# Morphology, Ontogeny, and Biomineralization of Trichomes of Selected Higher Plants

**Dissertation**

zur
Erlangung des Doktorgrades (Dr. rer. nat.)
der
Mathematisch-Naturwissenschaftlichen Fakultät
der
Rheinischen Friedrich-Wilhelms-Universität Bonn

vorgelegt von


## Adeel Mustafa

aus Shakargarh, Pakistan


Bonn, 2017

Angefertigt mit Genehmigung der Mathematisch-Naturwissenschaftlichen Fakultät der
Rheinischen Friedrich-Wilhelms-Universität Bonn

Erstgutachter: Prof. Dr. Maximilian Weigend

Zweitgutachter: Prof. Dr. Thorsten Geisler-Wierwille

Tag der mündlichen Prüfung: 21.02.2018

Erscheinungsjahr: 2018

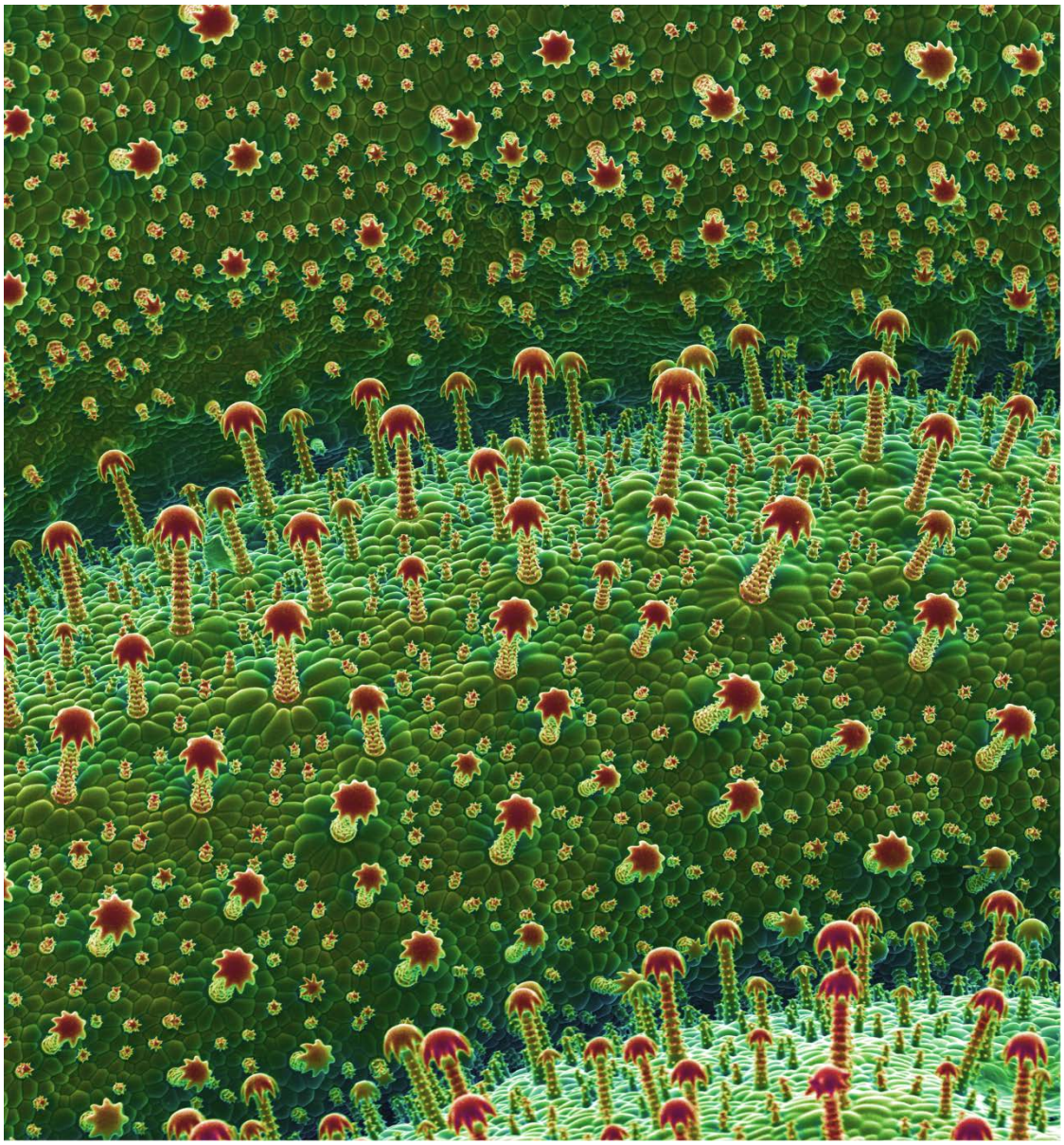

Cryo-scanning electron image of the mineralized trichomes cover on the fruit capsule of *Blumenbachia insignis* (Loasaceae).

# ACKNOWLEDGEMENTS

First of all, I would like to express my sincere gratitude to my supervisor Prof. Dr. Maximilian Weigend for his remarkable mentorship and excellent guidance throughout the PhD project. I owe earnest thankfulness for all his contributions of time, ideas, and funding, which allowed me to successfully complete my PhD. I am particularly grateful for his open door conveying me that I am always welcome to ask questions, and for our inspiring and insightful discussions. I highly appreciate his valuable advice in writing scientific articles, which ended up in the successful publications of our work.

My special thanks go to my co-author, Hans-Jürgen Ensikat, for teaching me SEM, EDX techniques and all preparation methods applied in this research work. I am grateful for his support in getting the results of this thesis and writing the manuscripts of this thesis. I am glad that I could profit from his expertise. My grateful thanks are extended to Prof. Dr. Thorsten Geisler-Wierwille (Steinmann-Institut für Geologie, Mineralogie und Paläontologie), not only for agreeing to be the second supervisor of this thesis but also for introducing me to the Raman spectroscopy technique.

Many thanks also go out to our Nees-Institute working group: Dr. Stefan Abrahamczyk, Rafael Acuña-Castillo, Tim Böhnert, Dr. Juliana Chacón, Dr. Bernadette Große-Veldmann, Dr. Norbert Holstein, Dr. Federico Luebert, Andreas Mues, Dr. Jens Mutke, Constantin Poretschkin, and Nicole Schmandt, for their helpful discussions, guidance and support on various aspects during my PhD time. I thank Elisabeth Gebhard and Elke Hedke for their support in administrative procedures.

I would especially like to thank Dr. Federico Luebert (Nees Institut für Biodiversität der Pflanzen, Bonn), Dr. Martin A. Hamilton (Research Leader, UKOTs; Royal Botanical Garden, Kew, UK), Dr. Tilo Henning (Botanischer Garten und Botanisches Museum Berlin-Dahlem), and Dr. Günter Gerlach (Botanischer Garten München-Nymphenburg) for organizing and transporting the plant specimens. I would explicitly like to thank Dr. Norbert Holstein for his useful suggestions, continuous support in figure arrangement as well as for proofreading the text of some chapters. I am grateful

to the enthusiastic and dedicated staff of the Botanical Gardens of Bonn for cultivation and supplying of the plant materials that I needed, especially to Mrs. Birgit Emde and Mr. Michael Neumann. I am grateful to Thomas Joßberger for vouchering the collections and preparing the herbarium specimens.

Finally, I thank my parents and all other family members for their unconditional and immeasurable support and care.

# TABLE OF CONTENTS

# CHAPTER 1

# General introduction

## 1.1 Biomineralization: A general overview

Biomineralization refers to the processes by which living organisms deposit minerals in different tissues often leading to the hardening or stiffening of the mineralized structures (Lowenstam and Weiner, 1989). It is a relatively common and widely observed phenomenon among plants and animals (Nitta et al., 2006; He et al., 2014). Biomineralized tissues have been described in detail in vertebrates (antlers and bones), mollusk shells, algae and microorganisms (Boskey, 2007; Thamatrakoln and Hildebrand, 2008). In each group, biomineralization evolved to adapt to different selective pressures, such as defense, foraging or sexual attraction. Biomineralization with calcium carbonate is particularly common in marine invertebrates (Sommerdijk and Cusack, 2014), as is silica in algae, sponges and diatoms (Thamatrakoln and Hildebrand, 2008), as well as calcium carbonate and calcium phosphate in vertebrates (Omelon et al., 2009). The size, shape, location, chemical and structural composition of the minerals produced by living organisms are essentially controlled by genetic factors (Rahn-Lee and Komeili, 2013; Krieger et al., 2017). Several specific enzymes have been identified in living organisms that contribute actively to the processes of biomineral formation in diverse biological models, such as algae, bacteria and metazoans (Weiss and Marin, 2008).

Biominerals, including calcium and phosphate ions as the main components of higher vertebrates bones (Lowenstam, 1981), are mainly involved in mineral ion metabolism through dissolution, precipitation and crystallization processes. In unicellular organisms, biomineral calcium phosphate occurs in an amorphous phase (Combes et al., 2016), whereas in more highly evolved organisms, notably in vertebrates, it mainly occurs as apatite structures and is produced abundantly (Elliott, 2002). Biomineralization is also widely prevalent in plants and has been reported in a variety

of plant organs: fruits, flowers, seeds, leaves, stems and roots (Fu et al., 2002; Lins et al., 2002; Currie and Perry, 2007; Bauer et al., 2011). Three common biominerals (calcium oxalate, calcium carbonate and silicon dioxide) have been identified in higher plants and have gained valuable attention due to their widespread distribution (Arnott, 1982). The biomineral calcium oxalate occurs in the inner tissues of plants, whereas calcium carbonate ($CaCO_3$) and silicon dioxide ($SiO_2$) are mainly present on plant surface structures (Pollard and Briggs, 1984; Lin et al., 2002; Nitta et al., 2006; Bauer et al., 2011). The presence of biominerals in or on plant surfaces defines their functional properties such as the mechanical stability and protection of soft tissues.

Biomineralization is an interdisciplinary field involving three major disciplines: biology, chemistry and physics, which are interlinked with each other. Therefore, the study of the origin and the properties of biominerals has received significant scientific attention from different fields, such as medicine (bones and teeth), material science, mineralogy and crystallography. Biominerals are crucially important in geo- and bio-sciences due to their prominent role in global biochemical cycles (Van Cappellen, 2003). Lowenstam (1981), Mann (1983), Weiner and Addadi (1997) and Addadi and Weiner (2014) comprehensively described the mechanisms employed by biological organisms to produce mineral phases and factors controlling these biological processes. This includes structural, spatial and chemical properties, including the significance of amorphous biominerals. The process of mineralization is followed by two different fundamental processes: (a) *biologically induced* (intracellular level of regulation), where the living organism is modified according to physio-chemical conditions of its environment and has little control over the type and shape of minerals; (b) *biologically controlled* (both intra- and extracellular), where the shape of crystallites and crystal growth is controlled by biomolecules (Lowenstam, 1981; Mann, 1983; Franceschi and Nakata, 2005).

The variability in morphology and structure by which organisms are capable of depositing biominerals is remarkable. Each type of biomineral has evolved unique strategies for building up inorganic/organic composite materials. They are optimally adapted to their specific functions and often equipped with distinctive mechanical properties. Living organisms employ these mechanical, optical and even magnetic

properties for a range of characteristic purposes. Biominerals are shaped by living organisms under natural conditions (temperature, water, pressure and pH) and are composites of a complex organic macromolecular matrix of proteins, polysaccharides and amorphous or crystalline minerals (Lowenstam, 1981; Weiner and Dove, 2003). Explaining the specific mechanisms leading to the formation of any particular biomineralized structure appears to be difficult. However, some basic mechanisms of biomineralization are prevalent in the majority of living organisms (Arnott, 1982).

### 1.1.1 Characteristic functions of biominerals

The functional properties of an individual biomineral might be variable depending on its location, elemental compositions, shapes and sizes (Franceschi and Nakata, 2005). The deposits of biominerals in plants, animals and microorganisms provide mechanical stability to the organism in the form of skeletons or hard defence structures. In vertebrates, the shapes of bones and teeth have evolved to optimize their functionality, whereas microstructure and composition determine their physical properties. Hardness, elasticity, density and solubility depend on microstructural features, such as crystallinity, crystallite orientation, porosity and the ratio of mineral to organic matrix components. The chemical nature of the bone and teeth biominerals is quite uniform, as a carbonated calcium phosphate (bio-apatite), and is of substantial interest to chemists and material scientists. The remarkable stability of mollusc shells results from the microstructure of their calcium carbonate composite material (Sommerdijk and Cusack, 2014). Microorganisms, such as diatoms, foraminifera and corals produce enormous amounts of biominerals such as silica and calcium carbonate, despite of their small size (Weiner and Addadi, 2011; de Nooijer et al., 2014). Through shells and crustacean exoskeletons, the toxic level of heavy metals can be reduced. Tudor et al. (2006) demonstrated that the biomineralized shell of clam (*Mercenaria mercenaria*) exhibit very rapid sequestration of metal ions, for example, a solution with a concentration of 10,000 mg/l Pb can be reduced by up to 0.5 mg/l in less than six minutes.

Genes encode the matrix proteins of biominerals that have profound effects on the structural properties of the mineral, including elasticity and hardness (Wilt and Killian,

2008). High and low concentrations of biominerals in surface structures define their functional properties; Currie and Perry (2007) and others (Franceschi and Horner, 1980; Franceschi and Nakata, 2005; Bauer et al., 2011) have described that high concentrations of biominerals in plants are enhancing the hardness, stiffness and mechanical stability of surface structures, helping them to work as the first line of defence against plant consumers prior to the initiation of feeding. Numerous studies show that biomineralization is an ecologically and physiologically important phenomenon. It exhibits a variety of characteristic functions, such as regulating calcium levels, detoxifying high concentrations of aluminum, heavy metals, oxalic acid and creating structural barriers to protect above-ground organs (Franceschi and Horner, 1980; Lins et al., 2002; Iwano, et al., 2004; Mazen, 2004; He et al., 2012). Soil is not only a basic growth medium for plants, but also a geochemical sink (Kirpichtchikova et al., 2006) for naturally existing heavy metals, such as Cu, Zn, Pd, Cr and other harmful pollutants (Malizia et al., 2012). The negative effects of heavy metals for soils, biological functions and microbial community are well known (Abay et al., 2005). Plants have evolved various defensive strategies against heavy metals. The accumulation of toxic metals inside trichomes – specialized cells located at leaf surfaces – has been documented in several species such as *Arabidopsis thaliana* (L.) Heynh. and *A. halleri* (L.) O'Kane & Al-Shehbaz (Zhao et al., 2000; Sarret et al., 2009), *Brassica juncea* (Salt et al., 1995), *Alyssum lesbiacum* (Krämer et al., 1997), and *Cucrurbita moschata* (Iwasaki and Matsumura, 1999). Tobacco plants excrete heavy metals (Zn and Cd) through their trichomes, which have demonstrated powerful detoxification mechanisms (Sarret et al., 2007).

### 1.2 Most common inorganic elements in biominerals

Three inorganic chemical elements are the basis of most common biominerals: calcium (Ca), phosphorus (P) and silicon (Si). Together with carbon and oxygen they form the biominerals calcium carbonate, calcium oxalate, calcium phosphate and silica (Lowenstam and Weiner, 1989; Knoll, 2003).

### 1.2.1 Calcium

Calcium (Ca) is an essential element and it plays fundamental roles in plant physiological and biochemical processes (White and Broadley, 2003). $Ca^{2+}$ is the principle cation of choice for most organisms involved in biomineralization (Lowenstam and Weiner, 1989). It is required by plants to regulate developmental and metabolic functions (Franceschi and Horner, 1980; Pritchard et al., 2000), cell membrane integrity, cell wall rigidity, cell division, cell elongation and membrane permeability (Wyn Jones and Lunt, 1967; Burstrom, 1968; White et al., 2002; Hepler, 1994, 2005). During cell wall formation, the acidic pectin residues, for example, galacturonic acids, are secreted as methyl esters and afterwards de-esterified by pectin methyl esterase enzyme, liberating the carboxyl groups that bind $Ca^{2+}$ (Hepler, 2005). Low concentrations of $Ca^{2+}$ consequently make the cell walls more fragile, whereas contrarily high concentrations of $Ca^{2+}$ may enhance the rigidity of the cell walls, binding with phospholipids and stabilizing lipid bilayers, thus increasing the structural integrity to the cellular membrane (Hepler, 2005; Guerini et al., 2005). Cell walls provide an enormous reservoir of $Ca^{2+}$ in comparison to the cytosol. High concentrations of $Ca^{2+}$ are required on the outer surface of the plasma membrane to maintain its functional integrity (Guerini et al., 2005). Calcium is an important component of several primary and secondary minerals in the soil, which is absorbed through plant roots and transported through the shoot via the xylem (Rengel, 1992). Ca-deficiency may limit or disturb the growth of new tissues due to incomplete cell wall formation. In most soils, $Ca^{2+}$ is abundant, However, deficits of Ca cause various symptoms, including poor root development, fruit cracking, leaf necrosis and curling (White and Broadley, 2003).

### 1.2.2 Phosphorus

Phosphorus (P) is classified as a major and essential plant nutrient and plays a key role in many physiological and biochemical processes, such as cell growth, fruit formation, seed development, lipid metabolism and the biosynthesis of nucleic acids (Pigott, 1971; Ha and Tran, 2014). P is involved in controlling key enzyme reactions and regulation of metabolic pathways. It serves as an energy source for a variety of

biological functions (Ha and Tran, 2014). Phosphorus is also an important component of cell membranes, deoxyribonucleic acid (DNA), ribonucleic acid (RNA), adenosine triphosphate (ATP) and the complex nucleic acid structure of plants (Vance et al., 2003). Phosphorous deficiency is considered as a major abiotic stress and inadequate supply of phosphorus can weaken the genetic processes such as cell division and plant growth (Wissuwa, 2003).

### 1.2.3 Silicon

Silicon (Si) plays an essential function in plant healing in response to biotic (pathogen, insect pests) and abiotic stresses, including metal toxicity, salinity, drought, nutrient imbalance, heat and lodging (Ma and Yamaji, 2006; Sahebi et al, 2015). Plants and microorganisms require silicon to form stable cell walls or special hard structures (Epstein, 1994). Silicon has been found to act as an essential agronomic element, particularly for the production of rice (*Oryza sativa*) (Agostinho et al., 2017). High accumulation of silicon is needed for plant development, growth and high crop yield (Datnoff et al., 1997), whereas low silicon accumulation not only affects crop yield but also makes plants more susceptible towards diseases. Some studies have reported that insufficient accumulation of silicon results in a significant loss of crop yield (Tamai and Ma, 2008). Silicified trichomes of *Oryza sativa* have been found to exhibit physiological functions in addition to their role in maintaining the cell shape and to offer benefits to the plants by enhancing their resistance to certain microorganisms (Yamanaka et al., 2009; Ye et al., 2013). Silicon is the second most abundant chemical element in the earth's crust, exceeded only by oxygen. The available amount of silicon in soils can vary substantially (Sommer et al., 2006; Epstein, 1994). Plant roots take up silicon in the form of silicic acid [$Si(OH)_4$] (Ma and Yamaji, 2015). Land plants contain a substantial amount of silicon, composing 1 to 10% of their dry matter; however, in some species this percentage might be even higher (Hodson et al., 2005). Plants of the families, such as Cyperaceae, Equistaceae and Poaceae have been found to accumulate more than 4% silicon, whereas some families of the order Commelinids, Cucurbitales and Urticales contain 2 to 4% Si (Perry, 2009). Temperate zone plants, due to high temperature and solubility relationship, acquire higher silicon contents than arctic plants. Individual plants may differ in their ability to accumulate silica, but

the presence of even small concentrations of silica in plant parts may help alleviate stresses (Debona et al., 2017).

### 1.3 Common biominerals in higher plants

Plants and their different organs contain various types of minerals. The three most common and largely distributed biominerals in angiosperms include calcium oxalate, which occurs in more than 75% of angiosperms (Franceschi and Horner, 1980) and is found mainly in plants as intracellular crystals (Arnott et al., 1965), calcium carbonate ($CaCO_3$) and silicon dioxide ($SiO_2$), which are primarily found in epidermal cells in the form of phytoliths and cystoliths (Bauer et al., 2011; Gal et al., 2012a) and in the outer cell walls of trichomes (Sowers and Thurston, 1979; Pollard and Briggs, 1984).

#### 1.3.1 Calcium oxalate

Calcium oxalate is a common biomineral in plants. It has been found in many organs, such as roots, leaves, stems, seeds, floral organs and fruits (Horner et al., 2000; Franceschi, 2001; Ekici and Dane, 2007). Biosynthesis of calcium oxalate has been considered a basic and crucial physiological process in higher plants. Some plants accumulate this biomineral, consisting up to 10% of their dry weight (Libert and Franceschi, 1987). Calcium oxalate crystals vary substantially in their sizes, shapes and number of crystals among different species (Konyar et al., 2014). Based on their distinct morphology, they have been classified into five major forms: prism, styloids, raphides, druses and crystal sand (Webb, 1999). In angiosperms crystal formation is intracellular and often occurs within the vacuoles of specialized cells called crystal idioblast (Franceschi, 2001). Ilarslan et al. (2001) suggested that crystal formation within the cell is genetically controlled. Calcium oxalate crystals consist of either monohydrate whewellite ($CaC_2O_4 \cdot H_2O$) or dihydrate weddellite ($CaC_2O_4 \cdot 2H_2O$) forms. Both have been found as biominerals in many organisms. Several functions have been attributed to calcium oxalate crystals in plants, such as tissue support, contributing to calcium homeostasis, light gathering and reflection, removal of excess oxalate or metal detoxification (Franceschi and Horner, 1980). The presence of raphides – needle-shaped calcium oxalate crystals – in specialized cells of some

flowering plants has been suggested to function primarily in sequestering excess calcium and to defend against herbivores (Sakai et al., 1972; Konno et al., 2014). The presence and absence of crystals may represent useful taxonomic characters.

### 1.3.2 Calcium carbonate

Calcium carbonate ($CaCO_3$) is an important and widespread biomineral in nature. In terrestrial plants, remarkably high concentrations of $CaCO_3$ have been found particularly in cystoliths (Arnott, 1980). These calcified cystoliths are formed in specialized cells called lithocysts (Wu and Kuo-Huang, 1997). Cystoliths are conglomerate crystals of $CaCO_3$ deposited on a stalked projection of cell wall cellulose. The main mineral component of cystoliths by volume is amorphous calcium carbonate and the minor biomineral component is the biomineral silica (Gal et al., 2012a). They have been reported to function as internal light scatterers that reduce the steep light gradient and distribute the light flux more evenly inside the leaf (Gal et al., 2012b). Regular distributions of cystoliths are well-known in several plant families, for example, Acanthaceae, Cucurbitaceae, Moraceae, Urticaceae and Ulmaceae (Arnott 1980; Wu and Kuo-Huang, 1997; Gal et al., 2012a). Cystoliths have been documented to be composed of four different mineral phases including their distinct chemical properties (Gal et al., 2012a). Plant cell walls contain mineral deposits of different chemical natures. Thus, mineralized cell walls help confer rigidity on the tissues and may provide protection against herbivores. Deposits of $CaCO_3$ in the cell walls of several marine algae (Carvalho et al., 2017) and in *Capsicum annuum* (Solanaceae) have been frequently reported (Horner and Wagner, 1992). The deposition of $CaCO_3$ in the upper epidermal layer of mulberry (*Morus alba* cv. Minamisakari) leaves has also been described in large, rounded idioblast cells (Nitta et al., 2006).

### 1.3.3 Calcium phosphate

Although phosphates are common ingredients in all living cells, with calcium phosphate being especially common in animals, the deposits of calcium phosphate in plant leaves and other parts have been rarely documented. By using EDX-analysis, Lin

et al. (2004) reported Ca and P as the two main mineral elemental components of cystoliths in the leaves of *Justicia procumbens* L. Furthermore, Krieger et al. (2017) demonstrated that leaves and bark contain higher concentrations of biominerals in comparison to wood. However, they found particles with high concentrations of Ca, P or Mg in ray cells of beech (*Fagus sylvatica* L.) and in roots of sycamore maple (*Acer pseudoplatanus* L.). Hydroxyapatite (HAp, commonly referred to as "biological apatite") is thought to be the most stable form of calcium phosphate and the primary inorganic component of natural hard tissues. It has only recently been discovered in plant trichomes. Ensikat et al. (2016) described that calcium phosphate [apatite, $Ca_{10}(PO_4)_6(OH)_2$] as a structural biomineral contributes to the biomineralization of certain types of trichomes in Loasaceae. It was the first ever report on calcium phosphate as a structural biomineral in higher plants and indicated the presence of a complex complement of biominerals in individual trichomes.

### 1.3.4 Silica

Terrestrial plants play a crucial role in the silica cycle through accumulation and synthesis of amorphous biominerals composed of silica, known as phytoliths or silica bodies. They represent a major pool of silica in tree foliage, wood and on surface structures of grasses, which use silica for mechanical stability and structure stiffening (Sangster et al., 2001). Silica deposits have been frequently reported in stinging trichomes, bristle trichomes tips and grainy surface structures. This enhances their hardness, stiffness and mechanical stability (Sowers and Thurston, 1979; Selvi and Bigazzi, 2001). They are well known to be present in grasses, horsetails and several other plant groups as amorphous silica associated with cell walls and cell lumens (Sangster and Parry, 1981; Trembath-Reichert et al., 2015). The occurrence of silica in the plant cell lumen and cell wall helps to produce phytoliths (Hodson, 2016). Phytoliths (plant opal silica bodies) have been considered as an essential tool for systematic botanists (Prychid et al., 2003), archaeologists and paleontologists to reconstruct historic environments, human and plant interactions and the pathway of plant domestication (Piperno, 2006). Silica deposits occur in a wide range of plant tissues, however, the highest concentrations of silica occur in the leaves, roots, inflorescence bracts of cereals (Sangster, 1978; Hodson and Sangster, 1989; Larcher et

al., 1991) and trichome breaking zones (i.e. tips), which makes them enough hard to make a hypodermic syringe such as *Urtica* stinging hairs (Thurston, 1974). Moreover, high concentrations have also been reported in stomata of horsetails (*Equisetum* spp.) and ordinary epidermal cells (Kaufman et al., 1971; Currie and Perry, 2007). Grasses are particularly well described to mobilize remarkable amounts of silicon in the form of silica biominerals, which are widely used within plants for structural support and pathogen defense (Cooke and Leishman, 2011). To agronomists, silica is of great concern because of its efficiency in optimizing the yield of economically important crops (Vandevenne et al., 2012).

## 1.4 Trichomes gross morphology, ontogenetic development and mineral formation

The scientific interest in trichomes of higher plants is based on their widespread distribution, taxonomic significance, structural and functional properties and the complex patterns of mineralization. Generally, trichomes are divided into two main categories: glandular trichomes and non-glandular including stinging trichomes, and are found commonly in several angiosperm plant families (Werker, 2000; Ensikat et al., 2016). Trichomes usually start developing from cells of the aerial epidermis very early during organ development (An et al., 2011). Different trichome types begin developing their distinctive morphology at very early developmental stages, showing great diversity in their morphology, such as strait, hooked and branched shapes and smooth or sculptured surfaces (Fig. 1), with varying density from one organ to another (Payne, 1978). Loasaceae usually possess numerous conspicuous trichomes on both vegetative (leaves and stems) and reproductive parts of plants (sepals, petals, stamens, and fruits; Weigend, 2004). It consists of three types of small trichomes: (i) unicellular scabrid trichomes equipped with a grainy surface and barbed or hooked; (ii) unicellular glochidiate trichomes with upwards and downwards directed sharp barbs, T-shaped apex; and (iii) multicellular glandular trichomes (Weigend, 2004; Ensikat et al., 2016). The complexity of Loasaceae trichomes is not limited to the surface morphology. More than 100 years ago, Küster-Winkelmann (1914) – using light-microscopy – described morphological details such as the increase of wall thickness by depositions on the inner side finally leading to massive trichomes and the

remarkable chemical heterogeneity of wall structures in stained samples. Mechanical defense, ontogeny, distribution, density, classification and taxonomic significance of bristle trichomes and stinging trichomes have been widely described by morphologists and taxonomists (Thurston and Lersten, 1969; Pollard, 1986; Cano-Santana and Oyama, 1992; Tuberville et al., 1996; Werker, 2000; Diane et al., 2003; Farmer, 2014) but the complexity of their mineralization has not been recognized. The formation of biogenic minerals in the outer cell walls of trichomes is indeed a widespread phenomenon across many plant groups, but their mineral abundance and distribution in different types of trichomes varies widely between taxa (Thurston and Lerste, 1969; Ensikat et al., 2016). These mineralized structures on plant surfaces can offer considerable ways for understanding some intriguing aspects of cell and developmental biology. Mineralized stinging trichomes and bristle trichome tips with $CaCO_3$ and $SiO_2$ have been extensively reported, underscoring their important role on plant surfaces (Sowers and Thurston, 1979; Pollard and Briggs, 1984; Hilger et al. 1993; Selvi and Bigazzi, 2001).

Several analytical methods are available to identify and characterize biominerals. Scanning electron microscopy (SEM) with an integrated system for element analyses by energy dispersive X-ray analysis (EDX) is nowadays a standard method to identify and quantify typical biomineral elements, such as Si, Ca, P, C and O (Qi et al., 2003). EDX element-mapping enables the localization of elements with micrometer-resolution. For several biominerals, the exact identification requires additional information, e.g. for discrimination between calcium carbonate and oxalate. Electron diffraction in a transmission electron microscope (TEM) or X-ray diffraction is used to identify crystalline minerals such as the different polymorphs of calcium carbonate and oxalate (Ensikat et al., 2016). Raman spectroscopy is a useful method for the identification of mineral anions (carbonate, phosphate) as well as many organic components with micrometer resolution (Butler et al., 2016). However, some biominerals, particularly calcium carbonate may be displaced during the specimen preparation procedure for SEM, thereby making it difficult to determine their accurate location. SEM studies and EDX element analyses revealed mostly surface views of the specimens, measuring only a part of the mineral content near the surface, dependent

on the penetration depth of the electron beam. A comprehensive recognition of the biominerals requires in depth analysis of the specimens.

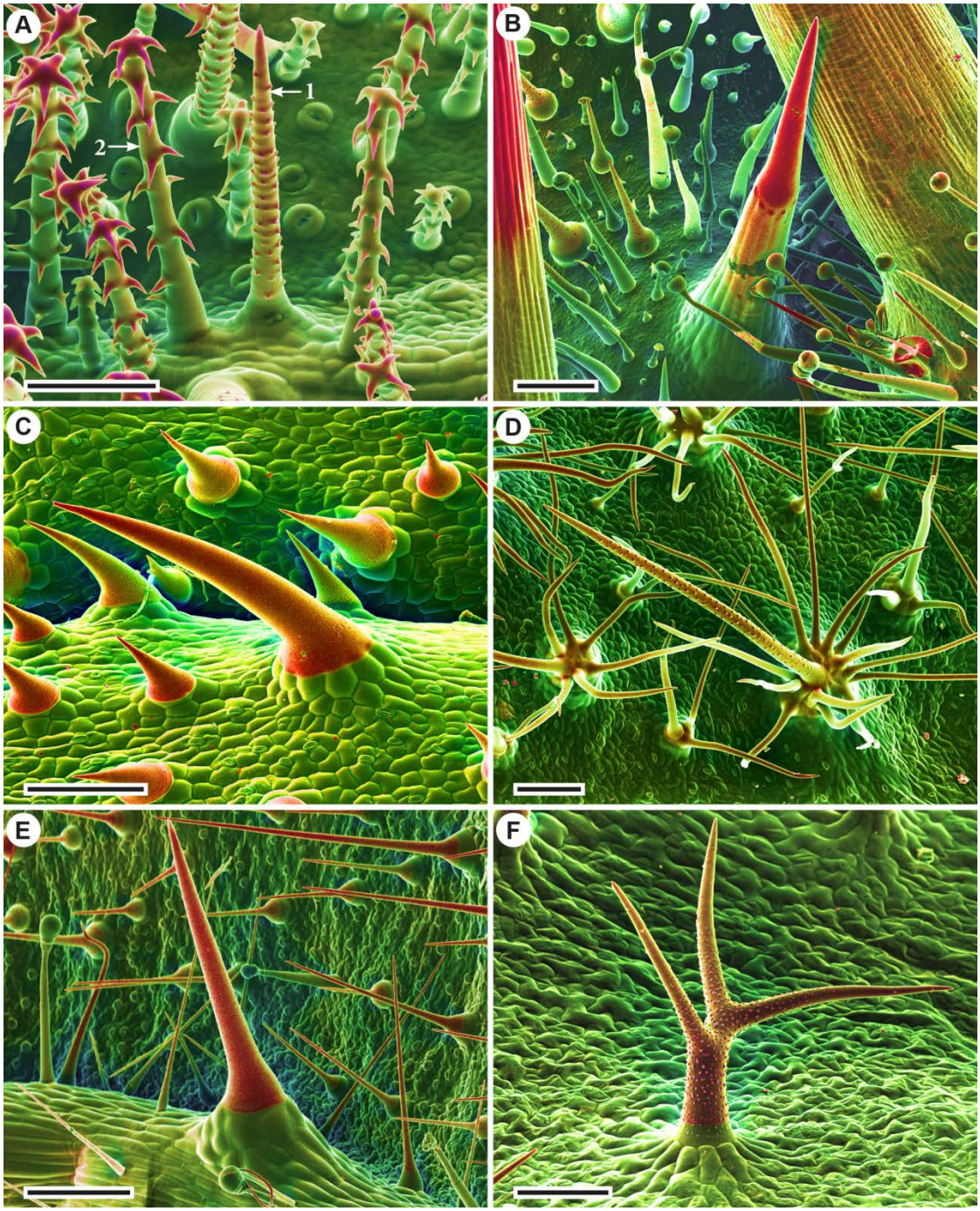


**Figure 1.** Cryo-SEM micrographs of typical trichomes on the leaves of different plant families. (A) *Loasa pallida* Gillies ex Arn. (Loasaceae); scabrid ("1, arrow" in A; sharp tipped with granular surface), glochidiate trichomes ("2, arrow" in A; T-shaped apex, upwards and downwards directed hooks). (B) *Codon royenii* D. Royen (Codonaceae); large trichomes consist of a mineralized single apical cell located on a high pluricellular, distally mineralized pedestal. In between are numerous small, partially

mineralized trichomes and non-mineralized glandular trichomes. (C) *Borago pygmaea* (DC.) Chater & Greuter (Boraginaceae); unicellular hispid trichomes with granular surface pattern, mineralized (yellow to red color). (D) *Onosma alborosea* Fisch. & C. A. Mey. (Boraginaceae); stiff unicellular trichomes with granular surface pattern, basal region covered by number of bristle trichomes, mineralization (yellow to red color). (E) *Phacelia malvifolia* Cham. (Hydrophyllaceae); sharp-tipped unicellular trichomes with a smooth surface, multicellular base, mineralized trichomes inserting on one row of mineralized foot cells. (F) A single trichome of *Arabidopsis thaliana* (L.) Heynh. (Brassicaceae) exhibits a distinctive shape with a stalk and three branches (Image reference: *Chapter 6*). The combined topographical and compositional contrast images show regions with higher mineral concentrations in yellow to red, whereas green color indicates the absence of mineral elements. Scale bars: A, F = 100 µm; B, C, D, E = 200 µm.

## 1.5 Functional properties of trichomes

A dense cover of trichomes can be found on both vegetative and reproductive plant organs. They vary in their structure, size, density and region of occurrence but are very common in many angiosperms (Weston et al., 1989; Snyder et al., 1993; Frelichowski and Juyik, 2001; Kennedy, 2003; Zhang et al., 2008). Mineralized non-glandular trichomes are believed to serve multiple functions in plants (Hanley et al., 2007; Fürstenberg-Hägg et al., 2013). Mechanical defense against herbivores is likely the prevailing function of all mineralized trichomes in Loasaceae (Eisner et al., 1998) and Urticaceae (Pullin and Gilbert, 1989). In addition, a barrier function due to their density is considered as an additional mechanism of defense against pathogens and herbivores (Levin, 1973). Generally, the functions of mineralized trichomes are based on their morphology and orientation. The distribution of bristle trichomes may reduce the feeding efficiency (Medeiros and Moreira, 2002; Kariyat et al., 2017). The anti-herbivore function against large mammals achieved by stinging trichomes is so apparent that no existing studies have attempted to experimentally validate it. Similarly, there is little evidence for the functionality of small trichomes and particularly scabrid-glochidiate trichomes of Loasaceae. However, Eisner et al. (1998) documented the capture mechanism: the physical impaling of insect feet by the glochidiate trichomes of a species of *Mentzelia* (Loasaceae). A whole range of insects may be permanently trapped and mortally wounded by the sharp hooks of these

trichomes, clearly underscoring that this type of trichome also plays an important role in plant defense.

Glandular trichomes consist of a stalk that provides support to the secretory head (round, glandular head). These trichomes are able to produce large amounts of proteins with defensive functions, for example, proteinase inhibitor, polyphenol oxidases and phylloplanins (Yu et al., 1992; Shepherd et al., 2005; Liu et al., 2006). Ingestion of metabolites can consequently disturb or damage digestive tracts (Hurley and Dussourd, 2015). In their essence, glandular trichomes afford an outer line of chemical defense by advertising the presence of noxious compounds (Hanley et al., 2007). On the other hand, some secreted substances attract a great variety of pollinators and visitors (Johnson, 1975; Werker, 2000). Secreted mucilage composed of water and polysaccharides from digestive glands of sundew (*Drosera*) acts like glue (sticky trap) for insects (Outenreath and Dauwaldert, 1986). Some studies demonstrated that glandular trichomes have the capacity to store and secrete massive amounts of different secondary metabolites (Schilmiller et al., 2008). Moreover, glandular trichomes have commercially gained significant economic value due to their by-products, which can be used for a variety of applications and purposes such as secondary metabolite use in pesticides or reserves of medicinal compounds (Aharoni et al., 2006), for essential oil production (Amelunxen et al., 1969; Schilmiller et al., 2008), or for the treatment of malaria (Weathers et al., 2011).

Apart from physical and chemical defenses, a dense cover of trichomes on leaves and stems may contribute actively to non-defence functionalities, e.g. leaf cooling and protecting living cells by reducing the absorption of solar radiation and extensive light (Skaltsa et al., 1994; Bickford, 2016). Trichomes may also reduce water evaporation of leaves and increase significantly the water retention under unfavorable stress conditions (Naydenova and Georgiev, 2013). Finally, trichomes can also provide efficient mechanisms for seed dispersal (Zhao and Chen, 2016).

### 1.6 Morphology and chemistry of stinging trichomes

Stinging trichomes have been of scientific interest because of their distinct morphology and ability to inflict pain by releasing chemical substances (Hook, 1665). The generalized structure of a stinging trichome consists either of a symmetrical or asymmetrical bulbous tip, shaft, base and a multicellular pedestal (Thurston, 1974). The size of stinging trichomes varies considerably among different genera. The smallest stinging trichomes have been observed in *Urtica dioica* L. with 1 mm in length (Joshi et al., 2014), whereas stinging trichomes of *Cnidoscolus texanus* can be from 5 to 8 mm long (Pollard, 1986). They are well known to be present in genera of five different plant families: Euphorbiaceae, Caricaceae, Loasaceae, Namaceae, Urticaceae (Thurston and Lersten, 1969; Carvalho and Renner, 2013). These families host various numbers of genera and species: (a) Euphorbiaceae (Malpighiales), a spurge family of flowering plants, consists of about ca. 300 genera with over 7500 species distributed primarily in the tropics. Stinging trichomes are present in the particular genus *Cnidoscolus*, which grows in deep sandy soils. It has two relatives in the southern United States, the *Cnidoscolus texanus* and *Cnidoscolus stimulosus*. The species of genus *Cnidoscolus* that are distributed in different regions: *Cnidoscolus urens* occurs in the Atlantic Coast and the Gulf Coastal Plain, *Cnidoscolus texanus* from Southern Arkansas to Tamaulipas, *Cnidoscolus aconitifolius* from Northern Mexico to Central America (Webster, 2014); (b) Caricaceae (Brassicales) is a flowering plant family comprising 6 genera and more than 34 species, distributed in the tropical regions of Central and South America and Africa (Carvalho, 2013); (c) Loasaceae (Cornales) consists of 20 genera in four subfamilies with more than 300 species, largely restricted to the Neotropics (Weigend et al., 2004); (d) Namaceae [based on new familial classification; *pro part* of Hydrophyllaceae, (Boraginales)] consists of only 4 genera (*Eriodictyon; Nama, Turricula, Wigandia*) with more than 76 species (Luebert et al., 2016); and (e) Urticaceae (Rosales) comprises 54 genera with more than 2000 species, overall including remarkable morphological diversity (Kim et al., 2015; Wu et al., 2015). Most of its genera and species are distributed in the humid tropics.

The part of stinging trichomes that delivers stinging liquid is slightly variable among different plant families (Thurston and Lersten, 1969; Fu et al., 2007; Fig. 2). In Urticaceae, Loasaceae and Euphorbiaceae the apical bulb is clearly curved and asymmetrical, whereas in Caricaceae (*Horovitzia*) and Namaceae (*Wigandia*) the apex of the stinging hair is symmetrical. However, the breaking tip mechanism may be similar. As a result of the force of contact, the mineralized tip of the stinging hair breaks off and creates a sharp hypodermic syringe, which penetrates into the skin (Thurston, 1974; Fu et al., 2007; Fig. 3). The pressure exerted on the bladder-like base extrudes the irritating chemical liquid (Thurston and Lersten, 1969; Thurston, 1974). Previous studies on mineralization of stinging nettle show that the wall of *Urtica* stinging trichome is stiffened with silica (silicified) at the apex and with calcium carbonate (calcified) in the rest portion (Sowers and Thurston, 1979), so that a predefined breaking zone is formed in the heavily silicified apical region.

Out of five urticating plant families, the family Urticaceae is well known because of its wide use in medicine (Wagner et al., 1989; Motamedi et al., 2014), cosmetics (Bourgeois et al., 2016), fiber production (Vogl and Hartl, 2003), phytoremediation (Adler et al., 2008) and application as alternative fertilizer (Li, 1994). However, their stinging trichomes have introduced themselves unpleasantly into human experience because of irritating chemical substances. The extracts of *Urtica dioica* L. are alleged to contain numerous phytochemical and pharmacological properties, such as antibacterial, analgesic, antiviral, antioxidant, anti-inflammatory, anti-sterols and anti-colitis (Asgarpanah and Mohajerani, 2012). Most studies of the chemical substances of aggressive stinging trichomes have been focused on members of Urticaceae and Euphorbiaceae (Lookadoo and Pollard, 1991; Fu et al., 2006). An early study on the chemistry of *Urtica urens* L. stinging liquid has suggested the presence of only two detectable active chemical substances, histamine and acetylcholine and an unidentified smooth muscle contracting substance (Emmelin and Feldberg, 1947). Furthermore, an investigation by Collier and Chesher (1956), documented the occurrence of 5-hydroxytrypatamine as a third toxic substance in the stinging liquid of *Urtica dioica.* Different species of Urticaceae have been found to produce different substances. In 1969, Thurston was not able to identify histamine, acetylcholine, 5-hydroxytrypatamine in the stinging liquid of *Urtica chamaedryoides* Pursh, thus the

presence of these substances remained controversial. Later on, Fu et al. (2006), examined stinging liquid of *Urtica thunbergiana* Siebold & Zucc., and found three substances: histamine, oxalic acid (ca. 2%), tartaric acid (ca. 10%). Moreover, some studies on the members of Euphorbiaceae such as *Cnidoscolus texanus* Small (Lookadoo and Pollard, 1991), found histamine, acetylcholine, 5-hydroxytrypatamine and some other non-detectable high molecular weight substances, which might be responsible for the experience of sensational pain. A comprehensive gap remains for detailed studies on chemical substances in stinging trichomes.

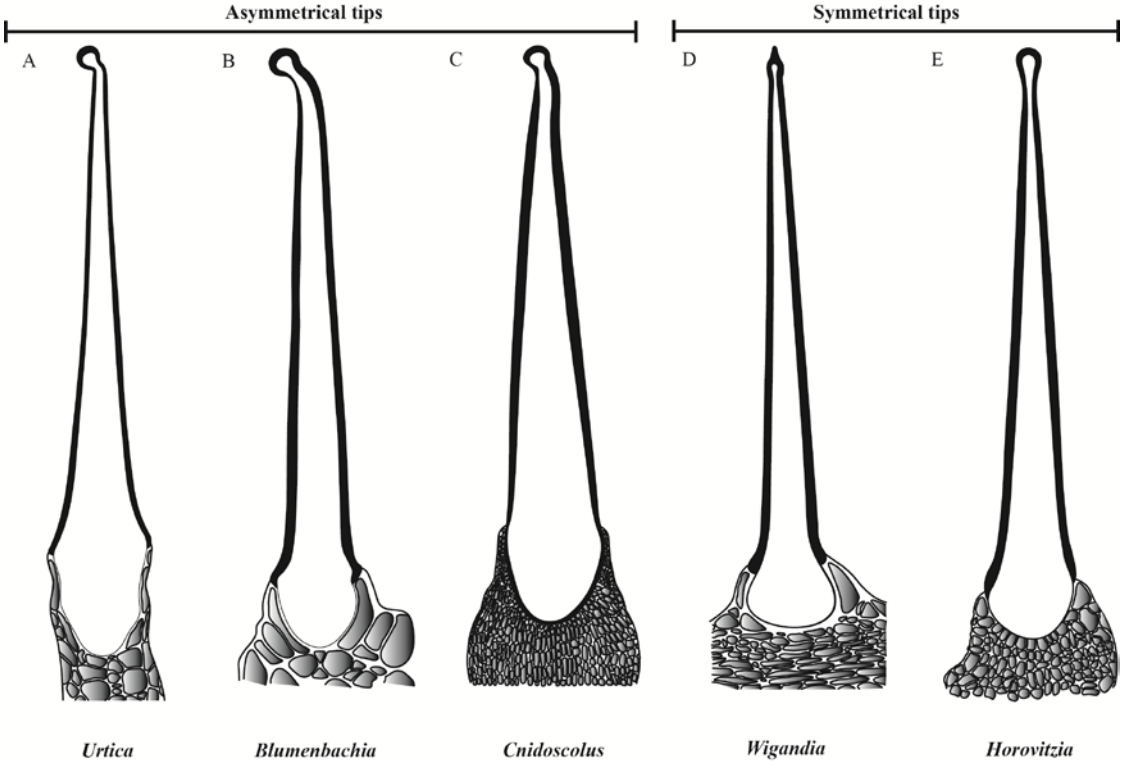


**Figure 2.** Schematic representation of stinging trichomes with asymmetrical and symmetrical tips of representative genera of five different plant families. (A) *Urtica* (Urticaceae). (B) *Blumenbachia* (Loasaceae). (C) *Cnidoscolus.* (Euphorbiaceae). (D) *Wigandia* (Namaceae). (E) *Horovitzia* (Caricaceae). Source: Drawn by Adeel Mustafa

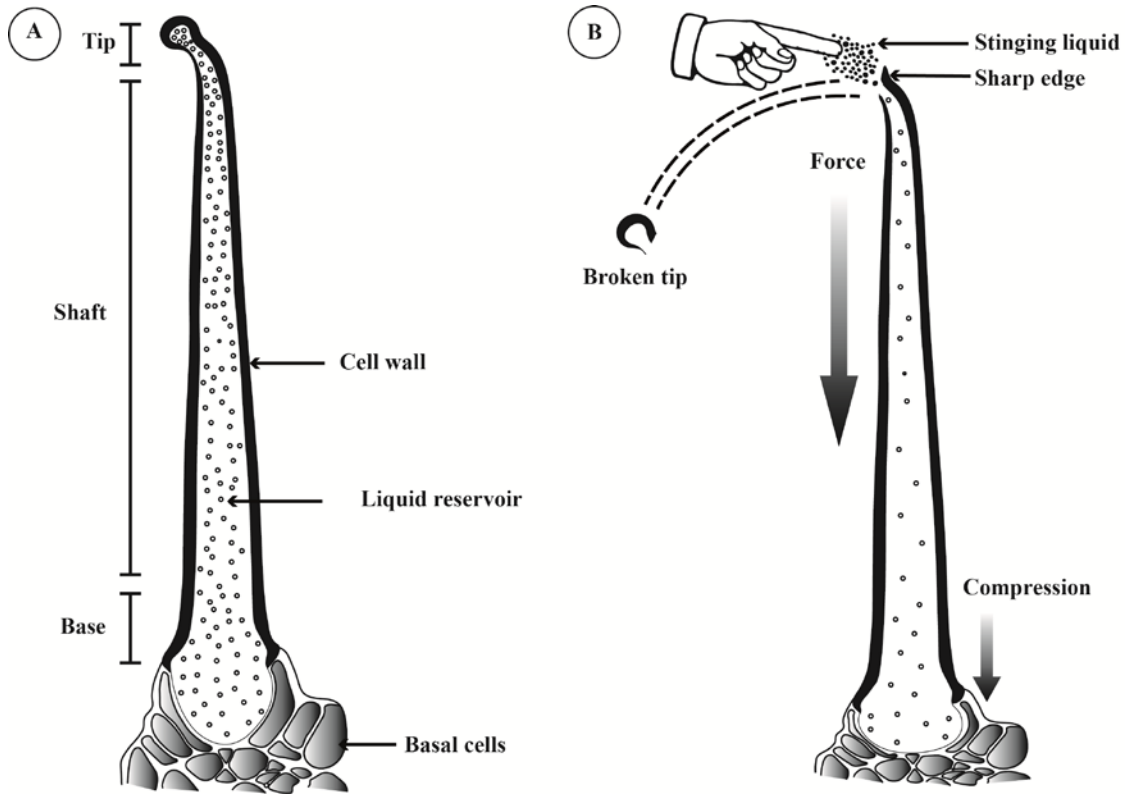


**Figure 3.** Schematic representation of *Blumenbachia insignis* Schrad. (Loasaceae) stinging trichome. (A) Three different regions/zones of a stinging trichome which include tip, shaft and base. The tube of the stinging trichome works as a stinging liquid reservoir. (B) Mechanism of tip breakage as a result of force of contact with an object or skin, creating a sharp point and the compression of the bladder-like base extrudes the chemical substances. Source: Drawn by Adeel Mustafa

## 1.7 Aims and scope of the study

The biomineral calcium phosphate, which is a primary component of bones and teeth in animals, has only recently been documented as a structural biomineral in higher plants. It was discovered in the stinging hairs and scabrid-glochidiate trichomes of the South-American plant family Loasaceae, where it was found to replace silica in stinging trichomes tips. Much research has been done on trichomes morphology, distribution and their diversity in different plant species. However, the ontogeny of these mineralized trichomes is poorly understood and the process of mineralization has not been studied previously. The essential aims of this study were to:

a) Elucidate the morphology and ontogeny of trichomes.

b) Document the ontogeny of stinging trichomes and their process of biomineralization.

c) Investigate the patterns of biomineralization in stinging trichomes and scabrid-glochidiate trichomes.

d) Compare stinging trichomes' biomineralization among different plant families.

e) Survey the distribution of the biomineral calcium phosphate, in combination with calcium carbonate and silica, across plant species of different plant groups.

Thus, the present study by using SEM, EDX-analysis, light microscopy (LM) and Raman spectroscopy was carried out in order to obtain a comprehensive data set describing the three-dimensional distribution of biominerals and particularly the co-occurrence of silica and calcium phosphate in morphologically distinct types of trichomes.

### 1.7.1 Research questions

The present study addresses these following questions:

**1.** What is the distribution of different types of trichomes (stinging, scabrid-glochidiate and glandular) on the plant surfaces of Loasaceae, e.g., on fruits, upper and lower side of leaves? How does the ontogenetic and morphological development of these complex trichomes proceed, and what are the sequences of their mineralization including deposition of different biominerals at certain locations of an individual trichome?

**2.** How are the three biominerals distributed in different types of trichomes (stinging, scabrid and glochidiate) across several different taxa of Loasaceae?

**3.** What are the patterns and differences of biomineralization in the outer cell walls of stinging trichomes, including their gross morphology across five angiosperm plant families (Urticaceae, Euphorbiaceae, Loasaceae, Caricaceae and Namaceae)?

**4.** What is the diversity of mineralization patterns with calcium phosphate, calcium carbonate and silica in representative species across seven families of the order Boraginales, and is there a possible presence of phylogenetic signals?

**5.** How common is the biomineral calcium phosphate in trichome walls of other plant groups, such as Boraginales, Brassicales, Malpighiales and Rosales?

### 1.8 Overview of the dissertation

This dissertation is a cumulative work of five manuscripts, published, accepted or submitted to different peer-reviewed scientific journals. They are presented as the author's version and publication information is provided in the beginning of each individual chapter. Bibliographic references cited through Chapter 1 and Chapter 7 are provided in a reference list after Chapter 7 and the supplementary data for published and non-published chapters are arranged as annexes after the bibliographic references.

Chapter 2 and Chapter 3 are purely SEM and EDX based studies, solely dedicated to the biomineralization of trichomes of Loasaceae – considered taxonomically the most interesting plant family – bearing a complex trichome cover. Chapter 2 describes the ontogenetic stages of stinging hairs, the morphologies of scabrid and glochidiate

trichomes and their differential development on different sites of plants. Moreover, it describes the diverging stages of mineralization and overall sequence of mineralization with three biominerals - silica, calcium carbonate and calcium phosphate.

Chapter 3 presents the patterns of biomineralization in single-celled trichomes such as scabrid-glochidiate trichomes and stinging hairs of the Loasaceae. It provides the first comprehensive overview of the diversity and distribution of biominerals between species and among genera, including 31 species containing two different biominerals in their trichomes, whereas 22 species contain three different biominerals (calcium phosphate, calcium carbonate, silica). This study moreover describes the extraordinary degree of physiological control in biomineralization.

Chapter 4 is dedicated to stinging trichomes biomineralization across the taxa. Stinging hairs have been reported from five plant families: Urticaceae, Euphorbiaceae, Loasaceae, Caricaceae and Namaceae. The results describe the remarkable diversity of mineralization patterns, often involving three different minerals differentially deposited in various zones of the stinging trichome.

Chapter 5 presents solely the patterns of mineralization in the trichomes of plant order Boraginales, demonstrating the striking phylogenetic, complex site-specific and differential patterns of biomineralization. Since no comprehensive biomineralization patterns have been documented previously on all these families collectively, the chapter includes and defines clear patterns of biomineralization among the 9 different plant families.

In chapter 6 a broader survey illustrates the wide distribution of calcium phosphate in trichome tips of several species in the orders Malpighiales, Rosales, Boraginales, Brassicales, Cornales and Cucurbitales. This chapter also includes trichome mineralization of the most extensively studied species *Arabidopsis thaliana* – where the presence of calcium phosphate had been completely overlooked.

## 1.9 Contribution to chapters

Chapter 2: **Mustafa A, Ensikat HJ, Weigend M. 2017.** Ontogeny and the process of biomineralization in the trichomes of Loasaceae. *American Journal of Botany* **104**: 367–378.
Own contribution: Designed work (together with M. Weigend and H. J. Ensikat), collected all plant materials, performed SEM and EDX work (together with H. J. Ensikat) and wrote the manuscript.

Chapter 3: **Ensikat HJ, Mustafa A, Weigend M. 2017.** Complex patterns of multiple biomineralization in single-celled plant trichomes of the Loasaceae. *American Journal of Botany* **104**: 195–206.
Own contribution: Collected all plant materials, prepared samples, performed SEM work and contributed to the final version of the manuscript (together with M. Weigend and H. J. Ensikat).

Chapter 4: **Mustafa A, Ensikat HJ, Weigend M. 2017.** Diversity of Biomineralization in stinging trichomes of different plant families: Silica, calcium phosphate, or neither?
Own contribution: Designed work (together with M. Weigend and H. J. Ensikat), performed SEM and EDX work (together with H. J. Ensikat) and wrote the manuscript (together with M. Weigend and H. J. Ensikat).

Chapter 5: **Mustafa A, Ensikat HJ, Weigend M. 2017.** Mineralized Trichomes in Boraginales – complex microscale heterogeneity and simple phylogenetic patterns.
Own contribution: Designed work (together with M. Weigend), performed SEM and EDX work (together with H. J. Ensikat) and wrote the manuscript (together with M. Weigend and H. J. Ensikat).

Chapter 6: **Weigend M, Mustafa A, Ensikat HJ. 2017.** Calcium phosphate in plant trichomes: the overlooked biomineral.
Own contribution: Collected all plant materials, prepared samples, performed SEM, EDX and Raman spectroscopy work (together with H. J. Ensikat) and contributed to the final version of the manuscript (together with M. Weigend and H. J. Ensikat).

# CHAPTER 2

## Ontogeny and the process of biomineralization in the trichomes of Loasaceae

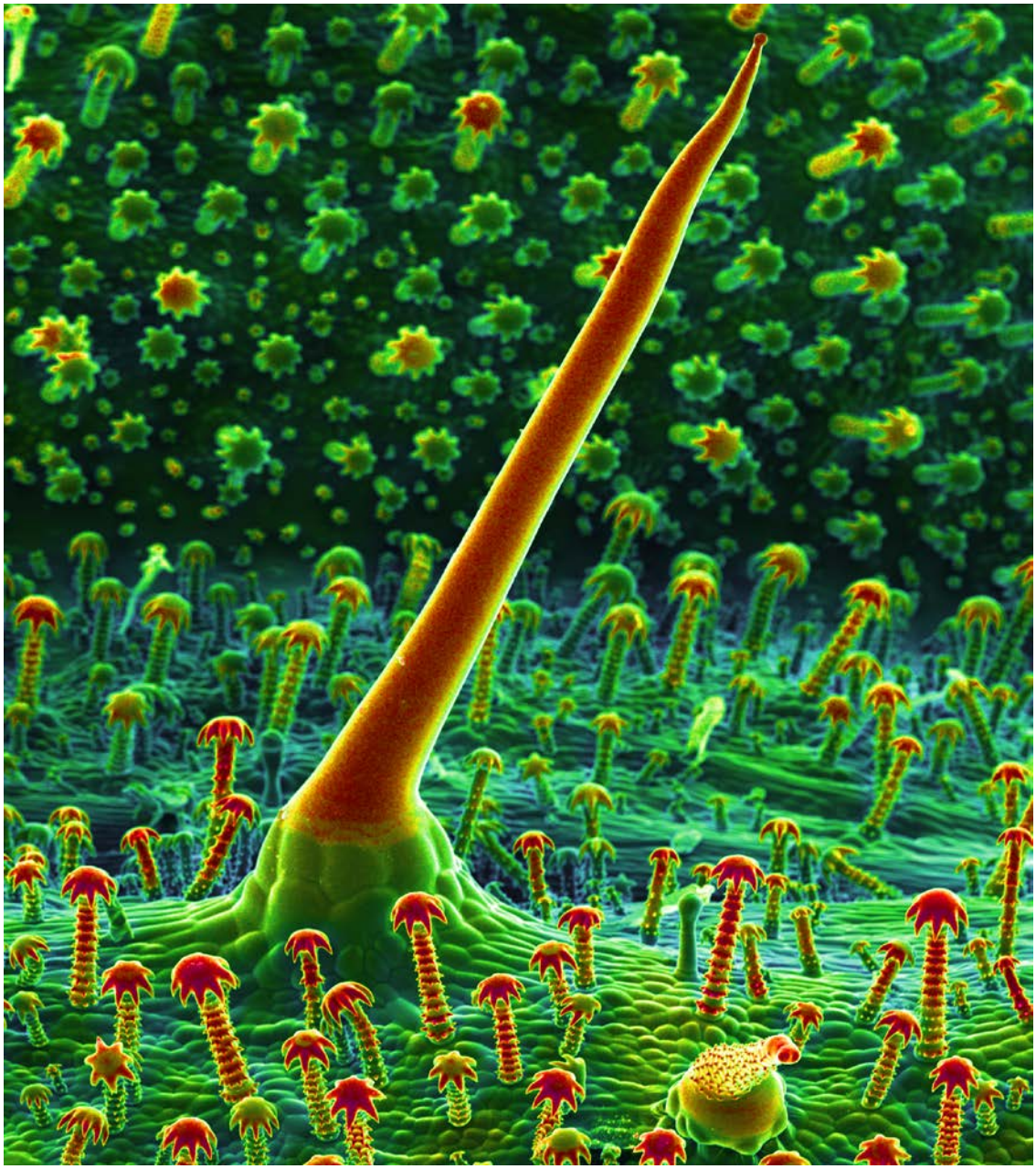

Cover image: A strongly mineralized unicellular stinging trichome consists of a bulbous tip and pluricellular base, is surrounded by unicellular scabrid-glochidiate trichomes (T-shaped and spiny) on the seed capsule of *Blumenbachia amana*.

RESEARCH ARTICLE

AMERICAN JOURNAL OF BOTANY

# Ontogeny and the process of biomineralization in the trichomes of Loasaceae[1]

Adeel Mustafa, Hans-Jürgen Ensikat, and Maximilian Weigend[2]

**PREMISE OF THE STUDY:** South American Loasaceae have a morphologically complex trichome cover, which is characterized by multiple biomineralization. The current study investigates the ontogeny of these complex trichomes and the process of their biomineralization, since both are very poorly understood.

**METHODS:** The development of stinging trichomes on various parts of the plants and the process of mineralization were studied using scanning electron microscopy (SEM) and energy-dispersive x-ray spectroscopy (EDX).

**KEY RESULTS:** Trichomes are initiated very early in organ development and the different trichome types begin developing their distinctive morphology at a very early developmental stage. Biomineralization in the stinging trichomes starts with the deposition of silica or calcium phosphate in the apex and then proceeds basipetally, with a more irregular, subsimultaneous mineralization of the base and the shaft. Mineralization of the scabrid-glochidiate trichomes starts on the surface processes and in the apex (silica, calcium phosphate), with a subsequent mineralization of the shaft with calcium carbonate.

**CONCLUSION:** Mineralized trichomes in Loasaceae provide an excellent model for the study of biomineralization. The overall sequence of mineralization is typically from distal and peripheral to proximal and central. Typically, three biominerals—silica, calcium carbonate, and calcium phosphate—are differentially and sequentially deposited in different parts of each unicellular stinging trichome.

**KEY WORDS** biomineralization; calcium carbonate; calcium phosphate; Cornales; development; energy-dispersive x-ray spectroscopy; Losaceae; morphology; scanning electron microscopy; silica

Loasaceae (Cornales) comprise 20 genera in four subfamilies with more than 300 species overall. They are typically covered with a dense, complex indument of various trichome types, including unicellular stinging hairs (Thurston, 1969; Thurston and Lersten, 1969; Dostert and Weigend, 1999; Weigend, 2003). Additionally, Loasaceae usually possess unicellular, scabrid trichomes (with a grainy surface, barbed, or hooked); unicellular, glochidiate trichomes (with a tack-shaped apex); and uniseriate, gland-tipped trichomes (Fig. 1; Weigend, 2003). These different trichome types are found on the entire aboveground plant surface, including the perianth. The two unicellular trichome types, the highly diversified scabrid-glochidiate trichomes and the relatively uniform stinging trichomes, are mineralized (Ensikat et al., 2016). Stinging trichomes are morphologically homogenous across the family, probably due to functional constraints. Stinging trichomes have been reported in a few genera from a range of different angiosperm families: Euphorbiaceae, Hydrophyllaceae, Loasaceae, Namaceae, and Urticaceae (Thurston and Lersten, 1969; Luebert et al., 2016). Trichomes can be defined based on their characteristic morphology, ontogeny, biomineralization, and ability to cause discomfort by the injection of irritant substances. Morphologically, stinging trichomes of Loasaceae are very similar to those of the family Urticaceae with an asymmetrical bulbous tip and a multicellular pedestal (Meyen, 1837; Greinert, 1886; Haberlandt, 1886; Küster-Winkelmann, 1914; Thurston, 1969). The mineralized, bulbous tip easily breaks off with the slightest touch, creating a sharp point, similar to that of a hypodermic needle, penetrating the skin and releasing the irritant. The morphology of stinging trichomes of Loasaceae has been of scientific interest for nearly 180 years (Meyen, 1837), but little is known about their development.

The scabrid-glochidiate trichomes of Loasaceae are more diverse and have been frequently used for taxon delimitation in the past

[1] Manuscript received 25 November 2016; revision accepted 7 February 2017.
Nees-Institut für Biodiversität der Pflanzen, Rheinische Friedrich-Wilhelms-Universität Bonn, Meckenheimer Allee 170, D-53115 Bonn, Germany
[2] Author for correspondence (e-mail: mweigend@uni-bonn.de)
**doi:10.3732/ajb.1600417**

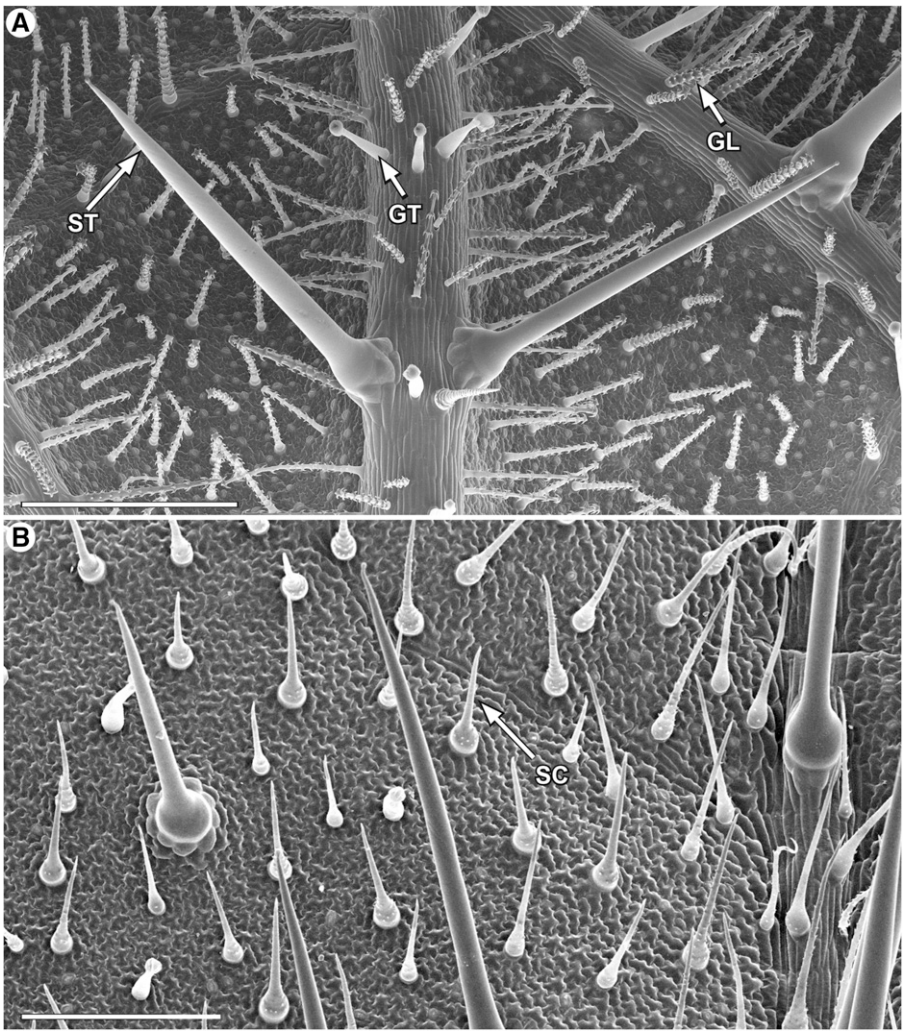


**FIGURE 1** Critical-point-dried (A) and cryo-SEM (B) micrographs of mineralized trichomes in Loasaceae. (A) Abaxial leaf surface of *Loasa insons* with large stinging trichomes, numerous smaller scabrid, glochidiate, and glandular trichomes. (B) Adaxial leaf surface of *Loasa insons* showing distribution of different types of trichomes over the surface. Scale bars: 500 µm in A; 300 µm in B. GL = glochidiate trichome; GT = glandular trichome; SC = scabrid trichome; ST = stinging trichome.

(Dostert and Weigend, 1999; Henning and Weigend, 2009; Weigend, 2000, 2003, 2004, 2007; Weigend and Rodriguez, 2003). The details of their surface sculpturing and overall shape show nearly endless variability, both between taxa and between different parts of the same plant. The basal portions of the stem typically differ in indument from the distal portions. Calyx, ovary, corolla, and leaves are typically differentiated in trichome cover, both in their trichome complement and the specific morphology of individual trichome types. One of the common phenomena with regard to the typical indument of many Loasaceae is that the adaxial leaf surfaces tend to be covered with scabrid trichomes, whereas glochidiate trichomes prevail on the abaxial leaf surface (Fig. 1). Mineralized trichomes are believed to have several functions in plants (Uphof, 1962; Levin, 1973; Gomez et al., 1980; Stipanovic, 1983; Jeffree, 1986; Agren and Schemske, 1993, 1994; Hanley et al., 2007; Fürstenberg-Hägg et al., 2013): mechanical defense against herbivores is likely the dominant function of all mineralized trichomes in Loasaceae. The antiherbivore function of the stinging trichomes is so obvious that apparently no one has been tempted to experimentally validate it, but there is also little evidence for the function of scabrid-glochidiate trichomes. However, Eisner et al. (1998) provided a range of images of small invertebrates trapped on the glochidiate trichomes of a species of *Mentzelia*, demonstrating that a variety of insects may be permanently trapped and mortally wounded by the sharp hooks of these trichomes, clearly underscoring that this trichome type also plays an important role in plant defense.

Biomineralized structures in plants are typically composed of calcium oxalate, calcium carbonate, or silica in a complex organic matrix of proteins and/or polysaccharides (Epstein, 2009; Bauer et al., 2011). Biomineralization in plants does not determine the shape of the organism to a comparable degree as in animals: Calcium oxalate is mainly found as intracellular crystals, while calcium carbonate ($CaCO_3$) and silicon dioxide ($SiO_2$) are mostly found on and in plant surfaces (Arnott, 1980; Wu and Kuo-Huang, 1997; Pollard and Briggs, 1984; Lins et al., 2002; Dietrich et al., 2003; Nitta et al., 2006; Bauer et al., 2011; Pérez Cuadra and Hermann, 2013), largely in the form of phytoliths and in the outer cell walls of trichomes. $CaCO_3$ and $SiO_2$ in stinging trichomes have been extensively reported from the plant kingdom, underscoring their important role on plant surfaces (Thurston and Lersten, 1969; Pollard and Briggs, 1984). Silicification and calcification of scabrid and glochidiate trichomes have also been reported, e.g., from Boraginaceae (Hilger et al., 1993; Selvi and Bigazzi, 2001). Recently, calcium phosphate biominerals (apatite, $Ca_5[PO_4]_3OH$) were reported to contribute to the biomineralization of certain trichomes in Loasaceae (Ensikat et al., 2016). This first report on calcium phosphate as a structural biomineral in higher plants indicated the presence of a complex complement of biominerals in individual trichomes. Ensikat et al. (2017) further demonstrated that trichomes in Loasaceae may undergo multiple mineralizations, with different minerals differentially deposited in different parts of the unicellular trichome, representing a remarkable example of chemical heterogeneity.

Plant trichomes in general develop from epidermal cells (Werker, 2000; Hülskamp, 2004) and may then differentiate into a range of uni- or multicellular structures of various shapes and sizes (Payne, 1978). However, the ontogeny of mineralized trichomes is poorly understood, and the development of the complex trichomes in Loasaceae and the process of their biomineralization have not been studied previously. The current study therefore provides a first insight into the ontogeny of typical Loasaceae trichomes and illustrates the process of their differential biomineralization using SEM and EDX techniques.

## MATERIALS AND METHODS

***Plant material***—The plant material (Table 1) used in this study was harvested from plants growing in the Botanical Gardens of the University of Bonn, Germany. All species are vouchered at the herbarium of the Nees-Institut für Biodiversität der Pflanzen (BONN).

***Sample preparation and scanning electron microscopy (SEM)***—Leaves between 3 and 40 mm long and young seed capsules were isolated for the SEM preparation. Very young leaf stages (<3 mm long) were accessible after removal of larger leaves and were left attached to the stem for further preparation. Topographical images were usually acquired by cryo-SEM of fresh, frozen samples. The fresh samples, e.g., leaves, were mounted on a cryo-holder and then cooled with liquid nitrogen. After insertion into the SEM, the samples were examined and imaged at temperatures of −100 to −70°C. Samples for EDX analyses were critical-point-dried after fixation in 70% ethanol + 4% formaldehyde for at least 24 h and dehydration with ethanol and acetone. Standard fixation solutions containing acetic acid were not used, because organic acids might alter the biomineral composition (especially calcium carbonate). Dried samples were sputter-coated with a thin layer (<30 nm) of palladium (Junker Edelmetalle, Waldbüttelbrunn, Germany), which does not compromise the detection of relevant elements such as silicon and phosphorus. To authenticate the element distribution results of the EDX mapping, we recorded element spectra of the regions of interest from fresh, hydrated samples, which tolerate the vacuum inside the SEM chamber for a sufficient time period for analysis.

Scanning electron microscopy was performed with a Cambridge S200 Stereoscan (Cambridge, UK) and a LEO 1450 SEM (Zeiss, Jena, Germany), equipped with an Oxford EDX system for element analyses. Images were recorded with a digital image acquisition system DISS 5 (Point Electronic, Halle, Germany). EDX mapping was performed on critical-point-dried samples. Color images were generated by combining secondary electron (SE) and backscattered electron (BSE) images or EDX element mapping. Image processing and color contrasting was carried out with standard image processing (Paint Shop Pro 9, Corel, Ottawa, Ontario, Canada) software (Ensikat et al., 2017).

**TABLE 1.** Examined plant species and their voucher details. All vouchers are housed at the herbarium BONN (Nees-Institut für Biodiversität der Pflanzen, Bonn University).

| Species | Accession | Herbarium |
|---|---|---|
| *Aosa uleana* | 36004 | *T. Jossberger 342* |
| *Blumenbachia amana* | 36584 | *T. Jossberger 1204* |
| *Blumenbachia insignis* | 36150 | *T. Jossberger 1210* |
| *Blumenbachia hieronymi* | 33609 | *T. Jossberger 1649* |
| *Caiophora clavata* | 33612 | *T. Jossberger 548* |
| *Caiophora cernua* | 33610 | *T. Jossberger 1653* |
| *Caiophora deserticola* | 37106 | *T. Jossberger 1562* |
| *Eucnide urens* | 29925 | *T. Jossberger 1501* |
| *Loasa elongata* | 37096 | *T. Jossberger TJH-067* |
| *Loasa insons* | 37108 | *T. Jossberger 1289* |
| *Loasa pallida* | 36565 | *T. Jossberger 666* |
| *Loasa triloba* | 37109 | *T. Jossberger 1624* |
| *Nasa contumazensis* | 37153 | *T. Jossberger 1309* |
| *Nasa weigendii* | 37116 | *T. Jossberger* 1242 |

## RESULTS

***Trichome distribution***—The aboveground surfaces of Loasaceae are densely covered with mineralized trichomes. Both sides of the leaves (Fig. 1A, B) are densely covered with stinging trichomes and a range of smaller trichomes, such as unicellular, scabrid (sharp-tipped, grainy surface), unicellular, glochidiate (T-shaped apex), and uniseriate, gland-tipped trichomes (round, glandular head). The typical structure of stinging trichomes consists of a single, elongate, conically tapering cell with a bulbous tip and mineralized cell walls, basally immersed in a pluricellular, nonmineralized pedestal. The outer cell wall of the stinging trichomes of most Loasaceae is perfectly smooth. A fine granular surface sculpturing is observed only on stinging trichomes of *Loasa pallida* (Appendix S1a, see Supplemental Data with online version of this article).

Maximum numbers of stinging trichomes ranged from 70 to 100 (adaxially) and 30 to 40 (abaxially) on leaves 17 to 45 mm long in the species studied. Individual leaves carried fewer or occasionally even no stinging trichomes (Appendix S1b, c). False-color SEM images of the adaxial leaf surface of *Blumenbachia hieronymi* and the abaxial leaf surface (Appendix S1d, e) of *Loasa pallida* show that both sides of the leaves are densely covered with smaller scabrid and/or glochidiate trichomes of variable sizes and a considerable number of large stinging trichomes, easily differentiated by their apical bulb and their smooth surface. Fully developed stinging trichomes are usually found in the intercostal part of the lamina on the adaxial leaf surface, while they are mostly found on the leaf veins on the abaxial leaf surface (Fig. 1A; Appendix S1d, e). Scabrid-glochidiate trichomes are quite variable in their morphology; they can be verrucose, spiny, or hooked (with erect or deflexed hooks, Appendix S2). Generally, glochidiate trichomes with long, reflexed barbs are more common on the abaxial leaf surfaces. Size, density, and details of the distribution of different trichome types vary substantially between the different taxa studied, on individual plants, and even between both sides of the leaf. On fruits of *Blumenbachia insignis*, e.g., are some large, fully developed stinging trichomes and numerous dramatically smaller glochidiate trichomes of variable sizes and in all developmental stages (Appendix S2d).

***Early ontogeny (before mineralization)***—Very young leaves in the earliest stages of development (<2 mm long, Fig. 2) were only accessible after removal of the larger leaves and opening of the terminal bud. Long before lamina and petiole differentiate in *Loasa pallida*, the leaves already carry a large number of surface protrusions, the first ones usually with the smooth surface typical of stinging trichomes. Trichome initiation proceeds from distal and marginal to basal and central, i.e., the first trichomes develop at the apex and the margins of the leaf. These young leaves of Loasaceae show various developmental stages of long stinging trichomes and smaller (scabrid or glochidiate) trichomes. Stinging trichomes develop from small surface protrusions into elongated, smooth cells, finally developing the characteristic apical bulb (arrows, Fig. 2A). The bulk of the trichomes on the young leaf of *Loasa pallida* (Fig. 2A, B) are evidently (smooth) stinging trichomes. The scabrid trichomes can be identified by the development of a roughly circular surface pattern at an early stage of development (arrow, Fig. 2C). From this sculpturing a granular pattern develops, finally turning into the conical surface sculpturing of the mature scabrid trichome (Fig. 2C and Appendix S3a). At these early stages, before leaf expansion, the trichomes are very narrowly spaced. Later, the spacing

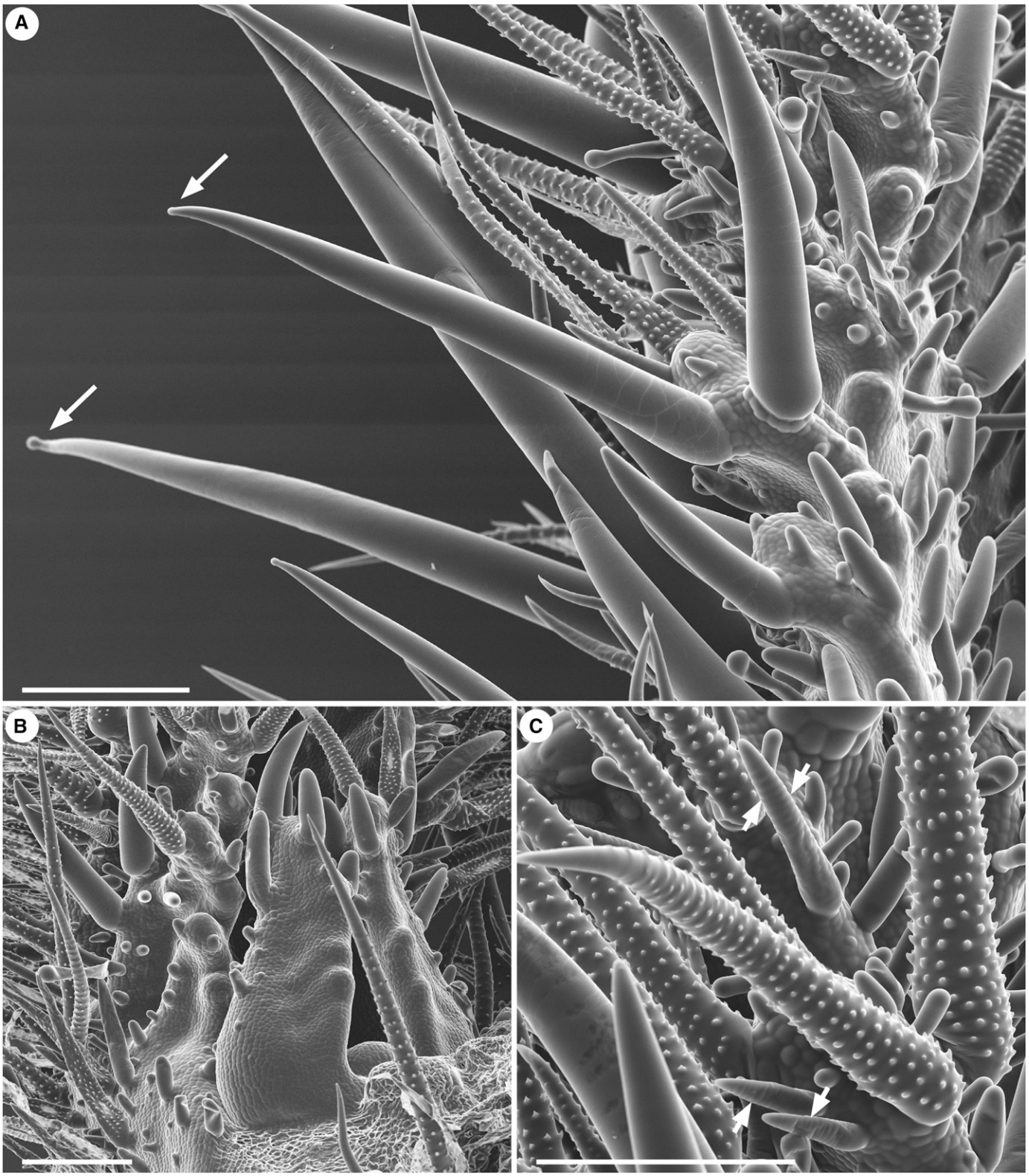


**FIGURE 2** Cryo-SEM images of very young leaves, of *Loasa pallida* showing early trichome development. (A) Early development of stinging trichomes; note the delicate cell walls (smooth) in unmineralized trichomes and incipient apical bulb formation (arrow). (B) Topographic image of very young *Loasa pallida* leaves at the vegetation point, showing first protrusions and outgrowing epidermal cells in the apical region and at the leaf margins. (C) Early stages of scabrid trichomes development. The stinging trichomes with their smooth surface can be distinguished from scabrid trichomes with an irregularly banded/granular surface. Formation of a faint circular pattern (arrows) allows the discrimination from the smooth stinging trichomes. Scale bars = 200 μm.

between stinging trichomes increases, while the total number of stinging trichomes per leaf remains roughly constant. The majority of stinging trichomes per leaf is thus established early in leaf development. The characteristic apical bulbs of stinging trichomes develop before the onset of mineralization. Trichome mineralization roughly follows the same topological sequence as trichome development, with mineralization starting along the leaf apex and margins (Appendix S3a–c) and then progressing more or less simultaneously over the entire leaf surface. At this stage, when mineralization is already progressing in the distal and marginal parts of the leaves, many stinging trichomes in the basal region of the leaf still appear nonmineralized, and some of them are collapsed, indicating their early ontogenetic stage (very thin and fragile walls, Appendix S3d, e).

***The process of biomineralization in stinging trichomes***—The process of mineralization at the early stages of stinging trichome development was additionally examined on selected stinging trichomes with EDX element mapping and the acquisition of spot spectra, particularly of the apical bulb and the shaft. Different stages of mineral deposition in stinging trichomes of *Aosa uleana* (Fig. 3A–F), and the stinging trichomes of *Nasa weigendii* and *Blumenbachia insignis* at various stages of biomineralization are shown in Figs. 4, 5). Previous examinations had revealed different biomineral compositions in the stinging trichomes of these species. The tips of *Aosa* were mineralized with silica, those of *Blumenbachia* and *Loasa* with calcium phosphate, whereas *Nasa* stinging trichome tips contained both (Ensikat et al., 2017). The figures clearly show that the process of biomineralization progresses basipetally from the apex of the stinging trichomes. The initially unmineralized trichomes of *Aosa* (Fig. 3A, arrow) start to be mineralized from the apex. The combined topography and EDX spectra indicate that silica is the first mineral to be deposited in the tip of stinging trichomes (Fig. 3B, C, arrow). Subsequently, silicification progresses basipetally (Fig. 3D and corresponding EDX spectra in Fig. 3E, arrow), with diffuse mineralization of the shaft and the base with both calcium carbonate and silica (Fig. 3F, Appendix S4) taking place more or less simultaneously. Biomineralization of the stinging hairs of *Nasa* showed a slightly different pattern. Two not fully mineralized stinging trichomes (Fig. 4A: ST1, ST2) contain Ca and P only, the shaft is not yet mineralized. Stinging trichome ST3 represents a more advanced stage, with the distal portion already heavily mineralized

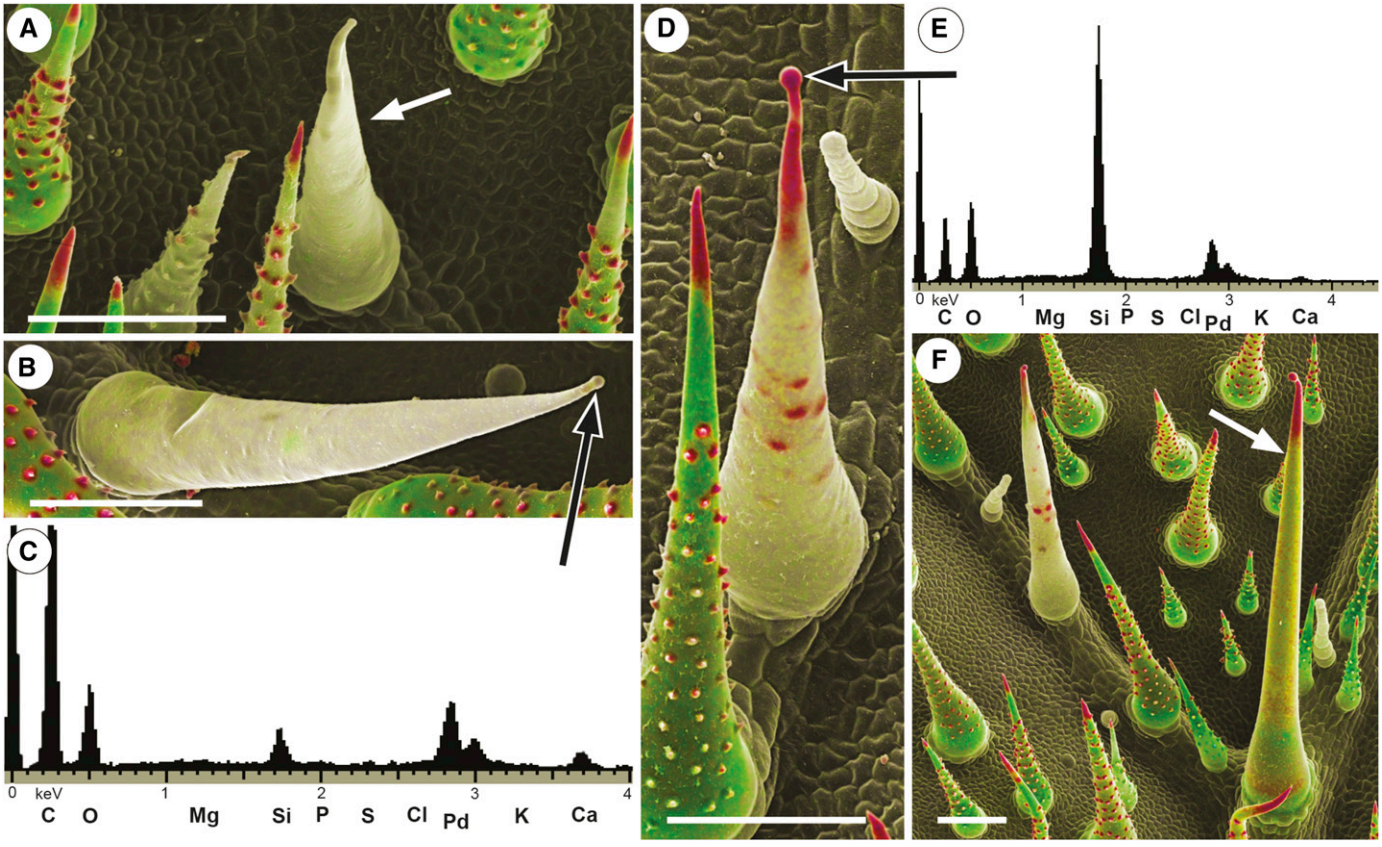


**FIGURE 3** Combined topography and EDX element-mapping images of critical-point-dried leaf material showing the element distribution (Si, Ca) and spectra of *Aosa uleana* stinging trichomes at different mineralization stages. (A) Unmineralized stinging trichome (colorless, arrow) with partially developed apical bulb surrounded by scabrid trichomes with near-complete mineralization. (B, C) Incipient mineralization of a stinging trichome tip. The EDX spectrum (C) from the tip (B, arrow) shows Si in low concentration and traces of Ca. Peaks corresponding to individual elements are labeled. (D, E) Partially mineralized stinging trichome with high Si concentration in the tip (arrow, corresponding spectrum in E); note the high Si peak in the spectrum (E). The shaft shows irregular deposition of Si, but no calcium deposition yet. (F) Fully mineralized stinging hair with silicified apex (red) and mostly calcified shaft (yellow to green, arrow) with traces of silica (red mottling). The colors indicate mineralization with Si (red) and Ca (green). Scale bars = 100 μm.

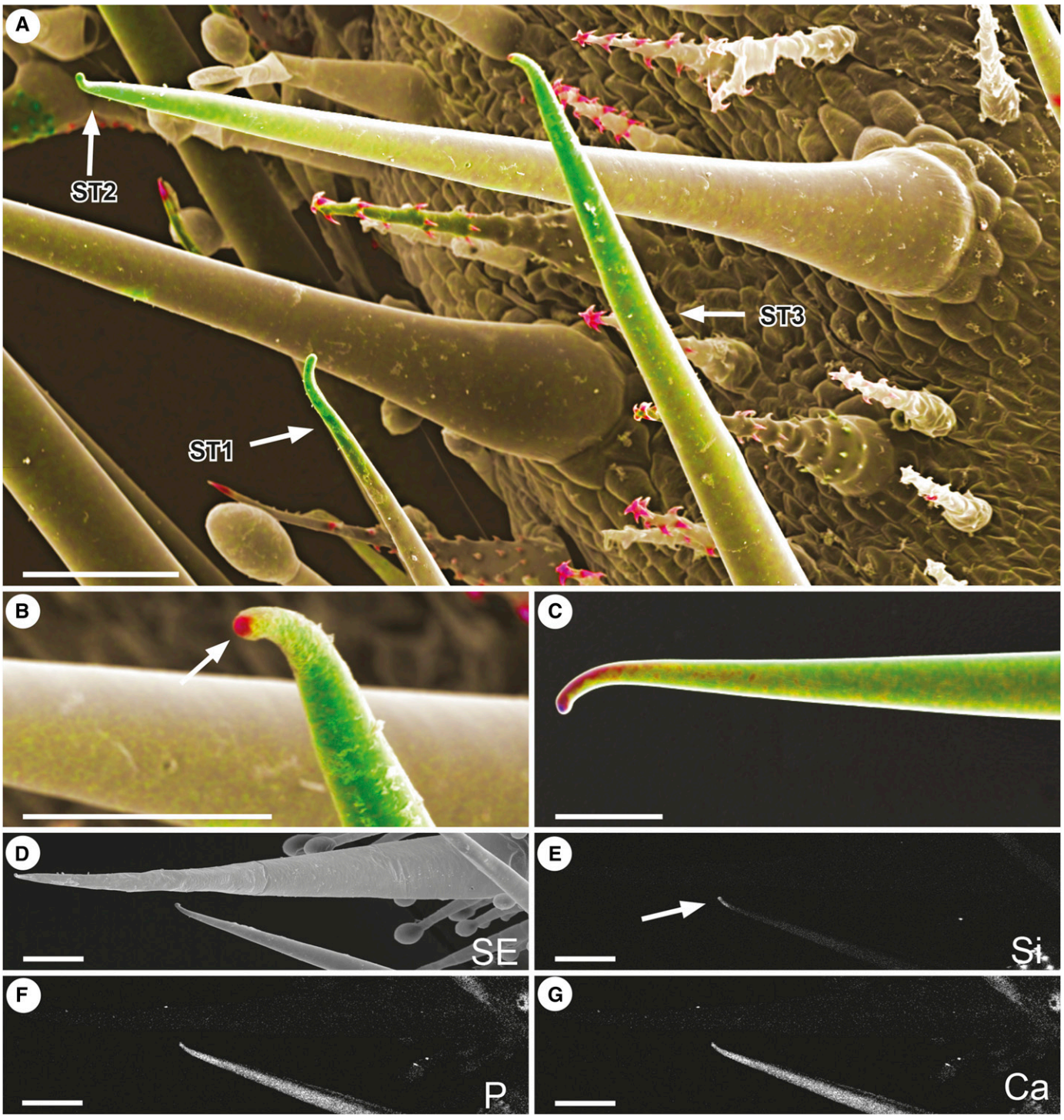


**FIGURE 4** SEM images of critical-point-dried leaf material. Combined topography and EDX element-mapping images showing the incipient mineralization of stinging and glochidiate trichomes of *Nasa weigendii*. (A) Tips of three stinging trichomes (ST1, ST2, ST3) in proceeding stages of beginning mineralization. The apical region containing calcium phosphate (green) extends from ST1 to ST3. The red dot at the tip of ST3 indicates incipient deposition of silica; see detail in (B). Note the progressive mineralization of glochidiate trichomes, beginning with silica (red) in the hooks. (B) Higher magnification of ST3 (arrow) with highly localized silica deposition. (C) Si distribution in a fully developed stinging trichome tip. (D–G) EDX-mapping of nonmineralized stinging trichome and apical part of a fully mineralized stinging trichome. (D) SE (secondary electron image) and distribution of (E) Si, (F) P, and (G) Ca. The nonmineralized (upper) trichome is visible only in the SE image. The fully mineralized one is clearly visible in the P and Ca images (F, G); the Si-mapping image (E) shows a high Si concentration only in the tip (arrow). Colors indicate mineralization with Si (red) and P (green). Scale bars: 100 µm in A; 50 µm in B, C; 100 µm in D–G.

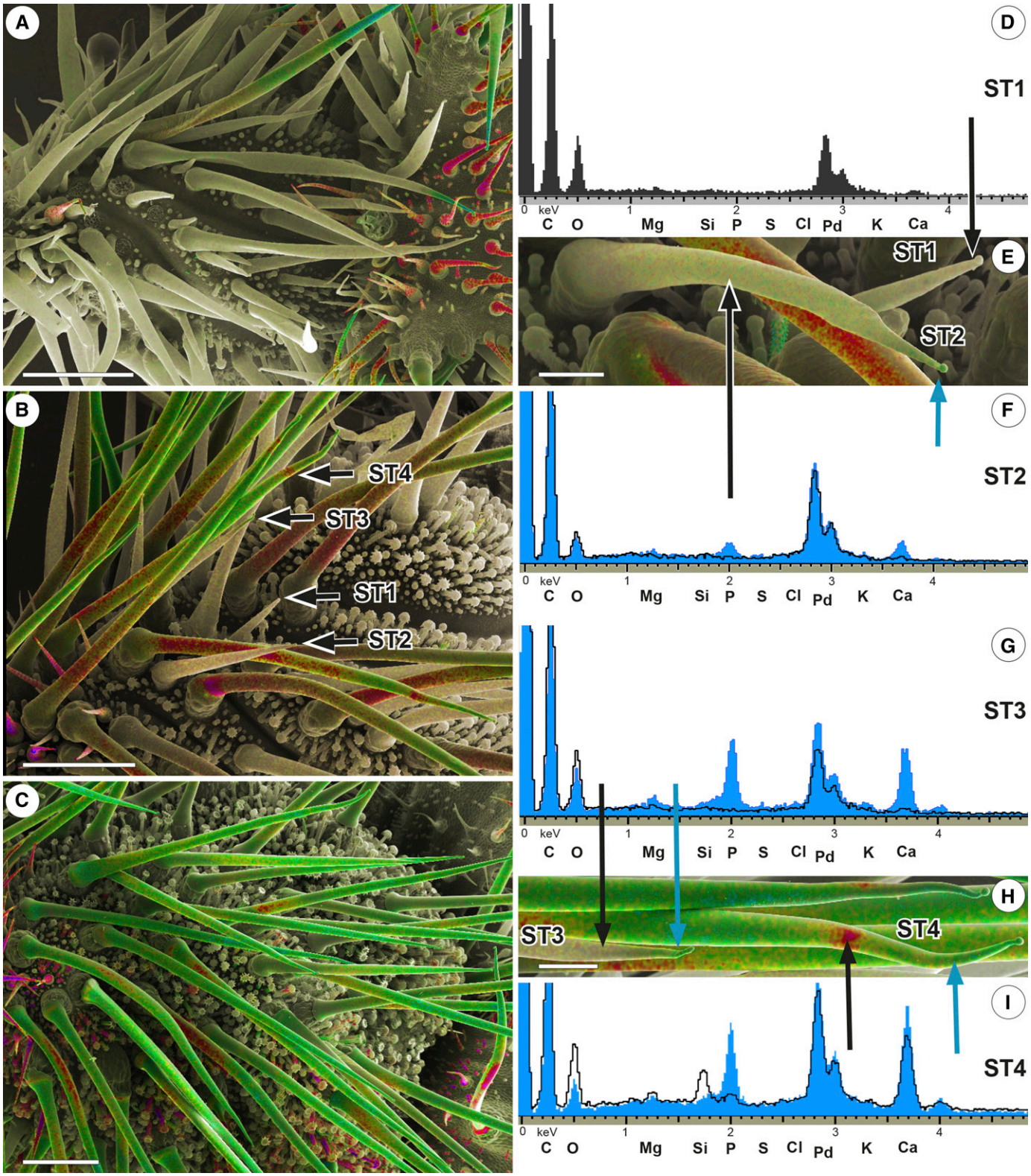


**FIGURE 5** SEM images of critical-point-dried ovaries of *Blumenbachia insignis* showing the development and biomineralization of the trichomes. (A) Very young ovary, <2 mm diameter, with numerous, nonmineralized stinging trichomes; only the largest ones show incipient calcification (green) at the apex. Sepals in the right part of the image are covered with numerous silicified (red) scabrid trichomes. (B) Ovary, ca. 3 mm diameter, with stinging trichomes (ST1, ST2, ST3, ST4) in various stages of mineralization. (C) Ovary, ca. 4 mm diameter, with fully developed and mineralized stinging trichomes and variously mineralized (red) and nonmineralized (gray) glochidiate trichomes. (D) Spectrum from the tip of nonmineralized stinging

with calcium phosphate and incipient deposition of silicon at the very tip (Fig. 4B). Silica is here deposited in the apex after calcium phosphate, deposition then proceeds over the curved region of the tip (Fig. 4C). Figure 4D–G shows the EDX-mapping images of one nonmineralized and one fully mineralized trichome each. The nonmineralized stinging hair is clearly visible in the topographic image (Fig. 4D), but is invisible in the element-mapping images due to the absence of the respective elements. The mineralized trichome contains Ca and P over the entire visible length, whereas silica is detected only at the tip (arrow).

***The process of differential mineralization in a mixed indument***—At very early ontogenetic stages, scabrid and stinging trichomes may look similar in some taxa, but on the twisted, inferior ovaries of *Blumenbachia insignis* stinging trichomes and glochidiate trichomes can be distinguished very early in their development because of their remarkably different sizes and distribution (Fig. 5). The ovary itself lacks scabrid trichomes (Fig. 5A, left), whereas a large number of scabrid trichomes are found on the adjacent sepals (Fig. 5A, right). On very young ovaries (<2 mm diameter), stinging trichomes appear on the ridges, along with numerous minute glochidiate trichomes (Fig. 5A). Scabrid trichomes on the sepal show incipient mineralization with silica. Most of the stinging trichomes on the ovary are not yet mineralized, but the longest ones show incipient mineralization with calcium at the apex. Once the ovary reaches a diameter of ca. 3 mm, its stinging trichomes have varying degrees of mineralization (Fig. 5B). At this stage, most of the stinging trichomes are fully or partially mineralized with calcium and some silica on the shaft, whereas glochidiate trichomes are still not mineralized. A larger ovary of ca. 4 mm diameter displays fully developed, long stinging trichomes that are already strongly mineralized, whereas the mineralization of glochidiate trichomes with silica is only starting (Fig. 5C). To illustrate the process of biomineralization in the stinging trichomes of *Blumenbachia*, therefore, we selected four stinging trichomes of the 3 mm seed capsule (Fig. 5B) for detailed analyses (Fig. 5E, H: ST1, ST2, ST3, ST4). In the element mapping images, ST1 appears nonmineralized (colorless) in Fig. 5E, while the mapping image of stinging trichome ST2 shows the first traces of Ca (green color in Fig. 5E) and P in the tip. The element composition can be estimated much better and with higher sensitivity in the corresponding EDX spectra (Fig. 5D, F). The blue area of each spectrum shows the composition of the apical bulbs, whereas the black line shows the spectrum of the corresponding shaft. The bulb of ST1 appears almost nonmineralized (Fig. 5D); negligible traces of P and Ca are close to the limits of sensitivity of the detector. Stinging trichome ST2 (Fig. 5F) shows both P and Ca in the bulb and apical region, indicating calcium phosphate deposition, whereas the shaft is still nonmineralized. The spectra of stinging trichome ST3 (Fig. 5G) show high concentrations of P and Ca in the apex, again with a peak height ratio that is characteristic for apatite-like calcium phosphate, whereas the shaft shows only traces of Ca. The spectra of stinging trichome ST4 (Fig. 5I) show high P and Ca contents in the apex, but mainly Ca and Si, and only traces of P, in the shaft. Overall, the element mapping images show an irregular distribution of Si in the shaft (Fig. 5B, C). Figure 6 schematically summarizes the process of biomineralization of the stinging trichomes in the four genera (*Aosa*, *Blumenbachia*, *Loasa*, *Nasa*). All of them show an overall basipetal progression of biomineralization, but display remarkable divergence in detail.

***The process of biomineralization in scabrid-glochidiate trichomes***—The biomineralization of scabrid-glochidiate trichomes proceeds slightly differently from that of stinging trichomes. Here, new trichomes are formed over a longer time, so that young trichomes of different development stages co-occur at any time until the leaf reaches its final size. As in stinging trichomes, characteristic morphological features, such as hooks and granular surface sculpturing, differentiate before mineralization. Figure 7A shows early developmental stages of glochidiate and scabrid trichomes on the abaxial side of a young *Loasa pallida* leaf. Mineralization starts with the deposition of Ca and P in the apices and the surface processes of scabrid trichomes; the shaft is mineralized later, and with Ca only. Glochidiate trichomes are here still unmineralized and in the process of morphological differentiation, as can be seen from the narrowly spaced and not fully differentiated hooks. Figure 7B and C show later stages with some trichomes already fully mineralized. Morphologically fully developed glochidiate trichomes contain high concentrations of calcium and phosphorus particularly in the hooks, and the process of biomineralization starts from the hooks and then progresses toward the shaft. The shafts of both scabrid and glochidiate trichomes contain calcium in variable concentrations. Trichomes of *Caiophora* contain the three biominerals silica, calcium carbonate, and calcium phosphate. Figure 7D through F show a complex and apparently more randomized mineralization pattern with nonmineralized and partially and fully mineralized glochidiate trichomes. Also, the precise type of biomineralization appears variable in scabrid-glochidiate trichomes. The majority of the glochidiate trichomes contain silica in the hooks (red), but several others contain calcium phosphate in their hooks (green and blue), indicating a considerable degree of variability in the type of biomineralization (Fig. 7E, F).

←

trichome (ST1). (E) Nonmineralized (colorless) stinging trichome (ST1; compare D) with fully developed apical bulb, and the stinging trichome (ST2, compare F) with first visible mineral traces in the tip and a nonmineralized shaft. (F) Spectra corresponding to the respective parts of panel E: ST2 shows small calcium and phosphorus peaks in the tip, whereas the shaft appears nonmineralized; carbon and oxygen represent the organic matrix (the palladium peaks result from the metal coating). The blue area of each spectrum shows the composition of the apical bulbs, whereas the black line shows the spectrum of the corresponding shaft. (G) EDX element spectra of the tip (bulbous) and shaft of the selected stinging trichome ST3 in H. The tip exhibits much higher Ca and P contents, whereas the shaft is still nonmineralized. (H) Two individual stinging trichomes from Fig. 5B were selected for detailed element mapping and local analyses. In the tip of stinging trichome ST3, the mineral content is clearly visible; in ST4, the tip and shaft appear mineralized. (I) EDX element spectra of the tip (bulbous) and shaft of the selected stinging trichome ST4 of H. The fully developed stinging trichome contains Ca and P in the tip; the shaft is mineralized with Ca (green) and Si (red) and contains only traces of P. Combined topography and EDX element-mapping images of critical-point-dried samples show Ca contents in green and silicon in red colors; nonmineralized structures appear colorless. Scale bars: 500 µm in A–C; 100 µm in E; 100 µm in H.

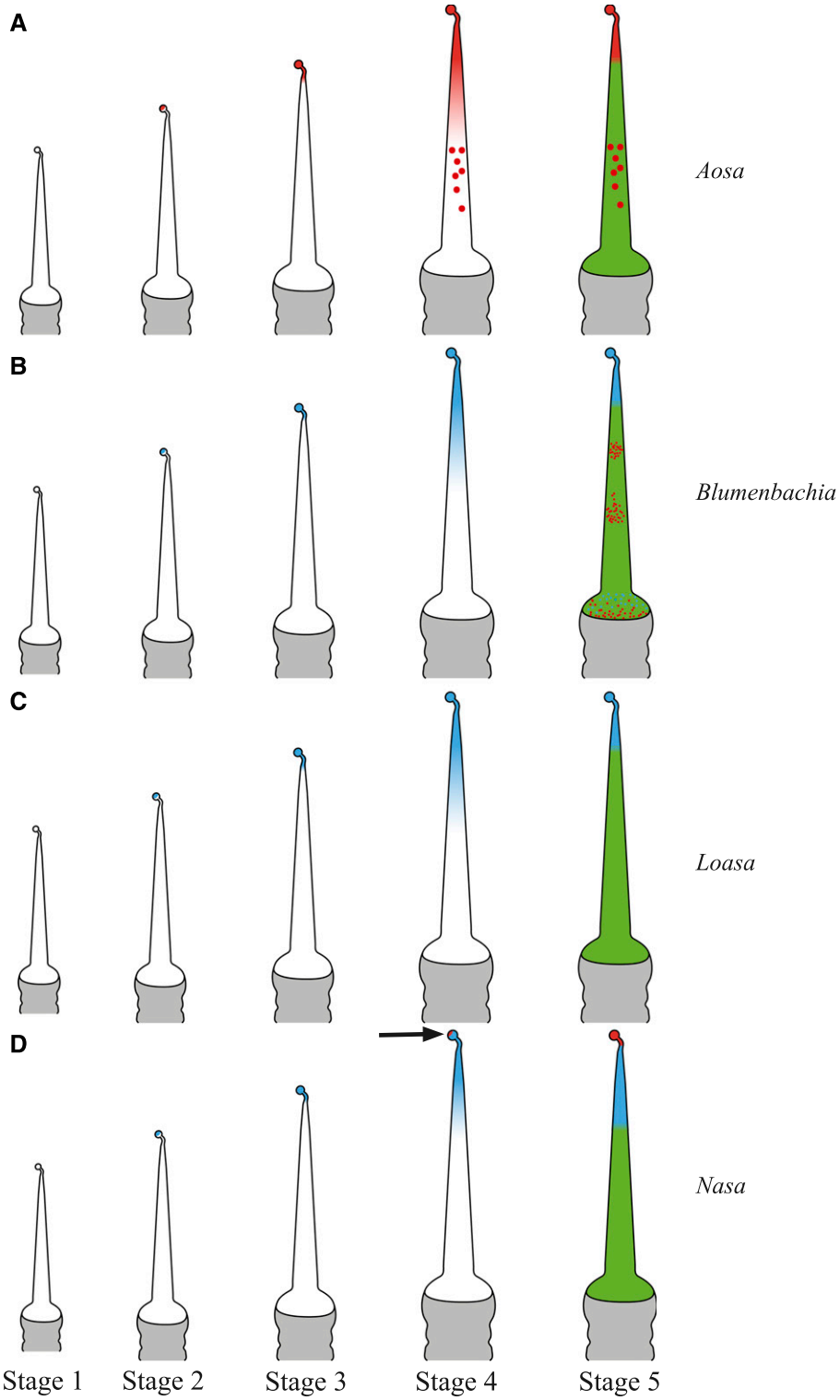


**FIGURE 6** Schematic representation of the process of biomineralization in the stinging hairs in different genera of Loasaceae: (A) *Aosa*, (B) *Blumenbachia*, (C) *Loasa*, (D) *Nasa*. Stage 1 = nonmineralized; Stage 2 = onset of mineralization; Stage 3 = tip mineralized; Stage 4 = partially mineralized; Stage 5 = fully mineralized. Biominerals are color-coded as follows: red = silica; green = calcium carbonate; blue = calcium phosphate.

## DISCUSSION

Previous morphological studies of *Urtica dioica* were mainly based on LM and SEM techniques or TEM cell ultrastructure (Thurston, 1974; Fu et al., 2007). For our studies, two SEM examination methods were most successful: cryo-SEM of fresh samples for morphology and EDX analysis with element mapping of critical-point-dried plant material, dramatically improving our understanding of the ontogeny and the process of biomineralization of the various mineralized trichomes. We clearly showed that stinging trichomes are developed early in ontogeny of the respective organs (e.g., leaves: Fig. 2B, ovaries: Fig. 5A). We further showed that up to three biominerals, silica, calcium carbonate, and calcium phosphate, are differentially and sequentially deposited in different parts of the individual, unicellular stinging trichome.

Both morphological trichome differentiation and biomineralization follow a general pattern starting from distal and marginal and progressing toward central and proximal. This general pattern of biomineralization is found in both scabrid-glochidiate and stinging trichomes, with the tips and—in the case of scabrid-glochidiate trichomes—the surface processes the first to be mineralized. In stinging trichomes, it is the tip that first shows mineral deposition, gradually extending in a proximal direction with an ultimately nearly simultaneous mineralization of the shaft and the base. In glochidiate trichomes, the hooks are the first to be mineralized; in scabrid trichomes, the apex and the surface processes are mineralized more or less simultaneously. The type of mineralization of stinging trichomes seems to be fairly conserved within species and genera. Figure 6 shows a schematic representation of the process of biomineralization of the stinging trichomes of the four genera in Loasaceae. In *Loasa*, *Blumenbachia*, and *Aosa* the process is straightforward: mineralization starts at the apex with calcium phosphate (*Loasa*, *Blumenbachia*) or respectively Si (*Aosa*), then a less regular mineralization of the shaft with calcium carbonate and silica takes place. *Nasa* diverges from this pattern: After the initial mineralization of the apex with calcium phosphate, the apical bulb becomes progressively silicified, followed by the mineralization of the shaft with calcium carbonate and varying amounts of the other minerals. Biomineralization of scabrid trichomes follows the same overall pattern, but appears to be more variable regarding the type of biomineral deposited.

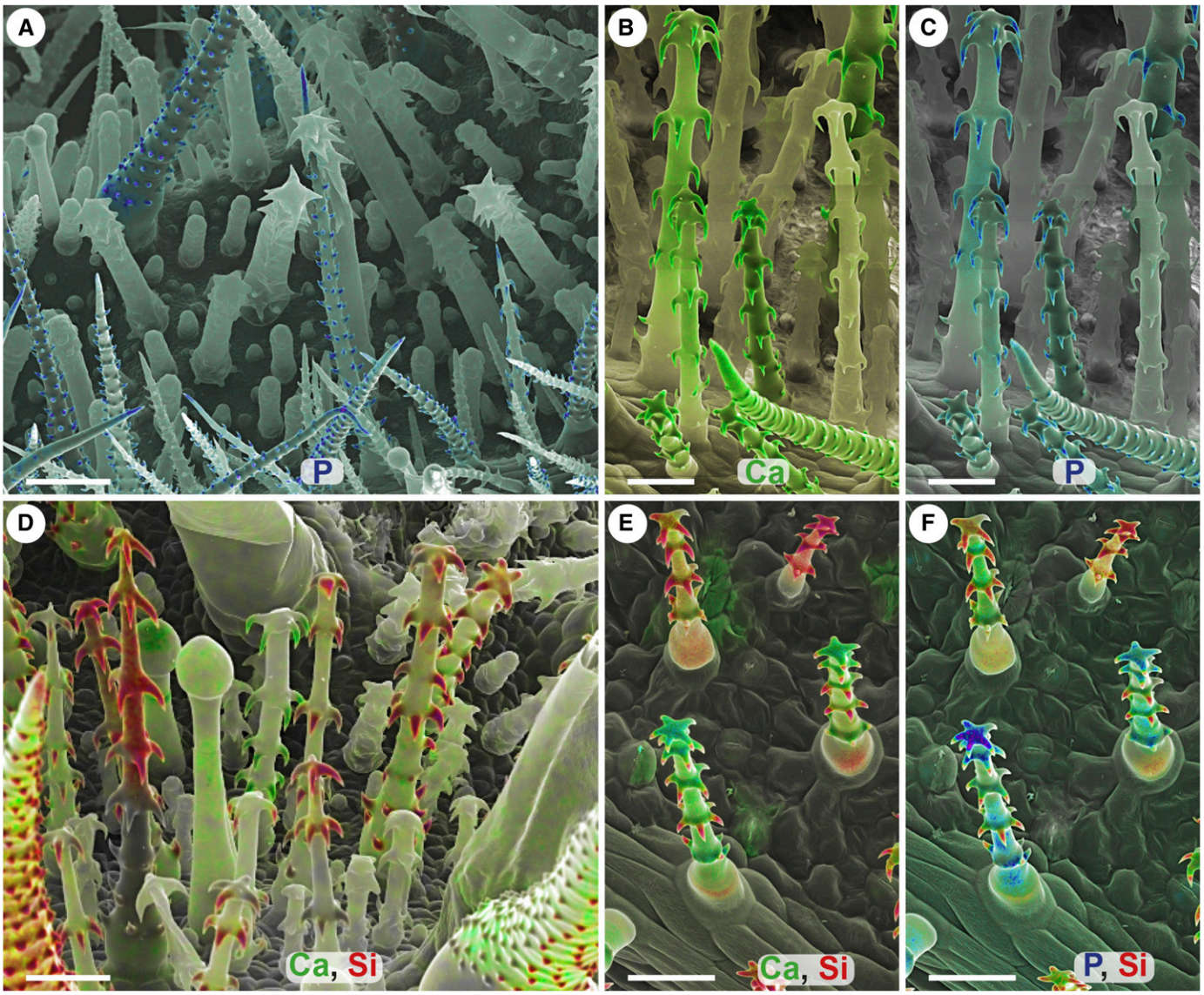


**FIGURE 7** SEM images of critical-point-dried leaves of *Loasa* and *Caiophora* showing the early stages of biomineral deposition in scabrid-glochidiate trichomes. (A) Abaxial leaf surface of *Loasa pallida* with glochidiate and scabrid trichomes, showing numerous nonmineralized glochidiate trichomes and partially mineralized scabrid trichomes at different developmental stages. Mineralization begins with deposition of Ca and P in the tips and hooks of scabrid trichomes. (B, C) Ca (green color) and P distribution (blue color) in partially and fully mineralized glochidiate trichomes on a *Loasa pallida* leaf, showing the occurrence of calcium along the shaft and hooks. In fully developed glochidiate trichomes, high concentration of P is restricted to the sharp hooks. (D–F) *Caiophora cernua* leaf surface, illustrating a mixed population of young trichomes with great biominerals variability (D) and later stages with fully mineralized glochidiate trichomes (E, F). Combined topography and EDX element-mapping images show calcium in green, phosphorus in blue and silica contents in red; colorless structures indicate nonmineralized state. Scale bars: 100 µm in A; 50 µm in B–F.

The overall distribution of stinging hairs on the plant and leaf surfaces in Loasaceae as found here corresponds to what has been documented in studies on other plants such as *Urtica*, *Cnidoscolus*, and *Tragia* (Thurston and Lersten, 1969; Thurston, 1974, 1976; Pollard and Briggs, 1982, 1984; Pollard, 1986; Fu et al., 2003, 2007). The stinging hairs themselves are designed as "hypodermic syringes" and are known to be fairly uniform throughout the Loasaceae. It would be expected that both their morphology and their mechanical properties, i.e., type and patterns of mineral deposition, are highly conserved since they should underlie functional constraints. The data shown here seem to confirm a relatively conserved pattern. The sequence of biomineralization is conserved, although the type of biomineralization found in different taxa diverges slightly. The late-ontogenetic biomineralization with silica in the apex of the stinging hairs of *Nasa* is striking, especially from a physiological perspective: Our data indicate that calcium phosphate on the outside of the stinging hair apex is secondarily replaced by silica. Clearly, ontogenetic studies of the stinging hairs in other and distantly related groups of Loasaceae (*Gronovia* L., *Eucnide* Zucc.; Weigend, 2003) would be very interesting to investigate in how far their putatively independent evolutionary origin is reflected in details of their ontogeny.

The functionally more simple "rough" hairs, i.e., scabrid-glochidiate trichomes, are more variable in morphology and also in their patterns of biomineralization. There can be little doubt that they also play a role in plant defense. Eisner et al. (1998: pp. 4412) described the effect of the glochidiate indument of *Mentzelia* on invertebrate herbivores in some detail and summarize that "*M. pumila* is a veritable killer plant. Its trichomes are potentially lethal to any number of insects." They show that the sharp hooks and spines on the glochidiate trichomes are of crucial importance for that function. The data here presented further indicate that—beyond the micromorphology—the micromechanical properties of these trichomes conveyed by the complex mineralization with extremely hard substances such as calcium phosphate and silica are likely of equally crucial importance to their function. The divergent morphologies of scabrid and glochidiate trichomes and their differential development on different parts of the plants likely reflect their ecological function, but studies to that end have not been done.

Our data generally indicate a complexity of biomineralization patterns in Loasaceae that is unique in the plant kingdom, with up to three different mineral-organic composites found in an individual unicellular structure and differentially and sequentially deposited in different parts of the cell wall. Clearly, this complexity invites further ontogenetic and functional studies in this and other plant groups with similar mineralized trichomes. These studies could focus on the distribution and the differential functionalities of distinct biominerals in their respective micromorphological contexts.

## ACKNOWLEDGEMENTS

We are very grateful to the enthusiastic and dedicated staff of the Botanical Garden of the University of Bonn, Germany, for growing and cultivating plants of the taxa studied. We express particular gratitude to B. Emde, M. Neumann, and T. Joßberger for vouchering the collections. We also thank J. Jeiter and N. Holstein for their suggestions and help in the arrangement of results figures. The reviewers' comments, that helped to substantially improve the manuscript, are gratefully acknowledged.

## LITERATURE CITED

Agren, J., and D. W. Schemske. 1993. The cost of defense against herbivores: An experimental study of trichome production in *Brassica rapa*. *American Naturalist* 141: 338–350.

Agren, J., and D. W. Schemske. 1994. Evolution of trichome number in a naturalized population of *Brassica rapa*. *American Naturalist* 143: 1–13.

Arnott, H. J. 1980. Carbonates in higher plants. *In* M. Omori and N. Watabe [eds.], Mechanisms of biomineralization in animals and plants, 211–218. Tokai University Press, Tokyo, Japan.

Bauer, P., R. Elbaum, and I. M. Weiss. 2011. Calcium and silicon mineralization in land plants: Transport, structure and function. *Plant Science* 180: 746–756.

Dietrich, D., S. Hinke, W. Baumann, R. Fehlhaber, E. Bäucker, G. Rühle, O. Wienhaus, and G. Marx. 2003. Silica accumulation in *Triticum aestivum* L. and *Dactylis glomerata* L. *Analytical and Bioanalytical Chemistry* 376: 399–404.

Dostert, N., and M. Weigend. 1999. A synopsis of the *Nasa triphylla* complex (Loasaceae), including some new species and subspecies. *Harvard Papers in Botany* 4: 439–467.

Ensikat, H. J., T. Geisler, and M. Weigend. 2016. A first report of hydroxylated apatite as structural biomineral in Loasaceae—plants' teeth against herbivores. *Scientific Reports* 6: 26073.

Ensikat, H. J., A. Mustafa, and M. Weigend. 2017. Complex patterns of multiple biomineralization in single-celled plant trichomes of the Loasaceae. *American Journal of Botany* 104: 195–206.

Eisner, T., M. Eisner, and E. R. Hoebeke. 1998. When defense backfires: Detrimental effect of a plant's protective trichomes on an insect beneficial to the plant. *Proceedings of the National Academy of Sciences, USA* 95: 4410–4414.

Epstein, E. 2009. Silicon: Its manifold roles in plants. *Annals of Applied Biology* 155: 155–160.

Fu, H. Y., S. J. Chen, R. F. Chen, L. L. Kuo-Huang, and R. N. Huang. 2007. Why do nettles sting? About stinging hairs looking simple but acting complex. *Functional Plant Science & Biotechnology* 1: 46–55.

Fu, H. Y., S. J. Chen, and L. L. Kuo-Huang. 2003. Comparative study on the stinging trichomes and some related epidermal structures in the leaves of *Dendrocnide meyeniana*, *Girardinia diversifolia*, and *Urtica thunbergiana*. *Taiwania* 48: 213–223.

Fürstenberg-Hägg, J., M. Zagrobelny, and S. Bak. 2013. Plant defense against insect herbivores. *International Journal of Molecular Sciences* 14: 10242–10297.

Gómez, F., L. Quijano, J. S. Calderón, and T. Rios. 1980. Terpenoids isolated from *Wigandia kunthii*. *Phytochemistry* 19: 2202–2203.

Greinert, M. 1886. Beiträge zur Kenntnis der Morphologie und Anatomie. Verhältnisse der Loasaceen, mit besonderer Berücksichtigung der Behaarung. Inaugural dissertation. Druck von C. Lehman, Freiberg, Germany.

Haberlandt, G. 1886. Zur Anatomie und Physiologie der pflanzlichen Brennhaare. *Sitzungsberatungen der Wiener Akademie der Wissenschaften* 93: 123–145.

Hanley, M. E., B. B. Lamont, M. M. Fairbanks, and C. M. Rafferty. 2007. Plant structural traits and their role in anti-herbivore defence. *Perspectives in Plant Ecology, Evolution and Systematics* 8: 157–178.

Henning, T., and M. Weigend. 2009. Systematics of the *Nasa poissoniana*-group (Loasaceae) from Andean South America. *Botanical Journal of the Linnean Society* 161: 278–301.

Hilger, H. H., J. R. Hoppe, and M. Hofmann. 1993. Energiedispersive Röntgenmikroanalyse (EDX) von Boraginaceae subfam. Boraginoideae—Klausenoberflächen. Sind Silicium- und Calcium-Einlagerungen in die Fruchtwand systematisch verwertbare Merkmale? *Flora* 188: 387–398.

Hülskamp, M. 2004. Plant trichomes: A model for cell differentiation. *Nature Reviews. Molecular Cell Biology* 5: 471–480.

Jeffree, C. E. 1986. The cuticle, epicuticular waxes and trichomes of plants, with reference to their structure, functions and evolution. *In* B. Juniper and R. Southwood [eds.], Insects and the plant surface, 23–64. Edward Arnold, London, UK.

Küster-Winkelmann, G. 1914. Das Haarkleid der Loasaceen. Doctoral dissertation. Friedrich-Alexander-Universität, Erlangen, Germany.

Levin, D. A. 1973. The role of trichomes in plant defense. *Quarterly Review of Biology* 48: 3–15.

Lins, U., C. F. Barros, M. Da Cunha, and F. C. Miguens. 2002. Structure, morphology, and composition of silicon biocomposites in the palm tree *Syagrus coronata* (Mart.) Becc. *Protoplasma* 220: 89–96.

Luebert, F., L. Cecchi, M. W. Frohlich, M. Gottschling, C. M. Guilliams, K. E. Hasenstab-Lehman, H. H. Hilger, et al. 2016. Familial classification of the Boraginales. *Taxon* 65: 502–522.

Meyen, F. J. F. 1837. Ueber die Secretions-Organe der Pflanzen. F. H. Morin, Berlin, Germany.

Nitta, I., A. Kida, Y. Fujibayashi, H. Katayama, and Y. Sugimura. 2006. Calcium carbonate deposition in a cell wall sac formed in mulberry idioblasts. *Protoplasma* 228: 201–208.

Payne, W. W. 1978. A glossary of plant trichome terminology. *Brittonia* 30: 239–255.

Pérez Cuadra, V., and P. Hermann. 2013. Characterization and macropattern of calcium oxalate phytoliths in Argentinean endemic species of Chenopodioideae (Amaranthaceae). *Quaternary International* 287: 83–88.

Pollard, A. J. 1986. Variation in *Cnidoscolus texanus* in relation to herbivory. *Oecologia* 70: 411–413.

Pollard, A. J., and D. Briggs. 1982. Genecological studies of *Urtica dioica* L. The nature of intraspecific variation in *U. dioica*. *New Phytologist* 92: 453–470.

Pollard, A. J., and D. Briggs. 1984. Genecological studies of *Urtica dioica* L. *New Phytologist* 97: 507–522.

Selvi, F., and M. Bigazzi. 2001. Leaf surface and anatomy in Boraginaceae tribe Boragineae with respect to ecology and taxonomy. *Flora* 196: 269–285.

Stipanovic, R. D. 1983. Function and chemistry of plant trichomes and glands in insect resistance: Protective chemicals in plant epidermal glands and appendages. *In* P. A. Hedin [ed.], Plant resistance to insects, 69–100. American Chemical Society, Washington, D.C., USA.

Thurston, E. L. 1969. An anatomical and fine structure study of stinging hairs in some members of the Urticaceae, Euphorbiaceae and Loasaceae. Ph.D. dissertation, Iowa State University, Ann Arbor, Michigan, USA.

Thurston, E. L. 1974. Morphology, fine structure, and ontogeny of the stinging emergence of *Urtica dioica*. *American Journal of Botany* 61: 809–817.

Thurston, E. L. 1976. Morphology, fine structure and ontogeny of the stinging emergence of *Tragia ramosa* and *T. saxicola* (Euphorbiaceae). *American Journal of Botany* 63: 710–718.

Thurston, E. L., and N. R. Lersten. 1969. The morphology and toxicology of plant stinging trichomes. *Botanical Review* 35: 393–412.

Uphof, J. C. T. 1962. Plant trichomes. *In* W. Zimmerman and P. G. Ozenda [eds.], Encyclopedia of plant anatomy, Band IV, Teil 5. Gebrüder Borntraeger, Berlin, Germany.

Weigend, M. 2000. A revision of the Peruvian species of *Nasa* ser. *Alatae*. *Nordic Journal of Botany* 20: 15–31.

Weigend, M. 2003. Loasaceae. *In* K. Kubitzki and C. Bayer [eds.], The families and genera of vascular plants, vol. 6, 239–254. Springer, Berlin, Germany.

Weigend, M. 2004. Four new species of *Nasa* ser. *Alatae* (Loasaceae) in the Amotape-Huancabamba zone of Peru. *Novon* 14: 134–146.

Weigend, M. 2007. Systematics of the genus *Mentzelia* (Loasaceae) in South America. *Annals of the Missouri Botanical Garden* 94: 655–689.

Weigend, M., and E. F. Rodriguez. 2003. A revision of the *Nasa stuebeliana* group [*Nasa* ser. *Saccatae* (Urb. & Gilg) Weigend, Loasaceae] with notes on morphology, ecology, and distribution. *Botanische Jahrbücher für Systematik und Pflanzengeographie* 124: 345–382.

Werker, E. 2000. Trichome diversity and development. *Advances in Botanical Research* 31: 1–35.

Wu, C.-C., and L.-L. Kuo-Huang. 1997. Calcium crystals in the leaves of some species of Moraceae. *Botanical Bulletin of Academia Sinica* 38: 97–104.

# CHAPTER 3

## Complex patterns of multiple biomineralization in single-celled plant trichomes of the Loasaceae

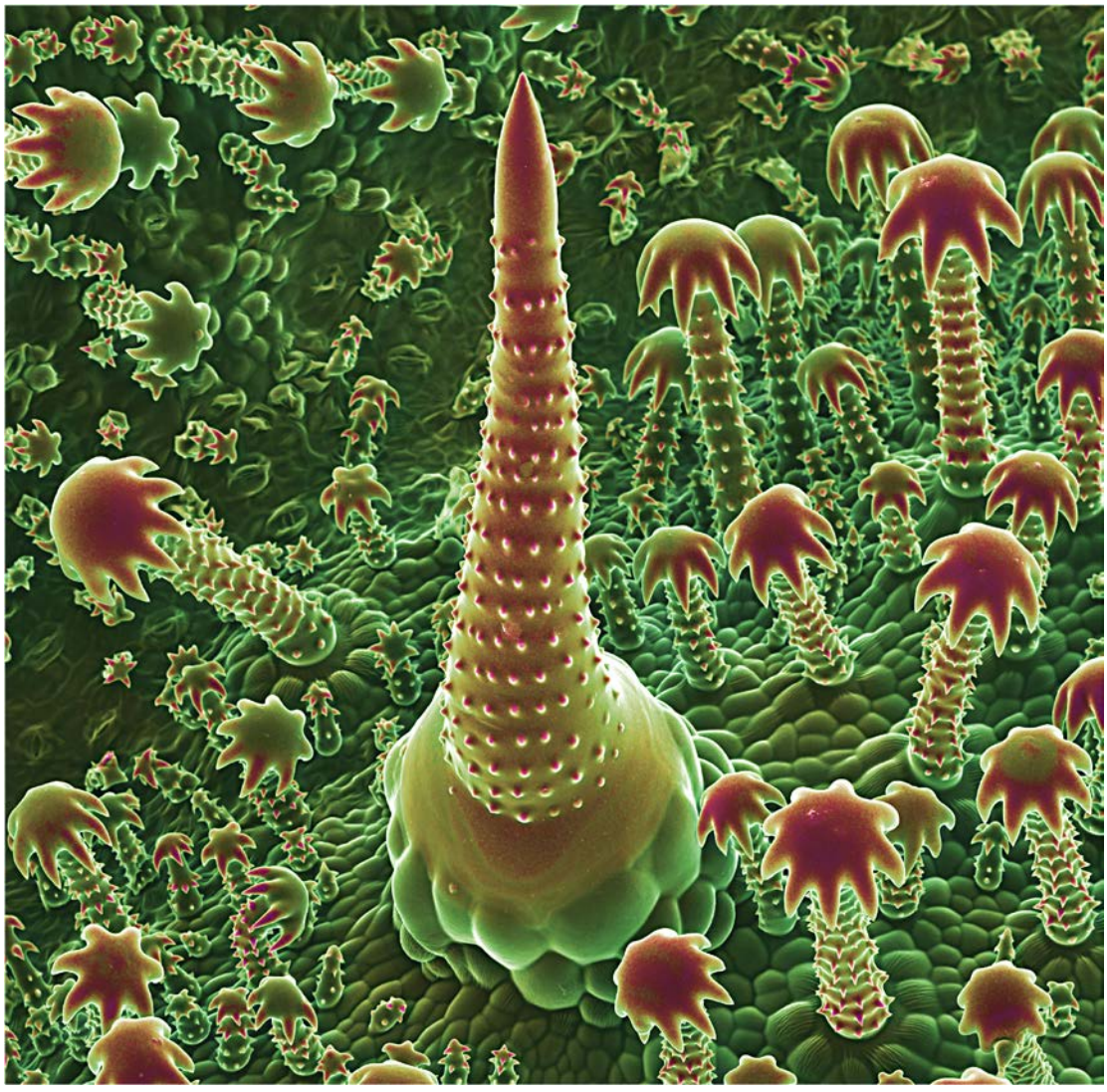

Cover image: Cryo-scanning electron micrographs of the trichomes cover on the capsule of *Blumenbachia amana* T. Henning & Weigend (Loasaceae). The glochidiate trichomes here have a spectacular, rounded, retrorsely barbed head; the towering trichome in the center is a scabrid trichome. The false colors of the image highlight mineralized portions in red and nonmineralized portions in green. The "heads" of the glochidiate trichomes and the granular and glochidiate processes on the trichomes are especially heavily mineralized. In "Complex patterns of multiple biomineralization in single-celled plant trichomes of the Loasaceae. See **Ensikat, H. J, Mustafa, A., Weigend, M. 2017**. *American Journal of Botany*, 104(2): 195-206.

RESEARCH ARTICLE

AMERICAN JOURNAL OF BOTANY

# Complex patterns of multiple biomineralization in single-celled plant trichomes of the Loasaceae[1]

Hans-Jürgen Ensikat, Adeel Mustafa, and Maximilian Weigend[2]

**PREMISE OF THE STUDY:** Plants of the family Loasaceae are characterized by a usually dense indument of various trichome types, including two basically different types of mineralized, unicellular trichomes (stinging hairs or setae and scabrid-glochidiate trichomes). Mineralized trichomes have long been known to have silicified or calcified walls, but recent studies demonstrated that trichomes of Loasaceae may also contain calcium phosphate. The current study investigates the distribution of different biominerals in the mineralized trichomes across several different taxa.

**METHODS:** Plants from cultivation were studied with scanning electron microscopy including energy dispersive x-ray analyses and element mapping.

**KEY RESULTS:** The vast majority of the 31 species investigated had at least two different biominerals in their trichomes, and 22 had three different biominerals in their trichomes. Thirty of the species had calcium phosphate in their trichomes. *Loasa* was mostly free of silica, but contained calcium phosphate in trichome tips and barbs, whereas calcium phosphate and silica were found in representatives of other genera of the family (*Blumenbachia*, *Caiophora*, *Nasa*).

**CONCLUSIONS:** Biomineralization is remarkably diversified between species, different trichome types and parts of the same trichome. Individual genera largely had different patterns of biomineralization. The presence of three biominerals in the trichomes of the basally branching *Eucnide urens* indicates either an early evolution and subsequent loss or several independent origins of multiple biomineralization. Differential biomineralization of the parts of individual, unicellular trichomes clearly indicates an extraordinary degree of physiological control over this process.

**KEY WORDS** apatite; biomineralization; calcium phosphate; cell walls; EDX; glochidiate trichomes; Losaceae; scanning electron microscopy; silica; stinging hairs

Biomineralization is a common process in higher plants, but the range of well-described biominerals is rather small and essentially limited to silica, calcium carbonate, and calcium oxalate (Lowenstam, 1981; Mann, 1993; Weiner and Addadi, 1997; Weiner and Dove, 2003; Franceschi and Nakata, 2005; Epstein, 2009; Bauer et al., 2011; He et al., 2014; Trembath-Reichert et al., 2015). Phytoliths, cystoliths, and mineralized trichomes are the most common forms of plant biomineralization, apart from diffuse biomineralization in, e.g., cell walls. Cystoliths and phytoliths continue to be the subject of intensive research from a range of perspectives, with a special emphasis on economically important plant families such as the Poaceae (Lanning and Eleuterius, 1987, 1989; Alexandre et al., 1997; Zhao et al., 1998; Franceschi and Nakata, 2005; Parr and Sullivan, 2005). A high morphological diversity is found in crystalline calcium oxalate deposits (Franceschi and Nakata, 2005; Hartl et al., 2007), which depend on crystallization conditions in their detailed conformation. The first report of silica in plant trichomes dates back to 1861 (Wicke, 1861), but overall there have been relatively few detailed studies. Mineralized trichomes, and especially stinging trichomes, are generally accepted to function primarily in herbivore deterrence (Pollard and Briggs, 1984; Tuberville et al., 1996; Fu et al., 2003; Hanley et al., 2007; Cardoso, 2008). Individual studies have added specific insights into patterns of biomineralization in plant trichomes, e.g., the differential deposition of silica and calcium in foot cells vs. trichome cells of *Helianthus tuberosus* L. (Lanning and Eleuterius, 1987). Stinging hairs of the greater stinging nettle (*Urtica dioica* L.) are certainly one of the most spectacular types of mineralized plant trichome. Their mineralization was studied by Thurston and Lersten (1969) and Thurston (1974). Thurston (1974) showed that the proximal part of the stinging hairs is mostly calcified, whereas the distal part of the hair is silicified. Loasaceae is the angiosperm plant family with possibly the most complex

[1] Manuscript received 13 September 2016; revision accepted 27 December 2016.
Nees-Institut f. Biodiversität d. Pflanzen, Rheinische Friedrich-Wilhelms-Universität Bonn, Meckenheimer Allee 170, D-53115 Bonn, Germany
[2] Author for correspondence (e-mail: mweigend@uni-bonn.de)
**doi:10.3732/ajb.1600331**

trichome cover, including also mineralized trichomes, among them stinging hairs (Weigend, 2003). There are three different basic trichome types (Dostert and Weigend, 1999; Weigend, 2003): nonmineralized uniseriate, glandular trichomes, and two mineralized types, stinging trichomes and scabrid-glochidiate trichomes. In their most typical expression (Weigend, 2007), the scabrid-glochidiate trichomes are quite distinctive—glochidiate trichomes are cylindrical and provided with curved hooks, and scabrid trichomes are tapering and provided with conical surface-sculpturing or spines. However, many transitional forms are found, combining characters of the two extremes. Both silica and calcium carbonate had been reported previously from Loasaceae trichomes (Hegnauer, 1966). However, Ensikat et al. (2016) recently demonstrated the presence of calcium phosphate as a structural biomineral in one representative of the family Loasaceae, providing a surprising addition to the range of structural biominerals known from higher plants. Ensikat et al. (2016) demonstrated that three biominerals, calcium phosphate, silica, and calcium carbonate occur at specific locations of the individual (unicellular) trichome. The study of Ensikat et al. (2016) focused on a single species of Loasaceae, *Loasa pallida* Gillies ex. Arn., but provided a first hint that the biomineralization of plant trichomes may be less uniform than generally believed. The current study therefore investigated biomineralization patterns across a range of representatives of the family Loasaceae to provide a first overview on the patterns and distribution of the three biominerals across taxa and trichome types.

## MATERIALS AND METHODS

***Plant material***—The plant material used in this study was cultivated at the Botanische Gärten der Universität Bonn, Germany. Fully developed, young leaves were used for this study. The following taxa and accessions were investigated: *Aosa rupestris* (accession [access.] 37104, *T. Jossberger 1258*); *Aosa uleana* (access. 36004, *T. Jossberger 342*); *Blumenbachia* hieronymi (access. 33609, *T. Jossberger 1649*); *Blumenbachia insignis* (access. 36150, *T. Jossberger 1210*); *Caiophora cernua* (access. 33610, *T. Jossberger 1653*); *Caiophora clavata* (access. 33612, *T. Jossberger 548*); *Caiophora coronata* (access. 34836, *T. Jossberger 052*); *Caiophora deserticola* (access. 37106, *T. Jossberger 1562*); *Caiophora lateritia* (access. 37012, *T. Jossberger 1654*); *Eucnide urens* (access. 29925, *T. Jossberger 1501*); *Huidobria fruticosa* (access. 33449, *T. Jossberger 1137*); *Loasa elongata* (access. 37096, *T. Jossberger 067*); *Loasa heterophylla* (access. 35601, *T. Jossberger 1650*); *Loasa insons* (access. 37108, *T. Jossberger 1289*); *Loasa pallida* (access. 36565, *T. Jossberger 666*); *Loasa tricolor* (access. 37098, *T. Jossberger 1209*); *Loasa triloba* (access. 37109, *T. Jossberger 1624*); *Nasa contumazensis* (access. 37153, *T. Jossberger 1309*); *Nasa lambeyequensis* (access. 37117, *M. Weigend 9669-C*); *Nasa magnifica* (access. 37112, *T. Jossberger 1656*); *Nasa poissoniana* (access. 37092, *T. Jossberger 1280*); *Nasa weigendii* (access. 37116, *T. Jossberger 1242*); *Presliophytum heucheraefolium* (access. 37168, *T. Jossberger 1322*); *Presliophytum incanum* (access. 37167, *T. Jossberger 1324*); *Urtica dioica* (access. 4919, *T. Jossberger 1665*). All vouchers are deposited at BONN.

***Scanning electron microscopy***—A Cambridge S 200 Stereoscan (Cambridge, UK) and a LEO 1450 (Cambridge, UK) scanning electron microscopes were used for imaging and energy dispersive x-ray (EDX) analyses. They were equipped with secondary electron (SE) and backscattered electron (BSE) detectors and an EDX analysis system (Oxford Instruments, Oxford, UK) using the Link ISIS software. Secondary electron and BSE images were usually acquired from frozen, hydrated samples at approximately −100°C using a cryostage without further sample preparation. Element mapping by EDX required samples with better long-term stability. For this purpose, stinging hairs and other trichomes were isolated, washed in ethanol and acetone, and dried within a few minutes to minimize potential displacement of components. The small trichomes were harvested from frozen leaves by scraping them off the lamina with a knife blade. The EDX samples were sputter-coated with silver or palladium (Junker Edelmetalle, Waldbüttelbrunn, Germany), because, in contrast to gold, the EDX spectra of these metals do not interfere with the characteristic x-ray peaks of relevant elements such as phosphorus and silicon. Synthetic apatite (penta-calcium hydroxytriphosphate, Carl Roth GmbH, Karlsruhe, Germany) was used as a reference substance for the EDX analysis.

***Image processing***—False-color SEM images were created by combining the SE image, showing the topography, with the corresponding BSE compositional contrast image, or combining the SE image with one or two element-mapping EDX images. Standard image processing software Corel Paint Shop Pro (Corel GmbH, Munich, Germany) was used. The topographical images contribute image brightness, whereas the compositional contrast is used to generate a color shift. The two-element-coded SEM images are suitable for visualizing only if the components occur at different locations; otherwise, there is signal overlap and loss of information. Thus, most of the following results are presented as separate element-mapping images. The elements silicon (Si), phosphorus (P), and calcium (Ca) were detected. As previously demonstrated (Ensikat et al., 2016), P is generally associated with Ca as calcium phosphate, whereas Ca (without P) is present as calcium carbonate, usually associated with organic matter such as cellulose. The images were therefore interpreted to document the presence of biomineralization with calcium carbonate (composites), calcium phosphate, and silica ($SiO_2$).

## RESULTS

The leaves of all species studied were densely covered with characteristic trichomes such as small glochids and larger stinging hairs. On the basis of their typical morphology, three basic types of trichomes could be distinguished (Fig. 1A–E; Appendix S1, see the Supplemental Data with this article): stinging trichomes (1), scabrid-glochidiate trichomes (2, 3), and uniseriate, glandular trichomes (4) (Appendix S1). The scabrid-glochidiate trichomes form two discrete groups in the taxa studied here, with the glochidiate trichomes (3) cylindrical and retrorsely barbed and the scabrid trichomes (2) tapering and with only short surface processes. Glochidiate trichomes were found mainly on the abaxial leaf surfaces, scabrid trichomes were predominantly found on the adaxial leaf surface, but also the abaxial, e.g., on the leaf veins. The stinging trichomes have a many-celled pedestal and a long, tapering, unicellular tip with an apical, oblique, bulbous appendage. Scabrid-glochidiate trichomes and the stinging hairs are mineralized (Fig. 1A–E, yellow and red), whereas the uniseriate, glandular trichomes are nonmineralized (Fig. 1A–E, green; Appendix S1B, D).

Scabrid trichomes were extremely variable in terms of size, surface sculpturing (Appendix S1A, B), and degree of mineralization,

rendering comparison difficult (results shown in online Appendices S1, S3). Conversely, stinging hairs and the glochidiate trichomes were found to be relatively uniform in size, shape, and degree of mineralization. Therefore, the following results concentrate on these two types. The apical region of the stinging hairs (Fig. 2A–E) and the barbs (hooks) of the glochidiate trichomes (Fig. 2F–I) were found to have highly characteristic mineralization patterns of silica and calcium phosphate within samples and taxa. Shafts of both trichome types contained mostly calcium (Ca, mainly as $CaCO_3$) and carbon (C), whereas silicon (Si) or phosphorus (P) often occurred at low and varying concentrations. High concentrations of Si or P were often found at the base of the trichomes, but were not uniformly distributed.

***Stinging hair morphology and mineralization***—The stinging hairs of all Loasaceae studied conformed to the same gross morphology, and many of them shared a uniform pattern of mineralization (Figs. 1A, 1C, 2A–E, 3A–F). The foot cells of the pedestal were not mineralized, but the unicellular stinging hair itself was heavily mineralized. Usually, the entire stinging hair was calcified; the presence of calcium carbonate was additionally confirmed by the formation of gas bubbles ($CO_2$) after addition of acids, as well as by Raman spectroscopy (Ensikat et al., 2016).

Figure 3 shows the element mapping images together with the topographical image (SE, secondary electron signal image) of stinging hairs of representative species from five genera of Loasaceae and from *Urtica dioica* for comparison. The distal portions of the stinging hairs contain different biominerals. Calcium phosphate was dominant in most species of Loasaceae (Table 1) in contrast to *Urtica*, where no phosphate was found. Stinging hair tips with high concentrations of calcium phosphate were generally found in all species investigated of *Loasa*, *Blumenbachia*, and *Caiophora* (Fig. 3A–C). Silica was found only in low amounts in the shafts of the stinging hairs in *Caiophora* and *Blumenbachia*. Conversely, all five species of *Nasa* examined contained silica and calcium phosphate in the stinging hair tips (Fig. 3D). Silica was, however, restricted to the very apex, proximally followed by a calcium phosphate-rich region, whereas calcium carbonate with traces of phosphorus made up the bulk of the shaft. Figure 4A illustrates the differential longitudinal distribution of the three elements in a stinging hair of *Nasa macrothyrsa*, with the very apex consisting mostly of silica, with some calcium phosphate, whereas the apical part of the trichome itself shows a near-uniform decrease in phosphorus content, while the calcium level is virtually unchanged, indicating a gradual replacement of calcium phosphate by calcium carbonate from distal to proximal. Figure 4B and C show details of the biomineralization

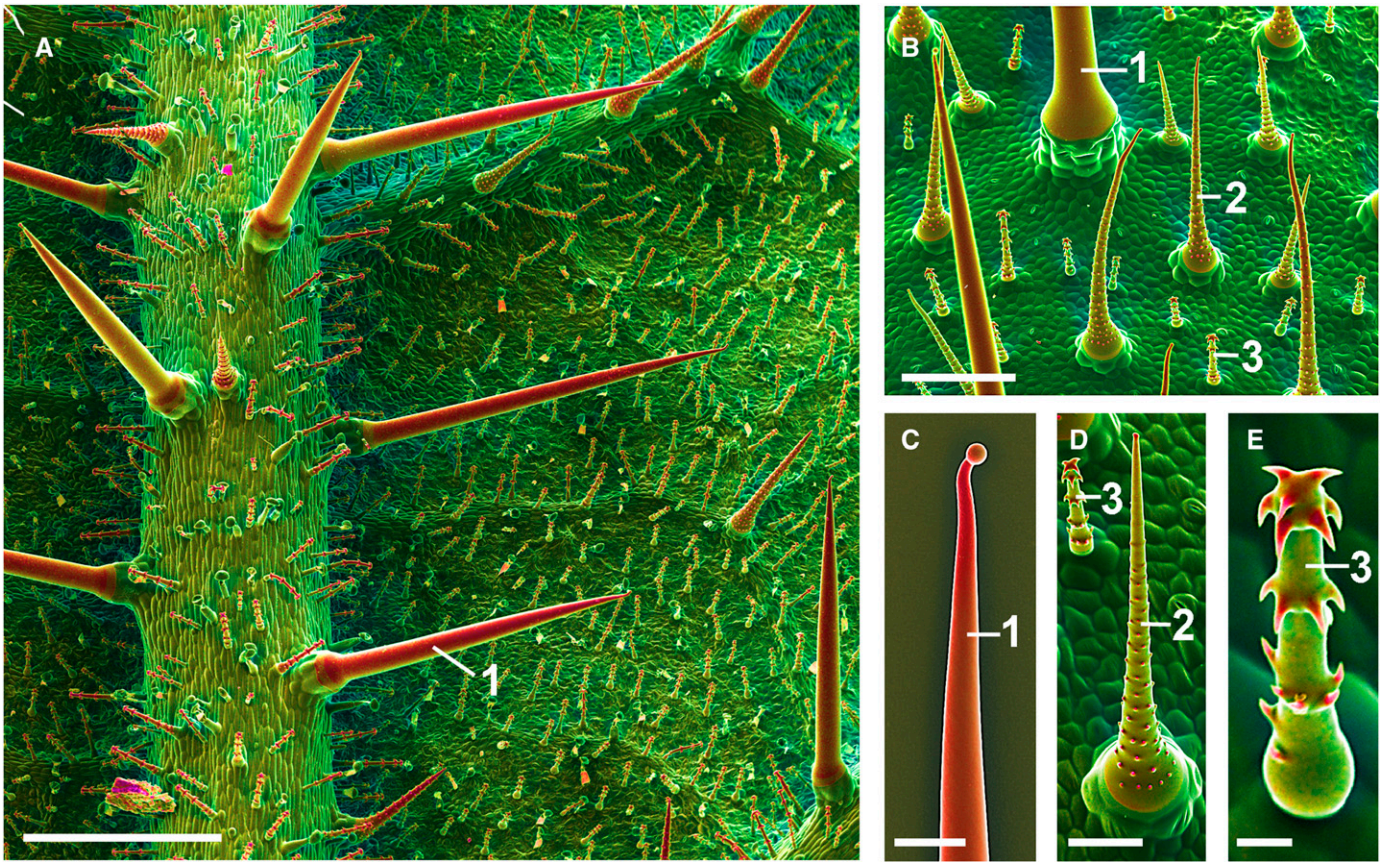


**FIGURE 1** Cryo-SEM image of a *Blumenbachia insignis* leaf densely covered with different trichomes. Stinging hairs ("1" in A, B, C) can be recognized by their smooth surface and the presence of an apical bulb; length may exceed 2 mm. Scabrid trichomes ("2" in A, B, D) have a pointy tip and a granular surface; their length varies strongly (up to ca. 1 mm maximum). Glochidiate trichomes ("3" in B, D, E) are much shorter and have a blunt apex with basiscopical hooks. Color SEM images are combined secondary electron (SE) and backscattered electron (BE) images using compositional contrast of the BE signal for providing a color shift. Red color indicates a high content of (heavier) mineral elements (Ca, P, Si). Scale bars: 500 µm in A; 200 µm in B; 50 µm in C, D; 10 µm in E.

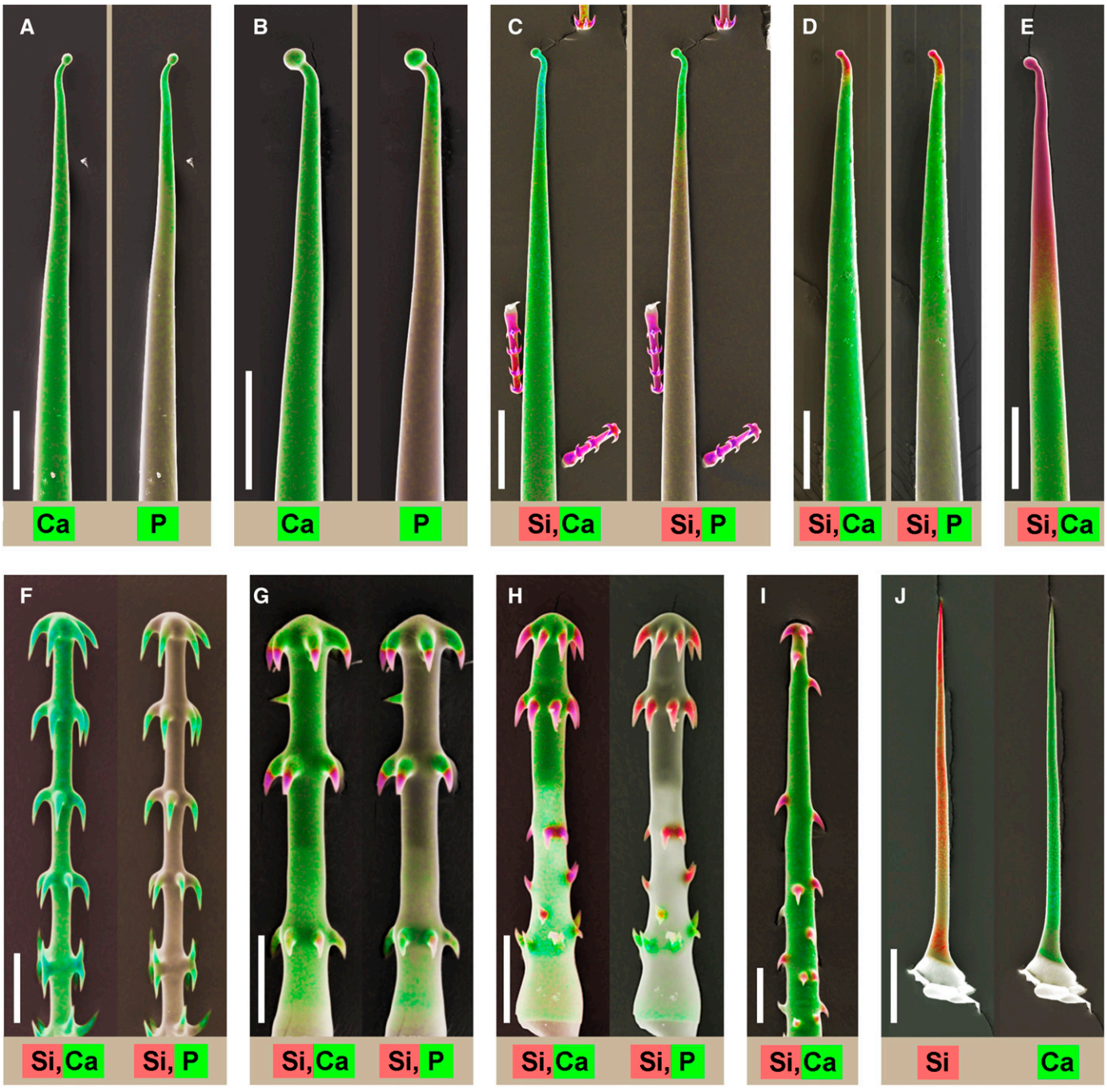


**FIGURE 2** Element distribution in stinging and glochidiate trichomes. SEM color images combining topographic SE image with EDX element mapping images indicate distribution of different elements. Image pairs showing high concentrations of either calcium (Ca) or phosphorus (P) in green, and silicon (Si) in red. (A–E) Stinging hairs and (F–I) glochidiate trichomes of various species: (A) *Loasa insons*; (B) *Caiophora deserticola*; (C) *Blumenbachia insignis*; (D) *Nasa macrothyrsa*; (E) *Urtica dioica*; (F) *Loasa insons*; (G) *Caiophora lateritia*; (H) *Blumenbachia hieronymi*; (I) *Nasa poissoniana*; (J) *Urtica dioica*. Stinging hairs of *Loasa*, *Caiophora*, and *Blumenbachia* and glochidiate trichomes of *Loasa* contain Ca and P (calcium phosphate) in tips and Ca in shafts. Stinging hairs of *Nasa* and glochidiate trichomes of *Caiophora* contain three biominerals simultaneously: silica (Si) in tips, followed by calcium phosphate (Ca and P), and calcium carbonate (Ca) in the shaft. Scale bars: 100 µm in A–E; 30 µm in F–I; 100 µm in J.

for two individual stinging hairs of *Nasa macrothyrsa,* documenting the minor differences between individual trichomes. Silica was always the dominant biomineral at the very apex; the remaining trichome was heavily mineralized with calcium as the dominant element. In the subapical region, phosphorus was abundant, and the trichome was thus incrusted with calcium phosphate, but toward the proximal portion, the phosphorus concentration fell dramatically, and biomineralization was increasingly and finally only with calcium carbonate. *Presliophytum* stinging hairs showed a very similar biomineralization to *Nasa*, with both silica and calcium phosphate

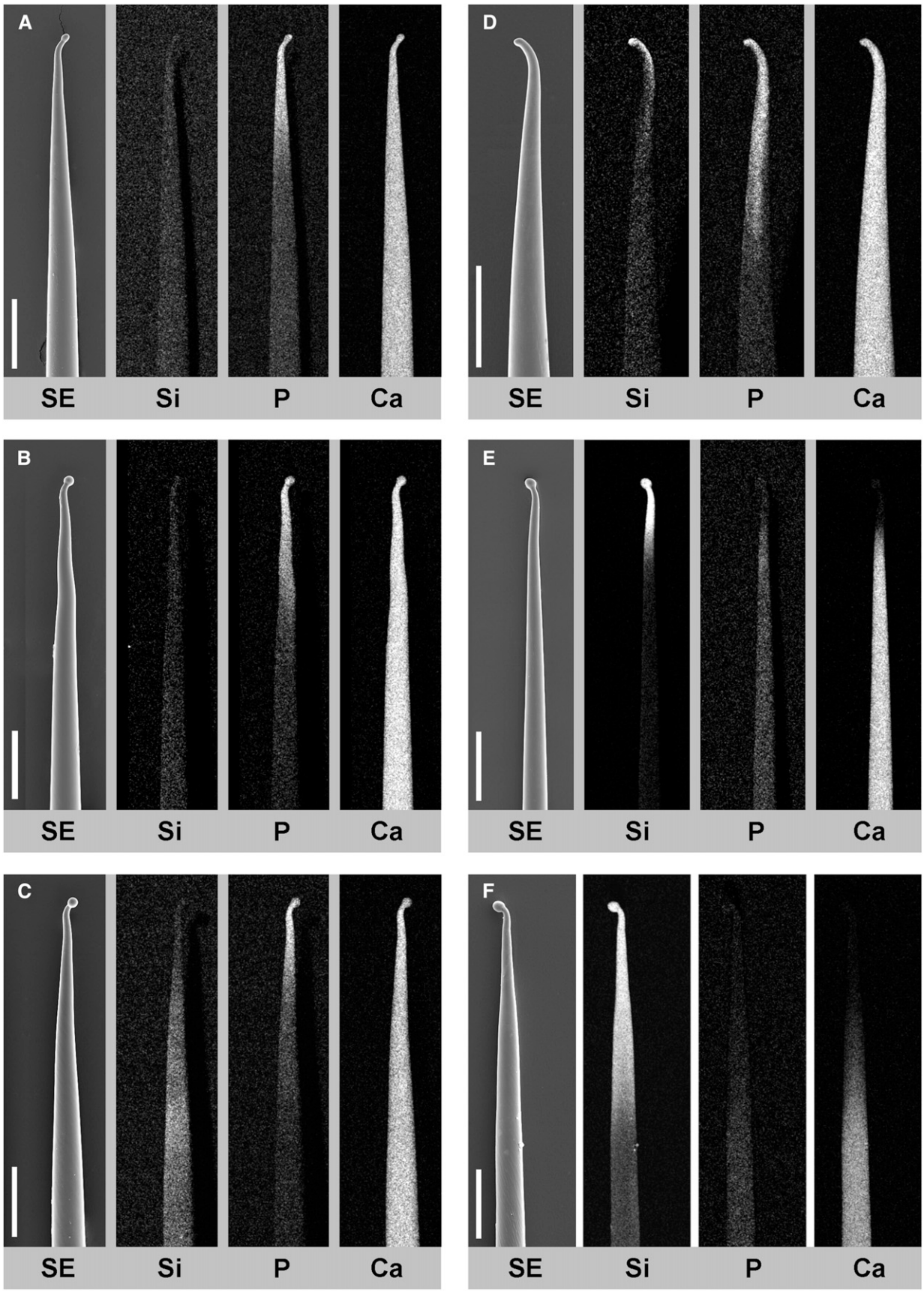
A
SE
Si
P
Ca
D
SE
Si
P
Ca
B
SE
Si
P
Ca
E
SE
Si
P
Ca
C
SE
Si
P
Ca
F
SE
Si
P
Ca

**TABLE 1.** Element distribution patterns in trichomes of all Loasaceae species examined.

| Pattern type | Stinging trichomes | | Glochidiate trichomes | | Species |
|---|---|---|---|---|---|
| | Tip / Bulbous | Shaft | Hooks | Shaft | |
| Loasa pattern | | | | | *Loasa acerifolia* |
| | | | | | *L. heterophylla* |
| | | | | | *L. insons* |
| | | | | | *L. pallida* |
| | | | | | *L. tricolor* |
| | | | | | *L. triloba* |
| Caiophora pattern | | | | | *Caiophora arechavaletae* |
| | | | | | *C. carduifolia* |
| | | | | | *C. cernua* |
| | | | | | *C. chuquitensis* |
| | | | | | *C. clavata* |
| | | | | | *C. coronata* |
| | | | | | *C. deserticola* |
| | | | | | *C. hibiscifolia* |
| | | | | | *C. lateritia* |
| | | | | | *Loasa elongata* |
| Blumenbachia pattern | | | | | *Blumenbachia hieronymi* |
| | | | | | *B. insignis* |
| Nasa pattern | | | | | *Nasa contumazensis* |
| | | | | | *N. lambeyequensis* |
| | | | | | *N. macrothyrsa* |
| | | | | | *N. magnifica* |
| | | | | | *N. poissoniana* |
| | | | | | *N. rudis* |
| | | | | | *N. usquiliensis* |
| | | | | | *N. weigendii* |
| | | | | | *Loasa acanthifolia* |
| Aosa pattern | | | | | *Aosa rupestris* |
| | | | | | *A. uleana* |
| Others | | | | | *Eucnide urens* |
| | - | - | | | *Huidobria fruticosa* |
| | | | | | *Presliophytum heucheraefolium* |
| | | | | | *Urtica dioica* |
| | Si P Ca | Si P Ca | Si P Ca | Si P Ca | |

present (Appendix S2A). On the other hand, stinging hairs of *Aosa rupestris* and *A. uleana* were distally silicified only, while calcium carbonate predominated in the median and proximal parts of the trichome; traces of phosphorus were found in the shaft (Fig. 3E). Stinging hairs of *Eucnide urens* had calcium (carbonate) as the principal mineral element, but silica was found in remarkably high concentrations in the proximal portions of some stinging hairs (Appendix S2B). *Huidobria* lacks stinging hairs (Appendix S2D).

***Glochidiate trichome morphology and mineralization***—Glochidiate trichomes are morphologically more diverse. The majority conform to the typical morphology with deflexed hooks along the shaft and a rounded apex with several deflexed hooks; in some cases, the shaft has acroscopical spines or hooks in the proximal part. The trichomes of *Huidobria* (Appendix S2D) are more reminiscent of arbuscular trichomes with long, porrect instead of deflexed hooks and a long, pointed tip. Figure 5A–F shows the element mapping and topography images of glochidiate trichomes of representative species of five genera of Loasaceae, with a small trichome of *Urtica dioica* for comparison. The shafts of all glochidiate trichomes were calcified, but the trichome hooks show remarkable variability in the presence or respective absence of Ca and P and/or Si. Five of seven *Loasa* species were almost free of silica, but the trichome hooks contained high concentrations of calcium phosphate (Table 1). The hooks of all species of *Caiophora* contained silica and calcium phosphate, like those of some species of *Nasa*. The glochidiate trichomes of the two species of *Blumenbachia* examined consisted of silica and were free of P. Even the shaft of *Blumenbachia insignis* contained both silica and calcium carbonate. The hooks of the trichomes of *Eucnide urens* (Fig. 6A, B) had Ca nearly exclusively as the mineral element. Only a more detailed look revealed the presence of calcium phosphate in high concentrations at the very tips of the distal ring of retrorse hooks. Glochidiate trichomes of *Presliophytum heucheraefolium* were found to contain Ca in the shaft and calcium phosphate in the hooks, whereas *Huidobria* trichomes were mainly mineralized with Ca, having high Si concentrations in the basal portion of the shaft only.

The mineralization patterns of scabrid trichomes are broadly similar to those of glochidiate trichomes. Appendix S3 shows the element distribution for five species. *Loasa pallida* trichomes (A) have calcium phosphate sculpturing on the shaft and tips and lack silica; trichomes of *Caiophora clavata* (B) contained both silica and calcium phosphate; scabrid trichomes of *Blumenbachia hieronymi*

**FIGURE 3** Biomineralization of stinging hairs. EDX element mapping images indicating localization of selected elements (Si, P, Ca) in comparison to the topographic (SE) image for various species: (A) *Loasa heterophylla*; (B) *Caiophora deserticola*; (C) *Blumenbachia insignis*; (D) *Nasa weigendii*; (E) *Aosa rupestris*; (F) *Urtica dioica*. Gray-scale images may also show lower concentrations not visible in the colorized combined images. Stinging hairs of *Loasa, Caiophora*, and *Blumenbachia* contain Ca and P (calcium phosphate) in apex and further Ca in shaft. Stinging hairs of *Nasa* contain silica and calcium phosphate in tip and calcium (carbonate) in shaft. Si (silica) is present only in outermost tip, whereas calcium phosphate occupies a larger region. Stinging hairs of *Aosa* contain Si in apex and Ca in shaft, similar to the pattern found in *Urtica dioica*. P occurs only in traces. Scale bars: 100 μm.

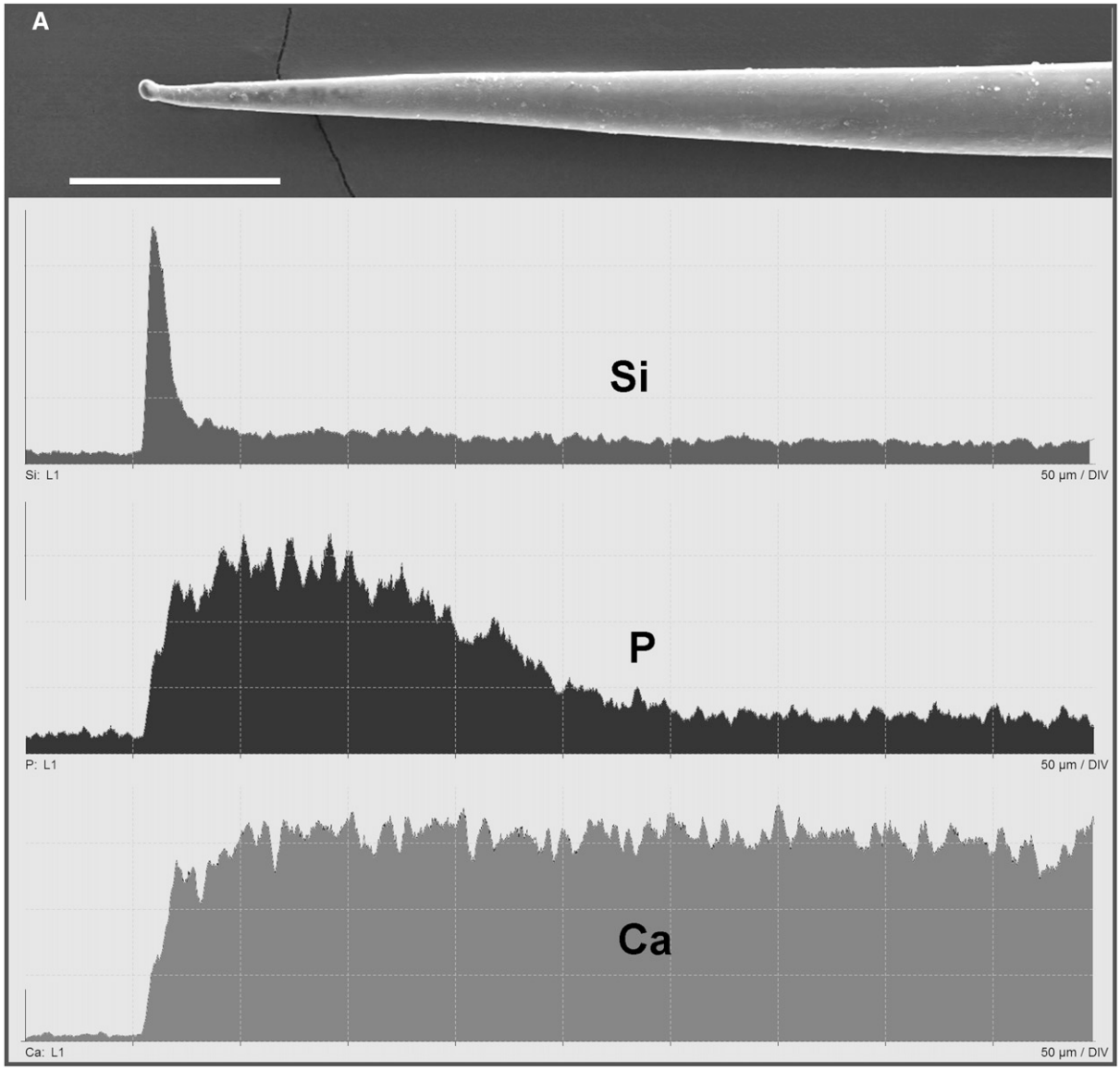
A
Si
Si: L1
50 µm / DIV
P
P: L1
50 µm / DIV
Ca
Ca: L1
50 µm / DIV

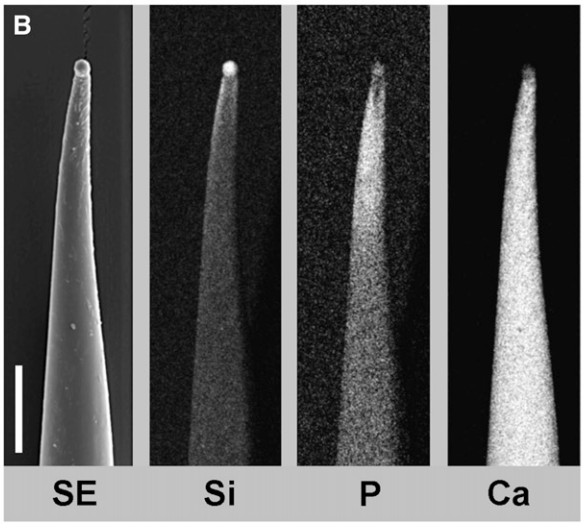
B
SE
Si
P
Ca

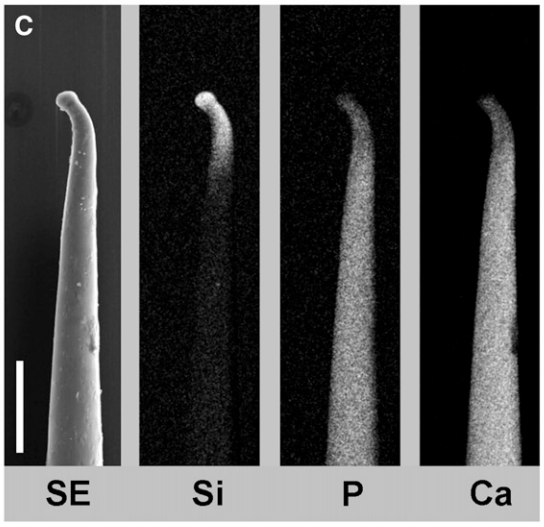
C
SE
Si
P
Ca

(C), *Nasa weigendii* (D), and *Aosa uleana* (E) are almost free of P and contain silica in tips and grains.

***EDX analyses***—EDX spectra of selected locations show the local composition, the main mineral elements, and the minor components. The spectra of *Loasa heterophylla* stinging hairs (Fig. 7A, B) confirm a high P and Ca content in the apical bulbous portion, but low P concentrations in the shaft, indicating the predominant presence of calcium carbonate. Magnesium (Mg) was frequently found at low and variable levels in the stinging hairs of various genera. Also, P was highly variable in its distribution, while Ca was very homogeneously distributed. In the regions with the highest P concentrations, the peak height ratio of P to Ca (Fig. 7C) was almost equal to that of pure apatite-calcium phosphate [$Ca_5(PO_4)_3OH$, Fig. 7D]. Spot spectra from a *Caiophora* glochidiate trichome hook (Fig. 7E, F) illustrate the presence of highly concentrated silica in the tip and both minerals, silica and calcium phosphate, in the basal part of the hook. We hesitate to present quantitative concentration values for the elements because the detection sensitivity particularly for the light elements C and O strongly depends on the surface geometry and orientation and various other factors such as surface layers (cutin, metal coating) and homogeneity of the samples. The peak height ratio for the elements P and Ca seems to be a good indicator for the presence of calcium phosphate as it fits well with that of apatite. Other calcium phosphates such as brushite and amorphous calcium phosphate have slightly different P to Ca ratios, and the additional presence of calcium carbonate can further shift this ratio, so that a definitive identification of the components would require high-resolution analytical techniques such as electron diffraction or EBSD (electron backscatter diffraction), which allows the crystalline structure to be visualized with SEM. The selected images illustrate the most typical distribution of the biomineral elements. However, the concentrations vary to some degree, and exceptions from the typical patterns were occasionally observed. For example, on leaves and petioles of *Nasa rudis* two types of stinging hairs were found; smaller colorless ones with calcium phosphate only in the tips, and larger, brown ones containing calcium phosphate and silica. While most trichomes of *Loasa pallida* were free from silica, small amounts were found in two cases; a low concentration of silica was detected in the shaft of one glochidiate trichome, and a higher concentration of silica occurred at the base of a trichome. Generally, the high concentrations of either calcium phosphate or silica in the trichome tips and hooks appeared to be the most consistent feature in a comparison among taxa.

## DISCUSSION

The different biominerals could be reliably detected and localized with a scanning electron microscope by EDX analyses and element mapping. Different crystalline and amorphous mineral phases cannot be identified with the techniques employed here—their identification would require another approach such as electron diffraction. Calcium carbonate in the trichome walls has previously been shown to be associated with organic components as a composite (Ensikat et al., 2016). The carbonate content can be easily confirmed by the development of gas bubbles ($CO_2$) after addition of acids; Raman spectroscopy also confirmed the presence of carbonate, and x-ray diffraction measurements of stinging hairs and glochidiate trichomes demonstrated that the calcium carbonate in the composite is amorphous. The high reactivity and possible solubility of calcium carbonate required an appropriate sample preparation to avoid displacement. Examination of deeply frozen cryosamples turned out to be the most suitable technique. For EDX element mapping, we used isolated trichomes immediately after obtaining them from the living plants, since some degree of displacement of carbonate-bound calcium was occasionally observed on samples that had been stored for several weeks in fixative (ethanol-formaldehyde). The calcium phosphate distribution in these samples remained unaltered.

The data reported here demonstrated both the considerable extent of biomineralization and the high degree of diversification in the detailed biomineralization patterns in Loasaceae. Calcium phosphate, recently reported from a single species (*L. pallida*, Ensikat et al., 2016), can be shown to be widespread as a biomineral in Loasaceae. It was found here in seven of the eight genera and 30 of the 31 species studied. Only one of the species studied has trichomes mineralized with a single compound (calcium carbonate), eight species have biomineralization with two compounds (calcium carbonate and calcium phosphate), the remaining 22 species are differentially mineralized with three biominerals, calcium carbonate, calcium phosphate, and silica. Multiple biomineralizations is not random, but is rather highly site specific. The tips of the stinging hairs in all but one species studied (*E. urens*) are mineralized with silica and/or calcium phosphate. These two minerals also play a prominent role in the mineralization of the fine hooks on the glochidiate trichomes. Conversely, calcium carbonate is universally present in all trichomes, but often restricted to the shaft. *Aosa*, with diffuse, triple biomineralization of the shaft, and *Presliophytum*, with both calcium phosphate and carbonate in the shaft, are notable exceptions.

Thus, biomineralization in Loasaceae is not only complex, but also highly diversified. The different taxa of the Loasaceae show remarkable differences in the mineralization, with overall patterns largely characteristic of individual genera. Table 1 summarizes the general patterns observed, which can be roughly sorted into the following groups:

*Loasa* pattern (6 of 8 species): Si absent; stinging trichome tips and glochidiate trichome barbs contain Ca and P (calcium phosphate). Exceptions are *Loasa elongata* with mineralization patterns corresponding to that of the *Caiophora* group (Si and P in hooks) and *Loasa acanthifolia* with mineralization patterns corresponding to that of the *Nasa* group (Si and P in stinging hair tips and the hooks of glochidiate trichomes).

*Caiophora* + *Blumenbachia* pattern (9 *Caiophora* species, 2 *Blumenbachia* species): stinging trichome tips contain Ca and P (calcium phosphate), glochidiate trichome barbs contain either silica only, or both silica and calcium phosphate.

**FIGURE 4** Distribution of three biominerals in stinging hairs of *Nasa macrothyrsa*. (A) EDX line scan along stinging hair displays relative concentrations of selected elements silicon (Si), phosphorus (P), and calcium (Ca). A high Si concentration is restricted to very apex. High P concentration extends over ca. 200 µm; Ca level is more or less uniform along the entire length of the trichome. (B, C) Variations in the size of silicified apical region. Silica deposits are sometimes smaller than the apical bulb, but may extend beyond curved part (C), followed by calcium phosphate toward the median portion of the trichome. Scale bars: 100 µm in A; 50 µm in B, C.

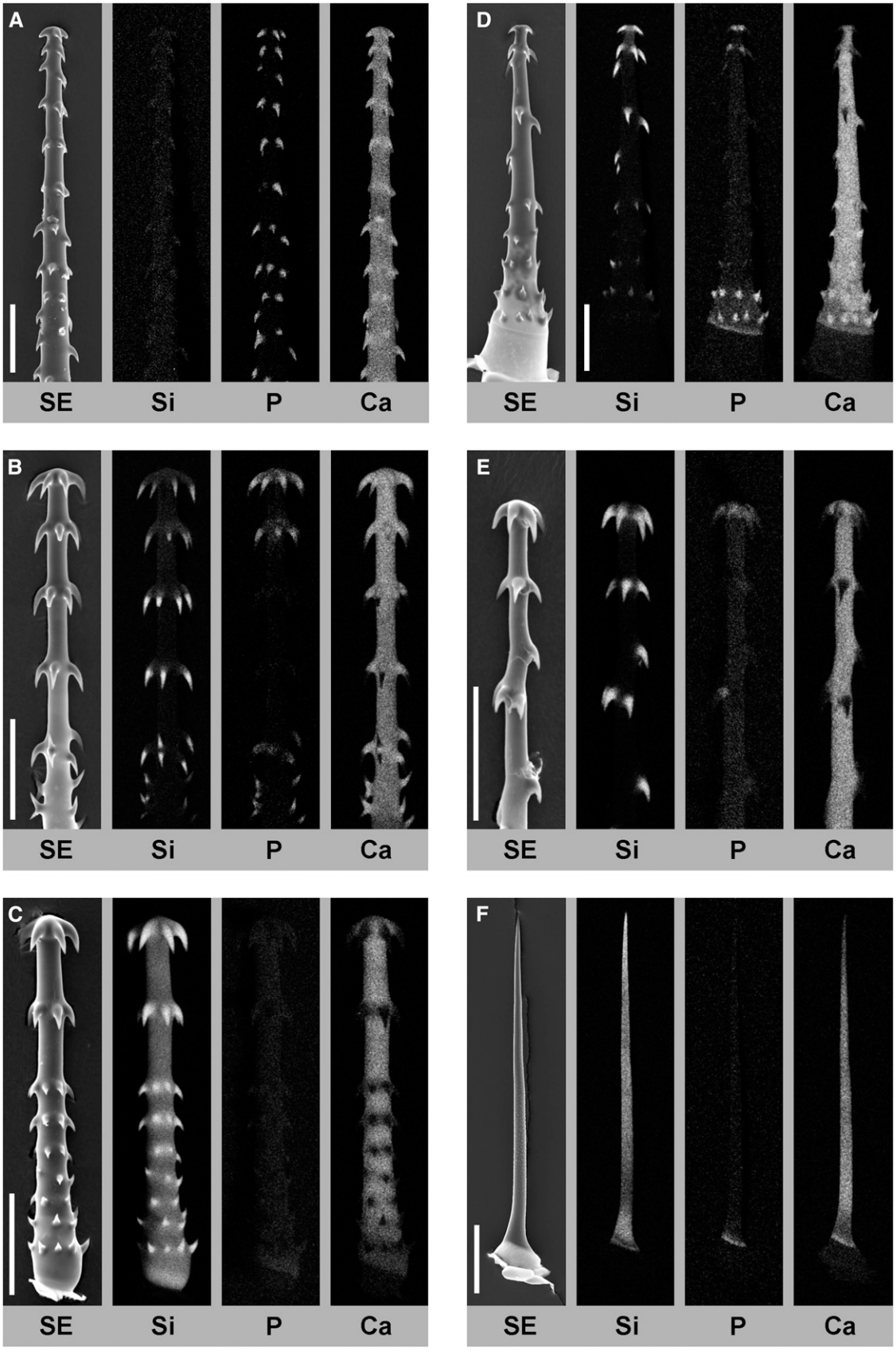
A
SE
Si
P
Ca
D
SE
Si
P
Ca
B
SE
Si
P
Ca
E
SE
Si
P
Ca
C
SE
Si
P
Ca
F
SE
Si
P
Ca

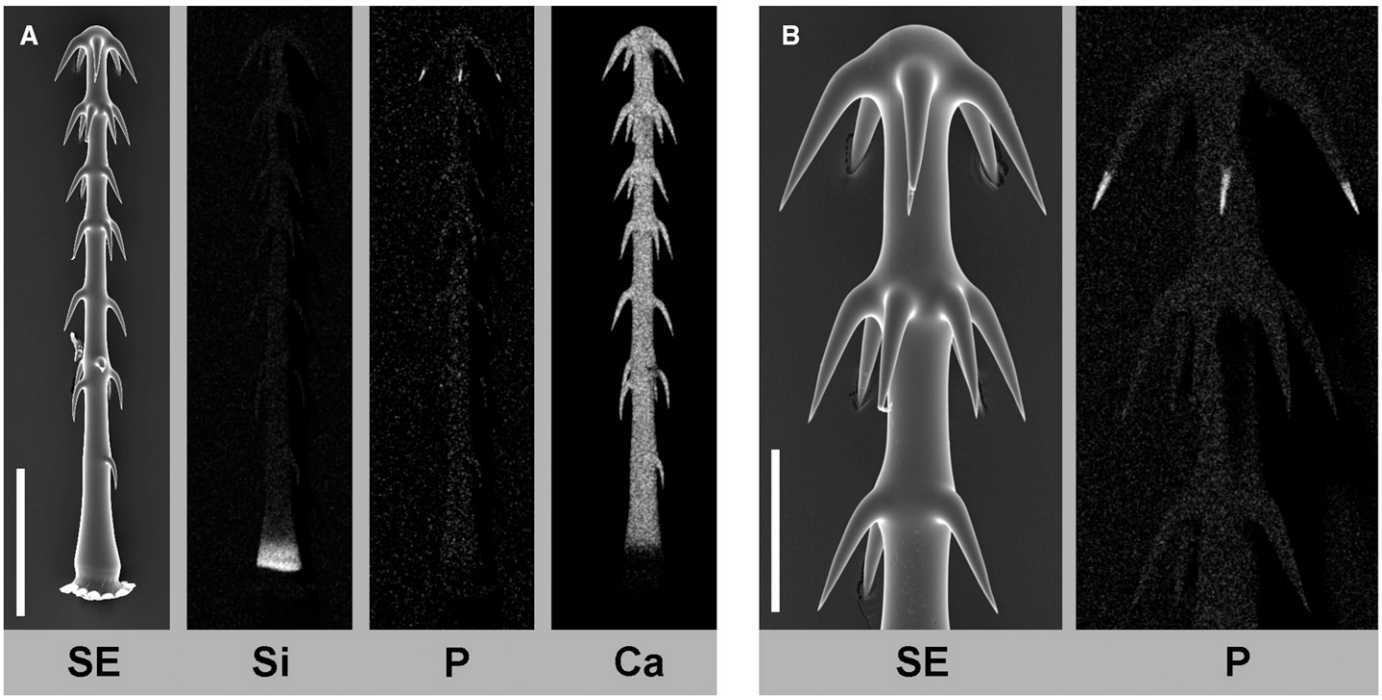


**FIGURE 6** Element distribution in glochidiate trichomes of *Eucnide urens*. (A) Entire trichome; only Ca appears as dominant biomineral with a high concentration of Si at base of trichome. (B) At higher magnification, content of P (calcium phosphate) in tips of distal hooks becomes evident. Scale bars: 300 μm in A; 100 μm in B.

*Nasa* pattern (8 of 8 species): stinging trichome tips contain silica and calcium phosphate; hooks of glochidiate trichomes contain either silica only, or both silica and calcium phosphate.

*Aosa* pattern (2 of 2 species): stinging trichome tips and glochidiate trichome barbs contain silica in high concentration; P is found at low concentrations only. The overall pattern is thus similar to what is found in *Urtica dioica*.

The other small genera of Loasoideae show slightly divergent patterns: *Presliophytum* is also mineralized with all three minerals, but with silica restricted to the tip of the stinging hairs. *Huidobria*, which lacks stinging hairs, has the simplest pattern of biomineralization limited to calcium carbonate.

## CONCLUSIONS

Our data demonstrate that biomineralization of glochidiate and stinging hairs is remarkably diversified in Loasaceae. There also appears to be some degree of phylogenetic sorting, and it is striking that *Huidobria*—representing the earliest-branching clade in Loasaceae subfam. Loasoideae (Hufford et al., 2003; Weigend et al., 2004)—has the simplest type of biomineralization and contains calcium carbonate only. This simple pattern could be interpreted as plesiomorphic. However, *Eucnide*, representing the most basally branching clade in the entire family, shows biomineralization with all three biominerals (silica at the base, calcium carbonate in the shaft and calcium phosphate in the very tips of the hooks of glochidiate trichomes). Triple biomineralization in individual trichomes of early-branching *Eucnide* indicates that the ability to deposit three different biominerals in a single trichomes either arose early in the evolution of the family (with subsequent losses)—or at least twice independently.

The data presented here include the bulk of the genera currently recognized, but cover only 31 of the ca. 200 species of Loasaceae subsp. Loasoideae (Weigend, 2003). The sampling can therefore not be considered as either comprehensive or even representative of this highly diversified family. Stinging hairs are present in at least three distantly related clades in Loasaceae (*Gronovia*, *Eucnide*, and subfam. Loasoideae) and the indument is extraordinarily diversified even within subgroups of the individual genera such as *Mentzelia* (Weigend, 2007) or *Nasa* (Dostert and Weigend, 1999; Henning and Weigend, 2009; Weigend, 2004; Henning et al., 2011). Based on our data, there seems to be some degree of phylogenetic sorting of the type of biomineralization (Table 1). However, the data on

**FIGURE 5** Biomineral distribution in glochidiate trichomes of various species. (A) *Loasa heterophylla*; (B) *Caiophora deserticola*; (C) *Blumenbachia insignis*; (D) *Nasa weigendii*; (E) *Aosa rupestris*; (F) *Urtica dioica*. Comparison of different taxa shows remarkable differences in the presence/absence of Si and P; Ca is uniformly found in all samples. In *Loasa*, hooks contain Ca and P (calcium phosphate); silica was not detected. *Caiophora* and *Nasa* glochidiate trichomes contain three biominerals. Hooks contain both silica (Si) and calcium phosphate (Ca and P); Ca (calcium carbonate) is present in shafts. Hooks of *Blumenbachia insignis* contain only Si; traces of P were detected at the bases. This species was the only one with high concentrations of Si and Ca in shaft. *Aosa* has silicified hooks with traces of phosphorus. Small trichomes of *Urtica dioica*, for comparison, have a silicified tip; the shaft contains Si and Ca. Scale bars: 50 μm in A–E; 100 μm in F.

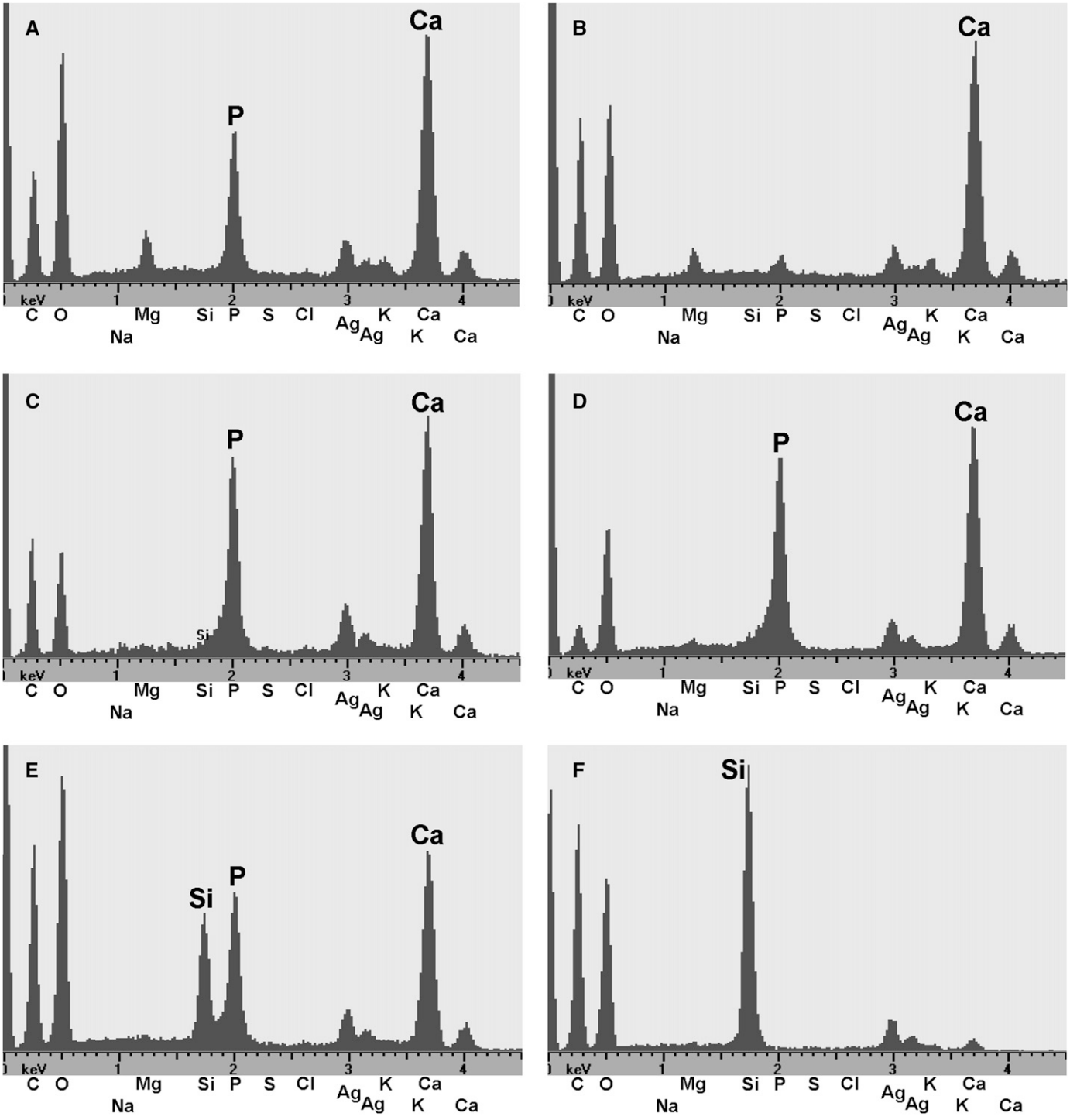


**FIGURE 7** EDX spectra of selected locations. High peaks in relation to the carbon peak (far left) indicate high concentrations of mineral elements, but low concentrations can also be recognized. (A, B) Spectra of a *Loasa heterophylla* stinging hair show high P and Ca concentrations in apical bulb (A) but only traces of P in shaft (B). (C, D) Locations with highest P concentrations such as hooks of *Loasa* glochids (C) show a P-to-Ca peak height ratio almost similar to that of mineral apatite (D), measured with 15 keV electron energy. (E, F) Spot-spectra of glochidiate trichome hook of *Caiophora deserticola* from a location with calcium phosphate and silica (E), and from a location with silica only (F).

*Loasa* show that even within genera there may be considerable interspecific variability. We therefore believe that both trichome morphology and biomineralization may follow similarly complex evolutionary patterns in the family and refrain from postulating general evolutionary trends. A detailed picture could only be obtained with greatly expanded sampling.

The functional significance of the different biominerals is also far from clear at present. Three biominerals were found in the

scabrid-glochidiate trichomes of the *Caiophora* species and in the stinging hairs of *Nasa*, and usually all three of them co-occurred in individual, unicellular trichomes with a differential distribution in different parts of the trichomes. Generally, the more delicate, terminal structures (bulbous stinging hair tip, apex of stinging hair, barbs on glochidiate trichomes) consist of calcium phosphate or silica, whereas the main wall structure is made of a calcium carbonate composite. At least in a first approximation, calcium phosphate and silica appear to be functionally equivalent and are employed in the same micromorphological context, apparently in those portions of the trichomes that require particular mechanical resilience of fine structures.

These data demonstrate an unprecedented degree of diversification in the biomineralization of plant trichomes, specifically in the Loasaceae, and invite a broad range of additional studies, since the patterns are clearly nonrandom and are likely to have an evolutionary and adaptive background. Future studies might look at the microscale chemical heterogeneity of plant trichomes and at mineralization patterns across other plant groups with a mineralized indumentum. Moreover, the process of biomineralization has so far not been investigated nor are the functional aspects of the differential biomineralization adequately understood.

## ACKNOWLEDGEMENTS

The authors thank the gardeners of the Botanische Gärten der Universität Bonn for cultivating the plants studied, especially Mrs. B. Emde and Mr. M. Neumann, and Mr. T. Jossberger for vouchering the collections. We are very grateful to two anonymous reviewers and the Associate Editor for detailed and helpful comments on the manuscript.

## LITERATURE CITED

Alexandre, A., J. D. Meunier, F. Colin, and J. M. Koud. 1997. Plant impact on the biogeochemical cycle of silicon and related weathering processes. *Geochimica et Cosmochimica Acta* 61: 677–682.

Bauer, P., R. Elbaum, and I. M. Weiss. 2011. Calcium and silicon mineralization in land plants: Transport, structure and function. *Plant Science* 180: 746–756.

Cardoso, M. Z. 2008. Herbivore handling of a plant's trichome: The case of *Heliconius charithonia* (L.) (Lepidoptera: Nymphalidae) and *Passiflora lobata* (Killib) Hutch. (Passifloraceae). *Neotropical Entomology* 37: 247–252.

Dostert, N., and M. Weigend. 1999. A synopsis of the *Nasa triphylla* complex (Loasaceae), including some new species and subspecies. *Harvard Papers in Botany* 4: 439–467.

Ensikat, H. J., T. Geisler, and M. Weigend. 2016. A first report of hydroxylated apatite as structural biomineral in Loasaceae—Plants' teeth against herbivores. *Scientific Reports* 6: 26073.

Epstein, E. 2009. Silicon: Its manifold roles in plants. *Annals of Applied Biology* 155: 155–160.

Franceschi, V. R., and P. A. Nakata. 2005. Calcium oxalate in plants: Formation and function. *Annual Review of Plant Biology* 56: 41–71.

Fu, H. Y., S. J. Chen, and L. L. Kuo-Huang. 2003. Comparative study on the stinging trichomes and some related epidermal structures in the leaves of *Dendrocnide meyeniana, Girardinia diversifolia,* and *Urtica thunbergiana. Taiwania* 48: 213–223.

Hanley, M. E., B. B. Lamont, M. M. Fairbanks, and C. M. Rafferty. 2007. Plant structural traits and their role in anti-herbivore defence. *Perspectives in Plant Ecology, Evolution and Systematics* 8: 157–178.

Hartl, W. P., H. Klapper, B. Barbier, H. J. Ensikat, R. Dronskowski, P. Müller, G. Ostendorp, et al. 2007. Diversity of calcium oxalate crystals in Cactaceae. *Canadian Journal of Botany* 85: 501–517.

He, H., E. J. Veneklaas, J. Kuo, and H. Lambers. 2014. Physiological and ecological significance of biomineralization in plants. *Trends in Plant Science* 19: 166–174.

Hegnauer, R. 1966. Losaceae. *In* Chemotaxonomie der Pflanzen, vol. 19, 402–404. Birkhäuser Verlag, Basel, Switzerland.

Henning, T., E. F. Rodríguez Rodríguez, and M. Weigend. 2011. A revision of the *Nasa ranunculifolia* group (*Nasa* ser. *Grandiflorae pro parte*, Loasaceae). *Botanical Journal of the Linnean Society* 167: 47–93.

Henning, T., and M. Weigend. 2009. Systematics of the *Nasa poissoniana* group (Loasaceae) from Andean South America. *Botanical Journal of the Linnean Society* 161: 278–301.

Hufford, L., M. M. McMahon, A. M. Sherwood, G. Reeves, and M. W. Chase. 2003. The major clades of Loasaceae: Phylogenetic analysis using the plastid *matK* and *trnL-trnF* regions. *American Journal of Botany* 90: 1215–1228.

Lanning, F. C., and L. N. Eleuterius. 1987. Silica and ash in native plants of the central and southeastern regions of the United States. *Annals of Botany* 60: 361–375.

Lanning, F. C., and L. N. Eleuterius. 1989. Silica deposition in some $C_3$ and $C_4$ species of grasses, sedges and composites in the USA. *Annals of Botany* 63: 395–410.

Lowenstam, H. A. 1981. Minerals formed by organisms. *Science* 211: 1126–1131.

Mann, S. 1993. Dalton perspectives. Biomineralization: The hard part of bioinorganic chemistry! *Journal of the Chemical Society, Dalton Transactions: Inorganic Chemistry* 1: 1–9.

Parr, J. F., and L. A. Sullivan. 2005. Soil carbon sequestration in phytoliths. *Soil Biology & Biochemistry* 37: 117–124.

Pollard, A. J., and D. Briggs. 1984. Genecological studies of *Urtica dioica* L. *New Phytologist* 97: 507–522.

Thurston, E. L. 1974. Morphology, fine structure and ontogeny of the stinging emergence of *Urtica dioica. American Journal of Botany* 61: 809–817.

Thurston, E. L., and N. R. Lersten. 1969. The morphology and toxicology of plant stinging hairs. *Botanical Review* 35: 393–412.

Trembath-Reichert, E., J. P. Wilson, S. E. McGlynn, and W. W. Fischer. 2015. Four hundred million years of silica biomineralization in land plants. *Proceedings of the National Academy of Sciences, USA* 112: 5449–5454.

Tuberville, T. D., P. G. Dudley, and A. J. Pollard. 1996. Responses of invertebrate herbivores to stinging trichomes of *Urtica dioica* and *Laportea canadensis. Oikos* 75: 83–88.

Weigend, M. 2003. Loasaceae. *In* K. Kubitzki and C. Bayer [eds.], The families and genera of vascular plants, vol. 6, 239–254. Springer, Berlin, Germany.

Weigend, M. 2004. Four new species of *Nasa* ser. *Alatae* (Loasaceae) in the Amotape-Huancabamba zone of Peru. *Novon* 14: 134–146.

Weigend, M. 2007. Systematics of the genus *Mentzelia* (Loasaceae) in South America. *Annals of the Missouri Botanical Garden* 94: 655–689.

Weigend, M., S. Hoot, M. Gottschling, and M. Ackermann. 2004. A preliminary phylogeny of Loasaceae subfam. Loasoideae based on *trn*$L_{(UAA)}$ sequence data and its relation to systematics and historical biogeography. *Organisms, Diversity & Evolution* 4: 73–90.

Weiner, S., and L. Addadi. 1997. Design strategies in mineralized biological materials. *Journal of Materials Chemistry* 7: 689–702.

Weiner, S., and P. M. Dove. 2003. An overview of biomineralization processes and the problem of the vital effect. *Reviews in Mineralogy and Geochemistry* 54: 1–29.

Wicke, W. 1861. Über das Vorkommen und die physiologische Verwendung der Kieselsäure bei den Dicotyledonen. *Botanische Zeitschriften* 19: 97–100.

Zhao, Z., D. M. Pearsall, R. A. Benfer, and D. R. Piperno. 1998. Distinguishing rice (*Oryza sativa* Poaceae) from wild *Oryza* species through phytolith analysis, II: Finalized method. *Economic Botany* 52: 134–145.

# CHAPTER 4

## Diversity of biomineralization in stinging trichomes of different plant families: silica, calcium phosphate, or neither?

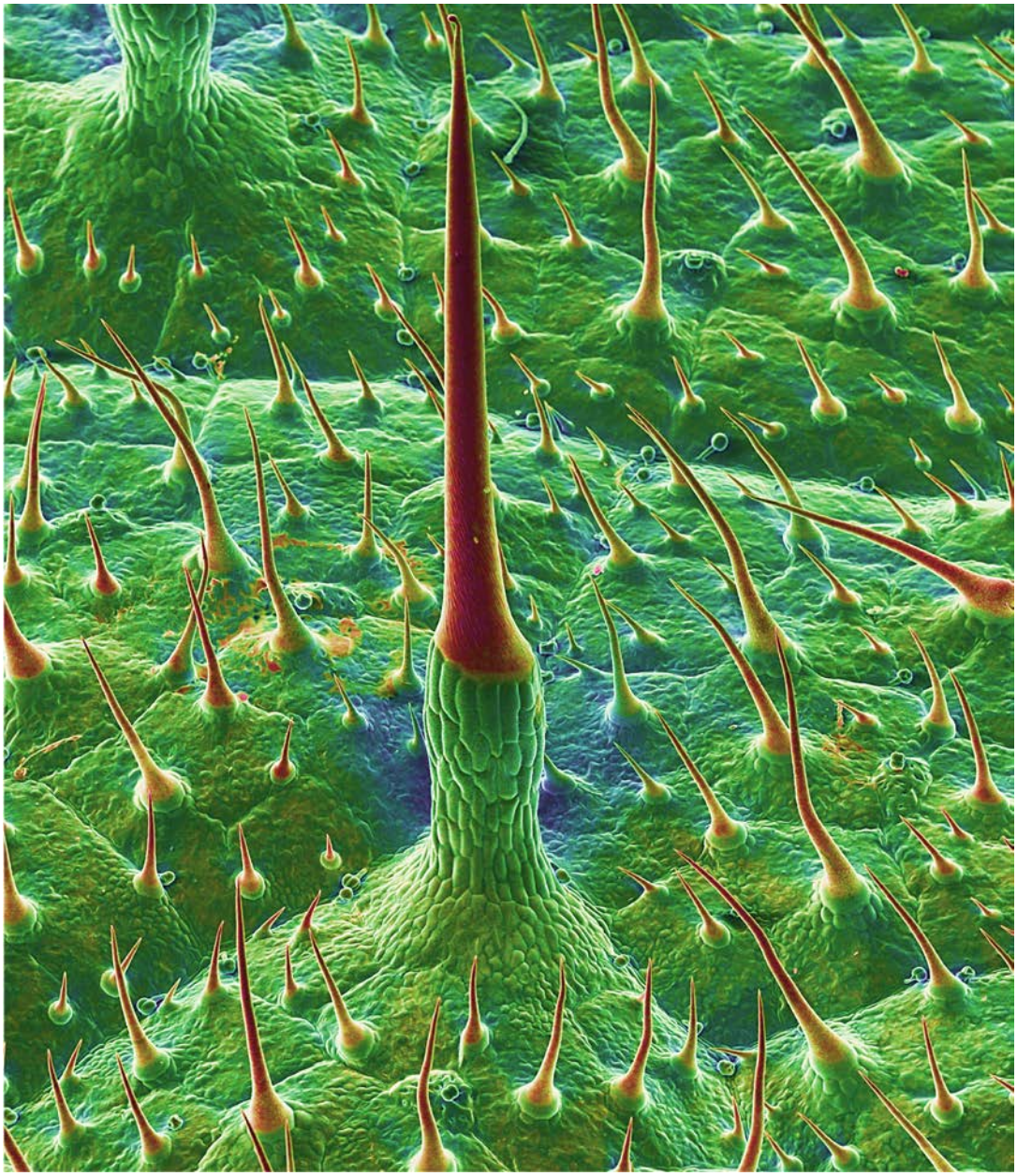

Cover image: Cryo-SEM micrograph of typical stinging trichome and small hairs on the leave of *Urtica dioica* L. (Urticaceae).

## Diversity of biomineralization in stinging trichomes of different plant families: silica, calcium phosphate, or neither?*


### Abstract

**PREMISE OF THE STUDY:** Stinging hairs are remarkable examples of plant microengineering – the plant equivalent of the hypodermic syringe. Their mechanical properties, required for this function are mostly achieved by cell wall mineralization. Stinging hairs of *Urtica dioica* have long been known to be mineralized with silica and calcium carbonate; those of Loasaceae have recently been shown to display a more complex pattern of biomineralization with also calcium phosphate involved. This discovery triggered renewed interest in trichome biomineralization across the taxa they are found in, namely Urticaceae, Euphorbiaceae, Loasaceae, Caricaceae and recently described Namaceae.

**METHODS:** Light microscopy and Scanning Electron Microscopy (SEM) with Cryo-SEM and EDX were used to analyze the distribution of biominerals in stinging trichomes surfaces and sections (block face imaging) of 17 representative species from five different plant families.

**KEY RESULTS:** Stinging hair mineralization patterns vary considerably between five plant families. Three regions of the trichomes showed different mineralization. Trichome apices contained either silica (Urticaceae), calcium phosphate (Caricaceae, Namaceae), both (some Loasaceae), or no minerals (Euphorbiaceae). Trichome shafts usually contained calcium carbonate, or calcium phosphate in few cases, whereas bases often had additional silica deposits. Cnidoscolus trichomes were completely unmineralized.

**CONCLUSIONS:** It has long been known that stinging hairs of *Urtica* are mineralized with calcium carbonate and silica, but few of the many species of


* Mustafa, A., Ensikat, H. J., Weigend, manuscript in preparation.

Urticaceae have been analyzed. Recently, reports of calcium phosphate in trichomes of Loasaceae indicated that stinging trichome mineralization may be a lot more complex than previously believed. In the present study, we document a surprising diversity of mineralization patterns, often involving three different minerals deposited in different parts of individual trichomes. This indicates that the physical properties of different wall regions of the stinging trichomes are fine tuned to optimizing their function via a modulation of wall thickness and differential composition.

**Keywords:** Biomineralization; calcium phosphate; calcium carbonate; Caricaceae; *Cnidoscolus*; Loasaceae; Namaceae; silica; stinging hairs; Urticaceae

## 4.1 Introduction

Plant defense is a broad topic in biology and a broad range of defense mechanisms are known, including structural and chemical defense and complex inducible defense pathways (Farmer, 2014). The crucial role of plant trichomes in herbivore defense continues to be intensively studied (Kaplan et al., 2009; War et al., 2012; Valverde et al., 2001). Glandular trichomes have long been known to be associated with chemical defense mechanisms (Wagner et al., 2004), but even morphologically simple, non-secretory trichomes are well known to convey some degree of herbivory protection, mainly against invertebrate herbivores (War et al., 2012; Sletvold et al., 2010; Kariyat et al., 2013; Kariyat et al., 2017). Stinging hairs have fascinated scientists for hundreds of years: The basic morphology and function of the stinging hairs of the Greater Stinging Nettle (*Urtica dioica* L.) was outlined more than 350 years ago in one of the early books on microscopy (Hook, 1665). Hooke in 1665 described the pluricellular pedestal and the long stinging cell "tapering in a very sharp point; it is of a substance very hard and stiff, exceedingly transparent and clear, and hollow from top to bottom" (Hook, 1665, p.142). Wicke (1861) was the first to characterize this "substance very hard and stiff" in 1861, demonstrating that the cell walls are mineralized with silica. Stinging hairs were subsequently discovered in several other plant families and discussed in a range of different publications, summarized by Thurston and Lersten (1969) and Fu et al. (2007). Stinging trichomes are a particularly intriguing defense form of combined structural/chemical defense, where the plant analogue of a hypodermic syringe injects a toxic substance into the skin of the herbivore upon touch. Consequently, much effort has been spent on identifying the active substances responsible for the painful sting (Collier and Chesher, 1956; MacFarlane, 1963; Thurston and Lersten, 1969; Lookadoo and Pollard, 1991; Corsi, 1992; Fu et al., 2007), and some effort has been spent on elucidating morphological and anatomical details of the trichomes (Thurston and Lersten, 1969; Thurston, 1974; Thurston, 1976; Pollard and Briggs, 1984; Fu et al., 2003). True stinging hairs with a pluricellular base and a single, hollow stinging cell are currently known from the Caricaceae (Brassicales), Euphorbiaceae (Malpighiales), Loasaceae (Cornales), Namaceae (Boraginales), and Urticaceae (Rosales). Overall stinging hair morphology is similar

across the different plant groups, in spite of their independent evolutionary origin, providing one of the most striking examples for the convergent evolution of complex plant structures. Unlike most other plant trichomes, stinging hairs appear to be specifically designed to prevent browsing by mammals, as has been argued for Urticaceae (Tuberville et al., 1996; Hurley, 2000), Loasaceae (Küster-Winkelmann, 1914), Namaceae (Cano-Santana and Oyama, 1994) and Euphorbiaceae (Pollard, 1986), while being largely ineffective against invertebrate herbivores. The direct and negative correlation between browsing and density of stinging hairs has been demonstrated in the past, underscoring the rather specific function of stinging hairs against mammalian herbivores (Pollard and Briggs, 1984; Iwamoto et al., 2014). Stinging hairs or urticant trichomes are thus highly specialized structures for herbivore deterrence (Farmer, 2014). Evidently, the specific function of the stinging hair as a type of hypodermic syringe requires a particular stiffness of the cell walls and this is usually achieved via biomineralization with calcium carbonate and silica (Thurston and Lersten, 1969). However, 150 years after the first demonstration of biomineralization in the stinging hairs of *Urtica*, there is still no detailed understanding of element distribution in the cell wall, with conflicting reports on the distribution of silica and calcium carbonate (Thurston and Lersten, 1969; Fu et al., 2007; Sowers and Thurston, 1979). Additionally, Ensikat et al. (2016, 2017) could demonstrate that the stinging hair tips of Loasaceae are mineralized with calcium phosphate, a substance not previously known as a structural biomineral in plants, thereby expanding the range of biominerals found in individual stinging hairs to three. Moreover, Mustafa et al. (2017) demonstrated that the apex of stinging hairs in the genus *Nasa* is first mineralized with calcium phosphate and subsequently with silica, raising the question as to what happens to the first deposited biomineral in the trichome tips. In spite of the long-standing interest in stinging hairs as unique structures for plant defense and examples of complex plant biomineralization, remarkably little research has been carried out on stinging hairs in general and the apparently complex biomineralization of the cell walls in particular. The present study aims at providing novel insights into the morphology and biomineralization patterns across all five plant families provided with these intriguing structures.

## 4.2 Materials and methods

### 4.2.1 Plant sample acquisition

Fresh plant material used for this study was cultivated at the Botanische Gärten der Universität Bonn, Germany, whereas the herbarium specimens were collected from the herbaria of the Nees-Institut für Biodiversität der Pflanzen (BONN); Royal Botanic Garden, Edinburgh, UK; Munich Botanical Garden, Nymphenburg, Germany. The following taxa from five different plant families were examined, such as Urticaceae: *Dendrocnide moroides* (access. 2001/1072), *Girardinia cuspidata* (*MW* 8656), *Laportea perrieri* (access. 18017, *T. Jossberger* 1719), *Urera baccifera* (access. 7690, *T. Jossberger* 1716), *Urtica dioica* (access. 4919, *T. Jossberger* 1665), *Urtica mairei* (access. 37176, *T. Jossberger* 1175); Loasaceae: *Blumenbachia amana* (access. 36584, *T. Jossberger* 1204), *Blumenbachia insignis* (access. 36150, *T. Jossberger* 1210) *Caiophora deserticola* (access. 37106, *T. Jossberger* 1562), *Nasa macrothyrsa* (access. 38261) *Nasa weigendii* (access. 37116, *T. Jossberger* 1242); Euphorbiaceae: *Cnidoscolus aconitifolius* (access. 38881, *TJH*-083), *Cnidoscolus urens* (*VE-0-M-1995/3660*), *Cnidoscolus vitifolius* (*RBGE: TMEX474*); Namaceae: *Wigandia ecuadorensis* (access. 34805, *T. Jossberger* 899), *Wigandia caracasana* (access. 37186, *T. Jossberge* 1619); Caricaceae: *Horovitzia cnidoscoloides* (*MX-0-M-2013/1841*).

### 4.2.2 Scanning electron microscopy (SEM)

Topographic imaging and EDX analyses were performed using a Cambridge S200 Stereoscan and a LEO 1450 SEM (Cambridge, UK), equipped with secondary electron (SE) and backscattered electron (BSE) detectors and an EDX analysis system (Oxford Instruments, UK) with Link ISIS software. SE and BSE images were usually acquired from frozen, hydrated samples at approximately -100°C using a cryo stage. Element mapping by EDX required samples with better long-term stability and were acquired from dried samples. All obtained images were recorded with a digital image acquisition system ‘DISS 5’ (Point Electronic, Halle, Germany). EDX element

mapping was used to analyse the distribution of the elements silicon (Si), phosphorus (P) and calcium (Ca). It has been demonstrated previously for trichome walls (Ensikat et al., 2016) that P was generally associated with Ca in form of calcium phosphate, whereas Ca without P occurred as a calcium carbonate-based composite, associated with organic matter such as cellulose. In the following, these calcium carbonate composites are named simply as calcium carbonate.

### 4.2.3 Light microscopy

Transmission views of isolated stinging trichomes were performed by using a Light Microscope (Axio Scope; Carl Zeiss Microscopy, Oberkochen, Germany) coupled to a digital camera and computer.

### 4.2.4 Sample preparation

Plant specimens were fixed in 70% ethanol + 4% formaldehyde for at least 24 h, dehydrated with ethanol and acetone. After dehydration, the specimens were critical-point dried (CPD 020 Balzers Union) using $CO_2$ as intermedium. Individual stinging trichomes were cut off the leaves with a razor blade, dehydrated with acetone, and air-dried out of acetone. Specimens were sputter-coated (SCD 040 Sputter-Coater: Balzers, Liechtenstein) with silver or palladium (Junker Edelmetalle, Waldbüttelbrunn, Germany) instead of gold, because the EDX spectra of palladium and silver do not interfere with the characteristic X-ray peaks of relevant biomineral elements. Samples for ultramicrotomy and block-face imaging were fixed in ethanol / formaldehyde, transferred into acetone, and embedded in resin (Agar Low viscosity kit, Plano GmbH, Wetzlar, Germany) according to standard instructions. Sectioning (longitudinal and transverse) was performed with a diamond knife in an ultramicrotome (Reichert OM-U3).

### 4.2.5 Element-mapping images processing

Material contrast color images were generated by combining secondary electron (SE) with backscattered electron (BSE) images. Image processing and color contrasting was

carried out with standard image processing software (Paint Shop Pro X8, Corel). Element distribution color images were generated by combining SE images with one or two corresponding element mapping images, either those of Ca, P or Si.

## 4.3 Results

### 4.3.1 Gross morphology of stinging hairs

We examined stinging trichomes from a total of 17 representatives of the families Caricaceae, Euphorbiaceae, Loasaceae, Namaceae and Urticaceae. The stinging hair itself is always a unicellular, elongate cell, distinctly tapering from bottom to top and with the emergent cell walls usually mineralized throughout (Fig. 1 A-E). Only the stinging hair of *Cnidoscolus* is completely unmineralized (Fig. 1 F). The size of the stinging trichomes varies considerably among different genera; the smallest stinging trichomes were observed in *Laportea* with 1 to 2 mm, whereas *Wigandia* and *Cnidoscolus* stinging trichomes may exceed 6 mm in length. The stinging cell itself is mounted on a pluricellular pedestal, into which the bulbous base of the stinging cell is immersed (Fig. 1 A-F, Fig. 7). The apical region of the stinging hair is always differentiated, forming a subapical 'preformed breaking point' with thinner cell walls. In Urticaceae, Loasaceae and Euphorbiaceae the apical bulb is distinctly curved and asymmetrical, with a bulbous tip set off to one side and the walls of the portion immediately below thinner on the concave and thicker on the convex side (Fig. 2 A-D). In *Horovitzia* (Caricaceae) and *Wigandia* (Namaceae), the apex of the stinging trichome is symmetrical (Fig. 2 E, F), with a symmetrically narrowed portion below the apical thickening. The stinging cells are essentially hollow from the base to the bulbous tip, and break off with the slightest touch. Breakage creates a sharp edge connected to a large liquid reservoir, similar to a hypodermic needle. Pressure applied to the trichome will compress the bladder-like base (Fig. 2 G-I) and eject the irritant fluid from the apex, performing an action analogous to the plunger in a hypodermic syringe (Appendix chapter 4, Fig. S1).

### 4.3.2 Biomineralization

Notable differences were found in the mineralization of stinging hairs. All Urticaceae stinging hairs examined had silicified tips (Fig. 3; Fig. S2). In contrast, the shafts and basal regions showed a strong variability in mineral composition. Si was found in most trichome shafts in minor amounts; only *Urera baccifera* had high Si concentration along the entire shaft (Fig. S2 C). Three species had very little or even no P in the shaft (*Urtica dioica, Girardinia cuspidata, Dendrocnide moroides*; Fig. S2 A, E, F). Three other species (*Urtica mairei, Urera baccifera, Laportea perrieri*; Fig. S2 B, C, D; Fig. 3 A) showed high P and Ca concentrations in shaft and base. Analyses of longitudinal sections were made to investigate mineral distribution across the cell wall. Element mapping images of the section of *Laportea perrieri* stinging hair Fig. 3 (B, C) showed high P and Ca concentrations from top to base and an outer layer with increasing amounts of Si towards the apex; lower amounts of Si are found along the entire shaft. Detailed mapping images show that the wall is evenly mineralized with calcium phosphate, whereas Si is concentrated in the outer part of the wall (Fig. 3 C). A line scan illustrates the concentration profiles (Fig. 3 D). EDX spectra show a uniform peak height ratio for P and Ca, similar to that pure apatite calcium phosphate, indicating that trichomes may be uniformly mineralized with calcium phosphate, while calcium carbonate may be absent. The shafts of the stinging hairs of Loasaceae were mainly mineralized with calcium carbonate, but the tips varied remarkably in their biomineralization. The bulbous apex and the immediately adjacent region of the cell wall were mineralized with calcium phosphate in the case of *Blumenbachia* (Fig. 4 A), whereas *Nasa* stinging hairs had silica and calcium phosphate at the very apex and calcium phosphate below (Fig. 4 B; Fig. S3 A). In *Nasa*, silica actually forms a cap over the calcium phosphate at the very apex (Fig. 4 C; Fig. S3 B). Towards the base, the calcium phosphate is gradually replaced by calcium carbonate (Fig. 4 illustrates the element distribution by colors; Fig. S3 shows grayscale mapping images of selected elements independently so that weaker signals can be recognized). A thin layer of silica on top of the calcium phosphate appears to be present also in other taxa, such as *Caiophora*. Here, it is barely noticeable in surface view, but clearly differentiated in longitudinal section. All sections of fully developed stinging trichomes clearly show that the entire wall is mineralized, not only the outer layers

(*Nasa*; Fig. 4 C-D; Fig. S3 B-C). *Cnidoscolus* (Fig. 5 A-G), while morphologically very similar to the other stinging hairs, shows no mineralization of the wall, but sections reveal traces of irregularly deposited calcium on the outer surface and in the cell lumen (Fig. 5 C-F). EDX spectra of the bulk of the wall (Fig. 5 G) and the oxygen distribution image (Fig. 5 E) indicate a low concentration, but an even distribution of oxygen, without any visible stratification, and no visible peaks of the mineral elements. Stinging trichomes of *Horovitzia* (Caricaceae) (Fig. 5 H-L) are heavily mineralized with calcium phosphate in the apex, the remainder of the shaft is mineralized primarily with calcium carbonate (and some phosphate), there is a considerably amount of silica occurs in the basal portion.

The stinging hairs of *Wigandia* (Fig. 6) are heavily mineralized with calcium phosphate only in the distal portion, less than $1/10^{th}$ of their overall length (Fig. 6 B, C), while the remaining shaft is mineralized with calcium carbonate. EDX spectra of selected locations (Fig. 6 H-J) reveal that P and Ca are the main mineral elements present in the tip, together with a minor and variable proportion of magnesium (Mg). The trichome shaft contains mainly calcium carbonate, and the basal region is only marginally mineralized with calcium carbonate. Figure 7 is a schematic representation of the structure and mineralization of stinging trichomes in representatives of the five plant families investigated. The locations of the different biominerals are shown in specific following color codes: red (silica); blue (calcium phosphate); green (calcium carbonate).

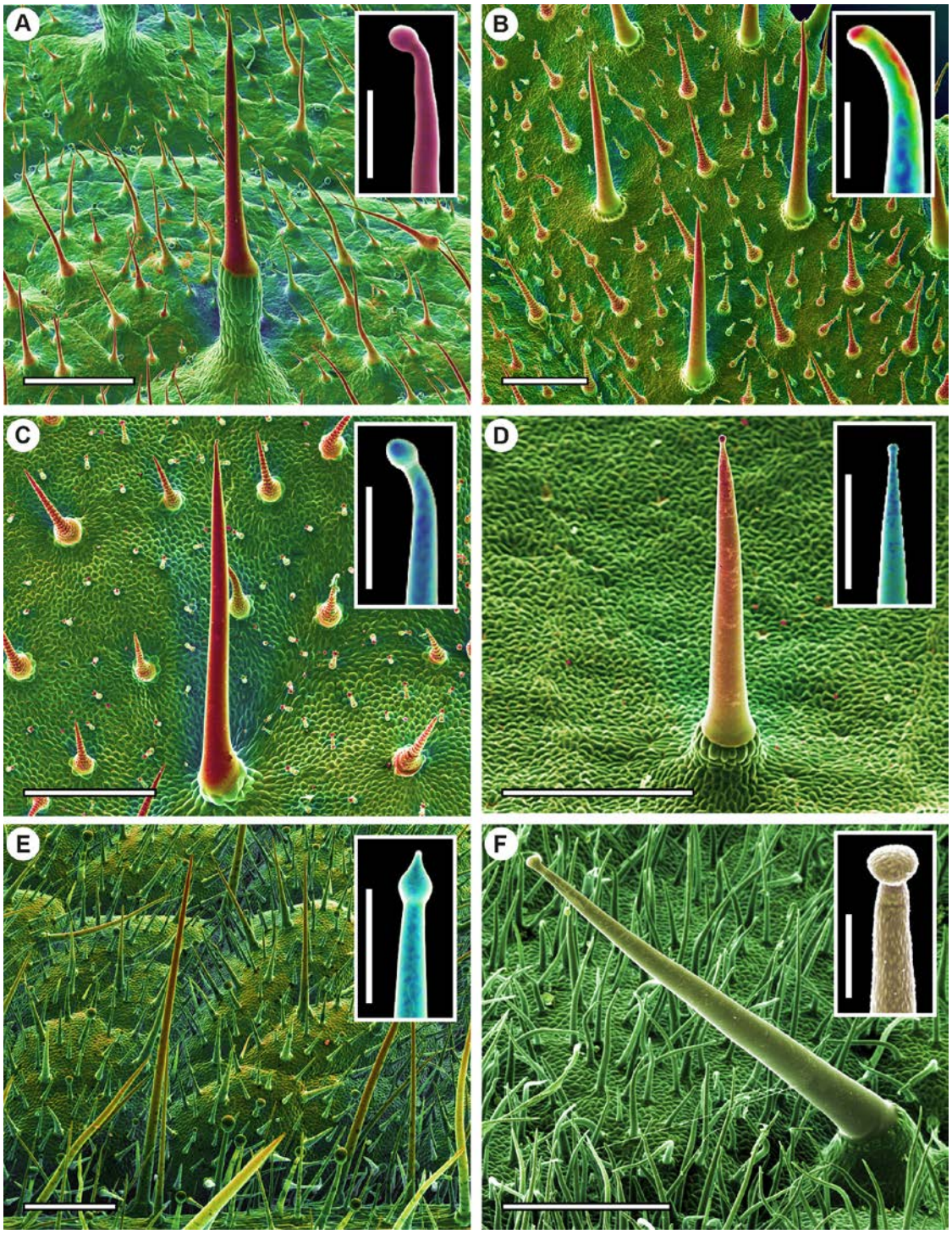


**Figure 1.** Cryo-SEM micrographs of typical stinging hairs on the leaves of six different plant families. The combined topographical and compositional contrast images show mineralized structures in yellow to red, green color indicates the presence of organic compounds only. Colorized inserts are combined topographic SE-images with EDX element-mapping images, displaying the mineralized apical regions with silica (red color), calcium phosphate (blue and green color) and non-mineralized (colorless). Scale bars of overview images A-F = 500 µm. (A) *Urtica dioica* (Urticaceae); single, elongate stinging hair,

apically tapering cell with a bulbous tip and pluricellular base. The insert shows the silicified bulbous tip of the stinging hair; the red color indicates high silicon content. Insert scale bar = 50 µm. (B) *Nasa weigendii* (Loasaceae); large mineralized stinging hairs and scabrid-glochidiate hairs cover the leaf surface. Insert: apical region of the stinging hair shows the occurrence of both, calcium phosphate (blue and green) and silica (red), in high concentration. Insert scale bar = 25 µm. (C) *Blumenbachia amana* stinging hair with multicellular base, accompanied by scabrid-glochidiate hairs. The insert shows the tip of *Blumenbachia amana* mineralized with calcium phosphate (blue). Insert scale bar = 50 µm. (D) *Horovitzia cnidoscoloides* (Caricaceae); individual, elongate stinging hair with symmetrical bulbous tip and multicellular base. The insert shows a high concentration of calcium phosphate (blue) in the apical region. Insert scale bar = 25 µm. (E) *Wigandia ecuadorensis* (Namaceae); leaf surface is covered by very thin and long mineralized stinging hairs, small mineralized hairs, and non-mineralized glandular hairs. Insert: apical knob of stinging hair strongly mineralized with calcium phosphate (blue). Insert scale bar = 50 µm. (F) *Cnidoscolus urens* (Euphorbiaceae); elongated stinging hair with apical bulb. The insert shows the non-mineralized apical bulb (colorless). Insert scale bars = 50 µm.

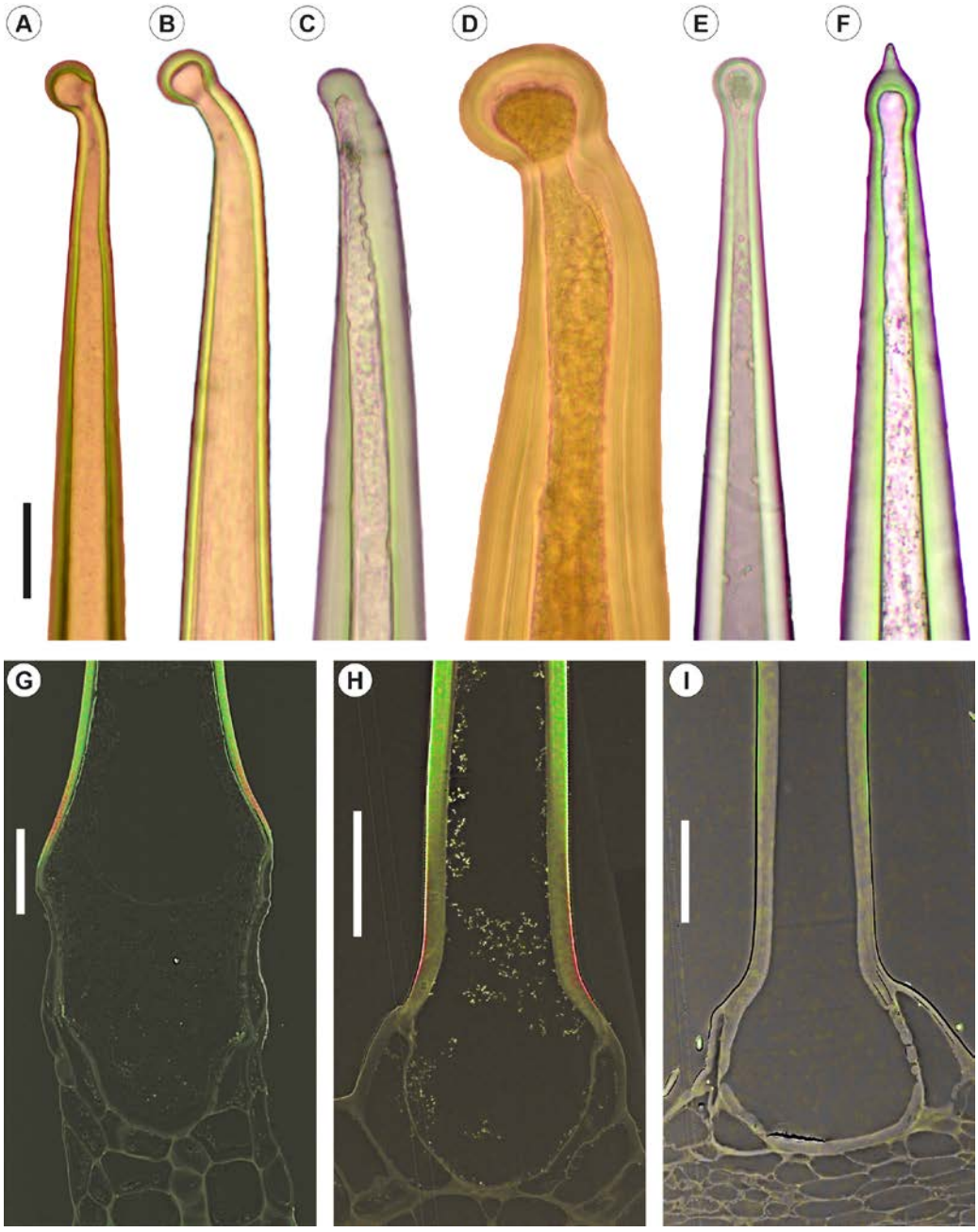


**Figure 2.** Light microscopic images of stinging hair apices and block-face SEM images of longitudinal sectioned stinging hair bases of different plant families. (A-D) Asymmetrical bulbous tip of stinging hairs of *Urtica dioica* (A), *Caiophora deserticola* (B), *Nasa weigendii* (C), and slightly asymmetrical tip of *Cnidoscolus aconitifolius* with a remarkable large diameter (D). (E) Symmetrical tip of stinging hair of *Horovitzia cnidoscoloides* and (F) lance-shaped tip of *Wigandia ecuadorensis* stinging hair. Calcified (green) base of *Urtica dioica* (G), calcified and slightly silicified (red) base of *Caiophora deserticola* (H); the base of *Wigandia caracasana* (*I*) appears unmineralized and Ca is found only in the outer region of the adjacent shaft. Combined element images indicate calcium in green color and silica in red. Scale bars: A-F = 30 µm, G-I =100 µm.

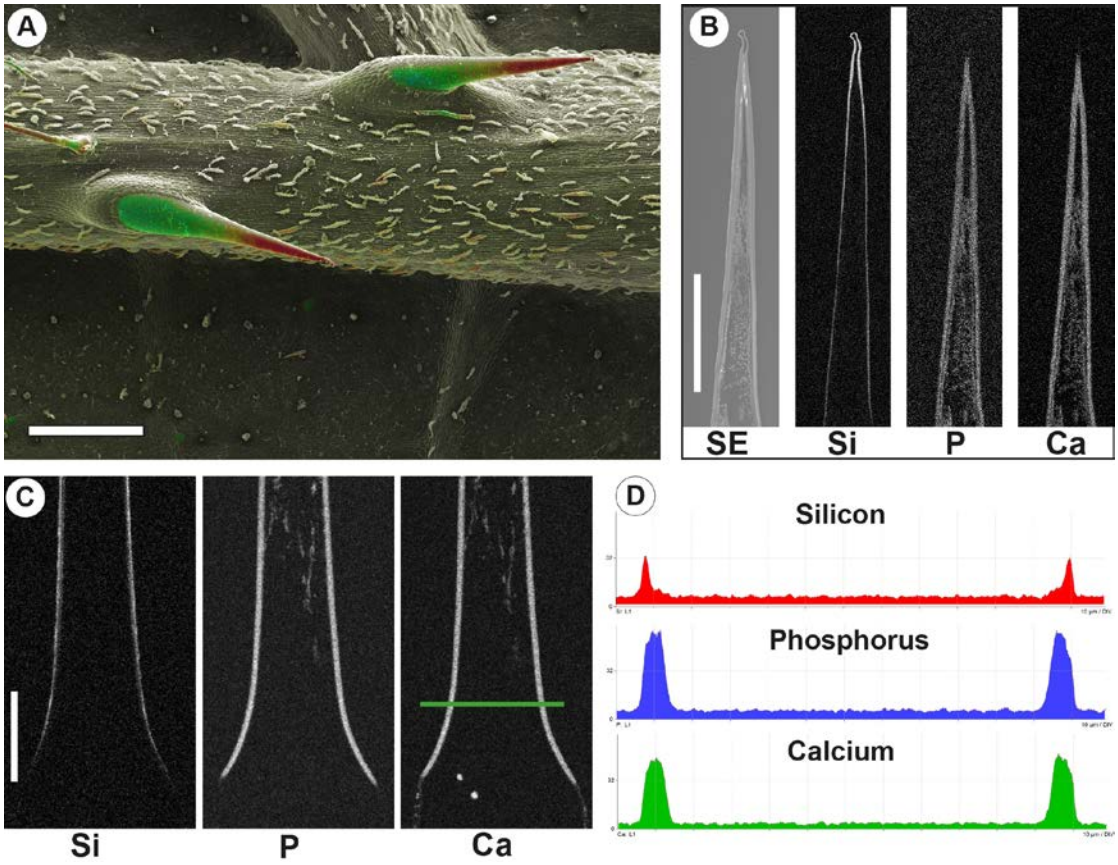


**Figure 3.** Element distribution in stinging hairs of *Laportea perrieri* an Urticaceae species primarily mineralized with calcium phosphate. (A) Element distribution image showing high concentrations of Si in red and P in green colors. (B-C) Element mapping images of longitudinal section of apical and basal part of a stinging hair, showing strong Ca and P signals over the entire length. The higher magnification (C) and the EDX line scan (D) reveal that the main part of the wall is impregnated with Ca and P, whereas Si is concentrated on the outer surface of the cell wall. Scale bars: A = 500 µm, B = 300 µm, C = 100 µm.

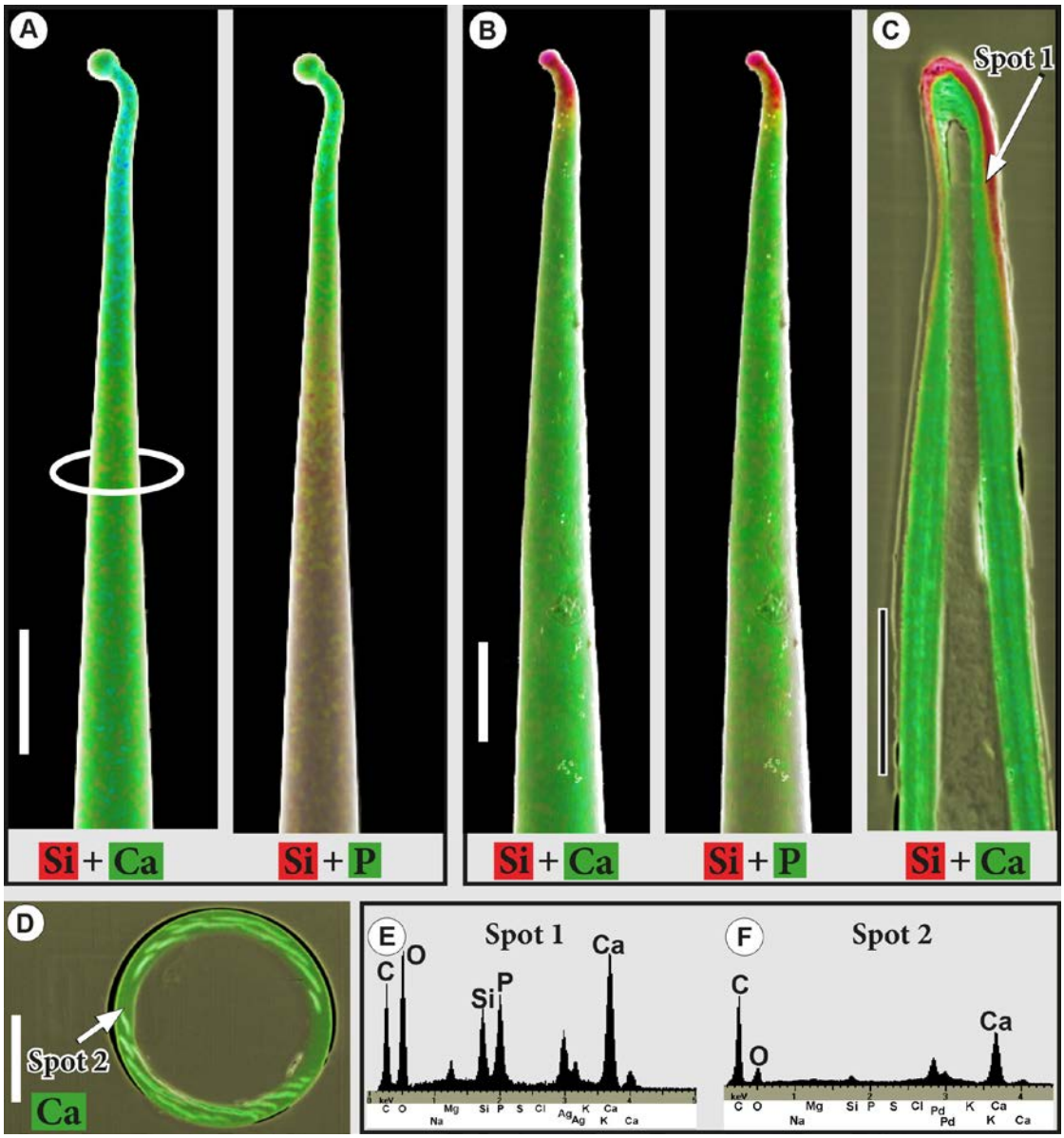


**Figure 4.** Surface views and sections showing the element distribution in stinging hairs of Loasaceae. Combined topographic and EDX element-mapping images display the distribution of calcium and phosphorous [Ca, P, (green)], and silica (Si, red) in stinging hairs of *Blumenbachia* and *Nasa*. (A) Stinging hair tip of *Blumenbachia insignis* contains calcium phosphate and Si is absent. Surface view (B) and longitudinal section (C) of *Nasa macrothyrsa*, showing a "cap" of silica on top of calcium phosphate apex. (D) Transverse section of *Blumenbachia insignis* stinging hair shaft [comparable to encircled region in (A)], displaying high Ca concentration across the entire wall thickness. The regions indicates by spot 1(C, arrow), spot 2 (D, arrow), and their corresponding EDX-spectra in E (Spot 1), F (Spot 2) indicate the different mineral compositions: the apex of the stinging hair of *N. macrothyrsa* contains both silica and calcium phosphate; the shaft in *Blumenbachia* (Spot 2) only shows Ca signature (calcium carbonate). Scale bars: A, B = 50 µm, C, D = 30µm.

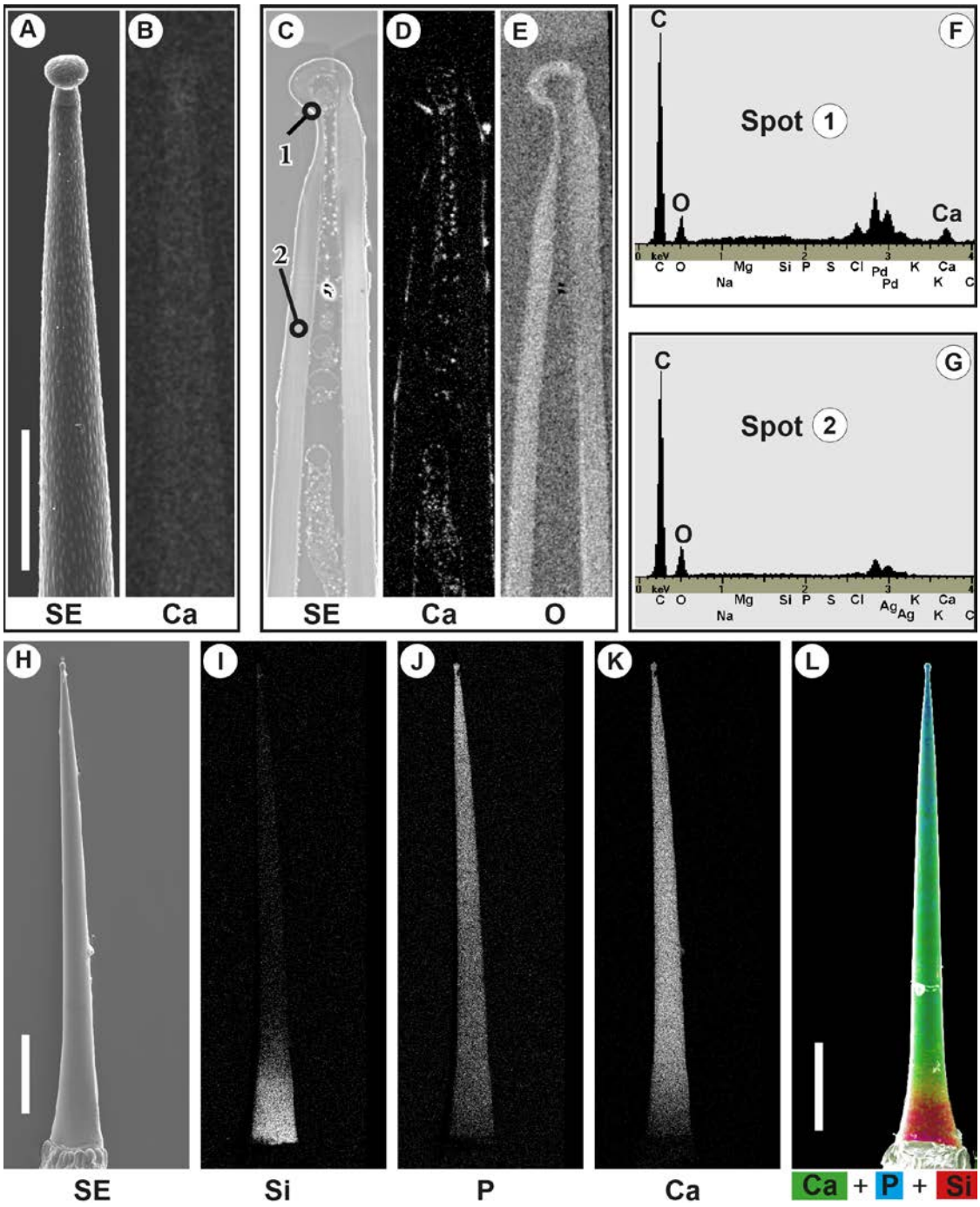


**Figure 5.** EDX element mapping and analysis of *Cnidoscolus aconitifolius* (Euphorbiaceae) and *Horovitzia cnidoscoloides* (Caricaceae) stinging hairs. (A) Topographic and (B) calcium distribution image of the surface, (C-G): SE image, element mapping images and spectra of the longitudinal section of a resin-embedded *Cnidoscolus aconitifolius* stinging hair. Traces of calcium (C; encircled), which were found occasionally in spectra, are localized by element mapping (D) of the section: minor Ca-rich deposits are found on the stinging hair surface (arrow) and in the cell lumen. The overview image (C) shows the locations where spectra were measured from a calcium-rich location (spot 1; corresponding

spectrum in F) and the regular cell wall (spot 2; corresponding spectrum in G) with no minerals detected. The spectrum of the regular wall shows high carbon and relatively low oxygen content. The oxygen mapping image (E) shows a homogeneous distribution without stratification. (H-K) Topographic overview and EDX mapping images of selected elements in *Horovitzia cnidoscoloides* stinging hairs. (I) Si distribution; indicating the high concentrations of silica at the base of stinging hair. (J) P distribution; documenting the presence of P along the entire stinging hair with gradually decreasing concentrations towards the base. (K) Ca distribution; showing a high concentrations of Ca over the entire shaft of the stinging hair. (L) Combined color image illustrating the differential distribution of three biominerals. Scale bars: A-E = 100 µm, H-L = 250 µm.

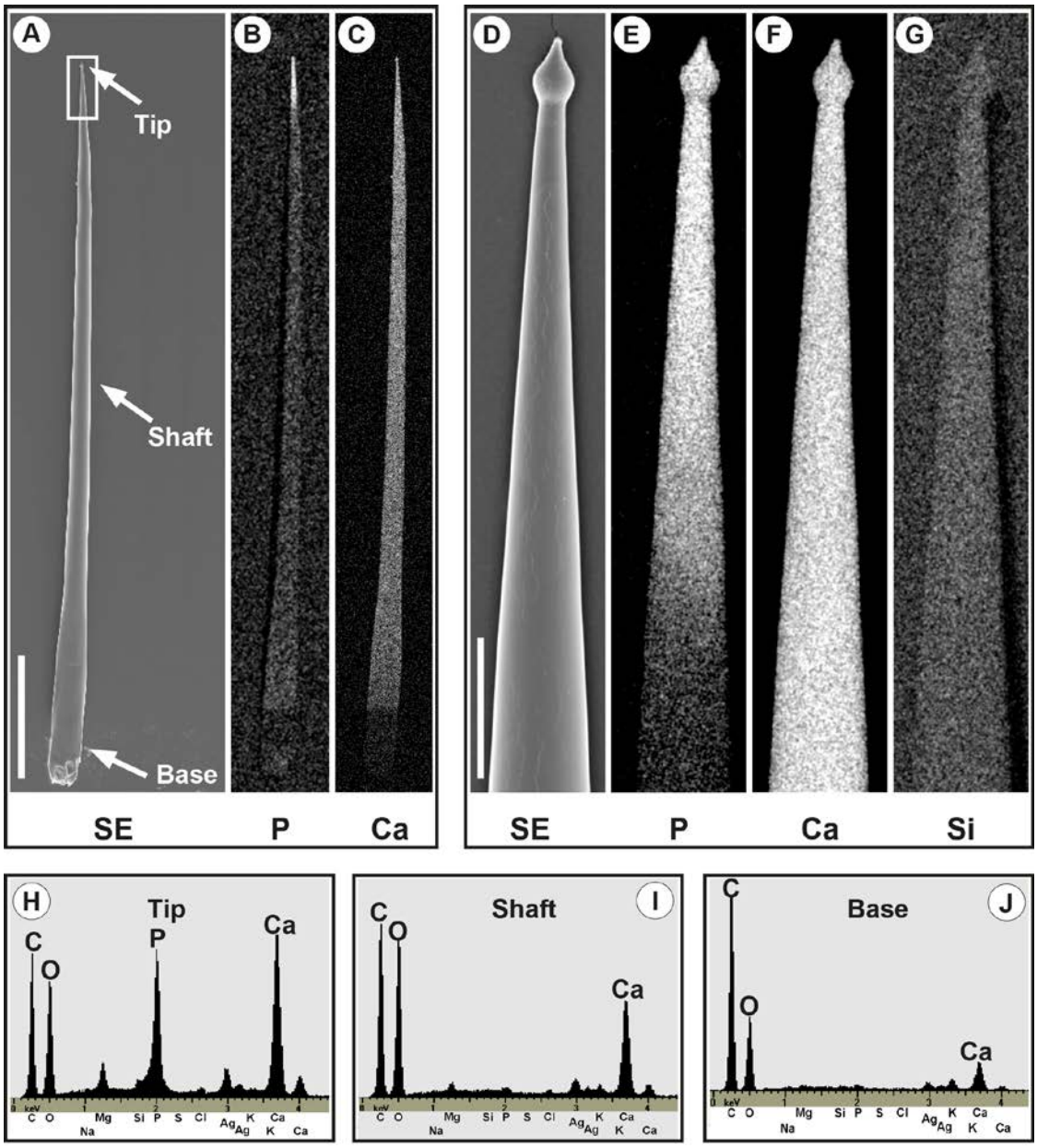


**Figure 6.** EDX element-mapping and corresponding spot spectra of *Wigandia ecuadorensis* stinging hairs. (A) SE-image of an isolated large *Wigandia* hair, with analyzed spots marked as tip, shaft and base (arrows). (B-C) Element-mapping of full length stinging hair shows that the higher concentration of P is restricted to the tip region, whereas Ca occurs in the entire shaft and only in low concentration in the base. (D-G) Higher-magnification micrographs of the tip region delimited by the white box in (A). (D) SE mode; (E-G) mapping of the elements P, Ca, Si. (H-J) EDX-spectra of locations pointed in (A) (arrows) show high concentration of calcium phosphate in the tip, calcium carbonate in the shaft and traces of calcium carbonate in the base. Scale bars: A-C = 500 µm, D-G = 50 µm.

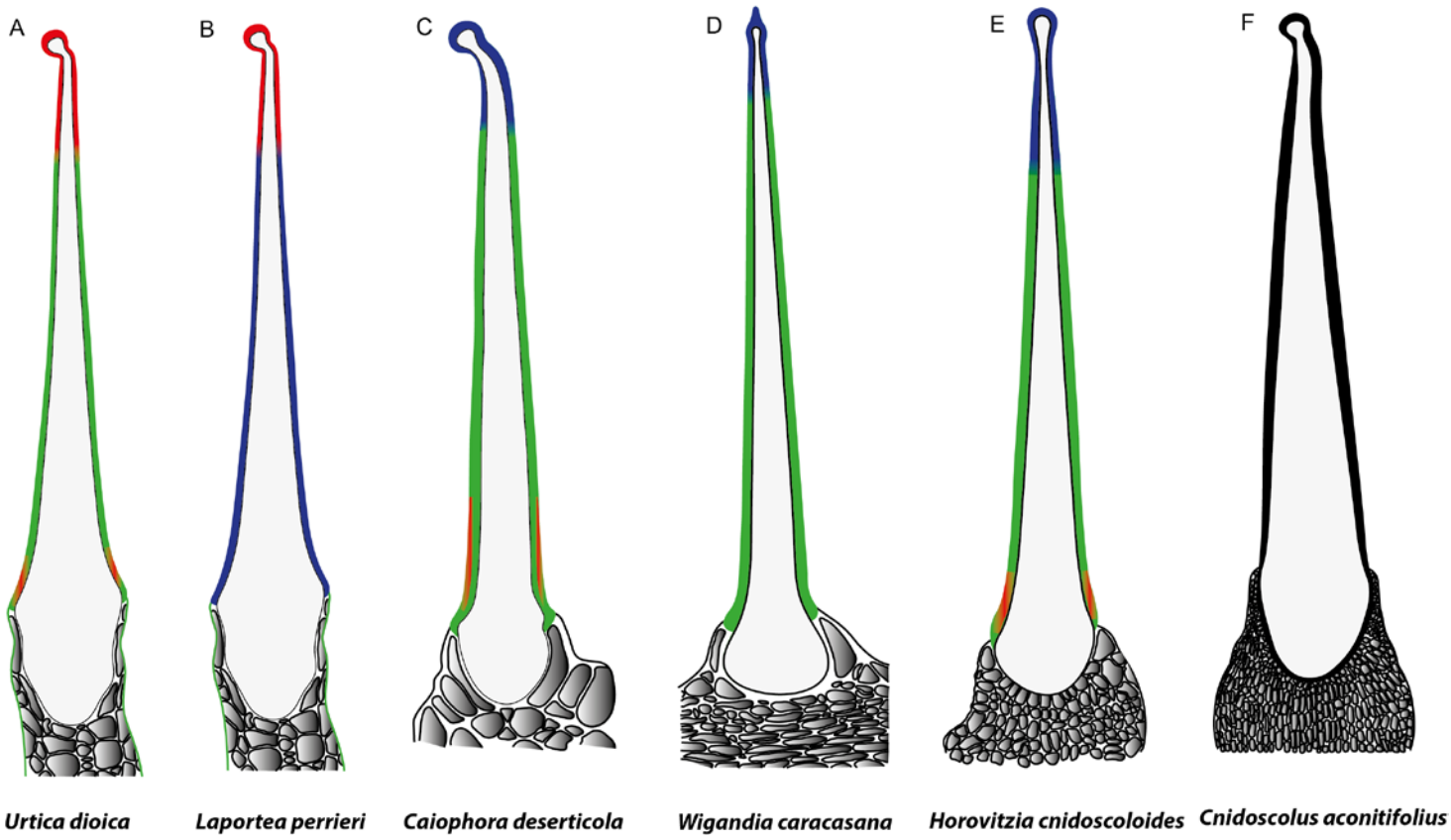


**Figure 4.7.** Schematic representation of stinging hair morphology and biomineralization in five different plant families. (A) *Urtica dioica* (Urticaceae). (B) *Laportea perrieri* (Urticaceae). (C) *Caiophora deserticola* (Loasaceae). (D) *Wigandia caracasana* (Namaceae). (E) *Horovitzia cnidoscoloides* (Caricaceae). (F) *Cnidoscolus vitifolius* (Euphorbiaceae). Biominerals are color-coded as follow: red = silica; green = calcium carbonate; blue = calcium phosphate; black = non-mineralized. The longitudinal sections (schematic, with different magnifications for tips and basal regions) show the typical differences in tip shape, mineral composition, and the morphology of basal region and pluricellular pedestal.

## 4.4 Discussion

Stinging hairs are highly specialized plant structures which evolved at least five times independently in distantly related orders of the flowering plants. The gross morphology is strikingly similar, especially the shape of the stinging cells in Urticaceae, Loasaceae and *Cnidoscolus* - with an asymmetrical, bulbous tip – are near-identical in shape (Fig. 7 A, B, C, F). The same structure with the same function is here realized with either two or three different biominerals, or without any biomineralization in the case of *Cnidoscolus*. However, the similar and relatively simple morphology is in stark contrast to the complex wall chemistry, with differential biomineralization in different parts of the trichome wall and a complex geometry of biomineral distribution. The classical view of *Urtica* stinging hairs as one of simple conical glass capillaries (Haberlandt, 1886) still prevails and little has been added to this concept in recent publications (Fu et al., 2007). Here, we demonstrate that different species of Urticaceae have different proportions of the three biominerals in different parts of their stinging hairs (Fig. S2), with calcium phosphate the dominant biomineral in some taxa. Similar, but different mineralization patterns prevail in the other mineralized stinging hairs found in Loasaceae, Namaceae and Caricaceae. In most mineralized stinging hairs, calcium carbonate makes up the bulk of the mineralization, but calcium phosphate and/or silica are commonly found at the base and the apex of the stinging hair, sometimes only as a superficial layer, but sometimes even in the entire wall. It has been shown previously that the exact type of biomineralization is quite diversified in the family Loasaceae (Ensikat et al., 2017). The present study shows that this phenomenon is not restricted to this family, but also present in the other plant taxa with mineralized stinging hairs. Morphologically, *Cnidoscolus* differs only by the much larger stinging hairs with much thicker walls, and this may well be due to the absence of biomineralization, requiring thicker cell walls for the same functionality. The overall relatively conserved morphology of the trichomes is in stark contrast to the divergence in biomineralization both within and between families.

In all stinging hairs, three different regions, often with specific mineralization can be defined: The tip with its preformed breaking point must be hard and brittle, so that the bulb breaks off easily and a sharp, mineralized edge is formed (Thurston and Lersten, 1969; Corsi, 1992; Tuberville et al., 1996; Farmer, 2014; Iwamoto et al., 2014). This is achieved with highly concentrated silica or calcium phosphate. The wall of the shaft forms a stiff, inelastic container, often formed by a calcium carbonate based or calcium phosphate-based composite material, which at its very base is often reinforced with a superficial coating of silica or calcium phosphate. The base is a flexible container with thin, unmineralized walls; its compression or deformation by mechanical force ejects the irritating liquid through the opened tip and injects it into the target. The different zones (tip, shaft, base) are also found in small trichomes which cover the leaf surfaces between the stinging hairs in many species. It seems remarkable that their mineralization patterns resemble those of the stinging hairs of the same species, with high silica or calcium phosphate concentrations in the tip and calcium carbonate in the shaft. Only in some Loasaceae species, scabrid-glochidiate trichomes contained different biominerals from the stinging hairs (Ensikat et al., 2017). Additional modifications are the layering of different biominerals in the tips of the stinging hairs of *Nasa*, or at the base of many stinging trichomes, even what appears to be a fine “silica-finish” across the entire surface of the stinging trichome in *Nasa* (Fig. S3 B).

### 4.5 Summary

Thurston and Lersten (1969) concluded “Stinging hairs, far from being merely classical text book objects, are instead complex structures with unusual characteristics and unsolved problems at all levels of organization”. This article, dealing solely with the walls of the stinging trichomes, clearly underscores this statement: complex, site-specific biomineralization is found in the bulk of the stinging trichomes investigated, indicating functional optimization of different parts of the cell wall using biomineral-composite structures of divergent composition and even using layering techniques, superimposing silica on calcium phosphate. Comparative biomechanical studies of the different stinging hairs and their differently mineralized parts would be required in order to come to a detailed functional understanding of the complex architecture of

stinging hairs. Stinging hairs – even as mechanical structures – are not simple cells with mineralized walls, but miracles of plant micro-engineering.

### 4.6 Acknowledgements

We kindly thank the staff of the Botanical Garden of the University of Bonn for growing and cultivation of plant species, Thomas Joßberger for vouchering specimens, and Dr. Federico Luebert for organizing and transporting herbarium specimens of *Cnidoscolus vitifolius* from the Royal Botanic Garden, Edinburgh, UK, and Dr. Günter Gerlach (Botanischer Garten München-Nymphenburg, Germany) for providing fresh plant samples of *Cnidoscolus urens*, *Dendrocnide moroides* and *Horovitzia cnidoscoloides*.

## 4.7 Literature cited


Cano-Santana, Z., and K. Oyama. 1994. *Wigandia urens* (Hydrophyllaceae): Un mosaico de recursos para sus insectos herbivoros. *Acta Botánica Mexicana* 28: 29–39.

Collier, H. O. J., and G. B. Chesher. 1956. Identification of 5-hydroxytryptamine in the sting of the nettle (*Urtica dioica*). *British Journal of Pharmacology* 11: 186–189.

Corsi, G. 1992. The stinging hair of *Urtica membranacea* Poiret (Urticaceae). II. Histochemistry. *Phyton* 32: 247–253.

Ensikat, H. J., T. Geisler, and M. Weigend. 2016. A first report of hydroxylated apatite as structural biomineral in Loasaceae - plants' teeth against herbivores. *Scientific reports* 6: 26073.

Ensikat, H. J., A. Mustafa, and M. Weigend. 2017. Complex patterns of multiple biomineralization in single-celled plant trichomes of the Loasaceae. *American Journal of Botany* 104: 195–206.

Farmer, E. E. 2014. Leaf Defense. *Oxford University Press*: 1–216.

Fu, H. Y., S. J. Chen, R. F. Chen, L. L. Kuo-Huang, and R. N. Huang. 2007. Why do nettles sting? About stinging hairs looking simple but acting complex. *Functional Plant Science and Biotechnology* 1: 46–55.

Fu, H. Y., S. J. Chen, and L. L. Kuo-Huang. 2003. Comparative study on the stinging trichomes and some related epidermal structures in the leaves of *Dendrocnide meyeniana*, *Girardinia diversifolia*, and *Urtica thunbergiana. Taiwania* 48: 213–223.

Haberlandt, G. 1886. Zur Anatomie und Physiologie der pflanzlichen Brennhaare. *Sitzungsber. Akad. Wiss. Wien* 93: 123–143.

Hooke, R. 1665. Micrographia: or some physiological descriptions of minute bodies made by magnifying glasses: with observations and inquiries thereupon. London: Allestry.

Hurley, M. 2000. Growth dynamics and leaf quality of the stinging trees *Dendrocnide moroides* and *Dendrocnide cordifolia* (family Urticaceae) in Australian tropical rainforest: implications for herbivores. *Australian Journal of Botany* 48: 191–201.

Iwamoto, M., C. Horikawa, M. Shikata, N. Wasaka, T. Kato, and H. Sato. 2014. Stinging hairs on the Japanese nettle *Urtica thunbergiana* have a defensive function against mammalian but not insect herbivores. *Ecological Research* 29: 455–462.

Kaplan, I., G. P. Dively, and R. F. Denno. 2009. The costs of anti-herbivore defense traits in agricultural crop plants: a case study involving leafhoppers and trichomes. *Ecologic*al *Applications* 19: 864–872.

Kariyat, R. R., C. M. Balogh, R. P. Moraski, C. M. De Moraes, M. C. Mescher, and A. G. Stephenson. 2013. Constitutive and herbivore-induced structural defenses are compromised by inbreeding in *Solanum carolinense* (Solanaceae). *American Journal of Botany* 100: 1014–1021.

Kariyat, R. R., J. D. Smith, A. G. Stephenson, C. M. De Moraes, and M. C. Mescher. 2017. Non-glandular trichomes of *Solanum carolinense* deter feeding by *Manduca sexta* caterpillars and cause damage to the gut peritrophic matrix. *In Proceedings of the Royal Society* 284: 20162323.

Küster-Winkelmann G. 1914. Das Haarkleid der Loasaceen. Doctoral dissertation. Friedrich-Alexander-Universität, Erlangen, Germany.

Lookadoo, S. E., and A. J. Pollard. 1991. Chemical contents of stinging trichomes of *Cnidoscolus texanus*. *Journal of Chemical Ecology* 17: 1909–1916.

MacFarlane, W. V. 1963. The stinging properties of *Laportea*. *Economic Botany* 17: 303–311.

Mustafa, A., H. J. Ensikat, and M. Weigend. 2017. Ontogeny and the process of biomineralization in the trichomes of Loasaceae. *American Journal of Botany* 104: 367–378.

Pollard, A. J., and D. Briggs. 1984. Geneocologial studies of *Urtica dioica* L. III. Stinging hairs and plant-herbivore interactions. *New Phytologist* 97: 507–522.

Pollard, A. J. 1986. Variation in *Cnidoscolus texanus* in relation to herbivory. *Oecologia* 70: 411–413.

Sletvold, N., P. Huttunen, R. Handley, K. Kärkkäinen, and J. Ågren. 2010. Cost of trichome production and resistance to a specialist insect herbivore in *Arabidopsis lyrata*. *Evolutionary Ecology* 24: 1307–1319.

Sowers, A. E., and E. L. Thurston. 1979. Ultrastructural evidence for uptake of silicon-containing silicic acid analogs by *Urtica pilulifera* and incorporation into cell wall silica. *Protoplasma* 101: 11–22.

Thurston, E. L., and N. R. Lersten. 1969. The morphology and toxicology of plant stinging hairs. *The Botanical Review* 35: 393–412.

Thurston, E. L. 1974. Morphology, fine structure, and ontogeny of the stinging emergence of *Urtica dioica. American Journal of Botany* 61: 809–817.

Thurston, E. L. 1976. Morphology, fine structure and ontogeny of the stinging emergence of *Tragia ramosa* and *T. saxicola* (Euphorbiaceae). *American Journal of Botany* 63: 710–718.

Tuberville, T. D., P. G. Dudley, and A. J. Pollard. 1996. Responses of Invertebrate Herbivores to Stinging Trichomes of *Urtica dioica* and *Laportea canadensis*. *Oikos* 75: 83–88.

Valverde, P. L., J. Fornoni, and J. Núñez-Farfán. 2001. Defensive role of leaf trichomes in resistance to herbivorous insects in Datura stramonium. *Journal of Evolutionary Biology* 14: 424–432.

Wagner, G. J., E. Wang, and R. W. Shepherd. 2004. New approaches for studying and exploiting an old protuberance, the plant trichome. *Annals of Botany* 93: 3–11.

War, A. R., M. G. Paulraj, T. Ahmad, A. A. Buhroo, B. Hussain, S. Ignacimuthu, and H. C. Sharma. 2012. Mechanisms of plant defense against insect herbivores. *Plant Signaling & Behavior* 7: 1306–1320.

Wicke, W. 1861. Über das Vorkommen und die physiologische Verwendung der Kieselsäure bei den Dicotyledonen. *Botanische Zeitschriften* 19: 97–100.

# CHAPTER 5

## Mineralized Trichomes in Boraginales – complex microscale heterogeneity and simple phylogenetic patterns

Cover image: Cryo-SEM compositional contrast image of the trichomes of *Codon royenii* (Codonaceae).

# Mineralized Trichomes in Boraginales – Complex Microscale Heterogeneity and Simple Phylogenetic Patterns*

**Running title: Biomineralization in Boraginales Trichomes**


## Abstract

**Background and Aims:** Boraginales are often characterized by a dense cover of stiff, mineralized trichomes, which may act as a first line of defence against herbivores. Recent studies have demonstrated that the widely reported silica and calcium carbonate may be replaced by calcium phosphate in plant trichomes. The present study investigates mineralization patterns in 42 species from 9 families of the order Boraginales in order to investigate detailed patterns of mineralization and the possible presence of a phylogenetic signal in different mineralization patterns.

**Methods:** The distribution of biominerals was analyzed by Scanning Electron Microscopy (SEM) including Cryo-SEM and EDX analyses with element mapping. The observed distribution of biominerals was plotted onto the phylogeny of the Boraginales by Luebert *et al.* (2016). Three colors were selected to represent the principle elements Si (red), Ca (green) and P (blue).

**Key Results:** Calcium carbonate was present in the mineralized trichomes of all 42 species, silica in 30 and calcium phosphate in 25 of the species investigated; multiple-mineralization with calcium carbonate and silica or calcium phosphate was found in all species, 13 of the species were mineralized with all three biominerals. Trichome tips featured the most regular pattern - nearly all were exclusively mineralized with either silica or calcium phosphate. Biomineralization of the trichome shafts and bases was found to be more variable between species. However, the trichome bases were also frequently mineralized with calcium phosphate or silica, indicating that not only the tip is under functional constraints requiring specific patterns of chemical



* Mustafa, A., Ensikat, H. J., Weigend, manuscript submitted to *Annals of Botany* (In press), 13/11/2017

heterogeneity. The complete absence of either silica or phosphate may be an additional feature with systematic relevance.

**Conclusions:** The study demonstrates that complex, site-specific and differential biomineralization is widespread across the order Boraginales. Calcium phosphate, only recently first reported as a structural plant biomineral, is common and appears to be functionally analogous to silica. A comparison with the phylogeny of Boraginales additionally reveals striking phylogenetic patterns. Most families show characteristic patterns of biomineralization, such as the virtual absence of calcium phosphate in Cordiaceae and Boraginaceae, the triple biomineralization of Heliotropiaceae and Ehretiaceae, or the absence of silica in Namaceae and Codonaceae. The complex chemical and phylogenetic patterns indicate that trichome evolution and functionalities are anything but simple and follow complex functional and phylogenetic constraints.

*Keywords***:** Biomineralization; Boraginales; Calcium phosphate; Silica; Calcium carbonate Trichomes; SEM; EDX

## 5.1 Introduction

Boraginales is a monophyletic plant group with subcosmopolitan distribution. It comprises ca. 2700 species in 125 genera and 11 families (Luebert *et al*., 2016). The order Boraginales falls into two major clades, Boraginales I resolved as [Codonaceae, [Wellstediaceae, [Boraginaceae]]], and Boraginales II resolved as [Hydrophyllaceae, [Namaceae, [Heliotropiaceae, [[Lennoaceae, Ehretiaceae], [Coldeniaceae, [Cordiaceae, Hoplestigmataceae]]]]]] (Weigend *et al*., 2014; Luebert *et al*., 2016). Leaves and stems of most Boraginales plants have long been known to be clothed in - often mineralized - trichomes (Jonová, 1926; Selvi and Bigazzi, 2001; Retief and van Wyk, 2005; Weigend and Hilger, 2010; Aleemuddin *et al*., 2011; Mehrabian *et al*., 2014; Weigend *et al*., 2014; Weigend *et al*., 2016). This is also reflected in the old Latin name for the group "Asperifoliae" and the modern German counterpart "Rauhblattgewächse" (= "rough leaf plants"). These mineralized trichomes show a range of structural features, including a large diversity of density, shape, and size, often dependent on their specific role and plant habitat (Diane *et al*., 2003). Mineralized trichomes are thought to play a crucial role in physical plant defense, e.g. via restricting herbivore movement in general and the access to vegetative and reproductive organs in particular (Reynolds and Rodriguez, 1981; Reynolds *et al*., 1986, 1989; He *et al*., 2012; Szyndler *et al*., 2013). Additional, non-defense functions of trichomes comprise a protection against water loss, high temperature and Ultraviolet-B radiation (Bickford, 2016). Mineral deposits in the sharp trichomes tips render them hard and enhance their mechanical stability (Johnson, 1975), but their relevance for other functionalities has not been studied. The formation of biogenic minerals in the outer cell walls of trichomes is indeed a widespread phenomenon found across many plant groups, but their mineral abundance and distribution in different types of trichomes varies widely between taxa (Thurston and Lersten, 1969; Ensikat *et al*., 2017; Mustafa *et al*., 2017). Calcium carbonate and silica have been widely reported as biominerals in the trichomes of a wide range of plant families in general, and Boraginales in particular (Hilger *et al*., 1993; Selvi and Bigazzi, 2001). In general, detailed patterns of biomineralization are poorly studied (He *et al*., 2014). However, our series of recent studies demonstrated the occurrence of multiple

biomineralization (calcium phosphate, calcium carbonate, silica) in stinging trichomes belonging to several angiosperm plant families, such as Caricaceae, Loasaceae, Urticaceae, Namaceae (Ensikat *et al*., 2016, 2017, Mustafa *et al*., 2017). Using scanning electron microscopy (SEM) and energy dispersive x-ray (EDX) analyses, the present study was undertaken in order to investigate the distribution of different biominerals across morphologically distinct types of trichomes in the order Boraginales. Preliminary data indicated that biomineralization in Boraginales is complex and variable and this triggered a more detailed study of biomineralization across the order Boraginales. The study addresses the following questions: (a) which biominerals are present in Boraginales trichomes and what is their distribution within trichomes; (b) can differential functionalities be inferred from the distribution patterns of individual biominerals; (c) are there phylogenetic patterns in the distribution of different biominerals?

## 5.2 Materials and methods

### 5.2.1 Sample preparation and microscopy

Fresh plant material was cultivated at the Botanical Garden of the University of Bonn, Germany, whereas the herbarium specimens were collected from the herbaria of the Nees-Institute for Biodiversity of Plants (BONN); Royal Botanical Garden, Kew, UK; and Institut für Biologie – Systematische Botanik und Pflanzengeographie, Freie Universität Berlin/ Botanische Gärten der Universität Berlin-Dahlem (BSB/B). At the Botanical Garden of the University of Bonn the plants were grown under three different temperature regimes depending on their regions of origin: temperate glasshouse with a minimum temperature of 13°C and an average temperature of 15°C to 17°C, a conservatory with minimum temperature of 10°C, and in the open during the summer months, respectively outdoor all year (most species). As a potting soil we used a peat-based mixture of 70% Einheitserde® ED73, and 30% sand. Einheitserde® ED73 consisting of 70% peat and 30% clay dust with a pH of 5.8 and pre-fertilized with a N: P: K ratio of 14: 16: 18 plus a slow-release fertiliser with a N: P: K ratio of 20: 10: 15. Plants were usually watered every other day. A total of 42 species

representing 9 families of the Boraginales were studied. Examined species with their voucher information are shown in Table 1. For EDX analysis and element mapping, fresh leaf samples were fixed in formaldehyde solution (70% ethanol + 4% formaldehyde) for 24 h, dehydrated, critical-point dried (CPD 020, Balzers Union, Liechtenstein), and sputter-coated with silver or palladium (SCD 040 Sputter-Coater: Balzers, Liechtenstein), using standard procedures described elsewhere (Ensikat *et al*., 2016).

Topographic imaging and EDX analyses were performed using a Cambridge S200 Stereoscan and a LEO 1450 SEMs (Cambridge, UK), which include secondary electron (SE) and backscattered electron (BSE) detectors and an EDX analysis system (Oxford Instruments, UK). Material contrast images were acquired from frozen, hydrated samples at ca. -100°C using a cryo stage (Ensikat *et al*., 2013). EDX was used for detection and mapping of the elements silicon (Si), phosphorus (P) and calcium (Ca). It has been previously demonstrated for trichome walls (Ensikat *et al*., 2017; Mustafa *et al*., 2017) that P is generally associated with Ca in the form of calcium phosphate, whereas Ca without P corresponds to a calcium carbonate-based composite, associated with organic compounds such as cellulose. This calcium carbonate composite is here simply referred to as calcium carbonate. All obtained images were recorded with a digital image acquisition system 'DISS 5' (Point Electronic, Halle, Germany). Image processing was carried out with standard image processing software (Paint Shop Pro X8, Corel GmbH, München, Germany). Material contrast color images were generated by combining secondary electron (SE) and backscattered electron (BSE) images, reflecting an increasing content of mineral elements (with higher atomic numbers than the main organic elements carbon and oxygen) in yellow to red hues, depending on the BSE contrast. Element color images were generated by combining SE images with one or two corresponding element mapping images, either Ca, P or Si distribution mappings. Three colors (red, green and blue) were chosen to demonstrate the distribution of the elements Si, Ca and P. The observed distribution of biominerals was plotted onto the phylogeny of the Boraginales by Luebert *et al.* (2016).

**Table 1.** Examined Taxon from nine plant families and their voucher information.

| Order | Family | Taxon | Region of origin | Herbarium |
|---|---|---|---|---|
| Boraginales | Codonaceae | *Codon royenii* D. Royen | Namibia | T. Joßberger 1247 |
| Boraginales | Codonaceae | *Codon schenckii* Schinz | Namibia | T. Joßberger 653 |
| Boraginales | Wellstediaceae | *Wellstedia dinteri* Pilg. | No Locality data | Dinter 4845 |
| Boraginales | Boraginaceae | *Borago officinalis* L. | France | T. Joßberger 1720 |
| Boraginales | Boraginaceae | *Borago pygmaea* (DC.) Chater & Greuter | Italy | T. Joßberger 1721 |
| Boraginales | Boraginaceae | *Echium italicum* S. G. Gmel. subsp. *Biebersteinii* (Lacaita) Greuter & Burdet | Georgia | T. Joßberger 759 |
| Boraginales | Boraginaceae | *Echium vulgare* L. | Germany | T. Joßberger 1037 |
| Boraginales | Boraginaceae | *Cerinthe major* L. subsp. *oranensis* (Batt.) Selvi & L. Cecchi | Germany | F. Selvi & M. Bigazzi 04.46 |
| Boraginales | Boraginaceae | *Myosotis sylvatica* Hoffm. | Hungry | T. Joßberger 1039 |
| Boraginales | Boraginaceae | *Ogastemma pusillum* (Coss. & Durieu ex Bonnet & Barratte) Brummitt | Israel | T. Joßberger 1609 |
| Boraginales | Boraginaceae | *Onosma alborosea* Fisch. & C. A. Mey. | Turkey | M. Ackermann 578 |
| Boraginales | Boraginaceae | *Podonosma orientalis* (L.) Feinbrun | Israel | T. Joßberger 1620 |
| Boraginales | Boraginaceae | *Symphytum caucasicum* M. Bieb. | Germany | T. Joßberger 1487 |
| Boraginales | Boraginaceae | *Symphytum officinale* L. | Germany | T. Joßberger 1723 |
| Boraginales | Boraginaceae | *Trachystemon orientalis* (L.) G. Don | Georgia | T. Joßberger 1438 |
| Boraginales | Boraginaceae | *Trichodesma africanum* (L.) Sm. | Israel | T. Joßberger 953 |

| | | | | |
|---|---|---|---|---|
| Boraginales | Hydrophyllaceae | *Hydrophyllum canadense* L. | No Locality data | T. Joßberger 1584 |
| Boraginales | Hydrophyllaceae | *Hydrophyllum virginianum* L. | Austria | T. Joßberger 1820 |
| Boraginales | Hydrophyllaceae | *Hydrophyllum tenuipes* A. Heller | USA | T. Joßberger 1556 |
| Boraginales | Hydrophyllaceae | *Nemophila menziesii* Hook. & Arn. | USA | T. Joßberger 1889 |
| Boraginales | Hydrophyllaceae | *Phacelia brachyantha* Benth. | Chile | F. Luebert 3182 |
| Boraginales | Hydrophyllaceae | *Phacelia malvifolia* Cham. | USA | T. Joßberger 1502 |
| Boraginales | Hydrophyllaceae | *Phacelia secunda* J. F. Gmel. | Chile | T. Joßberger 1722 |
| Boraginales | Hydrophyllaceae | *Draperia systyla* Torr. | USA | T. Joßberger 1752 |
| Boraginales | Hydrophyllaceae | *Eriodictyon crassifolium* Benth. | USA | T. Joßberger 1611 |
| Boraginales | Namaceae | *Nama rothrockii* A. Gray | USA | T. Joßberger 38768 |
| Boraginales | Namaceae | *Wigandia caracasana* Kunth | Peru | T. Joßberger 1619 |
| Boraginales | Namaceae | *Wigandia ecuadorensis* Cornejo | Ecuador | T. Joßberger 899 |
| Boraginales | Namaceae | *Wigandia urens* Ruiz & Pav.) Kunth | Peru | T. Joßberger 1717 |
| Boraginales | Heliotropiaceae | *Heliotropium corymbosum* Ruiz & Pav. | Peru | T. Joßberger 820 |
| Boraginales | Heliotropiaceae | *Heliotropium europaeum* L. | Turkmenistan, Turkestan | T. Joßberger 762 |
| Boraginales | Heliotropiaceae | *Heliotropium rufipilum* I. M. Johnst. | Ecuador | T. Joßberger 696 |
| Boraginales | Heliotropiaceae | *Tournefortia johnstonii* Standl. | No Locality data | Det. James S. Miller, 2000 |
| Boraginales | Heliotropiaceae | *Tournefortia cuspidata* Kunth | No Locality data | Jose Gonzalez 787; Det. James S. Miller |

| | | | | |
|---|---|---|---|---|
| Boraginales | Ehretiaceae | *Ehretia dicksonii* Hance | Germany | T. Joßberger 1220 |
| Boraginales | Ehretiaceae | *Ehretia microphylla* Lam. | No Locality data | T. Joßberger 1715 |
| Boraginales | Ehretiaceae | *Tiquilia* cf. *dichotoma* (Ruiz & Pav.) Pers. | Peru | M. Weigend, H. Förther and N. Dostert 688 |
| Boraginales | Ehretiaceae | *Tiquilia* cf. *elongata* (Rusby) A. T. Richardson | Peru | M. Weigend & F. Cáceres-H. 9081 (MW_06) |
| Boraginales | Coldeniaceae | *Coldenia procumbens* L. | Burkina Faso | T. Joßberger 1305 |
| Boraginales | Cordiaceae | *Cordia monoica* Roxb. | Kenya | T. Joßberger 1874 |
| Boraginales | Cordiaceae | *Varronia bahamensis* (Ubs.) Millsp. | Bahamas | M. A. Hamilton 64831000 |
| Boraginales | Cordiaceae | *Varronia rupicola* (Ubs.) Britton | Puerto Rico | M. A. Hamilton 2014-384 |

## 5.3 Results

### 5.3.1 Overview of trichome mineralization

Leaf surfaces of all investigated taxa are covered by morphologically different types of mineralized trichomes in variable densities and shapes. Figure 1 illustrates typical trichomes morphologies and the extent of the mineral deposits in their outer walls. The dual-detector cryo-SEM images show mineralized parts in yellow-to-red colors, reflecting an increasing content of mineral elements, such as Ca, P or Si. Many taxa from different families of the Boraginales have small non-mineralized glandular trichomes with a rounded apical cell and usually larger, eglandular, unicellular, mineralized trichomes with sharp tips (Fig. 1A-F). The mineralized trichomes generally consist of a single trichome cell, usually basally surrounded by a ring of foot cells. In most of the species examined the pluricellular bases are non-mineralized, but in some species they are found to be partially mineralized [e.g., *Onosma alborosea*, (*Phacelia malvifolia*, Fig. 1C)], sometimes extensively so. The foot cells may form a pedestal carrying the large trichome cell, with *Codon royenii* (Fig. 1A) representing an extreme case with the unicellular mineralized trichome sitting atop a massive, pluricellular "spine", which is distally heavily mineralized. Several species (e.g., *Codon royenii*, *Phacelia malvifolia*, Fig. 1A, C) carry clearly distinguishable trichomes of different sizes: large ones sitting atop a pluricellular pedestal and much smaller ones covering the epidermis without a pedestal and occurring at very high densities. The mineralized trichomes universally have a sharp tip; trichome surface is sometimes smooth (*Codon royenii*, *Phacelia malvifolia*, *Nama rothrockii*; Fig. 1A, C, D), sometimes grooved (*Onosma hispida*, *Heliotropium corymbosum*; Fig. 1B, E), or densely verrucose (*Coldenia procumbens*; Fig. 1F).

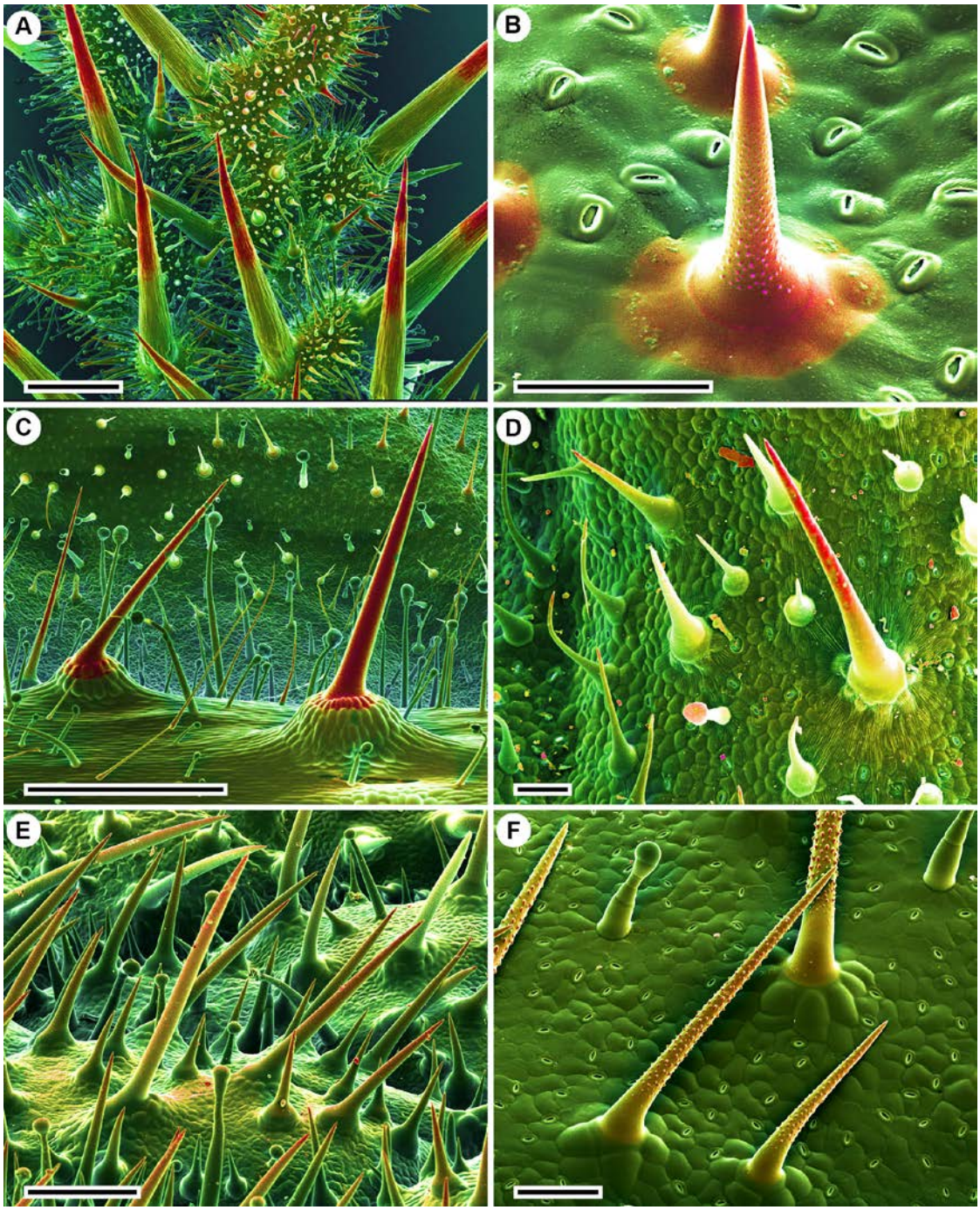


**Figure 1.** Cryo-SEM micrographs of typical trichomes on the leaves of different Boraginales plant families. (A) *Codon royenii* (Codonaceae); large trichomes consist of a mineralized single apical cell located on a high pluricellular, distally mineralized pedestal. In between are numerous small, partially mineralized trichomes and non-mineralized glandular trichomes. (B) *Onosma hispida* (Boraginaceae); stiff unicellular trichomes with a pointed tip, inserted on a ring of indistinct foot cells; mineralization (yellow to red color) extends onto the foot cells. (C) *Phacelia malvifolia* (Hydrophyllaceae); unicellular trichomes with multicellular base and needle-shaped unicellular, mineralized trichomes inserting on one row of mineralized foot cells, non-mineralized glandular trichomes are also abundantly represented. (D)

*Nama rothrockii* (Namaceae); sharp-tipped unicellular trichomes with a smooth surface. (E) *Heliotropium corymbosum* (Heliotropiaceae); unicellular hispid trichomes with granular surface pattern. (F) *Coldenia procumbens* (Coldeniaceae); spinulose, mineralized trichomes and non-mineralized glandular trichomes. The combined topographical and compositional contrast images show regions with higher mineral concentrations in yellow to red, whereas green color indicates the absence of mineral elements. Scale bars: A, C = 1000 µm; B, D, F = 100 µm; E = 300 µm.

### 5.3.2 Systematic distribution of patterns of biomineralization

Our data clearly document the widespread occurrence of the three elements, calcium (Ca), phosphorus (P), and silicon (Si), indicating the presence of three different biominerals in the plant trichomes: Ca in the absence of P indicates various inorganic or organic calcium carbonate compounds; plant trichomes usually contain calcium carbonate-based composites with organic material such as cellulose. Here we refer to this phenomenon as biomineralization with calcium carbonate. The simultaneous detection of Ca and P indicates the presence for calcium phosphate - P is always found in combination with Ca in trichome walls and appears to be present in the form of calcium phosphate-based composite with varying parts of organic matter and calcium carbonate. Si occurs as biomineral silica ($SiO_2$). The combined topography and element-mapping images in Fig. 2 show either Ca or P in green colors (Ca: yellow-to-green or P: green-to-blue, depending on increasing concentration) and Si in red. The colorized combined element distribution images of representative species of three different plant families show remarkable differences in the mineral components, particularly in the tips and in the bases of the trichomes. Ca (green color in Fig. 2A, E, I) over the entire shafts of trichomes was found in the majority of the taxa investigated. In contrast, the tips and bases of the trichomes show characteristic mineralization patterns, which can be assigned to three different basic patterns of biomineralization.

The first pattern represents calcified trichomes with calcium phosphate tips, e.g., *Codon royenii* (Fig. 2A, B), and no silica at all. The second pattern represents calcified trichomes with calcium phosphate in the trichome tips, whereas silica is dominant in the bases, e.g., *Tiquilia* cf. *elongata* (Fig. 2E, F). In some cases silica and calcium phosphate are found side-by-side at the trichome bases. The third pattern represents

calcified trichomes with silica in high concentrations in their tips and in varying amounts at their bases, sometimes accompanied by calcium phosphate (e.g., *Borago officinalis*, Fig. 2I, J). Magnesium (Mg) was frequently found at low and variable concentrations in the trichomes of several plant species of Boraginales (Fig. 2C, D, G, H, L). It occurred together with Ca in the entire trichomes, but the concentration ratio of Mg to Ca was highly variable, arguing against a fixed mineral formation. Thus, the trichome tips were found to show relatively uniform mineralization pattern across all species examined, containing either silica or calcium phosphate in high concentration. In many cases the occurrence of calcium phosphate or silica in the tips was restricted to a very small region at the very apex of the trichomes, but in several species they extended over wider parts of the shafts (e.g., Fig. 2F). In contrast to the trichome tips, the shafts showed rather less characteristic patterns. Calcium carbonate was mostly dominant, but silica and calcium phosphate were also found in varying concentrations. The biomineral patterns of the trichome bases generally differed from the shafts, but the variability was much higher than in the trichome tips. Particularly, basal regions of young, developing trichomes or partially mineralized trichomes appeared non-mineralized, because mineralization usually starts at the apex and thus the bases are the last part of the trichome to become fully mineralized (Mustafa *et al*., 2017). EDX spectra of tips and bases of the selected examples illustrate the high mineral concentrations particularly in the tips. A comparison of the height ratios of the P and Ca peaks with those of pure apatite-like calcium phosphate shows that many trichome tips contain (more or less pure) calcium phosphate, whereas lower P-to-Ca ratios indicate mixed phases containing both calcium phosphate and carbonate. We hesitate to present quantitative data, because the concentrations of the light elements carbon and oxygen cannot be determined with any accuracy with the technique here employed: Surface topography, detector position, surface coatings such as cutin and metal coating strongly influence the carbon and oxygen measurements. In Figure 3 the biomineralization data are mapped onto a phylogeny of Boraginales, differentiating between the occurrence of the three biominerals in the tips and basal regions of the species examined so far. It is obvious that particularly the mineral contents of the trichome tips correlate with the phylogenetic position of the species.

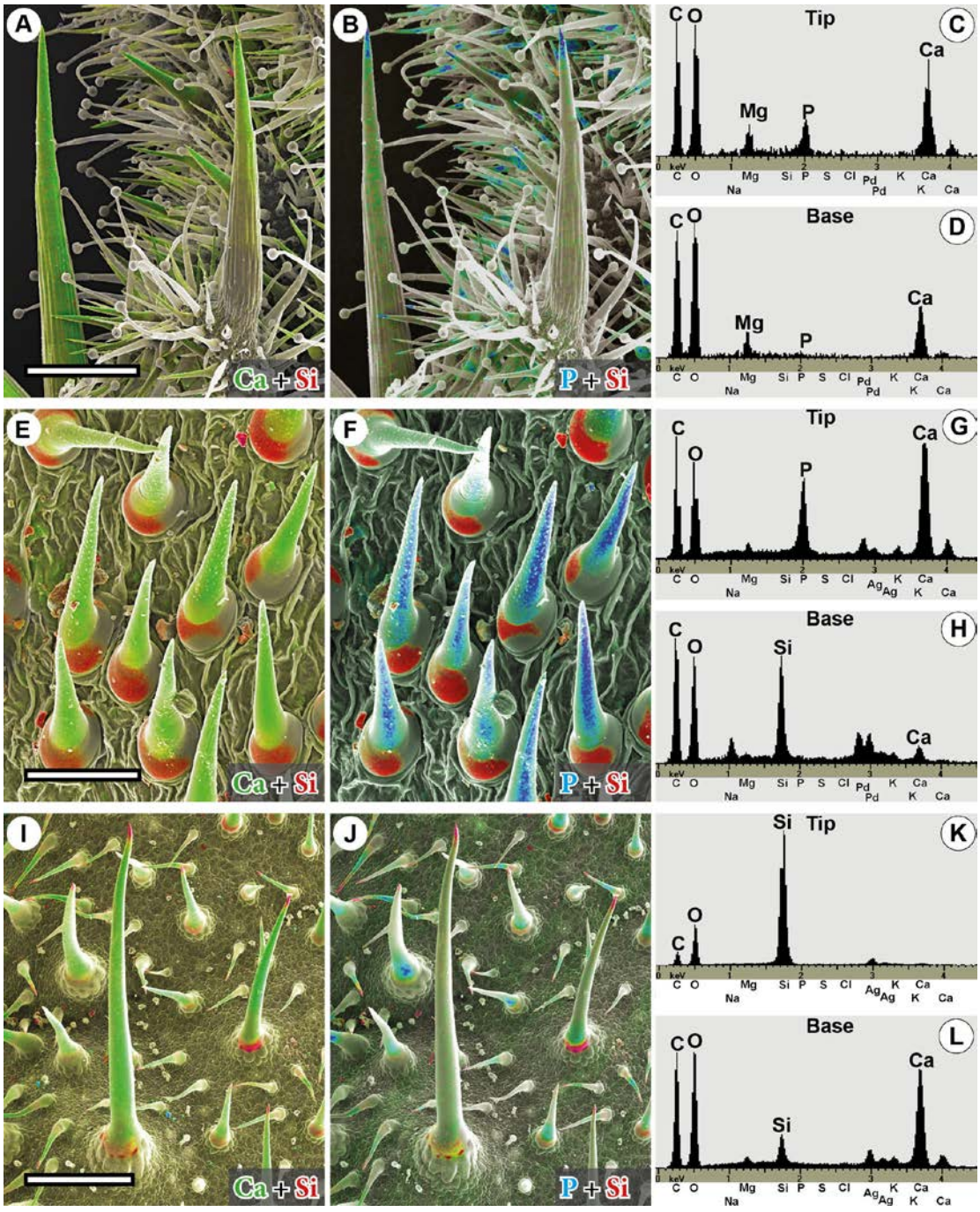


**Figure 2.** Combined topographic and element-mapping micrographs of critical-point dried leaves of representative species of *Codon royenii* (Codonaceae, A-D) *Tiquilia* cf. *dichotoma* (Ehretiaceae, E-H) and *Borago officinalis* (Boraginaceae, I-L) showing the various mineralization patterns. The colors identify the distribution of the elements Ca (green) and Si (red) in A, E, I respectively the elements P (blue) and Si (red) in B, F, J. The EDX spot spectra from the tips and bases of the trichomes illustrate the presence of the mineral elements Si, P, and Ca. The large trichomes of *Codon* contain Ca in the main cell and some adjacent cells of the pedestal, whereas P (calcium phosphate) is restricted to the tip.

Si is absent. The trichomes of *Tiquilia* contain Ca and P in high concentrations in their tips and shafts. The bases contain mostly Si, but also Ca and P in an adjacent area. *Borago* has very high concentration of Si in the tips; the bases contain Si and P; the shafts only Ca. The peaks of Ag or Pd in the spectra, due to sputter coating with these metals to avoid charging during SEM analyses. Scale bars: A, B = 500 µm; E, F =100 µm; I, F = 500 µm.

By and large, the families (with all their species studied so far) can be assigned to one of the mineralization patterns defined above. Based on Fig. 3, trichomes of Pattern 1 (calcium phosphate tips, no silica) occur in 12 out of 42 species. Trichomes with calcium phosphate tips in general (Patterns 1 and 2; trichome bases with or without silica) are reported from seven plant families, namely Codonaceae, Coldeniaceae, Ehretiaceae, Heliotropiaceae, Hydrophyllaceae, Namaceae and Wellstediaceae. In 16 species from two families, Boraginaceae and Cordiaceae, the trichomes tips were strongly mineralized with silica (Pattern 3). In our limited sampling of Heliotropiaceae we found species with silica tips (*Tournefortia*) and others with calcium phosphate tips (*Heliotropium*), but the sampling of these large genera appears too small to draw any conclusion at the genus level. Silica, sometimes co-occurring with calcium phosphate, was found in the trichome bases of a wider range of species, including representatives of Boraginaceae, Coldeniaceae, Cordiaceae, Ehretiaceae, Heliotropiaceae and some Hydrophyllaceae. Biominerals in the shafts showed a considerable variability within plant families; the main component calcium carbonate was often accompanied by silica or calcium phosphate in varying concentrations. Overall, the data here presented indicate a considerable phylogenetic signal in the detailed patterns of biomineralization. Only two of the 42 species had trichomes with aberrant mineral patterns for their respective phylogenetic group: *Ehretia microphylla* has short and stiff trichomes with pointed tips mineralized with silica and calcium phosphate; *Eriodictyon crassifolium* has long, thin, partially mineralized trichomes with calcium phosphate in the tips while the basal regions were not mineralized. Overall, both Boraginales I and Boraginales II appear to have clades which are mineralized predominantly or exclusively with calcium carbonate and phosphate, whereas the more derived families in both clades appear to be increasingly mineralized with silica.

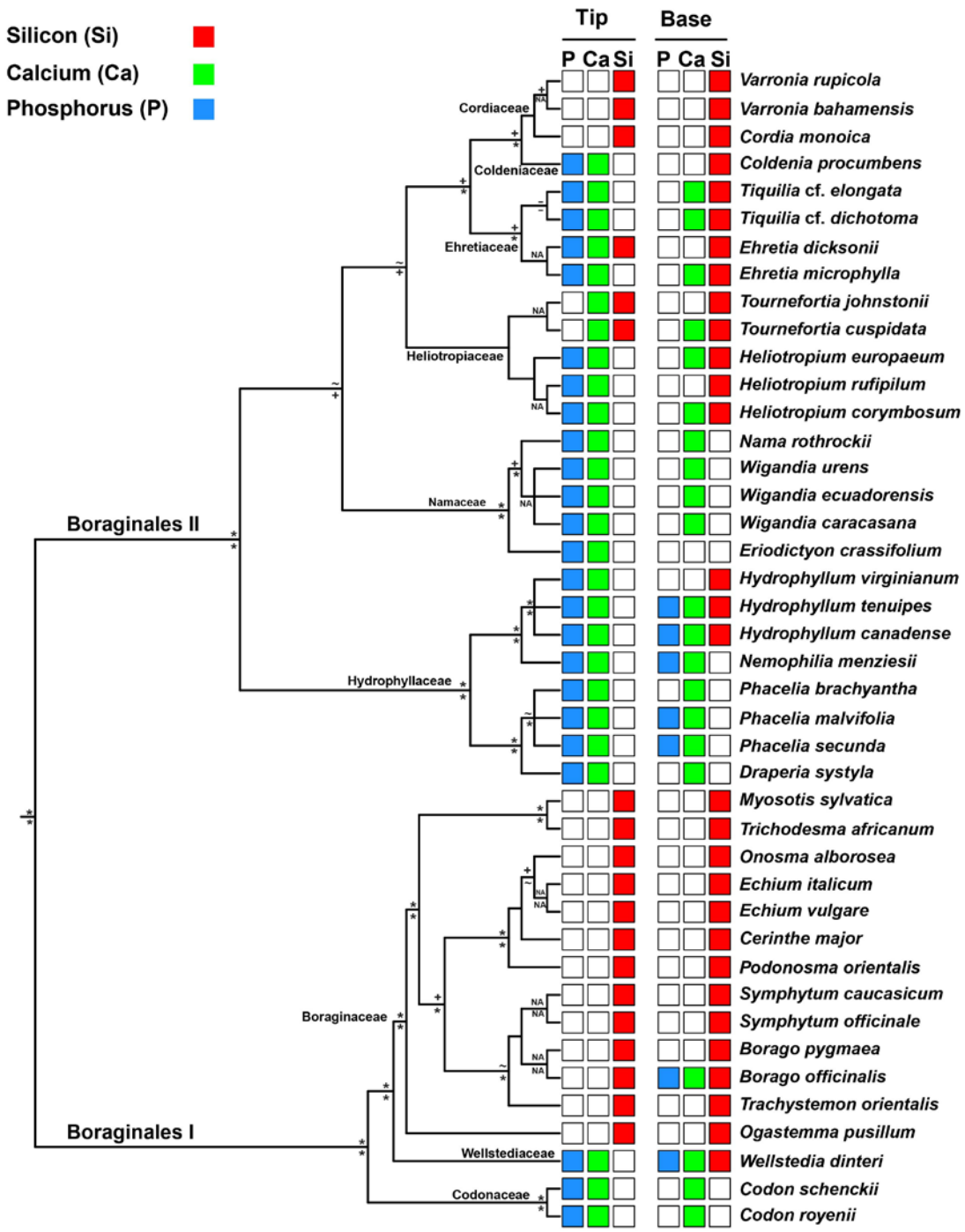


**Figure 3**. Phylogeny of the Boraginales with specific trichome zones plotted onto the terminal branches. The selected colors demonstrate the principle distribution of the elements Si (red), Ca (green) and P (blue). Backbone topology is based on Weigend *et al*. (2014). The topologies of some of the

individual families are based on following publications: Boraginaceae, Chacón *et al*. (2016); Ehretiaceae, Gottschling *et al*. (2014), Hydrophyllaceae Walden *et al*. (2014); Cordiaceae, Hamilton (2016). Supported values are taken from Weigend *et al*. (2014) and the above cited sources. Figures above the lines indicate Bayesian posterior probability, the symbols below the lines indicate maximum likelihood bootstrap support. The clade with an asterisk (*) are very highly supported groups (Bayesian posterior probability = 1.0, likelihood bootstrap value 100). The clades marked with a (+) are moderately supported (Bayesian posterior probability 0.99-0.9, maximum likelihood bootstrap values 99-75) in Weigend *et al*. (2014). The clades with a tilde (~) are weakly supported (Bayesian posterior probability 0.89-0.80, maximum likelihood bootstrap values 74-50). The clades with minuses (–) have no support (Bayesian posterior probability <0.80, maximum likelihood bootstrap values <50), whereas the not assigned support values are shown as "NA".

### 5.3.3 Detailed localization of the biominerals

Figure 4 and Supplementary figures 1-3 show some detailed patterns of biomineralization. The colorized images of one or a few representative species of each plant family illustrate the localization of calcium phosphate and silica, represented by the elements P and Si, in isolated single trichomes. Figure 4A-C shows three examples of 'Pattern 1' with calcium phosphate (green), but no silica (red). In *Codon schenckii* and particularly *Nama rothrockii*, calcium phosphate is limited to the very apex (Appendix chapter 5, Fig. S1). Separate grayscale mapping images are here used, since they are more suitable for illustrating co-localized elements present at low concentrations. In *Phacelia malvifolia*, calcium phosphate was found along the entire trichome, with elevated concentrations at the base and the apex. The examples of 'Pattern 2' (Fig. 4D-G; Fig. S2) show calcium phosphate in high concentrations in the tips. Three species have silica in the base (*Ehretia dicksonii*, *Heliotropium corymbosum*, *Coldenia procumbens* (Fig. 4E-G). One species, *Hydrophyllum canadense* (Fig. 4D), contains both silica and calcium phosphate in its base, but in two clearly delimited regions. The presence of three biomineral at different locations can also be demonstrated for *Wellstedia dinteri* (Fig. S3). Calcium is present in all parts of the trichomes (not colorised) except in locations with high Si concentrations. Figure 5 shows details of the element distribution in "Pattern 3" (trichomes with silica tips) in separate gray-scale mapping images for Si and Ca. The extent of the silicified regions varies strongly. Small silica deposits in the apex and at the base were found in *Echium*

*italicum* and *Tournefortia cuspidata*. In *Trichodesma africanum* and *Varronia bahamensis* the silicified regions is more extensive, whereas the trichomes of *Trachystemon orientalis* are completely silicified. Trichomes of *Borago officinalis* show high concentrations of Si in both the base and the apex and lower Si concentrations in the shaft. Ca is found in all parts except regions with high Si concentrations. Sometimes, P occurs at low concentrations, e.g., in *Trichodesma africanum* and in *Borago officinalis*.

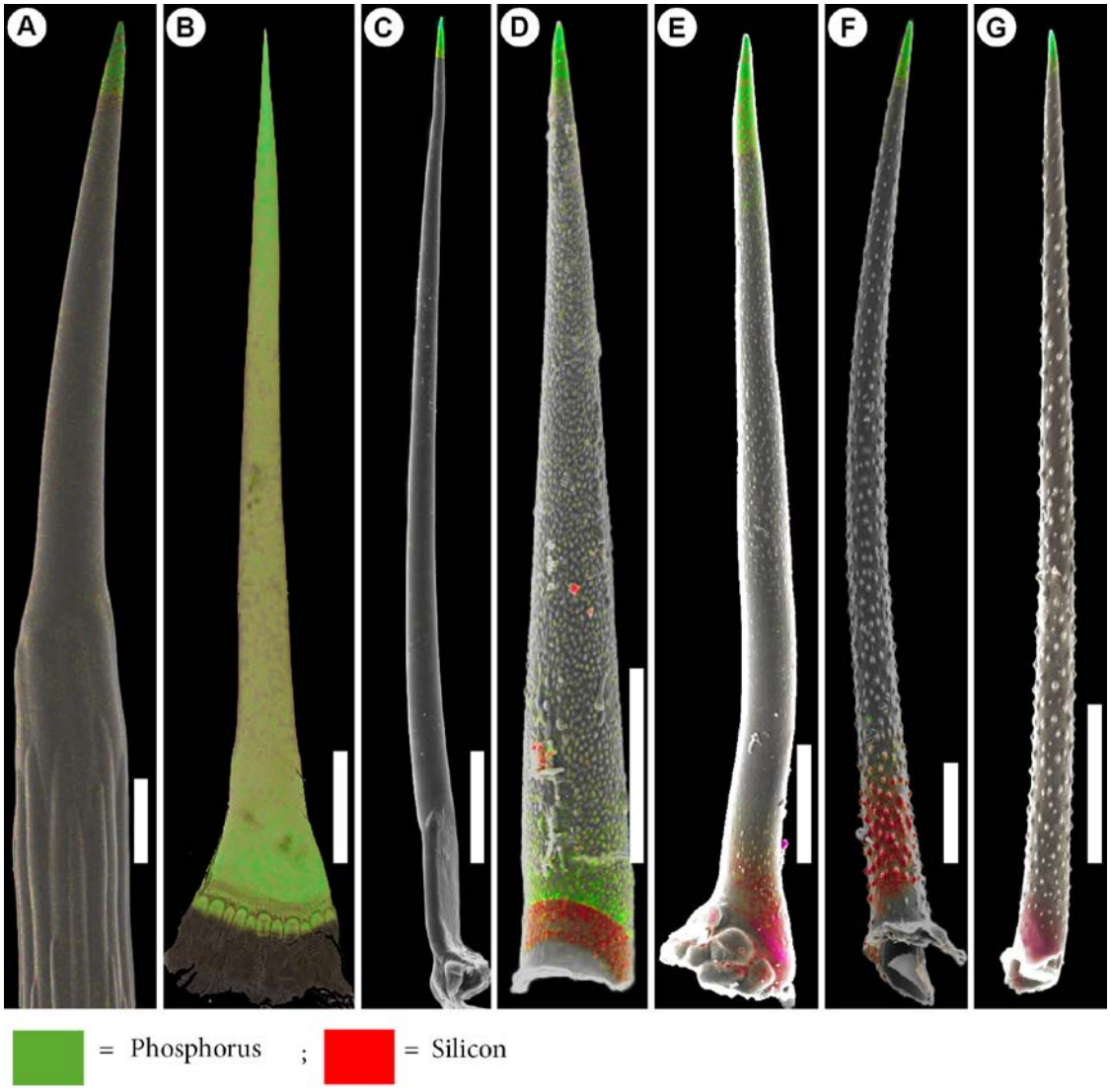


**Figure 4**. SEM images showing the element distribution in the trichomes of representative species of Codonaceae, Hydrophyllaceae, Namaceae, Heliotropiaceae, Ehretiaceae and Coldeniaceae. (A-C)

Occurrence of calcium phosphate but no silica at all; (A) *Codon schenckii*; high concentrations of calcium phosphate restricted to the tip regions. (B) *Phacelia malvifolia*; both tip and base regions mineralized with high concentrations of calcium phosphate, lower P concentrations in the shaft. (C) *Nama rothrockii*; calcium phosphate is restricted to a very short apical region of the trichome tip. (D-G) Calcium phosphate tips and silica in the bases; (D) *Hydrophyllum canadense*; (E) *Heliotropium corymbosum*; (F) *Ehretia dicksonii*; (G) *Coldenia procumbens.* Combined topographic and EDX element-mapping images show the distribution of P in green and Si in red. Calcium is present in the entire trichomes but not colorized. Scale bars: A, C, D, E, F, G = 100 µm; B = 250 µm.

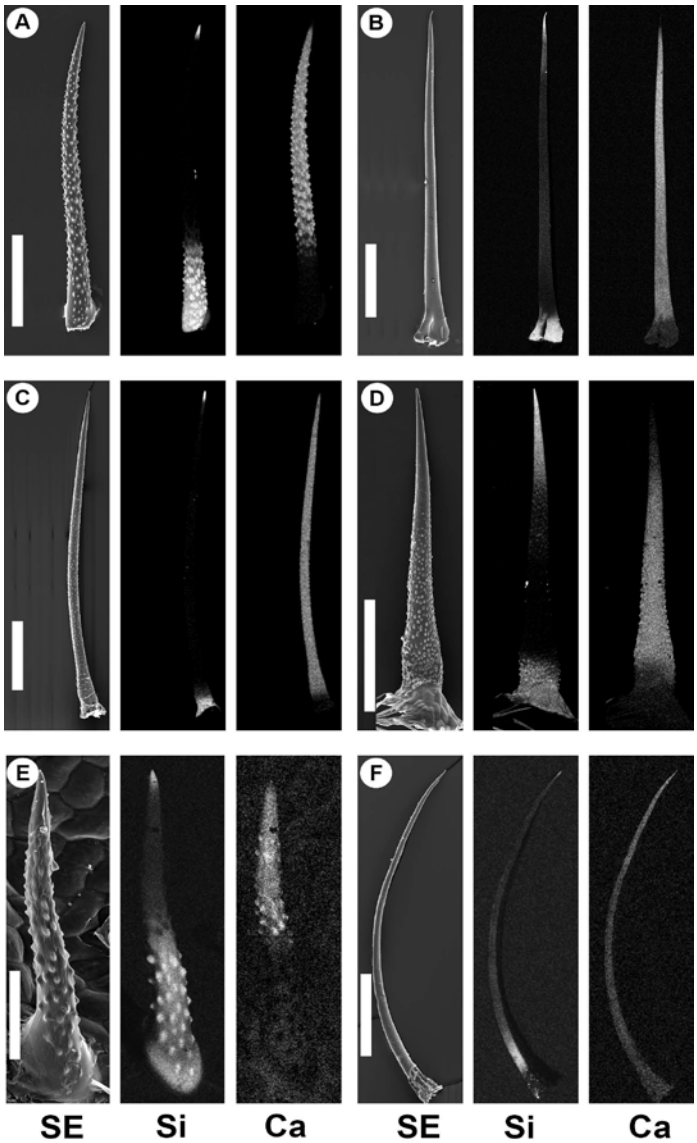


**Figure 5.** Topogaphic (SE) and element-mapping images of trichomes of selected Boraginaceae, Cordiaceae and Heliotropiaceae species with silicified tips. (A) *Ogastemma pusillum*; (B) *Borago*

*officinalis*; (C) *Echium italicum;* (D) *Trichodesma africanum*; (E) *Varronia bahamensis*; (F) *Tournefortia cuspidata.* The distribution of elements appears to be highly structured: The tips and bases of all trichomes are exclusively silicified, but the extent of the silica deposits varies strongly. Ca is present in all parts except the regions with high Si concentration. P was generally absent or present in traces only and therefore not shown here. Scale bars: A, E = 200 µm; B, C, D, F = 500 µm.

## 5.4 Discussion

The present study expands the range of structural biominerals in Boraginales from calcium carbonate and silica to calcium phosphate, recently documented for the first time as a structural plant biomineral in Loasaceae (Cornales, Ensikat *et al.*, 2016). Calcium carbonate is present in the mineralized trichomes of all 42 species investigated, silica in 30 and calcium phosphate in 25 of the species investigated, 13 species are mineralized with all three biominerals. Biomineralization is thus varied and complex across the plant order, similar to what has been reported from the family Loasaceae (Ensikat *et al.*, 2017).

Within the individual trichomes, there are clear patterns of biomineral distribution. The tips generally contain a hard biomineral in high concentration, either silica or calcium phosphate. The trichome shafts usually contain calcium carbonate, often with varying portions of silica or calcium phosphate. The bases of fully developed trichomes often contain silica or calcium phosphate at specific locations, together with calcium carbonate. The highly specific localization of silica and calcium phosphate deposits, found in most trichomes, indicates a strict cellular and genetic control of their deposition and - likely - a crucial functional component. The areas generally mineralized with calcium phosphate and silica are those where particular hardness is required. This is true for the apex of the trichomes, which is supposed to mechanically damage herbivore skin and which is mineralized with at least one of the two minerals in all 42 species studied. Similarly, the base of the trichome may need to be particularly stiff in order to ensure that the trichome is not easily broken off and has the required rigidity to perform its defensive role. This portion of the trichome is mineralized with one of the calcium phosphate and/or silica in 33 of the 42 species studied. Universally, wherever a particularly hard or stiff biomineral is required, either calcium phosphate or silica appears to be employed rather interchangeably across

Boraginales. The nine species without calcium phosphate or silica in their base comprise fives species (genera *Codon* and *Wigandia*) with massive, pluricellular pedestals, which evidently require no re-enforcement by biominerals to provide the requisite rigidity. The mineralized trichome bases are usually surrounded by a ring of foot cells. The remaining taxa are species of *Nama, Draperia, Eriodictyon* and *Phacelia* with very dense and relatively soft pubescence, likely with a primary role in drought protection rather than herbivore defense. This indicates, that biomineralization in the base is reduced in taxa where organic compounds take over their role due to larger size of the base (pedestal) and/or more massive cell walls respectively where mechanical rigidity is not a central aspect of trichome functions, because the defense function is secondary.

The detailed patterns of biomineral distribution show some degree of phylogenetic sorting. The early branching families in both major clades of Boraginales appear to be primarily (Namaceae, Hydrophyllaceae) or exclusively (Codonaceae, Wellstediaceae) mineralized with calcium carbonate and phosphate. Conversely, the more derived groups (Broaginales I – Boraginaceae, Boraginales II - Coldeniaceae, Ehretiaceae, Cordiaceae and Heliotropiaceae) show either triple mineralization, or silica largely replacing calcium phosphate. This, to the best of our knowledge, is the first time a clear phylogenetic signal can be documented for patterns of multiple biomineralization. In most of the species investigated the foot cells were non-mineralized, but in some species they were found to be heavily mineralized with silica i.e. *Wellstedia dinteri* (Fig. S3) and *Onosma hispida*. This is in agreement with a study of Selvi and Bigazzi (2001), demonstrating massive silica deposits in the trichome foot cells of *Anchusa formosa* and *Trachystemon orientalis*, indicating that this may be a wide-spread pattern at least in the corresponding subgroup Boraginaceae subfam. Boraginoideae (Chacón *et al*., 2016). Selvi and Bigazzi (2001) also mention the presence of phosphorus and sulfur in the tubercles of some species of *Nonea*, but without elaborating on the exact distribution. Calcium sulphate (gypsum) has been reported as a biomineral in plants, e.g., in the form of crystals in different plant tissues (*Acacia robeorum*, He *et al*., 2012; Caryophyllaceae, Cistaceae and Fabaceae, Palacio *et al*. 2014). A recent study on leaves collected from 23 gypsophiles and related non-endemic taxa growing on non-gypsum soils, demonstrated the presence of gypsum in

the leaves of several Chihuahuan Desert gypsum endemics, including the gypsophiles *Nama carnosa* and *Tiquilia hispidissima* (Muller *et al*., 2017) as representatives of the Boraginales. However, to date no conclusive evidence for structural biomineralization with gypsum has been brought forward, i.e., the incrustation of trichomes or glochidia with calcium phosphate as here demonstrated for calcium phosphate, calcium carbonate and silica. Future studies could investigate the possible presence of gypsum as a structural biomineral in gypsum endemic species of Boraginaceae such as *Cryptantha gypsophila* (Reveal and Broome, 2006) and *Moltkia gypsacea* (Rabizadeh *et al*., 2016). In general, it seems that biomineralization in Boraginales is more diversified than previously assumed. Evidently, the complex distribution of biominerals within individual plants and the phylogenetic patterns here demonstrated invite studies on the genetic basis of trichome evolution and mineralization, but also on the differential functionalities of mineralized trichomes across the taxa here investigated.

### 5.5 Acknowledgements

We are grateful to *F. Luebert* (Nees Institut für Biodiversität der Pflanzen, BONN); *M. Hamilton* (Research Leader, UKOTs; Royal Botanical Garden, Kew, UK); *T. Henning* (Botanischer Garten und Botanisches Museum Berlin-Dahlem) for organizing the plant specimens. We thank *J. Jeiter* for helping us in collecting plant material, coding phylogenetic tree and useful suggestions in writing manuscript. We would like to express our sincere gratitude to *T. Joßberger* for vouchering the collections and preparing the herbarium specimens.

## 5.6 Literature cited

**Aleemuddin MA, Karthikeyan M, Rajasekar S. 2011**. *Coldenia procumbens* Linn. – A phytopharmacological review. *International Journal of Pharmaceutical Sciences Review and Research* **11**: 133.

**Bickford CP. 2016.** Ecophysiology of leaf trichomes. *Functional Plant Biology* **43**: 807–814.

**Chacón J, Luebert F, Hilger HH, et al. 2016**. The borage family (Boraginaceae s. str.): A revised infrafamilial classification based on new phylogenetic evidence, with emphasis on the placement of some enigmatic genera. *Taxon* **65**: 523–546.

**Diane N, Jacob C, Hilger HH. 2003**. Leaf anatomy and foliar trichomes in Heliotropiaceae and their systematic relevance. *Flora* **198**: 468–485.

**Ensikat HJ, Geisler T, Weigend M. 2016.** A first report of hydroxylated apatite as structural biomineral in Loasaceae - plants' teeth against herbivores. *Scientific Reports* **6**: 26073.

**Ensikat HJ, Mustafa A, Weigend M. 2017**. Complex patterns of multiple biomineralization in single-celled plant trichomes of the Loasaceae. *American Journal of Botany* **104**: 195–206.

**Ensikat HJ, Weigend M. 2013.** Cryo-scanning electron microscopy of plant samples without metal coating, utilizing bulk conductivity. *Microscopy and Analysis* **27***:* 7–10.

**Gottschling M, Luebert F, Hilger HH, Miller JS. 2014.** Molecular delimitations in the Ehretiaceae (Boraginales). *Molecular Phylogenetics and Evolution* **72**: 1–6.

**Hamilton MA. 2016**. Boraginaceae *Varronia rupicola* (Urb.) Brtton: biogeography, systematic placement and conservation genetics of a threatened species endemic to the Caribbean. PhD thesis, Birkbeck, University of London, UK.

**He H, Bleby TM, Veneklaas EJ, Lambers H, and Kuo J. 2012.** Morphologies and elemental compositions of calcium crystals in phyllodes and branchlets of *Acacia robeorum* (Leguminosae: Mimosoideae). *Annals of Botany* **109**: 887–896.

**He H, Veneklaas EJ, Kuo J, and Lambers H. 2014.** Physiological and ecological significance of biomineralization in plants. *Trends in Plant Science* **19**: 166–174.

**Hilger HH, Hoppe JR, Hofmann M. 1993**. Energiedispersive Röntgenmikroanalyse (EDX) von Boraginaceae subfam. Boraginoideae - Klausenoberflächen. Sind Silicium- und Calcium- Einlagerungen in die Fruchtwand systematisch verwertbare Merkmale? *Flora* **188**: 387–398.

**Johnson HB. 1975**. Plant pubescence: an ecological perspective. *The Botanical Review* **41**: 233–258.

**Jonová, M. 1926.** Anatomie a morfologie trichomu u Borraginacei s ohledem na systematiku této celedi (L'anatomie et al morphologie des trichomes des Borraginées à l'égard du système de cette famille) [Anatomie und Morphologie der Trichome bei den Borraginaceen mit Rücksicht auf die Systematik dieser Familie]. Vestnik Král. Ceské Spolecn. Nauk, *Trida Mathematicko-Prirodovedecka*. **2**: 1–66.

**Luebert F, Cecchi L, Frohlich MW, et al. 2016.** Familial classification of the Boraginales. *Taxon* **65**: 502–522.

**Mehrabian AR, Sheidai M, Mozaffarian V. 2014**. Micromorphology of leaf trichomes in *Onosma* (Boraginaceae) and their systematic relevance in Iran. *Phytologia Balcanica* **20**: 41–56.

**Muller CT, Moore MJ, Feder Z, Tiley H, and Drenovsky RE. 2017.** Phylogenetic patterns of foliar mineral nutrient accumulation among gypsophiles and their relatives in the Chihuahuan Desert. *American Journal of Botany* **104**: 1442–1450.

**Mustafa A, Ensikat HJ, Weigend M. 2017.** Ontogeny and the process of biomineralization in the trichomes of Loasaceae. *American Journal of Botany* **104**: 367–378.

**Palacio S, Aitkenhead M, Escudero A, Montserrat-Martí G, Maestro M, Robertson AJ. 2014.** Gypsophile chemistry unveiled: Fourier transform infrared (FTIR) spectroscopy provides new insight into plant adaptations to gypsum soils. *Plos One* **9**: e107285.

**Rabizadeh F, Zare-Maivan H, and Kazempour S. 2017.** Endemic Gypsophytes Composition Delimitated by Soil Properties and Altitude from Calciphytes and Halophytes in the South-Central Alborz Ranges. *Nordic Journal of Botany*, in press. doi:10.1111/njb.01568

**Retief E, van Wyk AE. 2005**. Boraginaceae: Codonoideae, a new subfamily based on *Codon*. *Bothalia* **35**: 78–80.

**Reveal JL, Broome CR. 2006**. *Cryptantha gypsophila* (Boraginaceae: Boraginoideae), a New Species from Western Colorado. *Brittonia* **58**: 178–181.

**Reynolds GW, Epstein WL, Rodriguez E. 1986**. Unusual contact allergens from plants in the family Hydrophyllaceae. *Contact Dermatitis* **14**: 39–44.

**Reynolds GW, Gafner F, Rodriguez E. 1989**. Contact allergens of an urban shrub *Wigandia caracasana*. *Contact Dermatitis* **21**: 65–68.

**Reynolds GW, Rodriguez E. 1981**. Prenylated hydroquinones: contact allergens from trichomes of *Phacelia minor* and *P. parryi*. *Phytochemistry* **20**: 1365–1366.

**Selvi F, Bigazzi M. 2001.** Leaf surface and anatomy in Boraginaceae tribe Boragineae with respect to ecology and taxonomy. *Flora* **196**: 269–285.

**Szyndler MW, Haynes KF, Potter MF, Corn RM, Loudon C. 2013**. Entrapment of bed bugs by leaf trichomes inspires microfabrication of biomimetic surfaces. *Journal of The Royal Society Interface* **10**: 20130174.

**Thurston EL, and Lersten NR. 1969.** The morphology and toxicology of plant stinging hairs. *The Botanical Review* **35**: 393–412.

**Walden GK, Garrison LM, Spicer GS, Cipriano F W, Patterson R. 2014.** Phylogenies and chromosome evolution of Phacelia (Boraginaceae: Hydrophylloideae) inferred from nuclear ribosomal and chloroplast sequence data. *Madroño* **61**: 16–47.

**Weigend M, Hilger HH. 2010**. Codonaceae - a newly required family name in Boraginales. *Phytotaxa* **10**: 26–30.

**Weigend M, Luebert F, Gottschling M, Couvreur TL, Hilger HH, Miller JS. 2014.** From capsules to nutlets – phylogenetic relationships in the Boraginales. *Cladistics* **30**: 508–518.

**Weigend M, Selvi F, Thomas DC, Hilger HH. 2016**. Boraginaceae. In: Kubitzki K, ed. *The families and genera of vascular plants*, vol 14. Heidelberg: Springer, 41–102.

# CHAPTER 6

## Calcium phosphate in plant trichomes: the overlooked biomineral

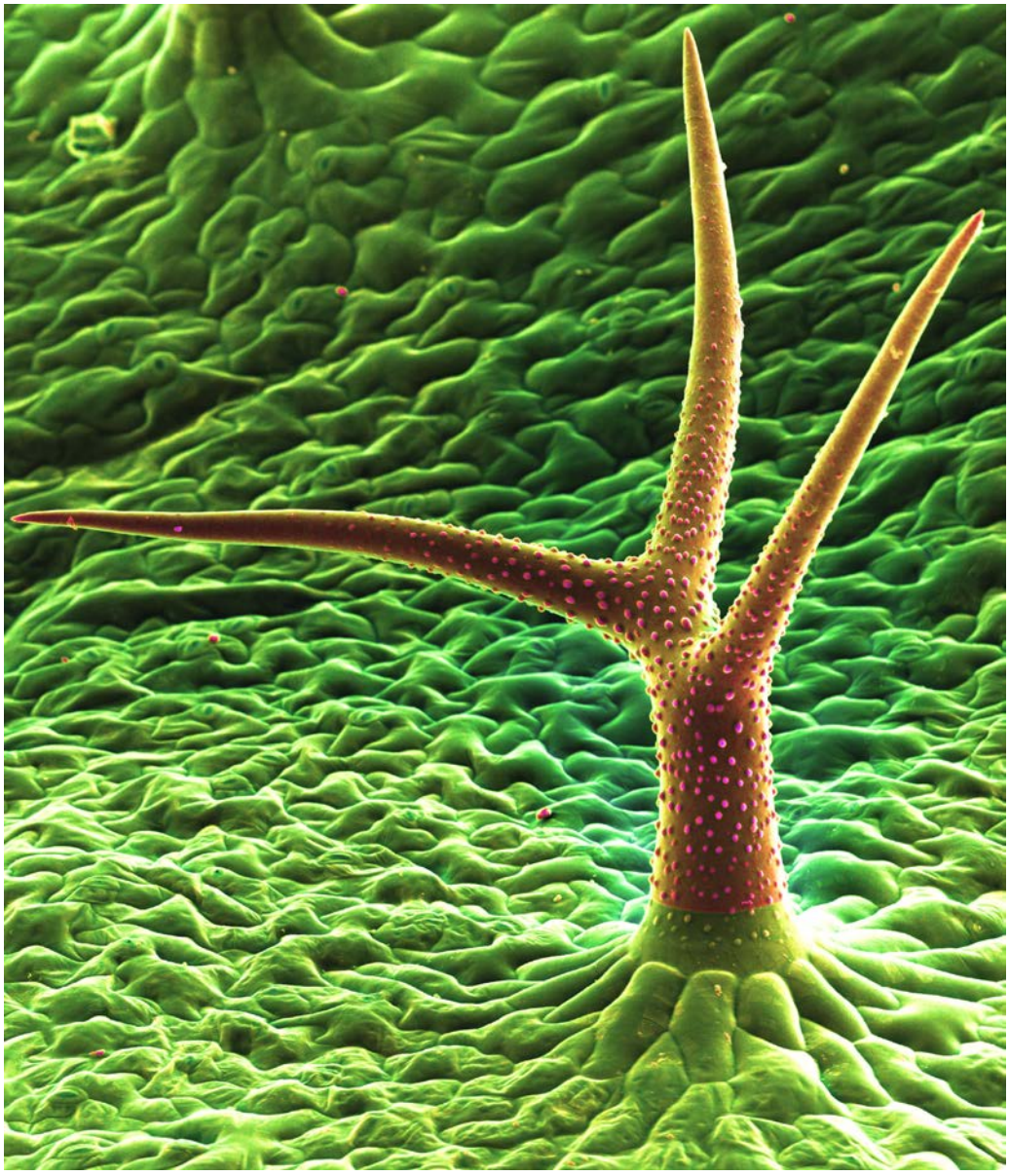

Cover image: Cryo-SEM micrograph of a trichome on the leaf of *Arabidopsis thaliana*. The false-color image highlights mineralized surfaces with calcium and phosphorus by a color shift towards yellow to red and non-mineralized surfaces in green.

# Calcium phosphate in plant trichomes: the overlooked biomineral*


## Abstract

### *Main Conclusion*

**Calcium phosphate was unknown as a plant biomineral until recently reported in Neotropical Loasaceae. Here we demonstrate its widespread occurrence in the trichomes of several plant families, including Brassicaceae.**

Calcium phosphate is the primary biomineral in, e.g., the bones and teeth of higher animals; in plants it was only recently discovered in the stinging hairs and scabrid-glochidiate trichomes of South American Loasaceae (Ensikat et al. in Sci Rep UK 6:26073, 2016), where it appears to be deposited highly specifically, often replacing the common plant biomineral silica. We initiated a broader survey in a range of different plant orders in order to investigate a possibly wider distribution of calcium phosphate biomineralization in plants. Scanning electron microscopy with EDX element analysis and mapping was used for the detection of the biominerals calcium phosphate, calcium carbonate, and silica in the trichomes of several common plant species of different orders. Results were authenticated with Raman-spectroscopy. Calcium phosphate was found in the trichomes of several species in the orders Malpighiales, Rosales, Boraginales and Brassicales. It occurred in trichome tips, replacing the more common silica, or together with silica and calcium carbonate at specific locations in the trichome cell walls. Most surprisingly, it was found in the trichomes of *Arabidopsis thaliana*, one of the most studied plant species – where it had been overlooked so far. The wide distribution of calcium phosphate as plant biomineral here demonstrated and the striking mineralization patterns with three different biominerals in the walls of single-celled trichomes underscore an unexpected complexity in plant biomineralization.



* Weigend, M., Mustafa, A., Ensikat, H. J. 2018. Calcium phosphate in plant trichomes: the overlooked biomineral. *Planta* 247(1), 277–285.

Keywords: *Arabidopsis thaliana*, biomineralization, calcium phosphate, plant trichomes, silica, calcium carbonate.

## Abbreviations

BSE Backscattered Electron

EDX Energy Dispersive X-Ray Analysis

## 6.1 Introduction

Phosphorus is widely recognized to play a major role in plant growth, and the mobilization of and access to phosphorus are considered to have had major impacts on the evolution of life on land (Oldroyd et al. 2009; Harpole and Stanley 2016) and in the sea (Guidry and Mackenzie 2000; Smith and Harper 2013). Phosphate is an essential component of basic structures in every living cell and occurs, e.g., in phospholipid molecules in cell membranes and is part of DNA and RNA molecules and adenosine phosphates (ADP, ATP; Vance et al. 2003). The crucial importance of phosphorus for plant growth and the limited availability of phosphate rocks for the productions of industrial fertilizers are a source of major concern (Cordell et al. 2013; George et al. 2016), and unravelling the molecular basis of phosphate uptake and utilization is the focus of dozens of scientific studies, especially on the model organism *Arabidopsis thaliana*, but also a range of important crop plants (Kaur et al. 2016). Phosphate has thus been abundantly documented to play a physiological role in plants, with the chemical properties of phosphate taking the lead role. The long list of plant uses for phosphorus was recently expanded by structural calcium phosphate biomineralization in the morphologically complex trichomes of Loasaceae (Cornales; Ensikat et al. 2016, 2017), where the physical properties of calcium phosphate appear to play the crucial role. Biomineralization as such is a fairly common phenomenon in plants (He et al. 2014), but calcium phosphate was previously not known to play a role in angiosperm biomineralization. It is, however, widely documented from the animals, with hydroxyl apatite the primary biomineral in teeth and bones (Lowenstam 1981; Franceschi and Nakata 2005; He et al. 2014). In plants, the combined occurrence of P and Ca has occasionally been reported, but calcium phosphate had not been confirmed

as being present as a biomineral. Thus, studies on heavy metal-accumulating plants demonstrate the co-occurrence of P, Ca (and other metals, e.g., Küpper et al. 2000), but the concentrations of P and other metals were much lower than the Ca concentration. Lin et al. (2004) found P and Ca in cystoliths of *Justicia procumbens* in a ratio close to that in apatite, but this does not qualify as proof of structural biomineralization.

In mineralized plant trichomes, the trichome tips usually contain hard minerals in high concentration, either silica or calcium phosphate, while the shaft and base are often less strongly mineralized typically with calcium carbonate only. This chemical heterogeneity has been previously reported from, e.g., *Helianthus tuberosus* L. with differential deposition of silica and calcium compounds in foot cells versus trichome cells (Lanning and Eleuterius 1987). After the first discovery of calcium phosphate replacing silica in the trichomes of Loasaceae (Ensikat et al. 2016, 2017; Mustafa et al. 2017), we investigated the possible presence and localization of calcium phosphate in the mineralized structures from other plant families. We selected taxa from the angiosperm orders Boraginales, Rosales, Brassicales, Cucurbitales and Malpighiales, thus focusing on plants which are known to possess mineralized trichomes.

## 6.2 Materials and methods

### 6.2.1 Plant material

All plants used were cultivated at the Botanische Gärten der Universität Bonn: *Arabidopsis thaliana* Columbia 0 (*TJH* 084); *Arabidopsis thaliana* (Accession 21507, *A. Mustafa* 01); *Aubrieta deltoidea* (Accession 12640, *TJH* 1803); *Blumenbachia insignis* (Accession 36150, *T. Jossberger* 1210); *Caiophora lateritia* (Accession 37012, *T. Jossberger* 1653); *Codon royenii* (Accession 34837, *T. Jossberger* 1247); *Fibigia clypeata* (Accession 8348, *TJH* 1804); *Loasa tricolor* (Accession 37098); *Phacelia malvifolia* (Accession 37883, *T. Jossberger* 1502);*Urtica dioica* (Accession 4919, *T. Jossberger* 1665); *Urtica fissa* (Accession 29914, *TJH* 1802). All species are vouchered at the herbarium of the Nees-Institut für Biodiversität der Pflanzen (BONN).

### 6.2.2 Scanning electron microscopy and sample preparation

A Cambridge Stereoscan S200 SEM (Cambridge, UK) with a custom-made cryo stage and a LEO 1450 SEM (Cambridge, UK) with an EDX system (Oxford Instruments, Oxford, UK) were used for microscopy and element analyses with mapping. EDX analyses were measured with acceleration voltages between 10 and 20 kV; usually 15 kV for surface analyses and 10 kV for element mapping of sections. Material contrast images were produced by cryo-SEM from frozen hydrated plant material at ca. -100°C with simultaneous acquisition of secondary electron (SE) images and backscattered electron (BSE) images. Cryo-preparation is described in detail by Ensikat and Weigend (2013). Color images were generated by combining SE images with BSE images or element mapping images of selected elements using image processing software. The separate grayscale SE-, BSE-, and element-mapping images, used for rendering of color images, are presented as supplementary data. Raman spectra were collected with a confocal Horiba Scientific HR800 Raman spectrometer at the Steinmann Institute of Bonn University, Bonn, Germany. (For details, see Ensikat et al., 2016.) Plant samples for EDX analyses and element mapping were fixed for at least 24 h in 70% ethanol with 4% formaldehyde, followed by dehydration with acetone and critical-point drying with carbon dioxide. Frozen samples were usually examined without a metal coating; dried samples were sputter-coated with a thin palladium layer of 10 to 15 nm thickness. In contrast to gold, palladium does not disturb the EDX-detection of certain elements of interest such as phosphorus and silicon.

## 6.3 Results

After the study of biomineralization of Loasaceae (Cornales) trichomes with their complex morphology and multiple mineralization with calcium carbonate, calcium phosphate, and silica (Fig. 1, Appendix chapter 6, Fig. S1a, b), we initiated a study on the mineralization patterns in the trichomes of other plant orders. Even in our limited survey we found a remarkable diversity in the mineralization patterns. Silicified trichome tips are widespread, but we also recognized calcium phosphate biomineralization in a range of different plant groups, such as Boraginales, Rosales,

Brassicales, Malpighiales, and Apiales. The order Boraginales has long been known for the widespread occurrence of mineralized trichomes. *Codon royenii* from the family Codonaceae is covered with particularly stiff trichomes (Fig. 2a-e). A detailed view with material contrast reveals that both the large apical cell and the uppermost cells of the pluricellular pedestal are strongly mineralized (Fig. 2a). Element mapping (Fig. 2b-e) shows largely Ca (calcium carbonate) in the selected part; only a small region of the tip of the trichome cell is strongly mineralized with calcium phosphate. *Phacelia malvifolia* (Hydrophyllaceae) from California also has notably stiff and spiny trichomes (Fig. 2f), mineralized with calcium carbonate and calcium phosphate; here calcium phosphate is present along the entire trichome, the concentration peaking at the apex (spectrum, Fig. 2h), decreasing towards the median portion of the stinging trichome and increasing again towards the base (line scan, Fig. 2i). The stinging trichomes of Stinging Nettles (genus *Urtica*, Urticaceae, Rosales, Fig. 3a) have long been known to be mineralized with silica and calcium carbonate. East Asian *Urtica fissa*, however, is mineralized with calcium phosphate along its entire shaft, with the highest concentration near the base; only the tip is silicified (Fig. 3b-h).

Thus, taxa across the orders Rosales, Boraginales and Cornales appear to be able to use calcium phosphate as a structural biomineral, always in combination with calcium carbonate and silica in different parts of the cell wall of the same individual cell. Surprisingly, an investigation of the comparatively small trichomes of Brassicaceae (Brassicales) could also demonstrate the occurrence of calcium phosphate. The branched, unicellular trichomes of *Arabidopsis thaliana* (Fig. 4) are heavily mineralized with calcium compounds, apart from their very base. The apices of its trichome branches and the granular structures on the trichome surface are incrusted with calcium phosphate in varying concentrations, as indicated by EDX spectra from selected spots (Fig. 4b-e), and by Raman spectra of *Arabidopsis thaliana* trichome tip (Fig. 5). A study of other representatives of Brassicaceae could demonstrate that the common ornamental plant *Aubrieta deltoidea* has also mineralized trichomes, but calcium phosphate occurs only in the very apices of the trichome branches (Fig. 6a-c). A similar pattern is found in the Mediterranean annual *Fibigia clypeata*, also from Brassicaceae. In these taxa calcium phosphate mineralization is restricted to very small distal parts of the trichome, in contrast to calcium carbonate which is present in the

entire trichomes. So far, we have analyzed 32 species of Loasaceae (Ensikat et al. 2017), 42 species from 9 families of the order Boraginales **(**Mustafa et al. In press), and ca. 20 species of other plant groups (data not shown). In total, 67 out of 94 species contained calcium phosphate (ca. 71%), mostly in trichome tips, where it replaced the more common silica. Remarkably, all Brassicales species contained calcium phosphate but no silica in their trichomes. Most of these results are to be published elsewhere.

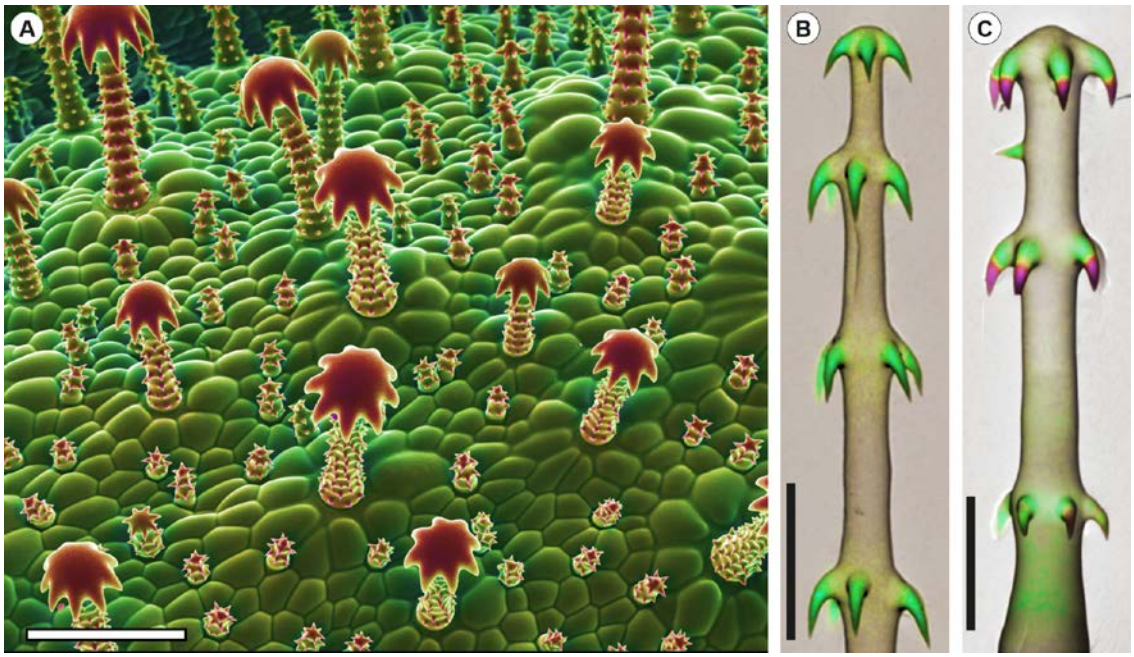


**Fig. 1** SEM images of glochidiate trichomes on Loasaceae. **a** The cryo-SEM image with combined topographical and compositional contrast of trichomes on the inferior ovary of *Blumenbachia insignis* shows mineralized structures in yellow-to-red tones, due to the high content of heavier element such as Ca, P, or Si. The apical caps and tips of the spiny protrusions are heavily mineralized. **b-c** Combined Si and P element mapping images of single glochidiate trichomes of *Loasa tricolor* (**b**) and *Caiophora lateritia* (**c**) show that not only the morphology, but also the mineralization patterns appear complex. The cell walls are mineralized with two or three different biominerals: The shafts contain Ca compounds (not colorized); P (green) occurs together with Ca as calcium phosphate in the hooks of *Loasa* trichomes and in hook shoulders and trichome bases of *Caiophora*; Si (red) indicates silica in the tips of the *Caiophora* trichome hooks. Scale bars = 100 µm (**a**), 30 µm (**b-c**). Corresponding grayscale SE-, BSE-, and element-mapping images, used for rendering of the color images, are presented as supplementary data.

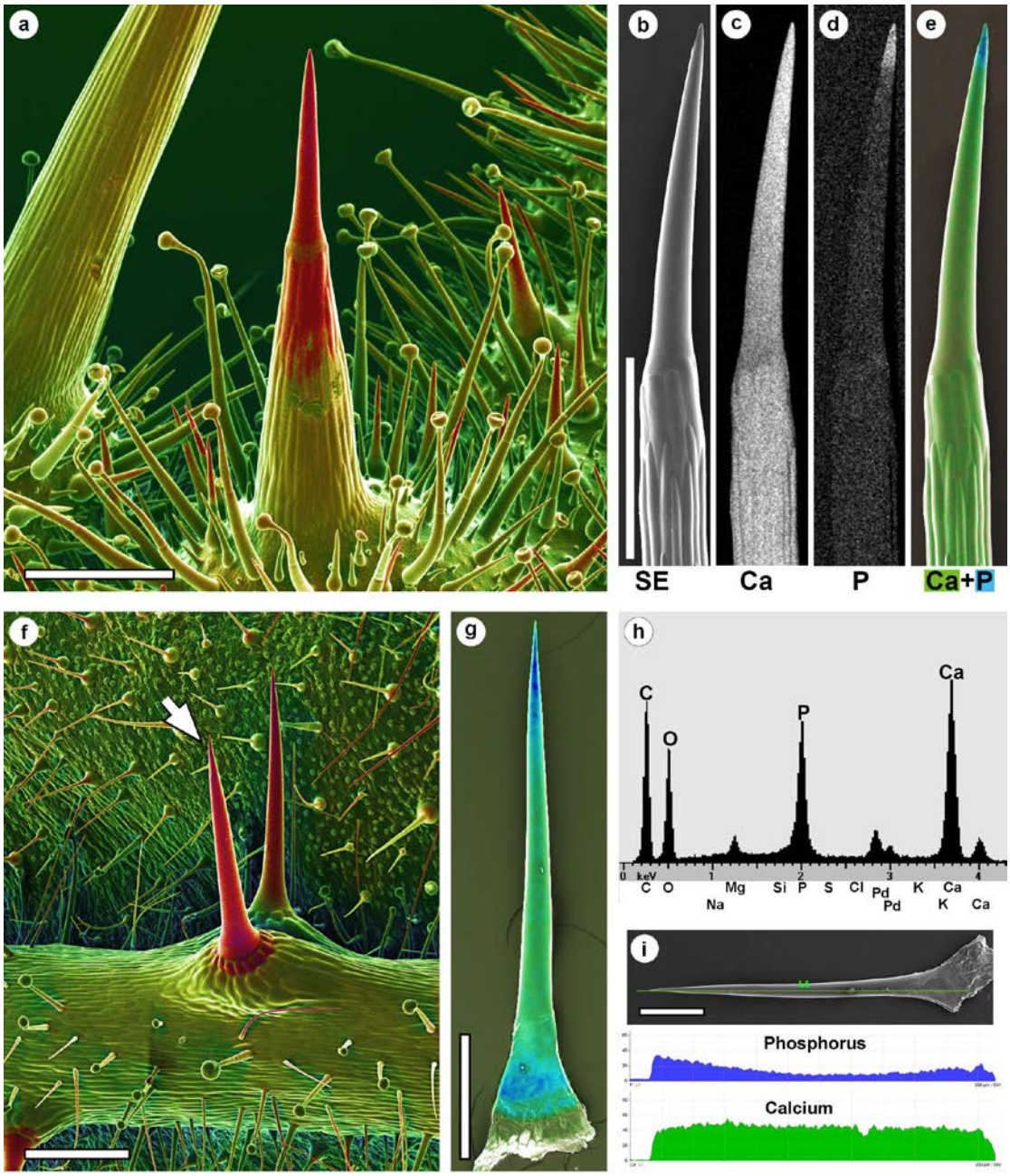


**Fig. 2** Mineralization patterns and calcium phosphate distribution in the trichomes of Codonaceae and Hydrophyllaceae. **a-e** *Codon royenii* with phosphate in the trichome tip only. **a** The cryo-SEM compositional contrast image shows strong mineralization in in the upper half of the trichome (red color), including some cells of the pedestal below the apical cell. A detailed view of the tip using SE imaging (**b)** and element mapping shows Ca in the entire mineralized part (**c**) whereas P (calcium phosphate) occurs only in the uppermost tip (**d**). The combined SE/Ca/P image (**e**) shows calcium phosphate in blue and calcium carbonate in green color. **f-h** *Phacelia malvifolia* with calcium phosphate in the entire trichome. The cryo-SEM image (**f)** shows the mineralized trichomes in red color. **g** Combined SE/Ca/P-mapping image showing areas with high P concentration in blue, high Ca

concentrations in green. The EDX spectrum (**h)** from the trichome tip (arrow in **f**) shows high concentrations of P and Ca in relation to carbon (C) from organic matter. The P-to-Ca ratio reaches almost that of pure apatite [$Ca_5(PO_4)_3OH$]. **i** An EDX line scan from tip to base of a single trichome shows the relative concentrations of P and Ca. The Ca concentration appears almost constant, the P concentration is highest at the tip, decreases towards the middle, and rises again towards the base. Scale bars = 400 µm (**a-h).**

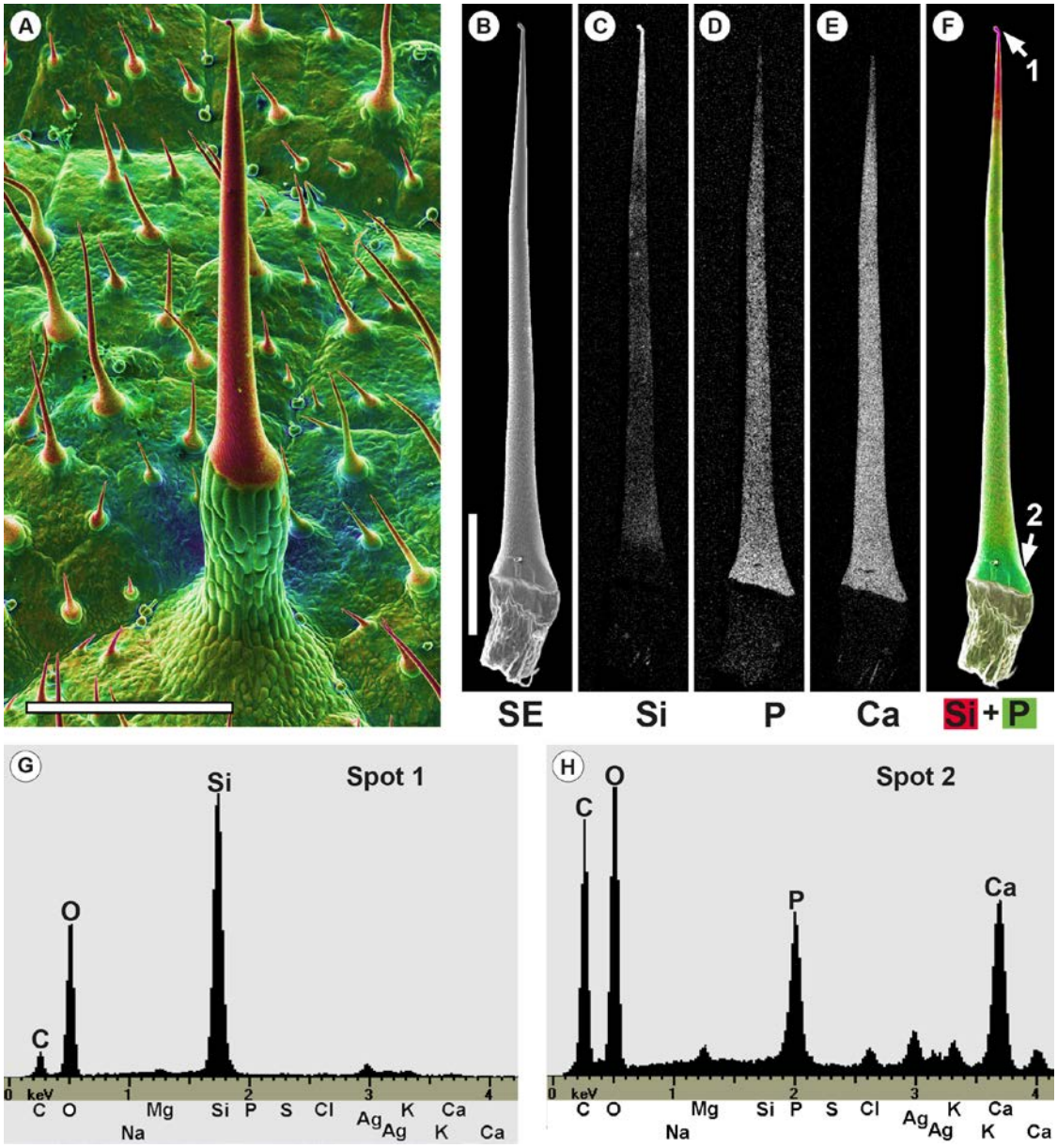


**Fig. 3** Cryo-SEM image and element distribution of Urticaceae stinging hairs. **a** The compositional contrast image of *Urtica dioica* shows the large stinging cell and numerous small trichomes in red color, indicating strong mineralization. **b-f** The element mapping images of a single stinging hair of *Urtica*

*fissa* show very high Si concentrations in the tip and high Ca concentrations in the shaft and base, and a high P concentration at the base, decreasing towards the tip. **f** The combined color image shows the Si distribution in red and P in yellow to green, depending on the concentration. **g, h** The spectra of two locations [Spot 1 and 2 marked in (**f**)] indicate the very high silica concentration in the tip and the apatite-like mineral composition at the base. Scale bars = 500 µm (**a-f).**

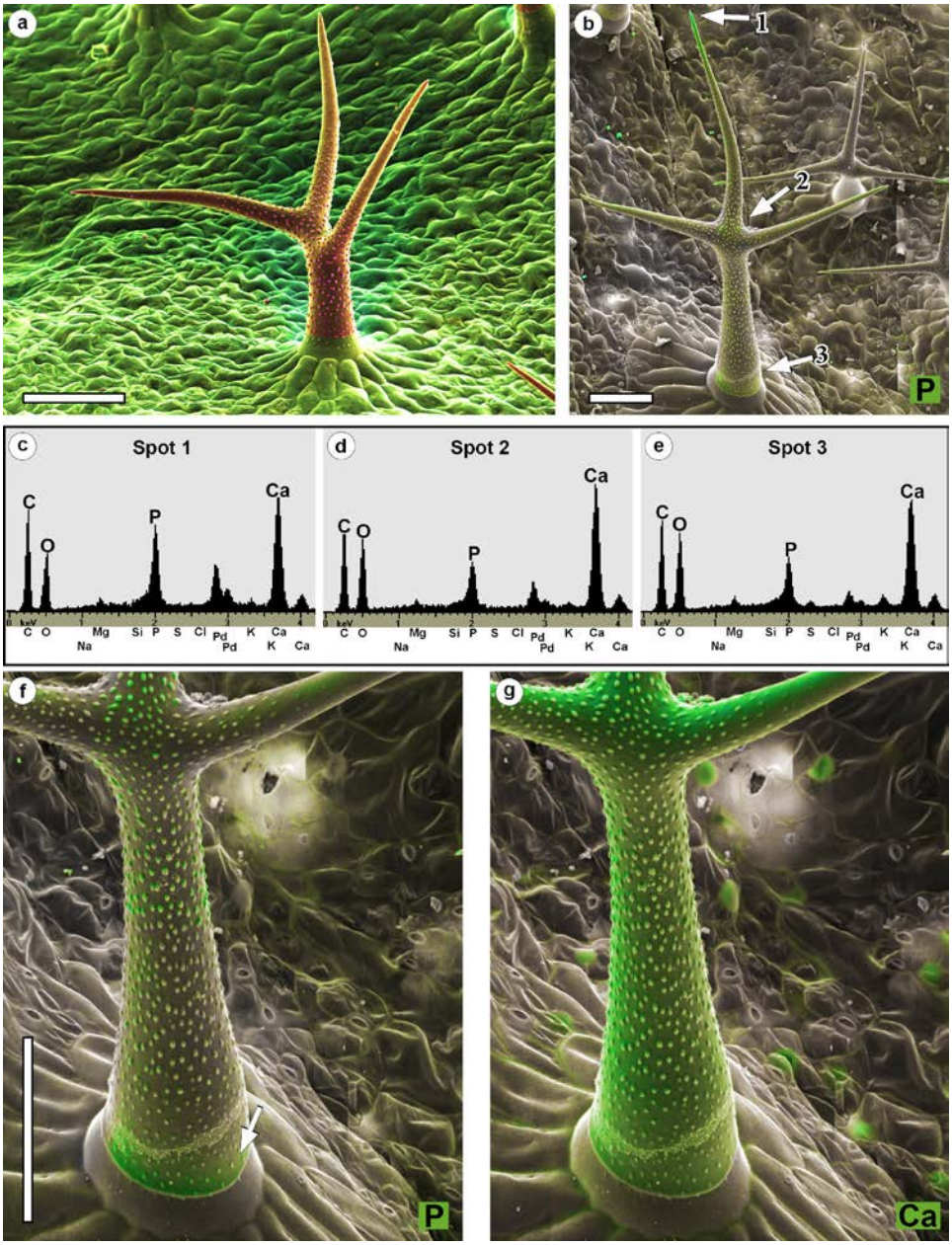


**Fig. 4** Mineralization of *Arabidopsis thaliana* trichomes. **a** Cryo-SEM image of an individual trichome, showing mineralized part in yellow-to-red; the very base appears non-mineralized. **b** Element-mapping

image of phosphorus (green), combined with the SE image shows high P concentrations in the trichome tips, and intermediate concentrations towards the base and in the granular surface structures. EDX spectra from three locations (marked in b) show the P-to-Ca ratios in the tip, on granular structures, and at the base. Element mapping images for P and Ca (Fig. 4**f-g**) of a trichome base show phosphorus mainly at the base and in the granular structures whereas Ca is evenly distributed, except for the non-mineralized lower end (arrow). Lab-grown plants (**a**) and those growing in open ground in the Botanical Garden (**b-g**) had similar Ca and P distributions. Scale bars = 100 µm.

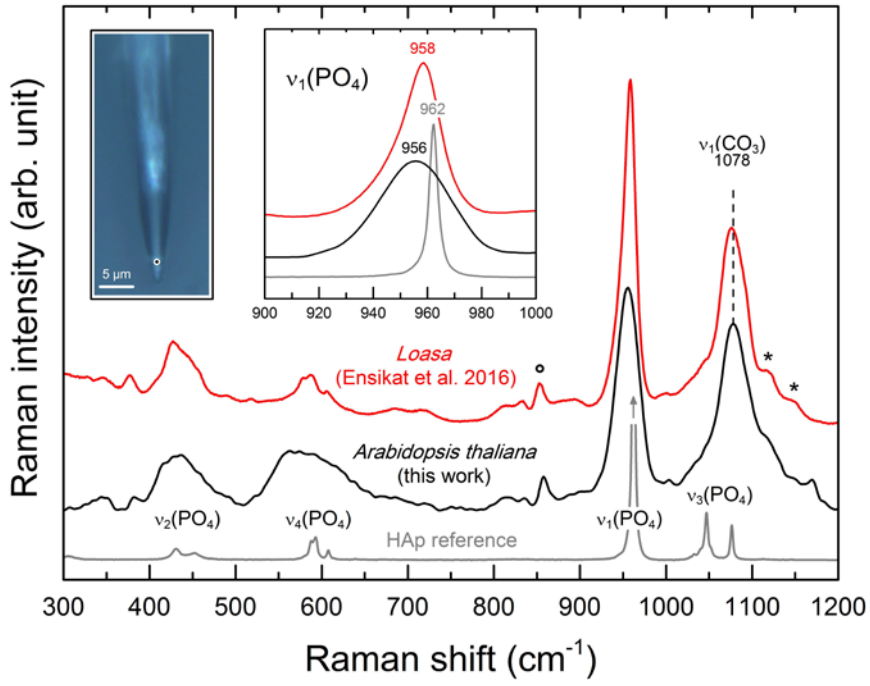


**Fig. 5** Raman spectra from *Arabidopsis thaliana* trichome tip in comparison to *Loasa* trichome. Insert shows the optical image (left) of the apical region with tip of *Arabidopsis thaliana* trichome. The spot Raman spectrum (location marked with black and white dot) indicates that the tip of trichome is mineralized with amorphous calcium phosphate. The spectra show a strong $v_1$ ($PO_4$) band around 958 $cm^{-1}$, whereas the detected band around 1078 $cm^{-1}$ is likely related to the symmetric $v_1$ ($CO_3$) stretching mode of the carbonate molecules. The band is overlain by a cellulose band around 1093 $cm^{-1}$.

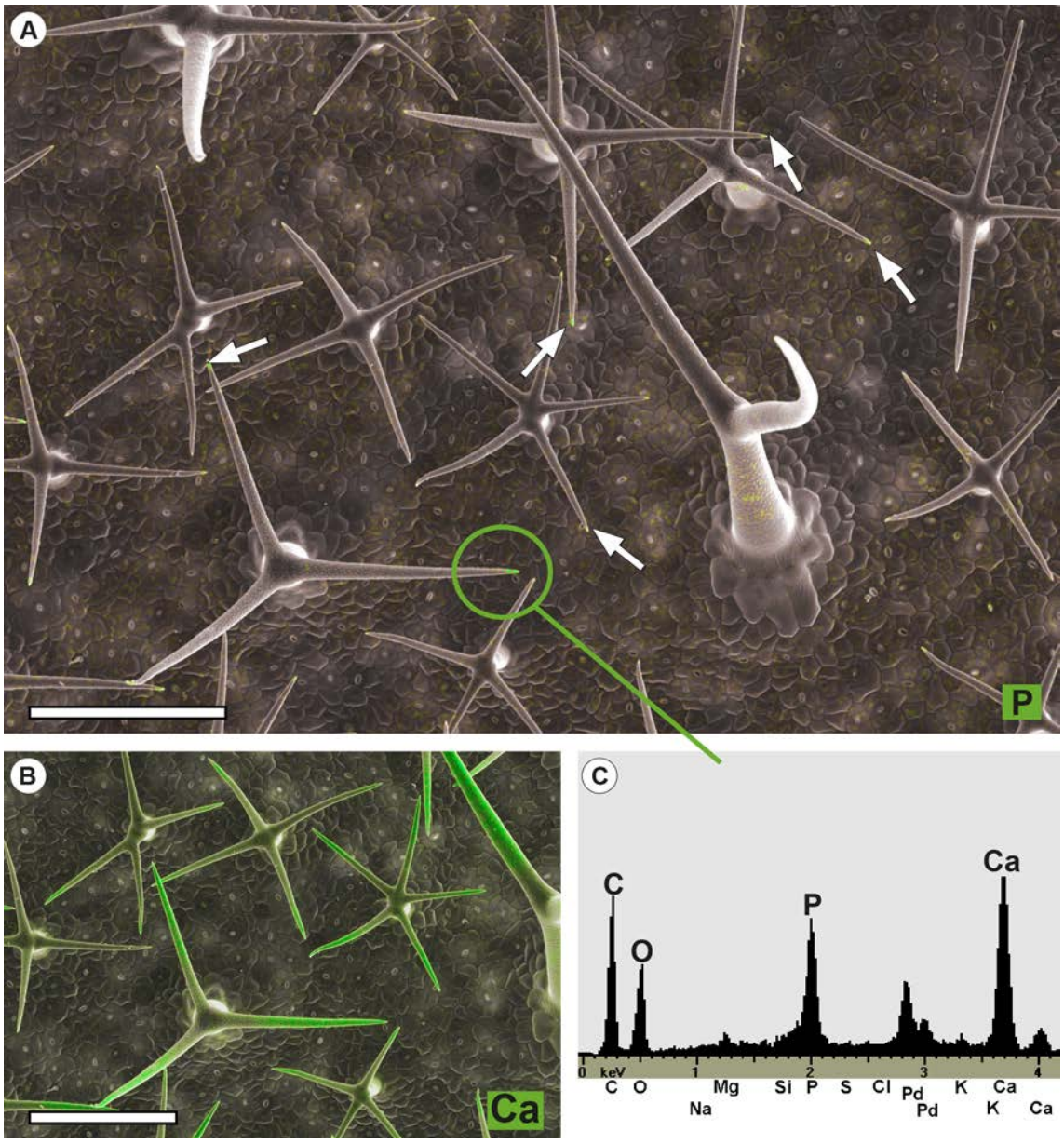


**Fig. 6** Combined topography (SE) and element mapping color images of CP-dried trichomes of *Aubrieta deltoidea*. Phosphorus (**a)** is only found in very small regions in the trichome tips, whereas Ca is present in the entire trichome (**b)**. The comparatively low P-to-Ca ratio indicates a mixture of calcium phosphate and calcium carbonate. Scale bars = 200 µm.

## 6.4 Discussion

Across the taxa studied, calcium phosphate tends to be concentrated at the trichome tips and often also the trichome bases, apparently providing additional hardness and/or stiffness to these regions. Calcium phosphate appears to be functionally equivalent to silica to some degree. We found that the tips of mineralized trichomes contain either silica (in the stinging hairs of Urticaceae and many other species not shown here, e.g. Cucurbitales and Heliantheae) or Calcium phosphate in most species presented in this work; only in very few cases (2 to 3% of the species examined) the entire trichomes contained only calcium as mineral element. Sometimes the deposits of these hard minerals were restricted to very small areas of the tips. In certain Loasaceae the stinging hair tips and the complex glochidiate trichomes of several Loasaceae contain silica and calcium phosphate at specific locations side-by-side (Fig. 1c; Ensikat et al. 2017). In *Urtica fissa* and *Phacelia malvifolia* calcium phosphate is found along the entire trichome and is the dominant biomineral. The presence of calcium phosphate has previously been reported from cystoliths (Lin et al., 2004). Overall, the results here presented clearly indicate that calcium phosphate is much more widespread as a plant biomineral than previously known and that the multiple roles of phosphorus in plant physiology have to be expanded to include its role in structural biomineralization. Evidence that calcium phosphate is located in the trichome walls and that here the phosphorus is generally associated with calcium has been shown by EDX analyses of transverse sections, published in Ensikat et al. (2016), and from other sections from various stinging trichomes and trichomes of Boraginaceae, which will be published separately. Further, EDX analyses with varying acceleration voltages (between 10 and 20 kV) for the electron beam confirmed that the detected mineral elements were located close to the sample surface in the cell wall.

EDX and Raman spectra show that the biominerals in trichomes generally are associated with organic material. The highest mineral concentrations (silica or calcium phosphate) were found in the trichome tips, whereas the shafts and bases had higher contents of organic material. Powder X-ray diffraction and electron diffraction measurements of several Loasaceae and Urticaceae trichomes indicated the presence of amorphous calcium carbonate and broad peaks indicating a nanocrystalline

structure for calcium phosphate (data not shown here, but compare Ensikat et al. 2016). Calcium carbonate is identified in the Raman spectra (Fig. 5), although its main signal overlaps with peaks of organic components such as cellulose. A simple chemical test for the presence carbonate is the formation of $CO_2$ gas bubbles after addition of acids. However, the aim of this study was to illustrate the wide distribution of the biomineral calcium phosphate in plants, regardless of its crystalline nature.

Interestingly, multiple biomineralization with different biominerals is not restricted to the typical "defensive" trichomes such as the stiff bristles on *Phacelia malvifolia* or the stinging hairs of *Urtica*, but is also present in the relatively small and soft trichomes of Brassicaceae, especially the trichomes of *Arabidopsis thaliana*, with surprisingly complex biomineralization. The most thoroughly studied plant in plant biology - both with regards to its genetics and physiology - has thus been hiding the secret of calcium phosphate biomineralization in plain sight. Trichome cover of *Arabidopsis* as such has been studied extensively from a genetic and physiological point of view (Traw and Bergelson 2003; Bloomer et al. 2014; Hauser 2014), and there is good evidence for trichomes in *Arabidopsis* functioning in herbivore deterrence, both for *Arabidopsis thaliana* (Handley et al. 2005) and closely related *A. lyrata* (Løe et al. 2007; Sletvold et al. 2010). A recent study further indicates that the trichomes of *Arabidopsis thaliana* may act as mechanosensoric switches (Zhou et al. 2016). The latter study describes in detail how the rigid upper part of the trichome transmits the pressure exerted onto the upper part of the trichome to its base, which shows elastic deformation. The elastic deformation of the trichome base in turn is translated into a signal in the skirt (foot) cells. It is argued that the differential elasticity of the cell wall, critical for this mechanism, is provided by differential cell wall thickening (Zhou et al. 2016). Our study demonstrates that differential biomineralization of the cell wall is likely a crucial factor: cell walls in the median and distal part of the trichomes are heavily mineralized, partly with calcium carbonate, partly with calcium phosphate, but the very base of the trichome cell wall was found to be non-mineralized and thus capable of elastic deformation.

Overall, the data demonstrate a remarkable degree of chemical heterogeneity of plant trichomes and the surprisingly widespread occurrence of multiple biomineralization

with two or three different biominerals. This appears to indicate that the micromechanical roles of the three different biominerals – silica, calcium carbonate and calcium phosphate - are divergent, but functional studies have not been carried out to date. Mineralized trichomes are thus not just some simple, stiffened structures, but turn out to be tiny miracles of micro-engineering. This sheds a new light on the function of mineralized trichomes in plant-environment interactions, inviting a broad range of studies. Especially a detailed study of the genetics, physiology and functional significance of differential biomineralization in the excessively well-studied model-organism *Arabidopsis* should be able to provide valuable insights.

### 6.5 Acknowledgments

The authors thank T. Jossberger for vouchering the collection. We thank Prof. Dr. Thorsten Geisler-Wierwille for his assistance in collecting the Raman spectra.

## 6.6 Literature cited

Bloomer RH, Lloyd AM, Symonds VV (2014) The genetic architecture of constitutive and induced trichome density in two new recombinant inbred line populations of *Arabidopsis thaliana*: phenotypic plasticity, epistasis, and bidirectional leaf damage response. BMC Plant Biol 14: 119

Cordell D, Jackson M, White S (2013) Phosphorus flows through the Australian food system: identifying intervention points as a roadmap to phosphorus security. Environ Sci Policy 29: 87-102

Ensikat HJ, Geisler T, Weigend M (2016) A first report of hydroxylated apatite as structural biomineral in Loasaceae - plants' teeth against herbivores. Sci Rep-UK 6: 26073

Ensikat HJ, Mustafa A, Weigend M (2017) Complex patterns of multiple biomineralization in single-celled plant trichomes of the Loasaceae. Am J Bot 104: 195-206

Ensikat HJ, Weigend M (2013) Cryo-scanning electron microscopy of plant samples without metal coating, utilizing bulk conductivity. Microsc Anal 27: 7-10

Franceschi VR, Nakata PA (2005) Calcium oxalate in plants: Formation and function. Annu Rev Plant Biol 56: 41-71

George TS, Hinsinger P, Turner BL (2016) Phosphorus in soils and plants – facing phosphorus scarcity. Plant Soil 401: 1-6

Guidry MW, Mackenzie FT (2000) Apatite weathering and the Phanerozoic phosphorus cycle. Geology 28: 631-634

Handley R, Ekbom B, Ågren J (2005) Variation in trichome density and resistance against a specialist insect herbivore in natural populations of *Arabidopsis thaliana*. Ecol Entomol 30: 284-292

Harpole WS, Stanley CJ (2016) Addition of multiple limiting resources reduces grassland diversity. Nature 537: 93-96

Hauser MT (2014) Molecular basis of natural variation and environmental control of trichome patterning. Front Plant Sci 5: 20-26

He H, Veneklaas EJ, Kuo J, Lambers H (2014) Physiological and ecological significance of biomineralization in plants. Trends Plant Sci 19: 166-174

Kaur G, Prabhavathi V, Bamel K, Sarwat M (2016) Phosphate signaling in plants: Biochemical and molecular approach. In: Sarwat M, Abdin AAMZ, Ibrahim MM (eds.) Stress signaling in plants: Genomics and proteomics perspective, 2nd Volume. Springer, Berlin, Germany, pp 83-110

Küpper H, Lombi E, Zhao FJ, McGrath SP (2000) Cellular compartmentation of cadmium and zinc in relation to other elements in the hyperaccumulator *Arabidopsis halleri*. Planta 212: 75-84

Lanning FC, Eleuterius LN (1987) Silica and ash in native plants of the central and southeastern regions of the United States. Ann Bot 60: 361-375

Lin ML, Yen TB, Kuo-Huang LL (2004) Formation of calcium carbonate deposition in the cotyledons during the germination of *Justicia procumbens* L. (Acanthaceae) seeds. Taiwania 49: 250-262

Løe G, Toräng P, Gaudeul M, Ågren J (2007) Trichome production and spatiotemporal variation in herbivory in the perennial herb *Arabidopsis lyrata*. Oikos 116: 134-142

Lowenstam HA (1981) Minerals formed by organisms. Science 211: 1126-1131

Mustafa A, Ensikat HJ, Weigend M (2017) Ontogeny and the process of biomineralization in the trichomes of Loasaceae. Am J Bot 104: 367-378

Oldroyd GE, Harrison MJ, Paszkowski U (2009) Reprogramming plant cells for endosymbiosis. Science 324: 753-754

Sletvold N, Huttunen P, Handley R, Kärkkäinen K, Ågren J (2010) Cost of trichome production and resistance to a specialist insect herbivore in *Arabidopsis lyrata*. Evol Ecol 24: 1307-1319

Smith MP, Harper DA (2013) Causes of the Cambrian explosion. Science 341: 1355-1356

Traw MB, Bergelson J (2003) Interactive effects of jasmonic acid, salicylic acid, and gibberellin on induction of trichomes in *Arabidopsis*. Plant Physiol 133: 1367-1375

Vance CP, Uhde-Stone C, Allan DL (2003) Phosphorus acquisition and use: critical adaptations by plants for securing a nonrenewable resource. New Phytol 157: 423-447

Zhou LH, Liu SB, Wang PF, Lu TJ, Xu F, Genin GM, Pickard BG (2016) The Arabidopsis trichome is an active mechanosensory switch. Plant Cell Environ 40: 611-621

# CHAPTER 7

## General discussion and conclusions

This dissertation, particularly from Chapter 2 to Chapter 6, focuses largely on the biomineralization of trichomes of higher plants. The overarching aim of this dissertation was to improve our understanding about mineralization at different zones of the trichomes among different plant groups. The chapters referring to the biomineralization in stinging hairs and scabrid-glochidiate trichomes of Loasaceae, represent the first comprehensive description of stringing trichome ontogeny and sequential mineralization processes in 13 out of 300 species (Chapter 2), and multiple-biomineralization patterns in 31 out of 300 species (Chapter 3). The comparison of stinging trichome biomineralization presented in Chapter 4 was an elaboration of the first studies by Thurston and Lersten (1969) and Thurston (1974), by expanding the study to 17 representative species from five different plant families (Caricaceae, Euphorbiaceae, Loasaceae, Namaceae and Urticaceae).

To investigate the distribution of biominerals, a broader survey with several species was performed. Their respective mineralization patterns were plotted in the phylogeny of the order Boraginales by Luebert et al. (2016), which demonstrate the presence of phylogenetic signals in biomineralization patterns (Chapter 5). It is also the first comprehensive biomineralization study across the order Boraginales and elaborates on the work of Hilger et al. (1993) and Selvi and Bigazzi (2001), by including 42 representative species from nine out of eleven families. An additional survey of species in other plant families, including *Arabidopsis thaliana* and several other Brassicaceae, is presented in Chapter 6. It describes the wide distribution of the biomineral calcium phosphate in trichomes, in combination with calcium carbonate and silica.

Several aspects of the morphology, ontogeny and biomineralization of trichomes in higher plants remained unclear in previous studies (Thurston and Lersten, 1969; Pollard and Briggs, 1984; Fu et al., 2003, 2007; Selvi and Bigazzi, 2001). Therefore,

our studies were based on scanning electron microscopy (SEM) and energy-dispersive X-ray spectroscopy (EDX) to study morphology and biomineral composition. These techniques provide the necessary resolution to identify even small biomineral deposits. Methods employed included cryo-SEM in order to avoid artefacts and dislocation of mineral contents. Additionally, EDX element mapping of critical-point dried samples was employed. Samples were sputter-coated with palladium (Pd) or silver (Ag) – to avoid interference with the detection of the relevant elements Si or P. Light microscopy (LM) was used for transmission views of isolated stinging trichomes. Raman spectroscopy was used for a specific identification of certain compounds, particularly hydroxyapatite (calcium phosphate), calcium carbonate and the organic components.

The morphology of stinging hairs of Loasaceae with an asymmetrical bulbous tip, functioning as hypodermic syringes, was found to be similar to that described for other species of the genera *Cnidoscolus* (Euphorbiaceae) and *Urtica* (Urticaceae; Thurston and Lersten, 1969; Pollard and Briggs, 1984; Fu et al., 2007). Small trichomes of Loasaceae have a surprising complexity in the form of glochidiate and scabrid trichomes, and show diversity in their surface structures as compared to trichomes of other plant families (Weigend, 2004). The distribution of stinging hairs on leaves varied strongly whereas small trichomes formed a dense cover on all leaf and stem surfaces of most species of Loasaceae.

Trichomes of Loasaceae were found to have complex mineralization patterns (Ensikat et al., 2016). The deposition of high concentrations of either silica or calcium phosphate in the tip is characteristic of all sharp-tipped small or bristle mineralized trichomes and provides additional hardness. The study of leaf and trichome ontogeny in Loasaceae provided new details on the morphological development of the diverse trichome types and the progress of their mineralization. Stinging hair and scabrid-glochidiate trichome morphology can be discriminated at early stages of development. Stinging trichomes develop with a smooth surface, whereas other small trichomes produce grainy surface structures (scabrid trichomes) and a circular surface pattern (glochidiate trichomes). The cryo-SEM and EDX-analysis-based study revealed that trichomes are initiated very early during organ development. Different trichome types

start developing their distinctive morphology at very early stages of the leaf development. The process of biomineralization in stinging trichomes progresses differently from that of scabrid-glochidiate trichomes. In stinging trichomes, the process begins with the deposition of silica or calcium phosphate in the apex and then proceeds towards the base and shaft, whereas in scabrid-glochidiate trichomes the process of biomineralization is initiated in the tips and hooks, followed by mineralization of the shaft. Only the stinging trichomes of genus *Nasa* showed a unique pattern of mineralization among the eight genera studied. Three biominerals were deposited in a single-celled trichome in different locations. Calcium phosphate and silica were found at the apical region of stinging hairs and in the barbs of glochidiate trichomes while calcium carbonate appeared dominant in the shafts. Further, longitudinal sections of the same trichomes (stinging hairs and glochidiate trichomes) showed that mineral depositions occurred in certain layers of trichomes, often in the outermost wall layers of stinging hairs. Scabrid-glochidiate trichomes deposit calcium carbonate in the shaft, which is extended to the cell lumen. These findings are consistent with a previous study reported by Küster-Winkelmann (1914), who described in her light-microscopic study that the wall thickness increases by deposition on the inner side, which subsequently led towards massive trichomes.

During the initial developmental stage, basal regions in trichomes are not yet mineralized. However, in fully developed stinging trichomes the base may need to be stiff in order to ensure that the trichome is not easily detached from plant surface. A previous study on fully developed stinging trichomes was documented by Thurston (1974), who performed X-ray microanalysis of the cell walls of *Urtica* stinging trichomes and suggested that the basal zone of stinging trichome is entirely unmineralized, whereas our analyses revealed strongly silicified trichome bases. Additionally, Thurston (1974) described the emergence of *Urtica dioica* stinging trichomes as starting from the epidermal and sub-epidermal cell layers. These findings are in line with our observation that trichomes initiate from the epidermis and the first trichomes initiate at the apex and margin of the leaf. Morphologically, stinging hairs from different plant families can be distinguished based on their apical regions. In Euphorbiaceae, Loasaceae and Urticaceae the apical bulb shows curved and asymmetrical shapes, whereas the stinging hairs of Caricaceae and Namaceae show

symmetrical apices. The morphology and ontogeny of the stinging trichomes of Loasaceae resembles those of Urticaceae more closely than those of representative genera of Namaceae (Hydrophyllaceae *p.p.;* Luebert et al., 2016) and Euphorbiaceae (Thurston and Lersten, 1969).

The analyses of Loasaceae trichomes (scabrid-glochidiate trichomes and stinging hairs) showed not only a fascinating surface morphology but also complex mineralization patterns with up to three biominerals – calcium phosphate in combination with calcium carbonate and silica – within the walls of single-celled trichomes. Different compositions were observed in trichomes of different genera of Loasaceae. Moreover, different zones of stinging hairs and small trichomes displayed distinct mineralization patterns. Notable differences were found in tips, shafts and base regions not only in Loasaceae, but also in mineralized trichomes of all plant families examined thus far. In nearly all species the trichomes contained high concentrations of silica or calcium phosphate in tips, while shafts in most species were mineralized with calcium carbonate in varying concentrations. The bases showed stronger variations in their mineralization, with all three minerals present either individually or in combination. Furthermore, chemical heterogeneity of wall structures, as reported by Küster-Winkelmann (1914) in stained samples, was also observed in our study. Data on the crystalline state and composition of trichome biominerals were obtained by using X-ray and electron diffraction and Raman spectroscopy (Ensikat et al., 2016), which showed nano-crystalline and amorphous mineral phases in trichomes of *Loasa pallida*. This finding triggered renewed interest in investigating the distribution of biominerals across the five plant families, which bear stinging trichomes. Touching stinging hairs break off their tips and transform them into sharp needles (Farmer, 2014; Iwamoto et al., 2014). In order to produce a sharp breaking point the tip of a stinging trichome must be hard and brittle, which can be achieved by high concentrations of biominerals. The tips of stinging hairs contained high concentrations of hard minerals: silica (Urticaceae), calcium phosphate (Caricaceae, Namaceae and Loasaceae), or no minerals (*Cnidoscolus,* Euphorbiaceae). The hardness and brittleness are suitable properties to form the predefined breaking point and a sharp, hard edge for penetration into the skin. It seems surprising that stinging trichomes of *Cnidoscolus* (Euphorbiaceae) can execute a similar function with non-

mineralized structures. It appears challenging to identify the mechanical properties of such non-mineralized stinging hairs. In previous studies, the stinging trichomes of *Urtica* have been widely reported as simple conical glass capillaries (Haberlandt, 1886; Thurston, 1974; Fu et al., 2007). In contrast to the tips, the shafts contained lower mineral concentrations and a higher content of carbon and oxygen (organic material), while trichome bases were mineralized with silica. These three zones play a crucial role in releasing the irritating liquid from the stinging trichome. Due to the compression or deformation by mechanical force, the irritating liquid in the shaft is injected through the opened tip into the skin (Emmelin and Feldberg, 1947; Fu et al., 2007).

The analyses of Loasaceae trichomes (scabrid-glochidiate trichomes and stinging hairs) showed not only a fascinating surface morphology but also complex mineralization patterns with up to three biominerals – calcium phosphate in combination with calcium carbonate and silica – within the walls of single-celled trichomes. Different compositions were observed in trichomes of different genera of Loasaceae. Moreover, different zones of stinging hairs and small trichomes displayed distinct mineralization patterns. Notable differences were found in tips, shafts and base regions not only in Loasaceae, but also in mineralized trichomes of all plant families examined thus far. In nearly all species the trichomes contained high concentrations of silica or calcium phosphate in tips, while shafts in most species were mineralized with calcium carbonate in varying concentrations. The bases showed stronger variations in their mineralization, with all three minerals present either individually or in combination. Furthermore, chemical heterogeneity of wall structures, as reported by Küster-Winkelmann (1914) in stained samples, was also observed in our study. Data on the crystalline state and composition of trichome biominerals were obtained by using X-ray and electron diffraction and Raman spectroscopy (Ensikat et al., 2016), which showed nano-crystalline and amorphous mineral phases in trichomes of *Loasa pallida*. This finding triggered renewed interest in investigating the distribution of biominerals across the five plant families, which bear stinging trichomes. Touching stinging hairs break off their tips and transform them into sharp needles (Farmer, 2014; Iwamoto et al., 2014). In order to produce a sharp breaking point the tip of a stinging trichome must be hard and brittle, which can be achieved by

high concentrations of biominerals. The tips of stinging hairs contained high concentrations of hard minerals: silica (Urticaceae), calcium phosphate (Caricaceae, Namaceae and Loasaceae), or no minerals (*Cnidoscolus,* Euphorbiaceae). The hardness and brittleness are suitable properties to form the predefined breaking point and a sharp, hard edge for penetration into the skin. It seems surprising that stinging trichomes of *Cnidoscolus* (Euphorbiaceae) can execute a similar function with non-mineralized structures. It appears challenging to identify the mechanical properties of such non-mineralized stinging hairs. In previous studies, the stinging trichomes of *Urtica* have been widely reported as simple conical glass capillaries (Haberlandt, 1886; Thurston, 1974; Fu et al., 2007). In contrast to the tips, the shafts contained lower mineral concentrations and a higher content of carbon and oxygen (organic material), while trichome bases were mineralized with silica. These three zones play a crucial role in releasing the irritating liquid from the stinging trichome. Due to the compression or deformation by mechanical force, the irritating liquid in the shaft is injected through the opened tip into the skin (Emmelin and Feldberg, 1947; Fu et al., 2007).

In most of the species investigated, the foot cells were nonmineralized. Only some species were found to be heavily mineralized with silica, i.e. *Wellstedia dinteri* Pilg., and *Onosma hispida* Wall. & G. Don. This is in line with a study of Selvi and Bigazzi (2001), which demonstrated massive silica deposits in the trichome foot cells of *Anchusa formosa* and *Trachystemon orientalis* (L.), thereby indicating that this may be a wide-spread pattern at least in the corresponding subgroup Boraginaceae subfamily Boraginoideae (Chacón et al., 2016). In a single study, the presence of phosphorus and sulfur in the tubercles of some species of *Nonea* (Boraginaceae) has been documented but without a comprehensive explanation about their exact distribution (Selvi and Bigazzi, 2001). Further analyses of specimens from other plant groups could document that calcium phosphate biomineralization is much more common than previously thought. Formerly, phosphate was reported as a minor component in studies of metal accumulating plant trichomes. Only one study reported Ca and P (calcium phosphate) in the cystoliths of *Justicia procumbens* L. (Acanthaceae), which usually consist of calcium carbonate particularly with high concentrations of Ca, deposited more in the core of the cystolith than in the peripheral areas (Lin et al.,

2004). So far all trichome tips in investigated species of Brassicaceae such as *Arabidopsis thaliana* (L.) Heynh., *Aubrieta deltoidea* (L.) DC., *Fibigia clypeata* (L.) Boiss. ex. Prantl, showed heavily mineralized trichome tips with calcium and no silica at all.

In conclusion, the work presented in this thesis provides a model for the study of biomineralization. The results of this research expand the current knowledge on trichome biomineralization and demonstrate that a single-celled trichome can contain three biominerals (calcium phosphate, calcium carbonate and silica) showing their site-specificity and complexity. The differential mineralization is not restricted only to one plant family or one plant group, but widespread across several common plant groups. Multiple patterns of biomineralization in the trichomes provide a new way of looking at trichomes in the light of systematic relationships and their functionality. It also sheds new light on the functions of mineralized trichomes in plant-environment interactions thereby inviting a broad range of subjects.

## Outlook

The results presented in this thesis have shown an unexpected complexity, stimulating additional research lines for future work. The discovery of multiple-biomineralization in trichome walls, particularly the deposition of calcium phosphate at different zones of trichomes, was not only restricted to the stinging hairs and scabrid-glochidiate trichomes of the family Loasaceae, but was shown to be widespread in many common plant groups. So far, the present studies described trichome biomineralization only in a few selected plant species from different plant groups. Further investigations could broaden our knowledge of plant biomineralization. Advanced microscopical and analytical methods are nowadays available to elucidate ultrastructure, crystalline and molecular order and physical properties of the inorganic/organic composite materials, e.g., high resolution microscopy techniques include transmission electron microscopy (TEM), electron tomography (ET) and analytical TEM methods, such as electron diffraction, electron energy loss spectroscopy (EELS) and atom probe tomography (APT). Moreover, improved preparation methods, such as freeze substitution, serial sectioning SEM and dual beam FIB-SEM, can be useful in order to minimize preparation artefacts.

The diversity highlighted in this work is not only limited to trichome morphology but could be extended to organic wall components and cell liquid toxins. The chemical composition of the irritating liquid in stinging hairs still seems to be controversial. Further investigation with advanced techniques such as liquid chromatography/mass spectrometry is needed here. The identification of organic components in the cell walls of mineralized and non-mineralized stinging trichomes, particularly of *Cnidoscolus* stinging trichomes, might be interesting in order to explore which organic components make them so hard and stiff that a mineralization – otherwise universally present in stinging hairs – is superfluous. Identification of the genes encoding proteins that regulate ion transport through the cell membrane for biomineral formation may be appropriate to compare biomineralization processes in plants, animals and humans. From a physiological perspective, further investigations are needed to identify the function of each biomineral and the dynamics of its formation. The present studies demonstrate that plant biomineralization is neither as uniform nor as simple as

universally assumed. The data here presented thus open up a wide range of research questions with regard to the physiological mechanisms, the ecological function and the evolutionary processes of this phenomenon. It also leads to new questions in the area of material science with the possibility of investigating biomimetic material based on plant templates.

# SUMMARY

***Mustafa, Adeel. 2017.*** Morphology, Ontogeny, and Biomineralization of Trichomes of Selected Higher Plants. Doctoral thesis, Mathematisch-Naturwissenschaftliche Fakultät, Rheinische Friedrich-Wilhelms-Universität Bonn, Germany.

This thesis describes the morphology and biomineralization of trichomes, which occur in different plant orders investigating: (i) The morphology and overall ontogenetic development stages of stinging hairs and scabrid-glochidiate trichomes in 14 representative species of Loasaceae, and the process of biomineralization; (ii) Patterns of multiple-biomineralization with calcium phosphate, silica and calcium carbonate in stinging trichomes and scabrid-glochidiate trichomes in 31 species of Loasaceae; (iii) Comparison of stinging trichomes biomineralization in 17 representative species from five different plant families; (iv) Distribution of the three biominerals in 42 species from nine families of the order Boraginales; (v) A broader survey of the distribution of the biomineral calcium phosphate, in combination with calcium carbonate and silica, in the walls of single-celled trichomes of several common and widespread plant species of different plant groups, extending to the total number of species analyzed up to 94.

Most of the SEM studies were performed on fresh plant materials from of the Botanical Garden of the University of Bonn, Germany, herbarium specimens were used only in few cases. SEMs equipped with an EDX element analysis system were used for the detection and localization of the mineral elements. Different SEM preparation methods were used, including cryo-SEM, critical point drying (CPD) and cryo-harvesting of trichomes. Further methods include Raman spectroscopy for the identification of biominerals and light microscopy for transmission views of isolated stinging trichomes.

It was revealed that trichomes of Loasaceae were mineralized with up to three different biominerals: calcium phosphate, calcium carbonate and silica. Very early stages of the different types of trichomes (stinging and scabrid-glochidiate) showed no mineralization. Trichome development initiated very early in organ

development, and the different trichome types started developing their distinctive morphology at a very early stage. The process of biomineralization starts with the deposition of calcium phosphate or silica in the apex and then proceeds irregularly in the shaft and base. Typically, up to three biominerals – calcium phosphate, calcium carbonate and silica – are deposited at three different zones of the trichomes. The tips contained either silica or calcium phosphate; shafts usually contained calcium carbonate, or calcium phosphate in few cases; and bases often had additional silica deposits. Surprisingly, the biomineral calcium phosphate was found in the trichomes of many species in the orders Boraginales, Brassicales, Cornales, Malpighiales and Rosales. Boraginales (Boraginales I and Boraginales II) trichomes displayed either triple-mineralization (calcium phosphate, calcium carbonate and silica) or silica replacing calcium phosphate. Stinging trichome tips of Urticaceae were generally mineralized with silica; Caricaceae and Namaceae with calcium phosphate; and Loasaceae deposit with both minerals. Only the stinging trichomes of the genus *Cnidoscolus* (Euphorbiaceae) were found to be unmineralized.

Overall, the studies have greatly expanded our knowledge and understanding of the biomineralization diversity in plants, among different genera, different trichome types and even in various parts of the same trichome. Disparate biomineralization of the parts of individual, unicellular trichomes clearly indicates an extraordinary degree of physiological control over this process.

## Zusammenfassung

***Mustafa, Adeel. 2017.*** Morphologie, Ontogenie und Biomineralisation von Trichomen ausgewählter höherer Pflanzen. Dissertation zur Erlangung des Doktorgrades der Mathematisch-Naturwissenschaftlichen Fakultät, Rheinische Friedrich-Wilhelms-Universität Bonn, Deutschland.

Die vorliegende Doktorarbeit beschreibt die Morphologie und Biomineralisation von Trichomen, die in verschiedenen Pflanzengruppen vorkommen. Untersucht wurden (i) die Morphologie und die allgemeinen ontogenetischen Entwicklungsstadien von Brennhaaren und scabrid-glochidiaten Trichomen in 14 repräsentativen Arten der Familie Loasaceae sowie der Prozess der Biomineralisation; (ii) die Muster multipler Biomineralisation mit Calciumphosphat, Silica (Siliciumdioxid) und Calciumcarbonat in Brennhaaren und scabrid-glochidiaten Trichomen in 31 Arten der Familie Loasaceae; (iii) ein Vergleich der Biomineralisation der Brennhaare in 17 repräsentativen Arten aus fünf verschiedenen Pflanzenfamilien; (iv) die Verteilung der drei Biomineralien in 42 Arten aus neun Familien der Ordnung Boraginales; (v) eine Erfassung der Verteilung des Biominerals Calciumphosphat, in Kombination mit Calciumcarbonat und Silica, in den Wänden einzelliger Trichome von bisher 94 verschiedenen häufig und weit verbreitetet vorkommenden Arten unterschiedlicher Pflanzengruppen.

Die Mehrzahl der Rasterelektronenmikroskopie-Untersuchungen (Rasterelektronen-mikroskop, REM) wurden mit frischem Pflanzenmaterial aus dem Botanischen Garten der Universität Bonn durchgeführt; Herbarmaterial wurde nur in wenigen Fällen verwandt. Zum Nachweis und zur Lokalisation der mineralischen Elemente wurden REMs mit Systemen zur energiedispersiven Röntgenanalyse (energy dispersive X-ray spectroscopy, EDX) eingesetzt. Es wurden verschiedene REM-Methoden wie Kryo-REM, Kritisch-Punkt-Trocknung (CPD) und Kryo-Abtrennung von Trichomen angewandt. Mit Hilfe der Raman-Spektroskopie wurde die Identifizierung der Biomineralien ergänzt. Aufnahmen per Lichtmikroskopie ermöglichten Einblicke in die Entwicklung der inneren Struktur von isolierten Brennhaaren.

Es hat sich gezeigt, dass Trichome der Familie Loasaceae mit bis zu drei verschiedenen Biomineralien mineralisiert sind: Calciumphosphat, Calciumcarbonat und Silica. Sehr frühe Stadien der verschiedenen Trichomtypen (Brennhaare und scabrid-glochidiate Trichome) zeigten noch keine Mineralisation. Die Entwicklung der Trichome setzte sehr früh in der Organentwicklung ein und die verschiedenen Trichomtypen begannen ihre charakteristische Morphology zu einem sehr frühen Stadium herauszubilden. Der Prozess der Biomineralisation begann mit der Ablagerung von Calciumphosphat oder Silica in der Spitze und setzte sich ungleichmäßig im Schaft und bis zur Basis fort. Üblicherweise wurden bis zu drei Biomineralien – Calciumphosphat, Calciumcarbonat und Silica – in drei verschiedenen Zonen der Trichome abgelagert: die Spitzen enthielten entweder Silica oder Calciumphosphat; der Schaft wies meistens Calciumcarbonat oder in wenigen Fällen Calciumphosphat auf; in der Basis wurde häufig zusätzlich Silica neben Calciumcarbonat nachgewiesen. Überraschenderweise wurde das Biomineral Calciumphosphat in den Trichomen vieler Spezies der Ordnungen Boraginales, Brassicales, Cornales, Malpighiales und Rosales gefunden. Trichome in den Boraginales (Boraginales I and Boraginales II) zeigten entweder eine Mineralisation mit allen drei Komponenten (Calciumphosphat, Calciumcarbonat und Silica) oder Silica ersetzte Calciumphosphat. Die Spitzen der Brennhaare von Urticaceae waren grundsätzlich mit Silica mineralisiert, Caricaceae und Namaceae mit Calciumphosphat, sowie Loasaceae mit Einlagerungen beider Mineralien. Lediglich Brennhaare der Gattung *Cnidoscolus* (Euphorbiaceae) waren nicht mineralisiert.

Insgesamt haben die Untersuchungen das Wissen und Verständnis der Diversität der Biomineralisierung in Pflanzen erweitert, sowohl zwischen unterschiedlichen Pflanzengattungen, als auch in verschiedenen Trichomtypen, bis hin zu verschiedenen Bereichen innerhalb eines Trichoms. Die differenzierte Biomineralisation von Teilen einzelner, einzelliger Trichome zeigt deutlich einen außerordentlichen Grad an physiologischer Kontrolle über diesen Prozess.

# LITERATURE

**Abaye DA, Lawlor K, Hirsch PR, Brookes PC. 2005.** Changes in the microbial community of an arable soil caused by long-term metal contamination. *European Journal of Soil Science* **56**: 93–102.

**Addadi L, Weiner S. 2014**. Biomineralization: mineral formation by organisms. *Physica Scripta* **89**: 098003.

**Adler A, Karacic A, Weih M. 2008.** Biomass allocation and nutrient use in fast-growing woody and herbaceous perennials used for phytoremediation. *Plant and Soil* **305**: 189–206.

**Agostinho FB, Tubana BS, Martins MS, Datnoff LE. 2017.** Effect of different silicon sources on yield and silicon uptake of rice grown under varying phosphorus rates. *Plants* **6**: 1–17.

**Aharoni A, Jongsma MA, Kim TY, Ri MB, Giri AP, Verstappen FW, Schwab W, Bouwmeester HJ. 2006.** Metabolic engineering of terpenoid biosynthesis in plants. *Phytochemistry Reviews* **5**: 49–58.

**Amelunxen F, Wahlig T, Arbeiter H. 1969.** Über den Nachweis des ätherischen Öls in isolierten Drüsenhaaren und Drüsenschuppen von *Mentha piperita* L. *Zeitschrift für Pflanzenphysiologie* **61**: 68–72.

**An L, Zhou Z, Yan A, Gan Y. 2011.** Progress on trichome development regulated by phytohormone signaling. *Plant Signaling & Behavior* **6**: 1959–1962.

**Arnott HJ, Pautard FGE, Steinfink H. 1965.** Structure of calcium oxalate monohydrate. *Nature* **208**: 1197–1198.

**Arnott HJ. 1980.** Carbonates in higher plants. In: Omori M, Watabe N, eds. *Mechanisms of biomineralization in animals and plants*. Tokyo: Tokai University Press, 211–218.

**Arnott HJ. 1982.** Three systems of biomineralization in plants with comments on the associated organic matrix. In: Nancollas GH, ed. *Biological mineralization and demineralization*. Heidelberg: Springer, 199–218.

**Asgarpanah J, Mohajerani R. 2012.** Phytochemistry and pharmacologic properties of *Urtica dioica* L. *Journal of Medicinal Plants Research* **6**: 5714–5719.

**Bauer P, Elbaum R, Weiss IM. 2011.** Calcium and silicon mineralization in land plants: transport, structure and function. *Plant Science* **180**: 746–756.

**Bickford CP. 2016.** Ecophysiology of leaf trichomes. *Functional Plant Biology* **43**: 807–814.

**Boskey AL. 2007**. Mineralization of bones and teeth. *Elements* **3**: 385–391.

**Bourgeois C, Leclerc ÉA, Corbin C, Doussot J, Serrano V, Vanier JR, Seigneuret JM, Auguin C, Pichon C, Lainé É, Hano C. 2016.** Nettle (*Urtica dioica* L.) as a source of antioxidant and anti-aging phytochemicals for cosmetic applications. *Comptes Rendus Chimie* **19**: 1090–1100.

**Burstrom HG. 1968.** Calcium and plant growth. *Biological Reviews* **43**: 287–316.

**Butler HJ, Ashton L, Bird B, et al. 2016.** Using Raman spectroscopy to characterize biological materials. *Nature Protocols* **11**: 664–687.

**Cano-Santana Z, Oyama K. 1992.** Variation in leaf trichomes and nutrients of *Wigandia urens* (Hydrophyllaceae) and its implications for herbivory. *Oecologia* **92**: 405–409.

**Carvalho FA. 2013.** Onward [continuously updated]. e-Monograph of Caricaceae, version 1, November 2013. http://herbaria.plants.ox.ac.uk/bol/caricaceae

**Carvalho FA, Renner SS. 2013.** Correct names for some of the closest relatives of *Carica papaya*: A review of the Mexican/Guatemalan genera *Jarilla* and *Horovitzia*. *PhytoKeys* **29**: 63–74.

**Carvalho RT, Salgado LT, Amado Filho GM, Leal RN, Werckmann J, Rossi AL, Campos APC, Karez CS, Farina, M. 2017.** Biomineralization of calcium carbonate in the cell wall of *Lithothamnion crispatum* (Hapalidiales, Rhodophyta): correlation between the organic matrix and the mineral phase. *Journal of Phycology*, **53**: 642–651.

**Chacón J, Luebert F, Hilger HH, et al. 2016**. The borage family (Boraginaceae s. str.): A revised infrafamilial classification based on new phylogenetic evidence, with emphasis on the placement of some enigmatic genera. *Taxon* **65**: 523–546.

**Collier HOJ, Chesher GB. 1956.** Identification of 5-hydroxytryptamine in the sting of the nettle (*Urtica dioica*). *British Journal of Pharmacology* **11**: 186–189.

**Combes C, Cazalbou S, Rey C. 2016.** Apatite Biominerals. *Minerals* **6**: 34.

**Cooke J, Leishman MR. 2011.** Is plant ecology more siliceous than we realise? *Trends in Plant Science* **16**: 61–68.

**Currie HA, Perry CC. 2007.** Silica in plants: biological, biochemical and chemical studies. *Annals of Botany* **100**: 1383–1389.

**Datnoff LE, Deren CW, Snyder GH. 1997.** Silicon fertilization for disease management of rice in Florida. *Crop Protection* **16**: 525–531.

**de Nooijer LJ, Spero HJ, Erez J, Bijma J, and Reichart GJ. 2014.** Biomineralization in perforate foraminifera. *Earth-Science Reviews* **135**: 48–58.

**Debona D, Rodrigues FA, Datnoff LE. 2017**. Silicon's role in abiotic and biotic plant stresses. *Annual Review of Phytopathology* **55**: 85–107.

**Diane N, Jacob C, Hilger HH. 2003.** Leaf anatomy and foliar trichomes in Heliotropiaceae and their systematic relevance. *Flora-Morphology, Distribution, Functional Ecology of Plants* **198**: 468–485.

**Eisner T, Eisner M, Hoebeke ER. 1998.** When defense backfires: detrimental effect of a plant's protective trichomes on an insect beneficial to the plant. *Proceedings of the National Academy of Sciences* **95**: 4410–4414.

**Ekici N, Dane F. 2007.** Calcium oxalate crystals in vegetative and floral organs of *Galanthus* sp. (Amaryllidaceae). *Asian Journal of Plant Sciences* **6**: 508–512.

**Elliott JC. 2002.** Calcium phosphate biominerals. *Reviews in Mineralogy and Geochemistry* **48**: 427–453.

**Emmelin N, Feldberg W. 1947.** The mechanism of the sting of the common nettle (*Urtica urens*). *The Journal of Physiology* **106**: 440–455.

**Ensikat HJ, Geisler T, Weigend M. 2016.** A first report of hydroxylated apatite as structural biomineral in Loasaceae - plants' teeth against herbivores. *Scientific Reports* **6**: 26073.

**Epstein E. 1994.** The anomaly of silicon in plant biology. *Proceedings of the National Academy of Sciences* **91**: 11–17.

**Farmer EE. 2014.** *Leaf Defence*. Oxford and New York: Oxford University Press.

**Franceschi V. 2001.** Calcium oxalate in plants. *Trends in Plant Science* **6**: 331.

**Franceschi VR, Horner HT. 1980.** Calcium oxalate crystals in plants. *The Botanical Review* **46**: 361–427.

**Franceschi VR, Nakata PA. 2005.** Calcium oxalate in plants: formation and function. *Annual Review of Plant Biology* **56**: 41–71.

**Frelichowski Jr JE, Juvik JA. 2001.** Sesquiterpene carboxylic acids from a wild tomato species affect larval feeding behavior and survival of *Helicoverpa zea* and *Spodoptera exigua* (Lepidoptera: Noctuidae). *Journal of Economic Entomology* **94**: 1249–1259.

**Fu F, Akagi T, Yabuki S. 2002.** Origin of silica particles found in the cortex of roots. *Soil Science Society of America Journal* **66**: 1265–1271.

**Fu HY, Chen SJ, Chen RF, Ding WH, Kuo-Huang LL, Huang RN. 2006.** Identification of oxalic acid and tartaric acid as major persistent pain-inducing toxins in the stinging hairs of the nettle, *Urtica thunbergiana*. *Annals of Botany* **98**: 57–65.

**Fu HY, Chen SJ, Chen RF, Kuo-Huang LL, Huang RN. 2007**. Why do nettles sting? About stinging hairs looking simple but acting complex. *Functional Plant Science and Biotechnology* **1**: 46–55.

**Fu HY, Chen SJ, Kuo-Huang LL. 2003.** Comparative study on the stinging trichomes and some related epidermal structures in the leaves of *Dendrocnide meyeniana*, *Girardinia diversifolia*, and *Urtica thunbergiana*. *Taiwania* **48**: 213–223.

**Fürstenberg-Hägg J, Zagrobelny M, Bak. S. 2013.** Plant defense against insect herbivores. *International Journal of Molecular Sciences* **14**: 10242–10297.

**Gal A, Brumfeld V, Weiner S, Addadi L, Oron D. 2012b.** Certain biominerals in leaves function as light scatterers. *Advanced Materials* **24**: OP77–OP83.

**Gal A, Hirsch A, Siegel S, Li C, Aichmayer B, Politi Y, Fratzl P, Weiner S, Addadi L. 2012a.** Plant cystoliths: A complex functional biocomposite of four distinct silica and amorphous calcium carbonate phases. *Chemistry-A European Journal* **18**: 10262–10270.

**Guerini D, Coletto L, Carafoli E. 2005.** Exporting calcium from cells. *Cell Calcium* **38**: 281–289.

**Ha S., and Tran LS. 2014.** Understanding plant responses to phosphorus starvation for improvement of plant tolerance to phosphorus deficiency by biotechnological approaches. *Critical Reviews in Biotechnology* **34**: 16–30.

**Haberlandt G. 1886.** Zur Anatomie und Physiologie der pflanzlichen Brennhaare. *Sitzungsberichte der Kaiserlichen Akademie der Wissenschaften* **93**: 123–143.

**Hanley ME, Lamont BB, Fairbanks MM, Rafferty CM. 2007.** Plant structural traits and their role in anti-herbivore defence. *Perspectives in Plant Ecology, Evolution and Systematics* **8**: 157–178.

**He H, Bleby TM, Veneklaas EJ, Lambers H, Kuo J. 2012.** Precipitation of calcium, magnesium, strontium and barium in tissues of four *Acacia* species (Leguminosae: Mimosoideae). *PLoS One* **7**: e41563.

**He H, Veneklaas EJ, Kuo J, Lambers H. 2014.** Physiological and ecological significance of biomineralization in plants. *Trends in Plant Science* **19**: 166–174.

**Hepler PK. 1994.** The role of calcium in cell division. *Cell Calcium* **16**: 322–330.

**Hepler PK. 2005.** Calcium: a central regulator of plant growth and development. *The Plant Cell* **17**: 2142–2155.

**Hilger HH, Hoppe JR, Hofmann M. 1993.** Energiedispersive Röntgenmikroanalyse (EDX) von Boraginaceae subfam. Boraginoideae - Klausenoberflächen: (Sind Silicium- und Calcium- Einlagerungen in die Fruchtwand systematisch verwertbare Merkmale?). *Flora* **188**: 387–398.

**Hodson MJ, Sangster AG. 1989.** Silica deposition in the inflorescence bracts of wheat (*Triticum aestivum*). II. X-ray microanalysis and backscattered electron imaging. *Canadian Journal of Botany* **67**: 281–287.

**Hodson MJ, White PJ, Mead A, Broadley MR. 2005.** Phylogenetic variation in the silicon composition of plants. *Annals of Botany* **96**: 1027–1046.

**Hodson MJ. 2016.** The development of phytoliths in plants and its influence on their chemistry and isotopic composition. Implications for palaeoecology and archaeology. *Journal of Archaeological Science* **68**: 62–69.

**Hooke R. 1665.** *Micrographia: or some physiological descriptions of minute bodies made by magnifying glasses: with observations and inquiries thereupon.* London: Martyn and Allestry.

**Horner HT., and Wagner BL. 1992.** Association of four different calcium crystals in the anther connective tissue and hypodermal stomium of *Capsicum annuum* (Solanaceae) during microsporogenesis. *American Journal of Botany* **79**: 531–541.

**Horner HT, Kausch AP, Wagner BL. 2000.** Ascorbic acid: a precursor of oxalate in crystal idioblasts of *Yucca torreyi* in liquid root culture. *International Journal of Plant Sciences* **161**: 861–868.

**Hurley KW, Dussourd DE. 2015.** Toxic geranium trichomes trigger vein cutting by soybean loopers, *Chrysodeixis includens* (Lepidoptera: Noctuidae). *Arthropod-Plant Interactions* **9**: 33–43.

**Ilarslan H, Palmer RG, Horner HT. 2001.** Calcium oxalate crystals in developing seeds of soybean. *Annals of Botany* **88**: 243–257.

**Iwamoto M, Horikawa C, Shikata M, Wasaka N, Kato T, Sato H. 2014.** Stinging hairs on the Japanese nettle *Urtica thunbergiana* have a defensive function against mammalian but not insect herbivores. *Ecological Research* **29**: 455–462.

**Iwano M, Entani T, Shiba H, Takayama S, Isogai A. 2004.** Calcium crystals in the anther of *Petunia*: the existence and biological significance in the pollination process. *Plant and Cell Physiology* **45**: 40–47.

**Iwasaki K, Matsumura A. 1999.** Effect of silicon on alleviation of manganese toxicity in pumpkin (*Cucurbita moschata* Duch cv. Shintosa). *Soil Science and Plant Nutrition* **45**: 909–920.

**Johnson HB. 1975**. Plant pubescence: an ecological perspective. *The Botanical Review* **41**: 233–258.

**Joshi B, Mukhija M, Kalia A. 2014.** Pharmacognostical review of *Urtica dioica* L. *International Journal of Green Pharmacy* **8**: 201–209.

**Kariyat RR, Smith JD, Stephenson AG, De Moraes CM, Mescher MC. 2017.** Non-glandular trichomes of *Solanum carolinense* deter feeding by *Manduca sexta* caterpillars and cause damage to the gut peritrophic matrix. *Proceeding of The Royal Society B* **284:** 20162323.

**Kaufman PB, Bigelow WC, Schmid R, Ghosheh NS. 1971.** Electron microprobe analysis of silica in epidermal cells of *Equisetum*. *American Journal of Botany* **58**: 309–316.

**Kennedy GG. 2003.** Tomato, pests, parasitoids, and predators: tritrophic interactions involving the genus *Lycopersicon*. *Annual Review of Entomology* **48:** 51–72.

**Kim C, Deng T, Chase M, Zhang DG, Nie ZL, Sun H. 2015.** Generic phylogeny and character evolution in Urticeae (Urticaceae) inferred from nuclear and plastid DNA regions. *Taxon* **64**: 65–78.

**Kirpichtchikova TA, Manceau A, Spadini L, Panfili F, Marcus MA, Jacquet T. 2006.** Speciation and solubility of heavy metals in contaminated soil using X-ray microfluorescence, EXAFS spectroscopy, chemical extraction, and thermodynamic modeling. *Geochimica et Cosmochimica Acta* **70**: 2163–2190.

**Knoll AH. 2003.** Biomineralization and evolutionary history. *Reviews in Mineralogy and Geochemistry* **54**: 329–356.

**Konno K, Inoue TA, Nakamura M. 2014.** Synergistic defensive function of raphides and protease through the needle effect. *PloS One* **9**: e91341.

**Konyar ST, Öztürk N, Dane F. 2014.** Occurrence, types and distribution of calcium oxalate crystals in leaves and stems of some species of poisonous plants. *Botanical Studies* **55**: 32.

**Krämer U, Grime GW, Smith JAC, Hawes CR, Baker AJM. 1997.** Micro-PIXE as a technique for studying nickel localization in leaves of the hyperaccumulator plant *Alyssum lesbiacum*. *Nuclear Instruments and Methods in Physics Research Section B: Beam Interactions with Materials and Atoms* **130**: 346–350.

**Krieger C, Calvaruso C, Morlot C, Uroz S, Salsi L, Turpault MP. 2017.** Identification, distribution, and quantification of biominerals in a deciduous forest. *Geobiology* **15**: 296–310.

**Küster-Winkelmann G. 1914.** *Das Haarkleid der Loasaceen.* Doctoral dissertation. Friedrich-Alexander-Universität, Erlangen, Germany.

**Larcher W, Meindl U, Ralser E, Ishikawa M. 1991.** Persistent super cooling and silica deposition in cell walls of palm leaves. *Journal of Plant Physiology* **139**: 146–154.

**Levin DA. 1973.** The role of trichomes in plant defense. *The Quarterly Review of Biology* **48**: 3–15.

**Li T. 1994.** Use of stinging nettle as a potential organic fertilizer for herbs. *Journal of Herbs, Spices & Medicinal Plants* **2**: 93–98.

**Libert B, Franceschi VR. 1987.** Oxalate in crop plants. *Journal of Agricultural and Food Chemistry* **35**: 926–938.

**Lin ML, Yen TB, Kuo-Huang LL. 2004.** Formation of calcium carbonate deposition in the cotyledons during the germination of *Justicia procumbens* L. (Acanthaceae) Seeds. *Taiwania* **49**: 250–262.

**Lins U, Barros CF, Da Cunha M, Miguens FC. 2002.** Structure, morphology, and composition of silicon biocomposites in the palm tree *Syagrus coronata* (Mart.) Becc. *Protoplasma* **220**: 0089–0096.

**Liu J, Xia KF, Zhu JC, Deng YG, Huang XL, Hu BL, Xu X, Xu ZF. 2006.** The nightshade proteinase inhibitor IIb gene is constitutively expressed in glandular trichomes. *Plant and Cell Physiology* **47**: 1274–1284.

**Lookadoo SE, Pollard AJ. 1991.** Chemical contents of stinging trichomes of *Cnidoscolus texanus*. *Journal of Chemical Ecology* **17**: 1909–1916.

**Lowenstam HA, Weiner S. 1989.** *On Biomineralization.* New York: Oxford University Press.

**Lowenstam HA. 1981**. Minerals formed by organisms. *Science* **211**: 1126–1131.

**Luebert F, Cecchi L, Frohlich MW, et al. 2016.** Familial classification of the Boraginales. *Taxon* **65**: 502–522.

**Ma JF, Yamaji N. 2006.** Silicon uptake and accumulation in higher plants. *Trends in Plant Science* **11**: 392–397.

**Ma JF, Yamaji N. 2015.** A cooperative system of silicon transport in plants. *Trends in Plant Science* **20**: 435–442.

**Malizia D, Giuliano A, Ortaggi G, Masotti A. 2012.** Common plants as alternative analytical tools to monitor heavy metals in soil. *Chemistry Central Journal* **6**: 1–10.

**Mann S. 1983.** Mineralization in biological systems. In: Connett PH, Follmann H, Lammers M, Mann S, Odom JD, Wetterhahn KE, eds. *Inorganic Elements in Biochemistry*. Heidelberg: Springer, 125–174.

**Mazen AMA. 2004.** Calcium oxalate deposits in leaves of *Corchorus olitorius* as related to accumulation of toxic metals1. *Russian Journal of Plant Physiology* **51**: 281–285.

**Medeiros L, Moreira GR. 2002.** Moving on hairy surfaces: modifications of *Gratiana spadicea* larval legs to attach on its host plant *Solanum sisymbriifolium*. *Entomologia Experimentalis et Applicata* **102**: 295–305.

**Motamedi H, Seyyednejad SM, Bakhtiari A, Vafaei M. 2014.** Introducing *Urtica dioica*, a native plant of Khuzestan, as an antibacterial medicinal plant. *Jundishapur Journal of Natural Pharmaceutical Products* **9**: e15904.

**Naydenova GK, Georgiev GI. 2013.** Physiological function of non-glandular trichomes in red clover (*Trifolium pratense* L.). *Journal of Agricultural Sciences, Belgrade* **58**: 217–222.

**Nitta I, Kida A, Fujibayashi Y, Katayama H, Sugimura Y. 2006**. Calcium carbonate deposition in a cell wall sac formed in mulberry idioblasts. *Protoplasma* **228**: 201–208.

**Omelon S, Georgiou J, Henneman ZJ, Wise LM, Sukhu B, Hunt T, Wynnckyj C, Holmyard D, Bielecki R, Grynpas MD. 2009.** Control of vertebrate skeletal mineralization by polyphosphates. *PLoS One* **4**: e5634.

**Outenreath RL, Dauwaldert M. 1986.** Ultrastructural and radioautographic studies of the digestive gland cells of *Drosera capensis* II. Changes induced by stimulation. *Journal of Ultrastructure and Molecular Structure Research* **95:** 164–174.

**Payne WW. 1978.** A glossary of plant trichome terminology. *Brittonia* **30**: 239 – 255.

**Perry CC. 2009.** An overview of silica in biology: Its chemistry and recent technological advances. In: Werner EG, Müller Mikhael A. Grachev, eds. *Biosilica in evolution, morphogenesis, and nanobiotechnology*. Heidelberg: Spreinger, 295–313.

**Pigott CD. 1971.** Analysis of the response of *Urtica dioica* to phosphate. *New Phytologist* **70**: 953–966.

**Piperno DR. 2006.** *Phytoliths: a comprehensive guide for archaeologists and paleoecologists*. New York: Rowman Altamira Press.

**Pollard AJ, Briggs D. 1984.** Genecological studies of *Urtica dioica* L. *New Phytologist* **97**: 507–522.

**Pollard AJ. 1986.** Variation in *Cnidoscolus texanus* in relation to herbivory. *Oecologia* **70**: 411–413.

**Pritchard SG, Prior SA, Rogers HH, Peterson CM. 2000.** Calcium sulfate deposits associated with needle substomatal cavities of container-grown longleaf pine (*Pinus palustris*) seedlings. *International Journal of Plant Sciences* **161**: 917–923.

**Prychid CJ, Rudall PJ, Gregory M. 2003.** Systematics and biology of silica bodies in monocotyledons. *The Botanical Review* **69:** 377–440.

**Pullin AS, Gilbert JE. 1989.** The stinging nettle, *Urtica dioica*, increases trichome density after herbivore and mechanical damage. *Oikos* **54**: 275-280.

**Qi Y, Lian K, Chin KL, Ford RL. 2003.** Using EDX/SEM to study heavy metal uptake and elemental composition in plant tissues. *Microscopy and Microanalysis* **9**: 1486–1487.

**Rahn-Lee L, Komeili A. 2013.** The magnetosome model: insights into the mechanisms of bacterial biomineralization. *Frontiers in Microbiology* **4**: 352 (1-8).

**Rengel Z. 1992.** The role of calcium in salt toxicity. *Plant, Cell & Environment* **15**: 625–632.

**Sahebi M, Hanafi MM, Siti Nor Akmar A, Rafii MY, Azizi P, Tengoua FF, Azwa JNM, Shabanimofrad M. 2015.** Importance of silicon and mechanisms of biosilica formation in plants. *BioMed Research International* 1–16.

**Sakai WS, Hanson M, Jones RC. 1972.** Raphides with barbs and grooves in *Xanthosoma sagittifolium* (Araceae). *Science* **178**: 314–315.

**Salt DE, Prince RC, Pickering IJ, Raskin I. 1995.** Mechanisms of cadmium mobility and accumulation in Indian mustard. *Plant Physiology* **109**: 1427–1433.

**Sangster AG, Hodson MJ, and Tubb HJ. 2001.** Silicon deposition in higher plants. *Studies in Plant Science* **8**: 85–113.

**Sangster AG. 1978.** Electron-probe microassays for silicon in the roots of *Sorghastrum nutans* and *Phragmites communis*. *Canadian Journal of Botany* **56**:1074–1080.

**Sangster AG., and Parry DW. 1981.** Ultrastructure of silica deposits in higher plants. In: Simpson TL, Volcani BE, eds. *Silicon and Siliceous structures in biological Systems*). New York: Springer-Verlag, 383–407.

**Sarret G, Isaure MP, Marcus MA, Harada E, Choi YE, Pairis S, Fakra S, Manceau A. 2007.** Chemical forms of calcium in Ca, Zn-and Ca, Cd-containing grains excreted by tobacco trichomes. *Canadian Journal of Chemistry* **85**: 738–746.

**Sarret G, Willems G, Isaure MP, Marcus MA, Fakra SC, Frerot H, Pairis S, Geoffroy N, Manceau A, Saumitou-Laprade P. 2009.** Zinc distribution and speciation in *Arabidopsis halleri* x *Arabidopsis lyrata* progenies presenting various zinc accumulation capacities. *New Phytologist* **184**: 581–595.

**Schilmiller AL, Last RL, Pichersky E. 2008.** Harnessing plant trichome biochemistry for the production of useful compounds. *The Plant Journal* **54**: 702–711.

**Selvi F, Bigazzi M. 2001.** Leaf surface and anatomy in Boraginaceae tribe Boragineae with respect to ecology and taxonomy. *Flora* **196**: 269–285.

**Shepherd RW, Bass WT, Houtz RL, Wagner GJ. 2005.** Phylloplanins of tobacco are defensive proteins deployed on aerial surfaces by short glandular trichomes. *The Plant Cell* **17**: 1851–1861.

**Skaltsa H, Verykokidou E, Harvala C, Karabourniotis G, Manetasi Y 1994.** UV-B protective potential and flavonoid content of leaf trichomes of *Quercus ilex*. *Phytochemistry* **37**: 987–990.

**Snyder JC, Guo Z, Thacker R, Goodman JP, Pyrek JS. 1993.** 2, 3-Dihydrofarnesoic acid, a unique terpene from trichomes of *Lycopersicon hirsutum*, repels spider mites. *Journal of Chemical Ecology* **19**: 2981–2997.

**Sommer M, Kaczorek D, Kuzyakov Y, Breuer J. 2006.** Silicon pools and fluxes in soils and landscapes–a review. *Journal of Plant Nutrition and Soil Science* **169**: 310–329.

**Sommerdijk NAJM, Cusack M. 2014.** Biomineralization: crystals competing for space. *Nature Materials* **13**: 1078.

**Sowers AE, Thurston EL. 1979.** Ultrastructural evidence for uptake of silicon-containing silicic acid analogs by *Urtica pilulifera* and incorporation into cell wall silica. *Protoplasma* **101**: 11–22.

**Tamai K, Ma JF. 2008.** Reexamination of silicon effects on rice growth and production under field conditions using a low silicon mutant. *Plant and Soil* **307**: 21–27.

**Thamatrakoln K, Hildebrand M. 2008.** Silicon uptake in diatoms revisited: a model for saturable and nonsaturable uptake kinetics and the role of silicon transporters. *Plant Physiology* **146**: 1397–1407.

**Thurston EL, Lersten NR 1969.** The morphology and toxicology of plant stinging trichomes. *The Botanical Review* **35**: 393–412.

**Thurston EL. 1969.** An anatomical and fine structure study of stinging hairs in some members of the Urticaceae, Euphorbiaceae and Loasaceae. Ph.D. dissertation, Iowa State University, Ann Arbor, Michigan, USA.

**Thurston EL. 1974.** Morphology, fine structure, and ontogeny of the stinging emergence of *Urtica dioica. American Journ*al *of Botany* **61**: 809–817.

**Trembath-Reichert E, Wilson JP, McGlynn SE, Fischer WW. 2015.** Four hundred million years of silica biomineralization in land plants. *Proceedings of the National Academy of Sciences* **112**: 5449–5454.

**Tuberville TD, Dudley PG, Pollard AJ. 1996.** Responses of invertebrate herbivores to stinging trichomes of *Urtica dioica* and *Laportea canadensis*. *Oikos* **75**: 83–88.

**Tudor HE, Gryte CC, Harris CC. 2006.** Seashells: detoxifying agents for metal-contaminated waters. *Water, Air, & Soil Pollution* **173**: 209–242.

**Van Cappellen P. 2003.** Biomineralization and global biogeochemical cycles. *Reviews in Mineralogy and Geochemistry* **54**: 357–381.

**Vance CP, Uhde-Stone C, Allan, DL. 2003.** Phosphorus acquisition and use: critical adaptations by plants for securing a nonrenewable resource. *New phytologist* **157**: 423–447.

**Vandevenne F, Struyf E, Clymans W, Meire P. 2012.** Agricultural silica harvest: have humans created a new loop in the global silica cycle?. *Frontiers in Ecology and the Environment* **10**: 243–248.

**Vogl CR, Hartl A. 2003**. Production and processing of organically grown fiber nettle (*Urtica dioica* L.) and its potential use in the natural textile industry: A review. *American Journal of Alternative Agriculture* **18**: 119–128.

**Wagner H, Willer F, Kreher B. 1989.** Biologically active compounds from the aqueous extract of *Urtica dioica*. *Planta Medica* **55**: 452–454.

**Weathers PJ, Arsenault PR, Covello PS, McMickle A, Teoh KH, Reed DW. 2011.** Artemisinin production in *Artemisia annua*: studies in planta and results of a novel delivery method for treating malaria and other neglected diseases. *Phytochemistry Reviews* **10**: 173–183.

**Webb MA. 1999.** Cell-mediated crystallization of calcium oxalate in plants. *The Plant Cell* **11**: 751–761.

**Weigend M. 2004.** Loasaceae. In: Kubitzki K, Bayer C, eds. *The families and genera of the vascular plants*. Heidelberg: Springer, 239–254.

**Weiner S, Addadi L. 1997.** Design strategies in mineralized biological materials. *Journal of Materials Chemistry* **7**: 689–702.

**Weiner S, Addadi L. 2011.** Crystallization pathways in biomineralization. *Annual Review of Materials Research* **41**: 21–40.

**Weiner S, Dove, PM. 2003.** An overview of biomineralization processes and the problem of the vital effect. *Reviews In Mineralogy and Geochemistry* **54**: 1–29.

**Weiss IM, Marin F. 2008.** The role of enzymes in biomineralization processes. In: Sigel A, Sigel H, Sigel RKO, eds. *Metal Ions In Life Science, Biomineralization: From Nature to Application.* West Sussex, UK: John Wiley & Sons, 71–126.

**Werker E. 2000**. Trichome diversity and development. *Advances in Botanical Research* **3**: 1–35.

**Webster, G. L. 2014.** Euphorbiaceae. In: Kubitzki K (eds) Flowering Plants Eudicots *The families and genera of vascular plants*, vol 11. Heidelberg: Springer, 51–216.

**Weston PA, Johnson DA, Burton HT, Snyder JC. 1989.** Trichome secretion composition, trichome densities, and spider mite resistance of ten accessions of *Lycopersicon hirsutum*. *Journal of the American Society for Horticultural Science* **114**: 492–498.

**White PJ, Bowen HC, Demidchik V, Nichols C, Davies JM. 2002.** Genes for calcium-permeable channels in the plasma membrane of plant root cells. *Biochimica et Biophysica Acta (BBA)-Biomembranes* **1564**: 299–309.

**White PJ, Broadley MR. 2003.** Calcium in plants. *Annals of Botany* **92**: 487–511.

**Wilt FH, Killian CE. 2008.** What genes and genomes tell us about calcium carbonate In: Sigel A, Sigel H, Sigel RKO, eds. *Metal Ions In Life Science, Biomineralization: From Nature to Application.* West Sussex, UK: John Wiley & Sons, 36–69.

**Wissuwa M. 2003.** How do plants achieve tolerance to phosphorus deficiency? Small causes with big effects. *Plant Physiology* **133**: 1947–1958.

**Wu CC, Kuo-Huang LL. 1997.** Calcium crystals in the leaves of some species of Moraceae. *Botanical Bulletin of Academia Sinica* **38**: 97–104.

**Wu ZY, Milne RI, Chen CJ, Liu J, Wang H, Li DZ. 2015.** Ancestral state reconstruction reveals rampant homoplasy of diagnostic morphological characters in Urticaceae, conflicting with current classification schemes. *PloS One* **10**: e0141821.

**Wyn Jones RG, Lunt OR. 1967.** The function of calcium in plants. *The Botanical Review* **33**: 407–426.

**Yamanaka S, Takeda H, Komatsubara S, Ito F, Usami H, Togawa E, Yoshino K. 2009.** Structures and physiological functions of silica bodies in the epidermis of rice plants. *Applied Physics Letters* **95**: 123703.

**Ye M, Song, Y, Long J, Wang R, Baerson SR, Pan Z, Zhu-Salzman K, Xie J, Cai K, Luo S, Zeng R. 2013.** Priming of jasmonate-mediated antiherbivore defense responses in rice by silicon. *Proceedings of the National Academy of Sciences* **110**: E3631–E3639.

**Yu H, Kowalski SP, Steffens JC. 1992.** Comparison of polyphenol oxidase expression in glandular trichomes of *Solanum* and *Lycopersicon* species. *Plant Physiology* **100**: 1885–1890.

**Zhang X, Thacker RR, Snyder JC. 2008.** Occurrence of 2, 3-dihydrofarnesoic acid, a spidermite repellent, in trichome secretions of *Lycopersicon esculentum* × *L. hirsutum* hybrids. *Euphytica* **162**: 1–9.

**Zhao FJ, Lombi E, Breedon TMSP. 2000.** Zinc hyperaccumulation and cellular distribution in *Arabidopsis halleri*. *Plant, Cell and Environment* **23**: 507–514.

**Zhao Q, Chen XY. 2016.** Development: A new function of plant trichomes. *Nature Plants* **2**: 16096.

# APPENDIX

## Appendix to Chapter 2

## Ontogeny and the process of biomineralization in the trichomes of Loasaceae*

* Mustafa A, Ensikat HJ, Weigend M. 2017. Ontogeny and the process of biomineralization in the trichomes of Loasaceae. *American Journal of Botany* 104: 367—378.

Mustafa et al. — *American Journal of Botany* 2017. DOI: 10.3732/ajb.1600417.s1 — Appendix S1

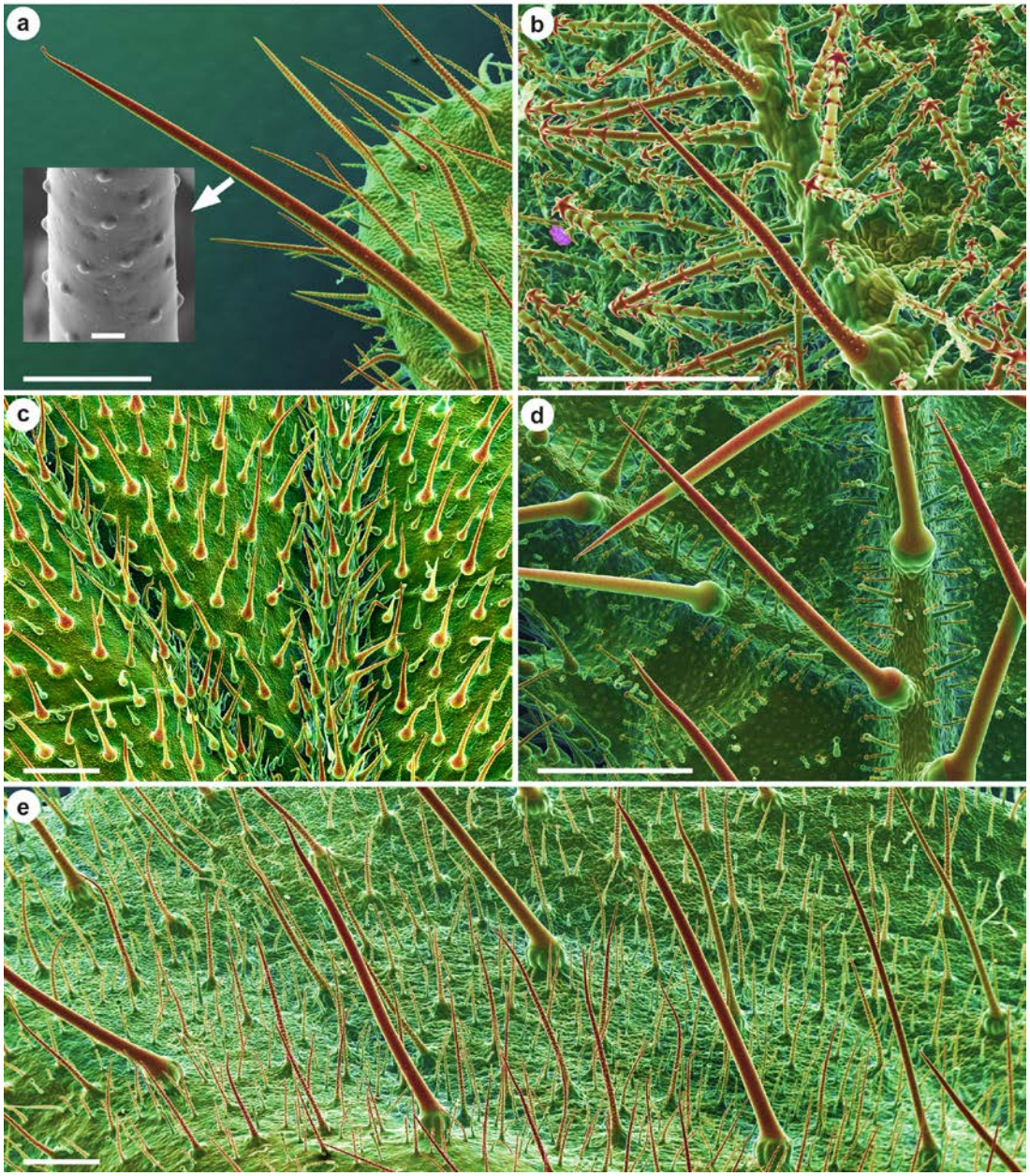


**Appendix S1.** Exemplary trichome distributions on adaxial and abaxial leaves surfaces**.** (a) Adaxial leaf surface of *Loasa pallida* with scabrid trichomes and fully developed stinging trichome at the apex of the leaf, showing a granular pattern on the shaft (high magnification inset, scale bar = 10 µm). (b) Scabrid and glochidiate trichomes on abaxial leaf of *Loasa pallida*. (c) Scabrid trichomes on adaxial leaf surface of *Nasa contumazensis*, showing surface area free from stinging trichomes. (d) Stinging trichomes and glochidiate trichomes on the abaxial leaf surface of *Blumenbachia hieronymi*; note the presence of stinging hairs on the leaf veins only. (e) Complex indument on adaxial leaf surface of *Loasa pallida* with long stinging trichomes and a range of different scabrid-glochidiate trichomes. Scale bars: 500 µm in a–e.

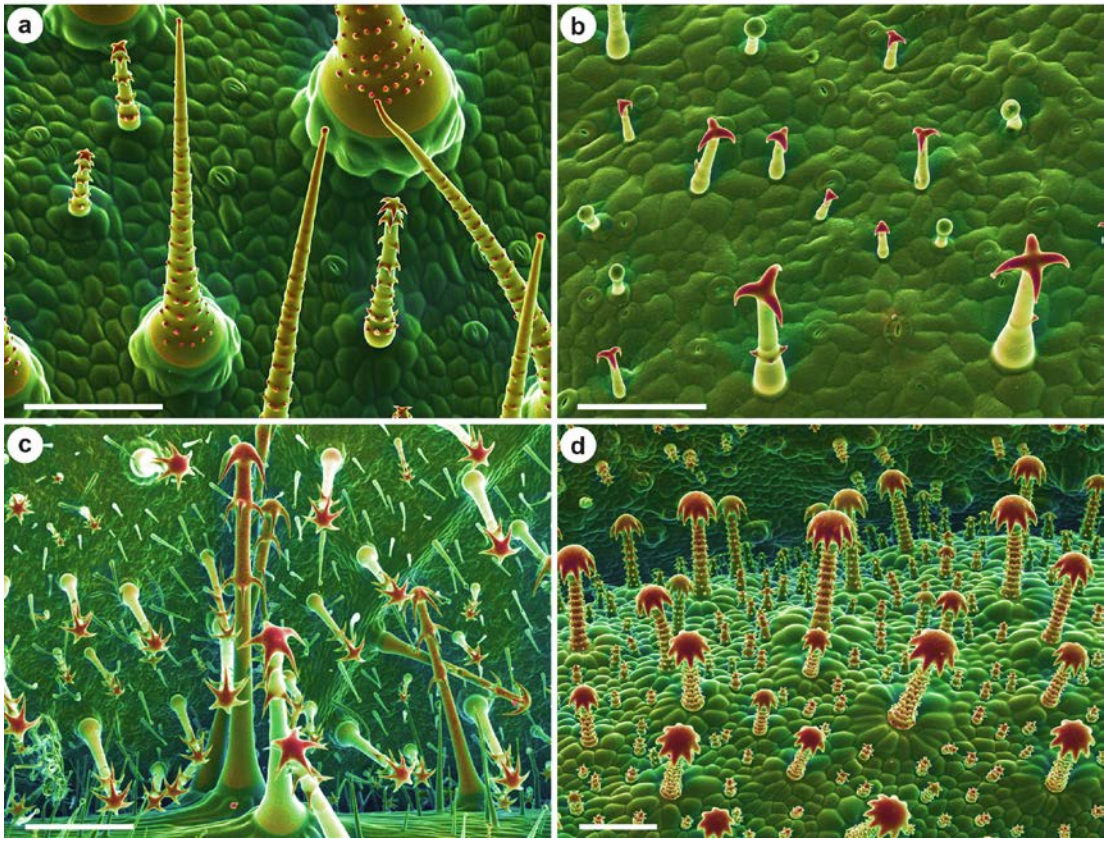


**Appendix S2.** Diversity of mineralized, glochidiate trichomes [combined secondary electron (SE) and backscattered electron (BE) images]. (a) Adaxial leaf surface of *Blumenbachia insignis*, showing mineralized scabrid trichomes and glochidiate trichomes in variable sizes with small retrorse barbs. (b) A range of different glochidiate (and glandular) trichomes on the abaxial leaf surface of *Loasa elongata*. (c) Glochidiate and scabrid trichomes on the abaxial lead surface of *Eucnide urens*, on and around the midvein. (d) Distinctive type of glochidiate trichomes on the fruit of *Blumenbachia insignis*. Scale bars: 100 µm in a,b,d; 500 µm in c.

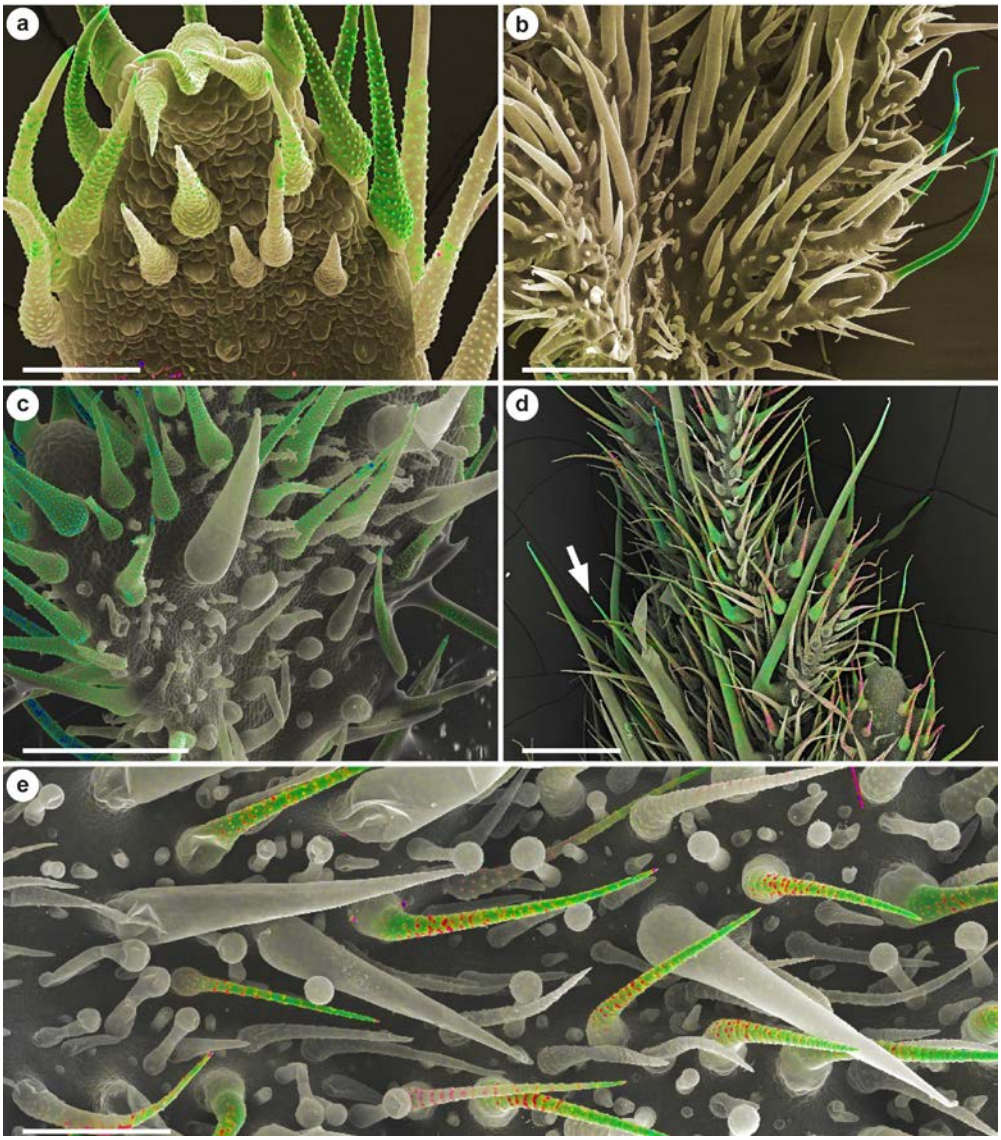


**Appendix S3.** Early trichome development. (a) Procurrent development of scabrid trichomes on the sepals of *Loasa triloba*, showing incipient mineralization (Ca = green color). Leaf base is at this stage without trichomes. (b-c) Adaxial leaf surface of *Loasa triloba*, showing developing stinging trichomes near the base. Non-mineralized trichomes appear colorless. (d) At a later stage, the stinging trichomes close to the leaf apex (*Blumenbachia hieronymi*) are mineralized with calcium compounds (green). The combined topography and EDX element-mapping image shows the presence of Ca contents in green and silicon in red colors. Some stinging trichomes have mineralized tips only (arrow). Most stinging trichomes in the basal region are non-mineralized and collapsed, indicating a very thin and fragile wall. Scabrid trichomes located between the stinging trichomes appear in red and green due to calcium and silicon contents. (e) Stinging trichomes of *Caiophora clavata* with fully developed globule on the adaxial leaf surface showing non-mineralized state. Scale bars: 100 µm in a; 500 µm in b,d; 300 µm in c,e.

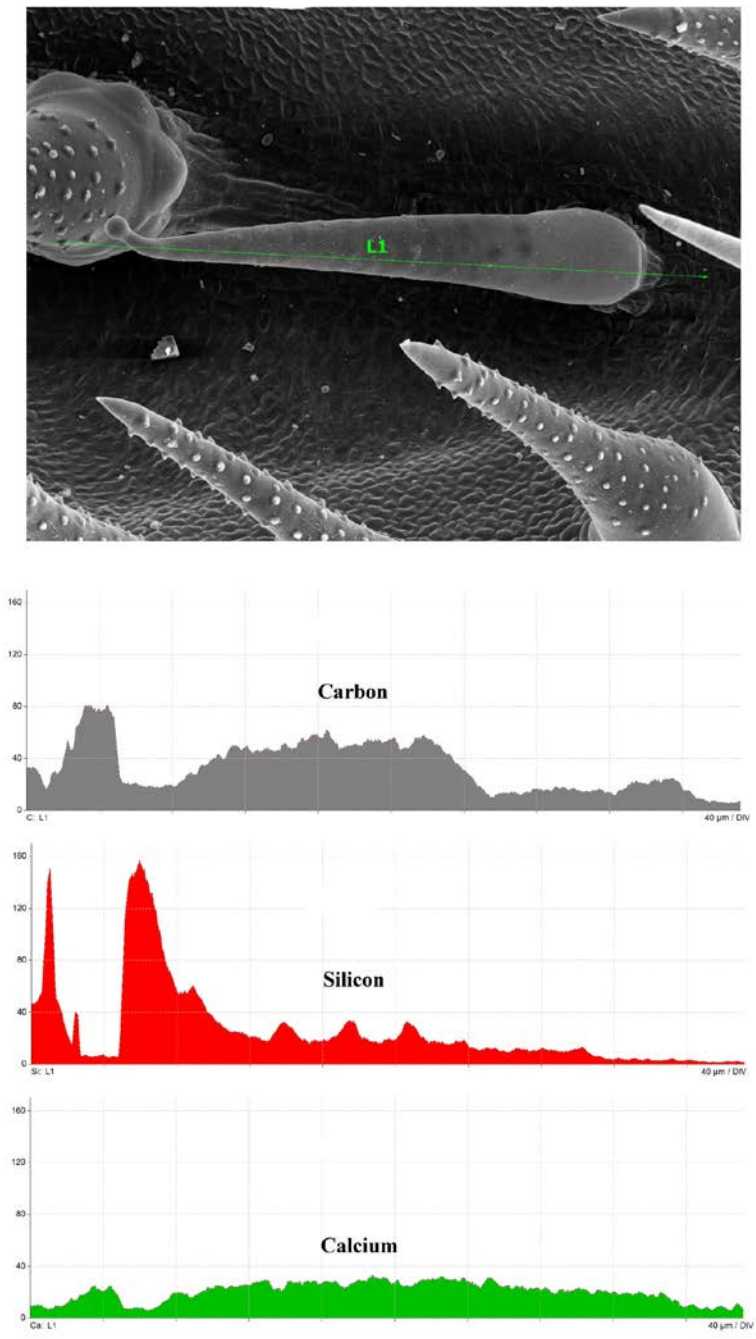


**Appendix S4.** Distribution of biominerals in a stinging trichome of *Aosa uleana*. EDX line scan from the tip to the base shows the occurrence and concentrations of silicon (Si), calcium (Ca) and carbon (C). High concentration of Si is limited to the apical region, whereas the shaft contains all three selected elements.

# Appendix to Chapter 3

## Complex patterns of multiple biomineralization in single-celled plant trichomes of the Loasaceae*

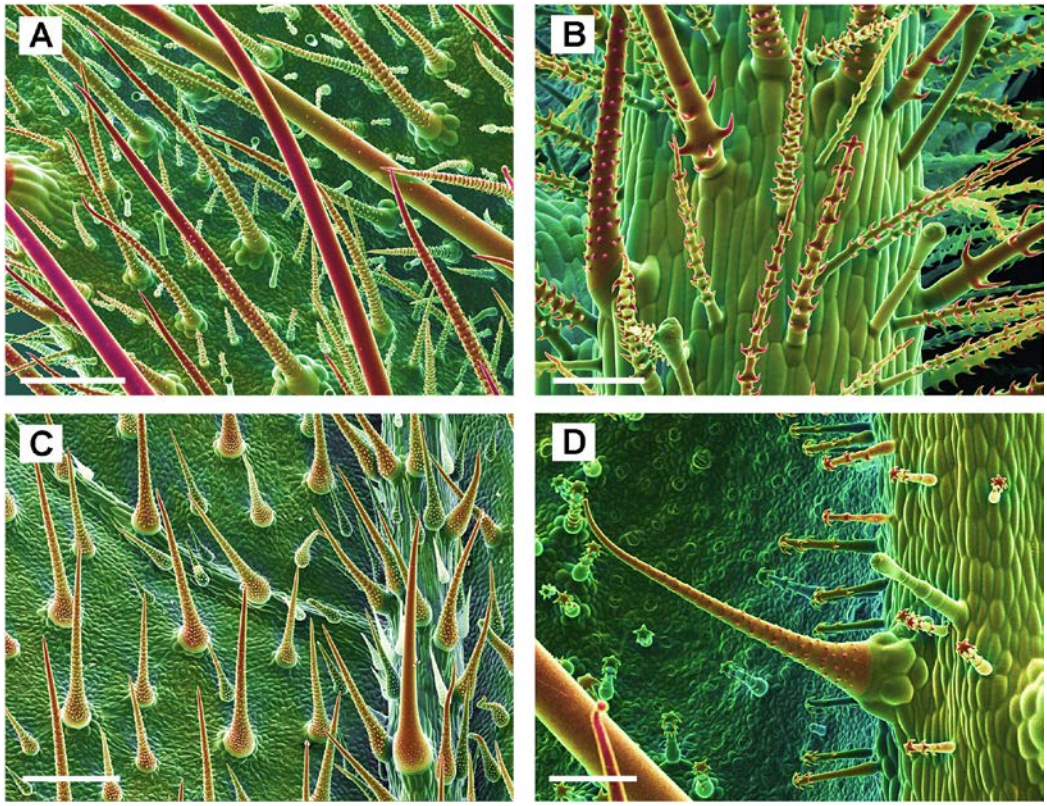


**Appendix S1.** Variability of scabrid trichomes. (A) Adaxial leaf surface of *Loasa pallida*, showing size variability of scabrid trichomes. (B) Trichomes on the veins of the abaxial leaf surface of *Loasa pallida* have sharp tips like those of scabrid trichomes, but surface sculpturing varies between grains and hooks (the latter resembling those of glochidiate trichomes). (C) Scabrid trichomes on the adaxial leaf surface upper side of *Nasa contumazensis* show sharp tips and a fine grainy surface structure. (D) *Blumenbachia hieronymi* scabrid trichomes have the typical granular surface pattern, but are provided with a rounded apex. Small glochidiate trichomes and a non-mineralized glandular trichome (4) can also be seen on this image. Scale bars: 300 µm in A, C; 100 µm in B, D.

* Ensikat HJ, Mustafa A, Weigend M. 2017. Complex patterns of multiple biomineralization in single-celled plant trichomes of the Loasaceae. *American Journal of Botany* 104: 195—206.

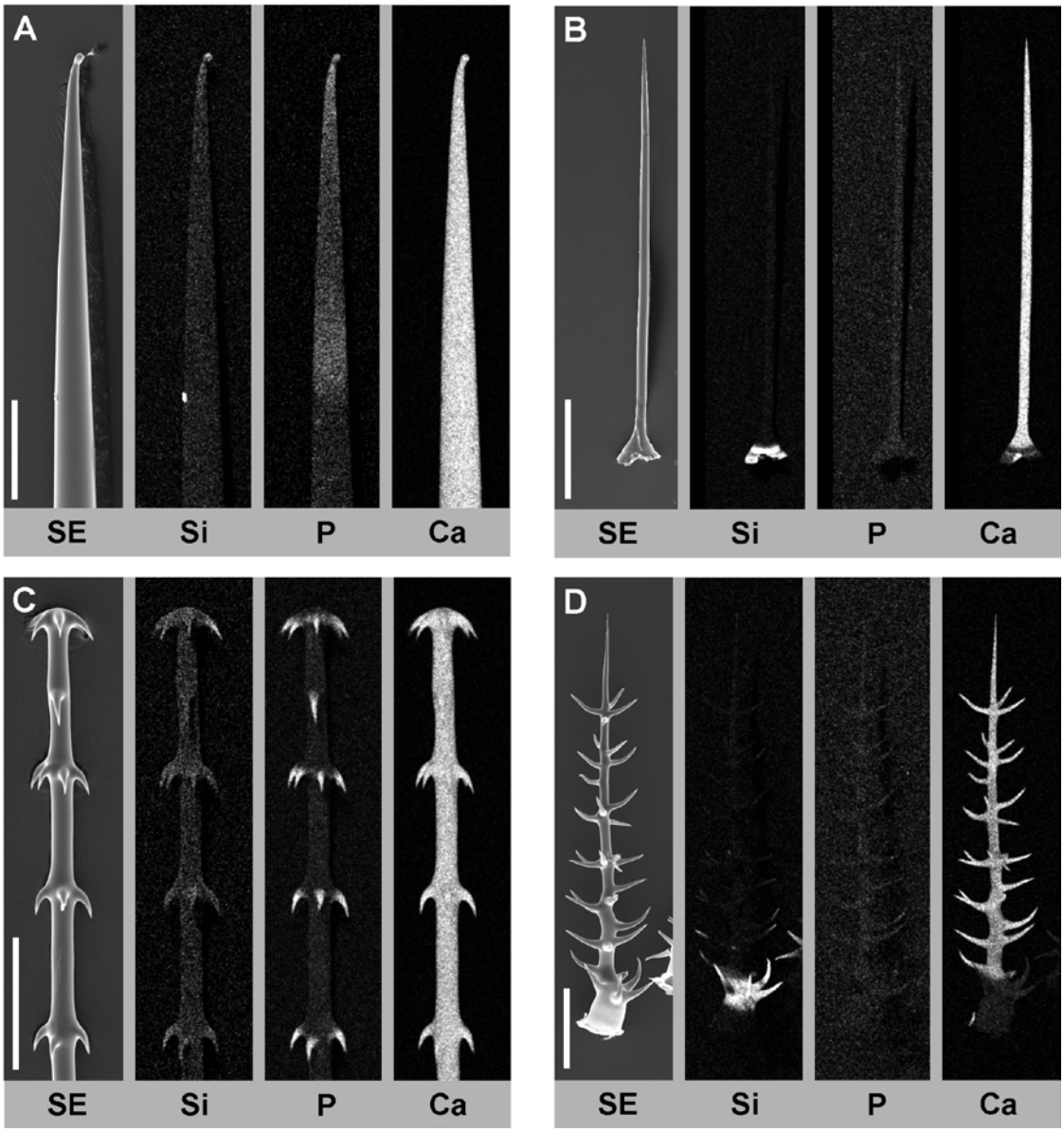


**Appendix S2.** Additional biomineral distribution patterns in stinging and glochidiate trichomes. (A) Stinging hairs of *Presliophytum heucheraefolium* resemble those of the *Nasa* species, with silica and calcium phosphate in the apex, and Ca in the shaft. (B) Stinging hairs of *Eucnide urens* are mineralized with calcium carbonate only, no phosphorus is detected in the apex. The base contains Si in high concentrations. (C) Glochidiate trichome hooks of *Presliophytum* contain mainly calcium phosphate and only traces of Si. (C) *Huidobria fruticose* trichomes are mineralized mainly with Ca; Si is found only at trichome base. Scale bars: 100 µm in A, C, D; 500 µm in B.

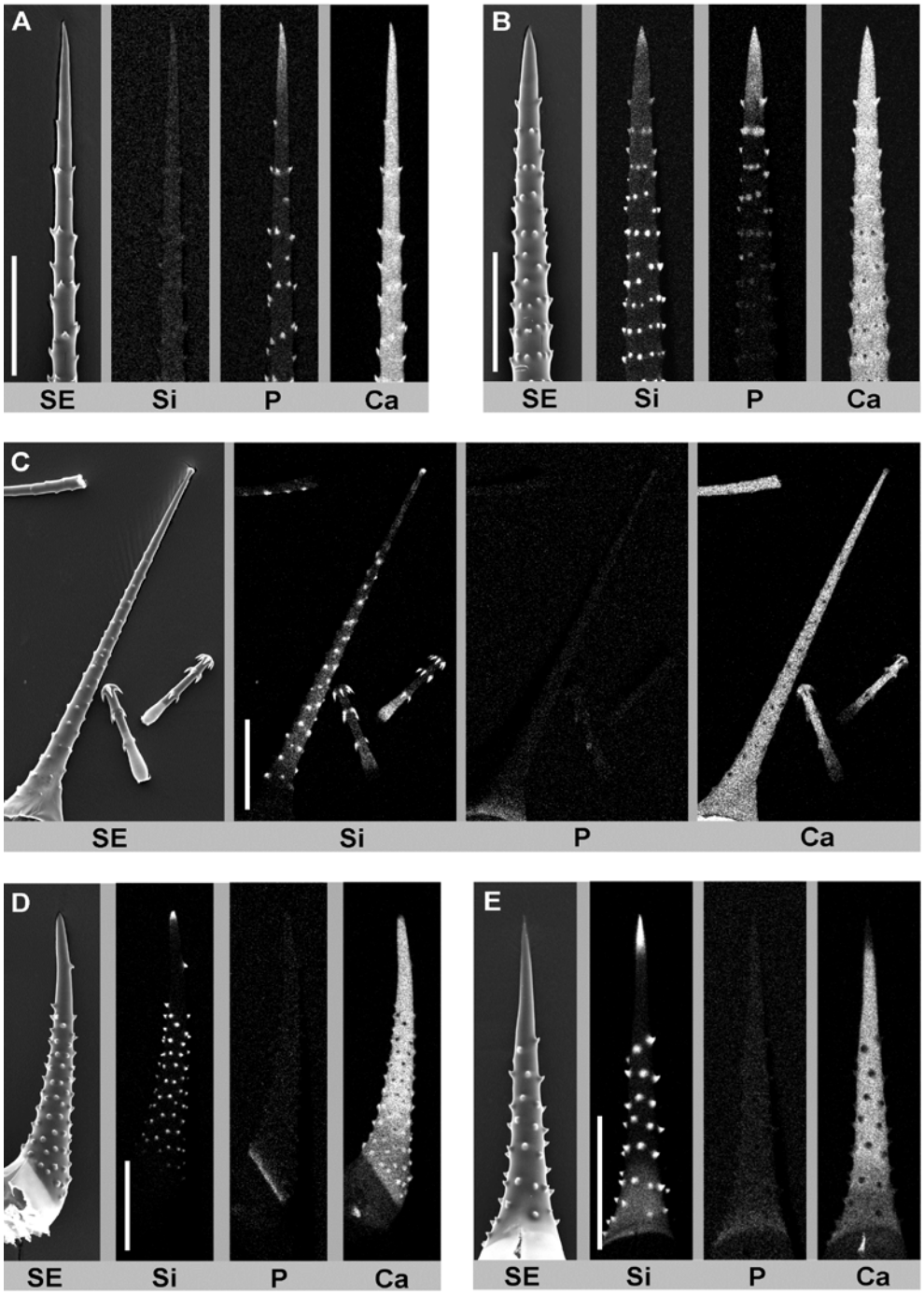


**Appendix S3.** Biomineral distribution in scabrid trichomes of various species. (A) *Loasa pallida*; (B) *Caiophora clavata*; (C) *Blumenbachia hieronymi*; (D) *Nasa weigendii*; (E) *Aosa uleana*. Element distribution in different taxa resembles largely that of corresponding glochidiate trichomes: Scabrid trichomes of *Loasa* are free from Si; those of *Caiophora* contain silica, calcium phosphate, and calcium carbonate; *Blumenbachia, Nasa,* and *Aosa* scabrid trichomes contain silica, but no calcium phosphate, except for traces at the trichome bases (D). Scale bars: 100 µm.

# Appendix to Chapter 4

## Diversity of Biomineralization in Stinging trichomes of Different Plant Families: Silica, Calcium phosphate, or neither?*

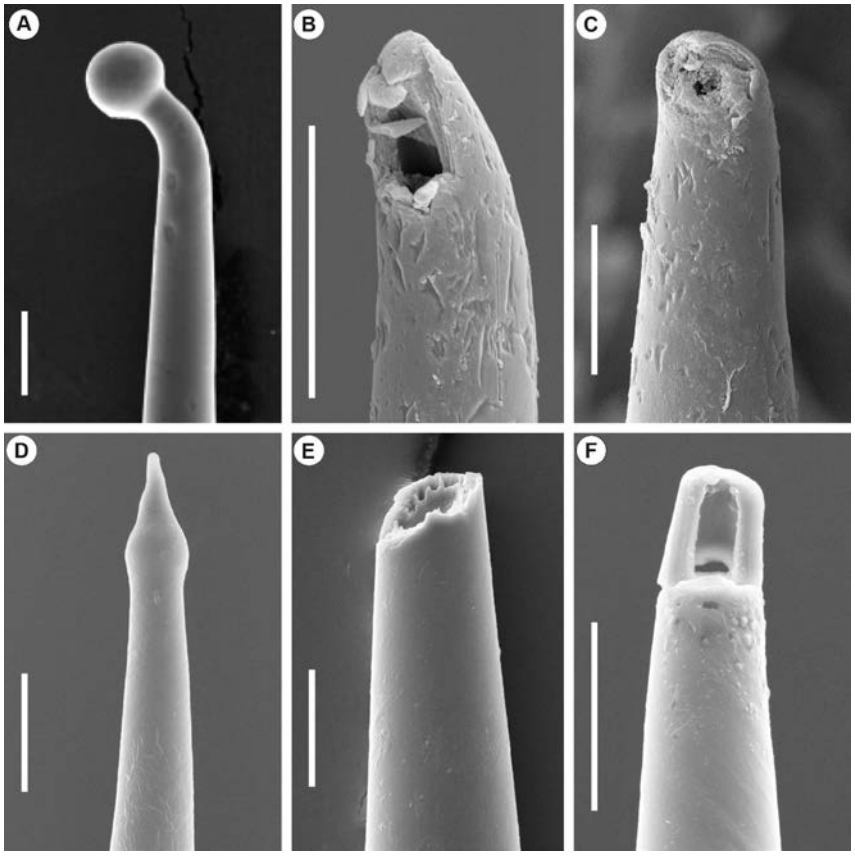


**Fig. S1.** Functional features of stinging hairs of Loasaceae and Namaceae. (A-C) Stinging hairs of *Caiophora deserticola*. (D-E) Stinging hairs of *Wigandia caracasana.* The stinging hair tips (A, D) on the left column are intact, whereas the stinging hair tips in the middle and right columns (B, C, E, F) are broken, illustrating their capability to act as a hypodermic syringe. The broken tips readily penetrate the skin and inject the irritating liquid into the skin. Scale bars: A-F = 20 µm.

* Mustafa, A., Ensikat, H. J., Weigend, manuscript in preparation.

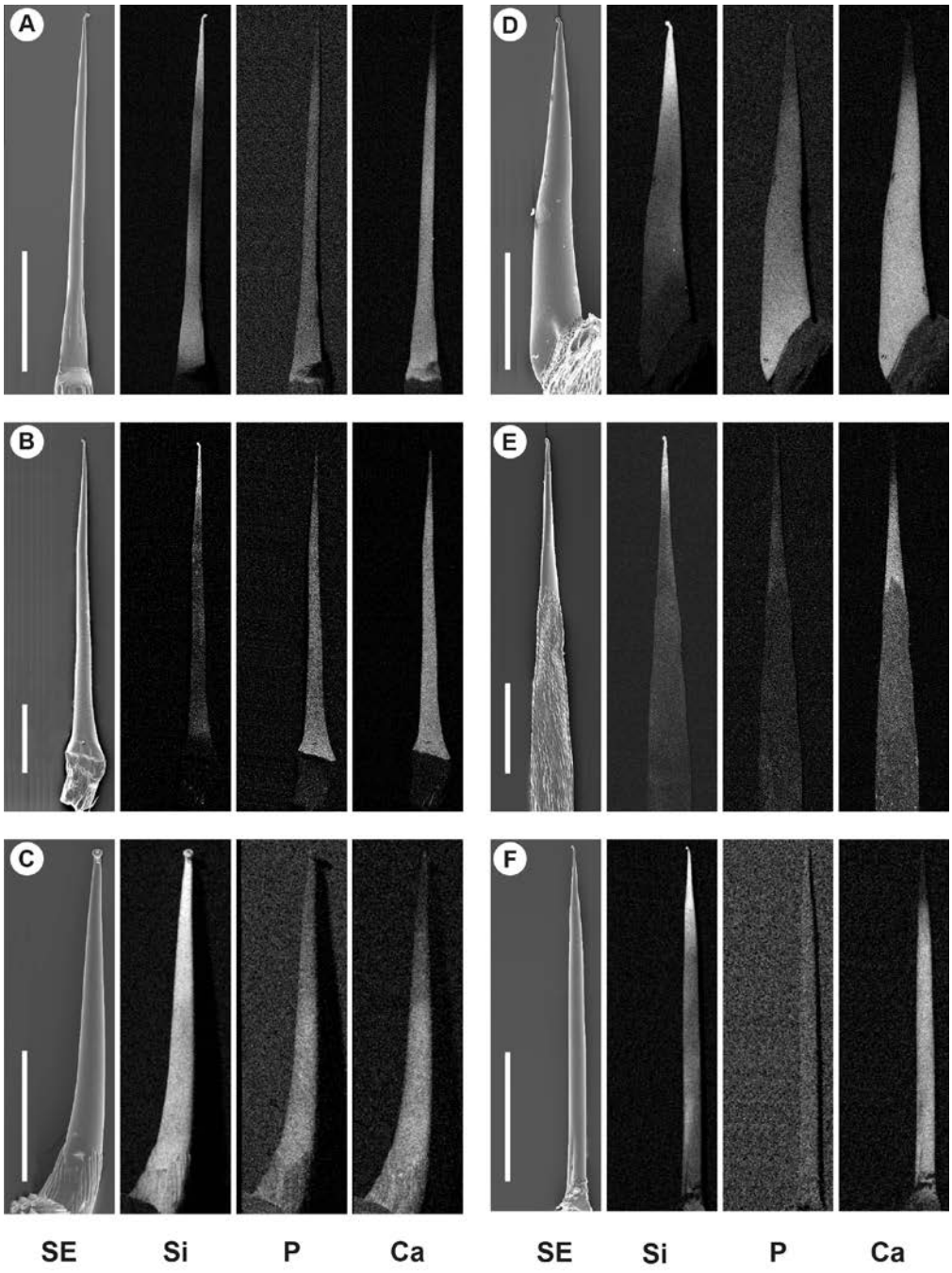


**Fig. S2.** EDX element-mapping micrographs of full length stinging hairs of Urticaceae. (A) *Urtica dioica*; (B) *Urtica mairei*; (C) *Urera baccifera*; (D) *Laportea perrieri*; (E) *Girardinia cuspidata*; (F) *Dendrocinide moroides*. A view of full length stinging hairs shows that the tips of all hairs are heavily mineralized with silica, and Ca is usually present in all parts except the regions with high Si concentration. P concentrations in the shaft vary strongly between taxa; *Urtica mairei*, *Urera baccifera*, and *Laportea perrieri* (B, C, D) show strong P signals, whereas *Urtica dioica*, *Girardinia cuspidata* and *Dendrocnide moroides* (A, E, F) have only traces or no P in the shafts. Scale bars: A, B, D, E, F = 500 µm, C = 300 µm.

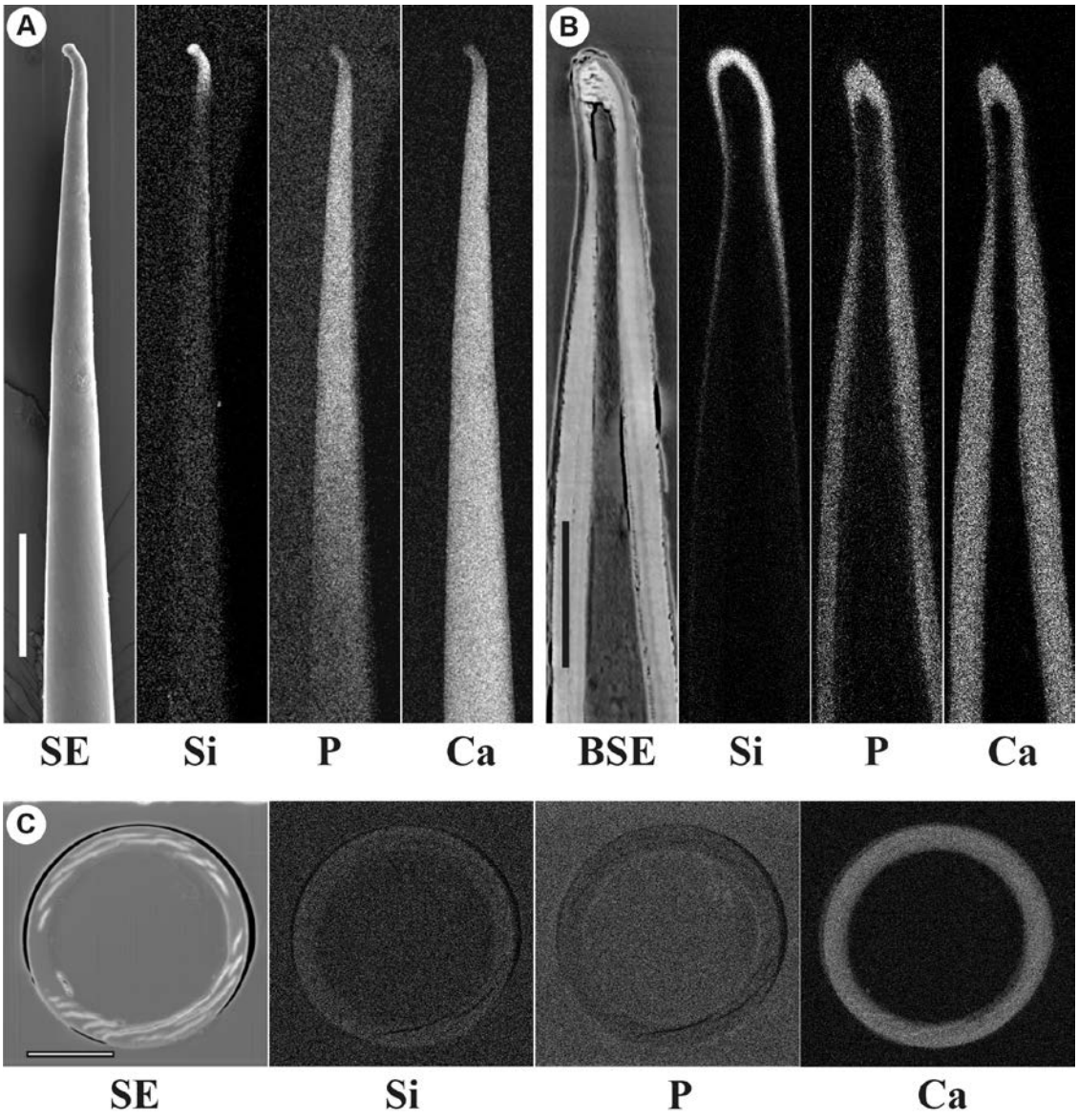


**Fig. S3.** EDX mapping images of selected elements of stinging hairs shown as color images in Fig. 4 B-D. In individual grayscale images the weaker signals (e.g., silica coating) can be more readily visualized than in combined color images. Scale bars: A = 100 µm; B, C = 30 µm.

# Appendix to Chapter 5

## Mineralized Trichomes in Boraginales – complex microscale heterogeneity and simple phylogenetic patterns*

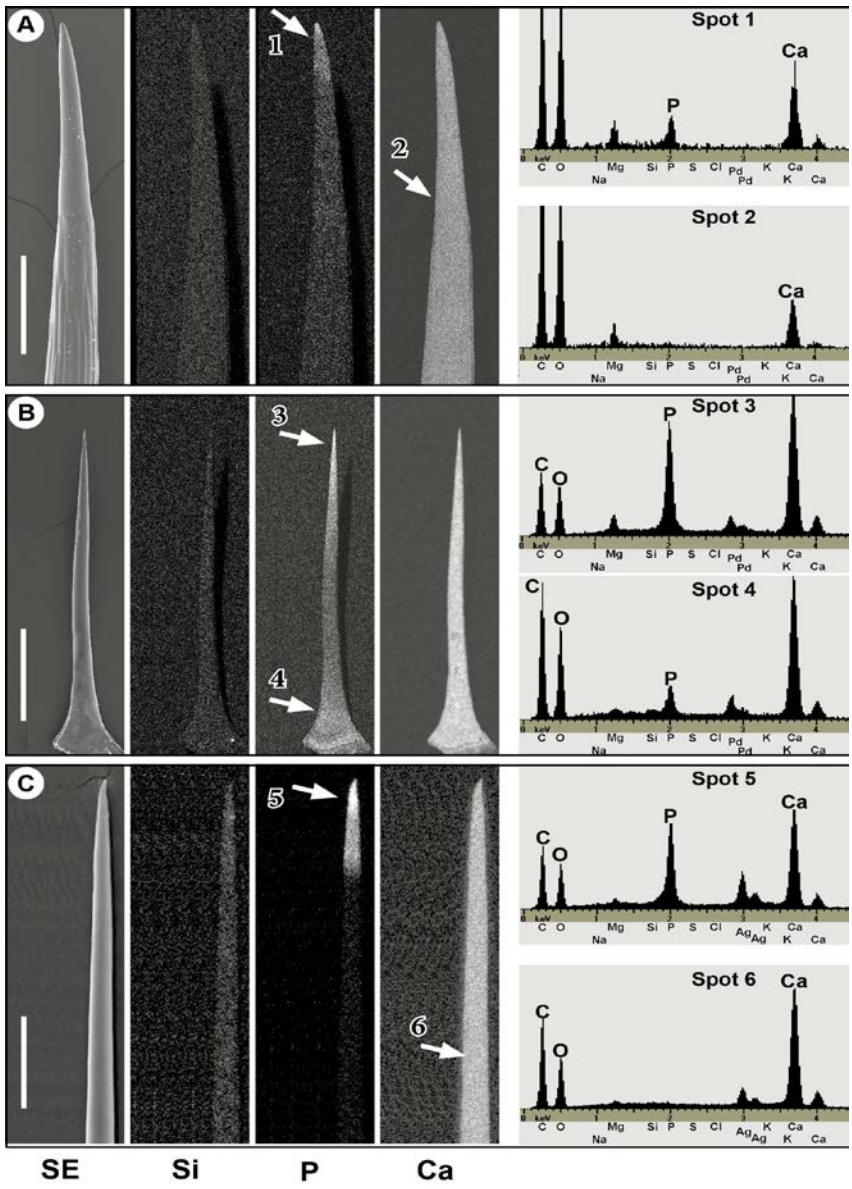


**Fig. S1.** EDX-mapping of selected trichomes: (A) *Codon schenckii*, (B) *Phacelia malvifolia and*, (C) *Nama rothrockii*. Arrows indicate locations of EDX spectrum acquisition. In *Codon* and *Nama*, P is restricted to a very small region in the trichome tip, whereas the *Phacelia* trichome contains P over the entire length. Scale bars: A = 300 µm; B = 600 µm; C = 30 µm.

* Mustafa, A., Ensikat, H. J., Weigend, manuscript submitted to *Annals of Botany* (In press), 13/11/2017

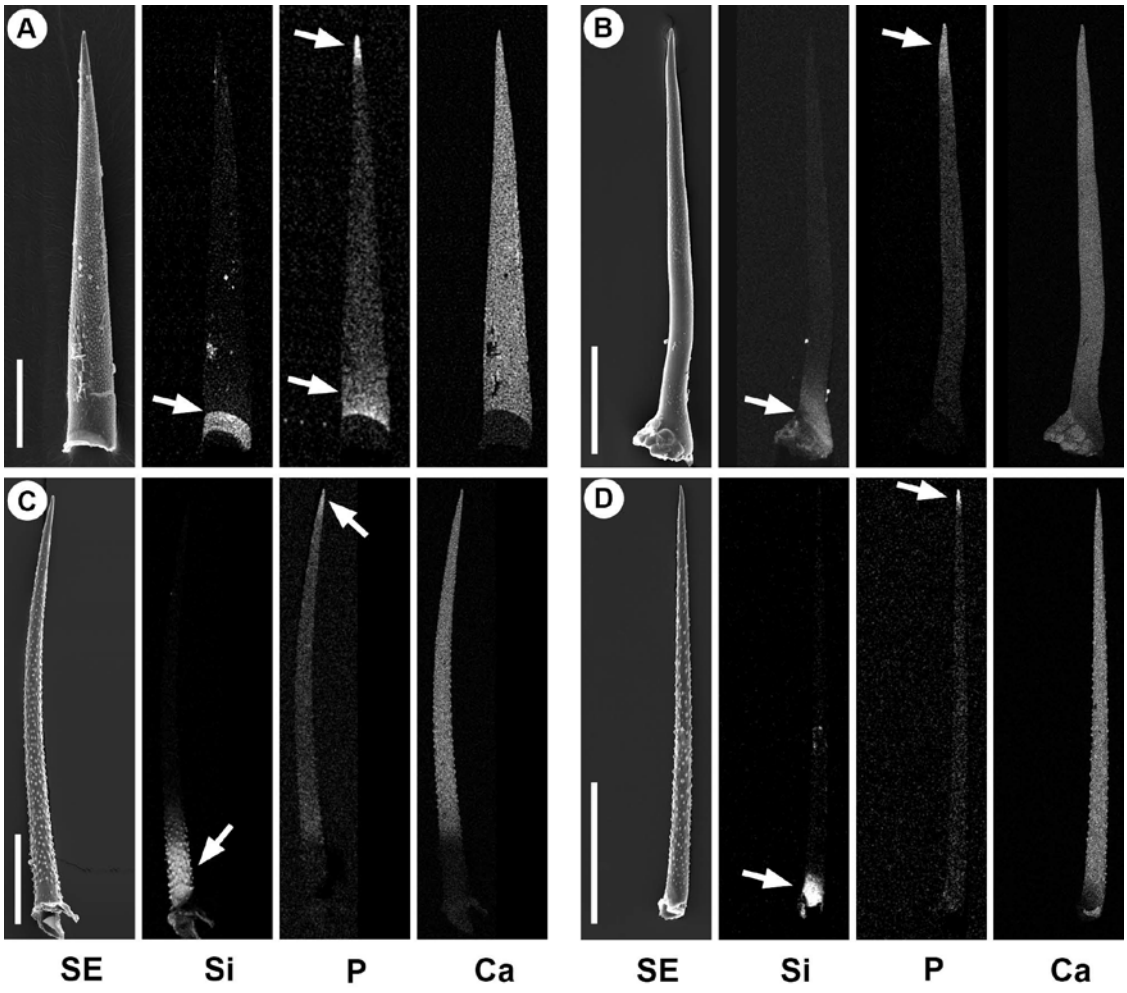


**Fig. S2.** EDX-mapping images of selected trichomes containing calcium phosphate in the tips and silica in the bases; separate gray-scale images of the trichomes shown in Fig. 4D-G: (A) *Hydrophyllum canadense*, (B) *Heliotropium corymbosum*, (C) *Ehretia dicksonii*, (D) *Coldenia procumbens.* High concentrations of Ca and P are restricted to tips of the trichomes, Si to the basal regions (arrows). In individual gray-scale mapping images lower concentrations of elements can be recognized than in combined colored images. Scale bars: A = 100 µm; B, C, D = 200 µm.

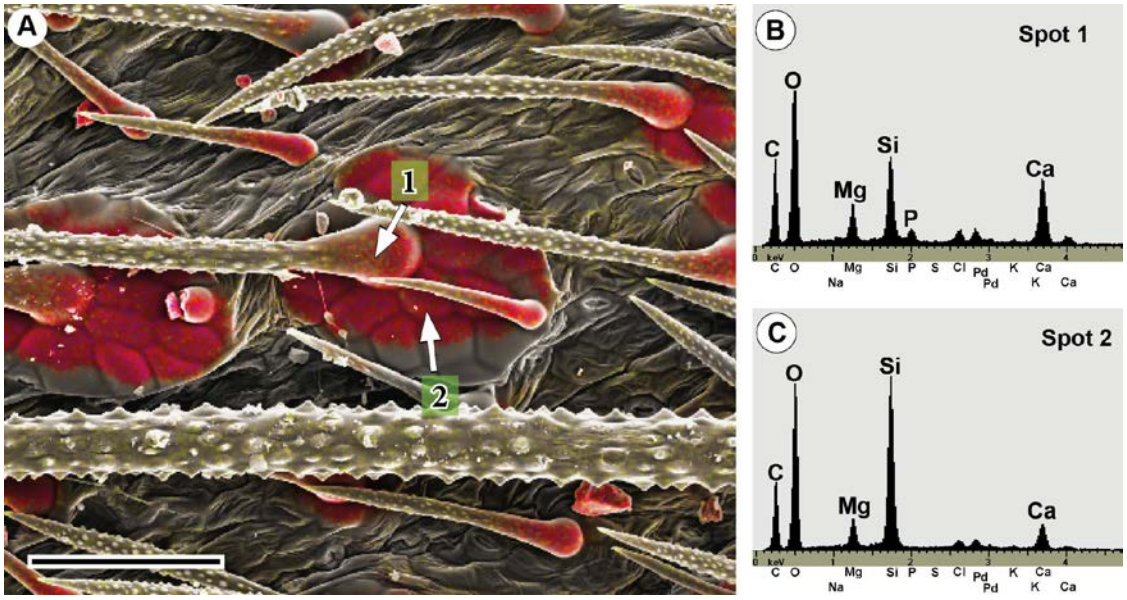


**Fig. S3.** Element distribution in the trichome foot cells of *Wellstedia dinteri*. (A) SEM-color image obtained by combining the SE image with EDX-element mapping images shows the distribution of Si (red) and P (green) in trichomes. Bases show high concentrations of Si along small traces of P (Spot 1), whereas foot cells are mineralized with high concentrations of Si (Spot 2). (B-C) EDX spectra from two locations [marked in A as 1, 2 (arrow)] show the high concentrations of Si, low concentrations of Ca at the base and foot cells. Scale bars: = 100 µm.

# Appendix to Chapter 6

## Calcium phosphate in plant trichomes: the overlooked biomineral*

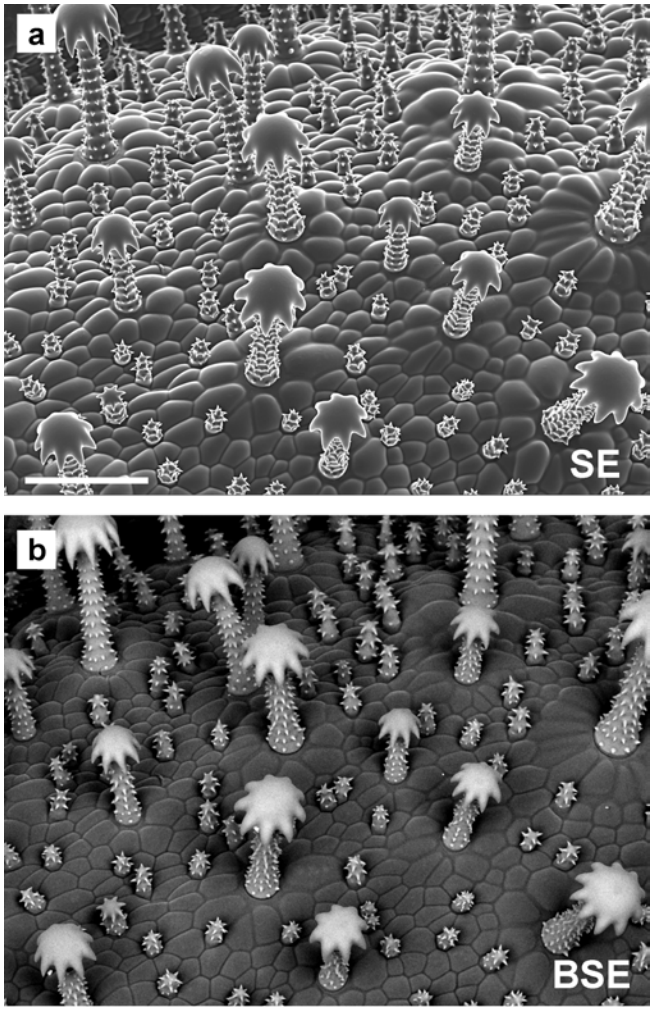


**Fig. S1.** Separate secondary electron (SE) and backscattered electron (BSE) images of Fig. 1a. The cryo-SEM images show (a) topographical and (b) compositional contrast of trichomes on the inferior

* Weigend, M., Mustafa, A., Ensikat, H. J. 2018. Calcium phosphate in plant trichomes: the overlooked biomineral. *Planta* 247(1), 277–285.

ovary of *Blumenbachia insignis*. Bright contrast in (b) indicates a high concentration of heavier element, such as Ca, P or Si. Scale bar = 100 µm.

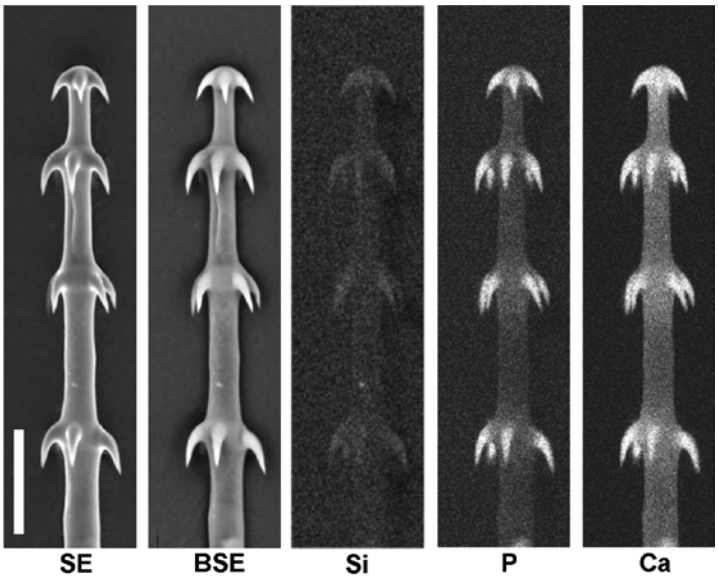


**Fig. S2.** SE-, BSE-, and element-mapping images of Fig. 1b. Glochidiate trichome of *Loasa tricolor* with high concentrations of P and Ca in trichome hooks and a lower Ca concentration in the shaft. Si is absent. Scale bar = 30 µm.

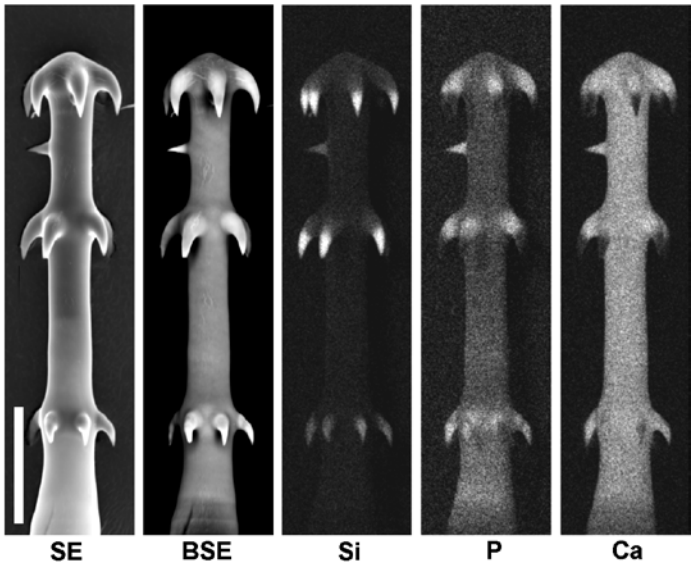


**Fig. S3.** SE-, BSE-, and element-mapping images of Fig. 1c. Glochidiate trichome of *Caiophora lateritia* with high Si concentration (= silica) in the hook tips, and high P and Ca concentrations (= calcium phosphate) in the hook shoulders. The shaft contains Ca in high and P in moderate

concentrations, but no Si (= calcium carbonate-based composite with traces of phosphate). Scale bar = 30 µm.

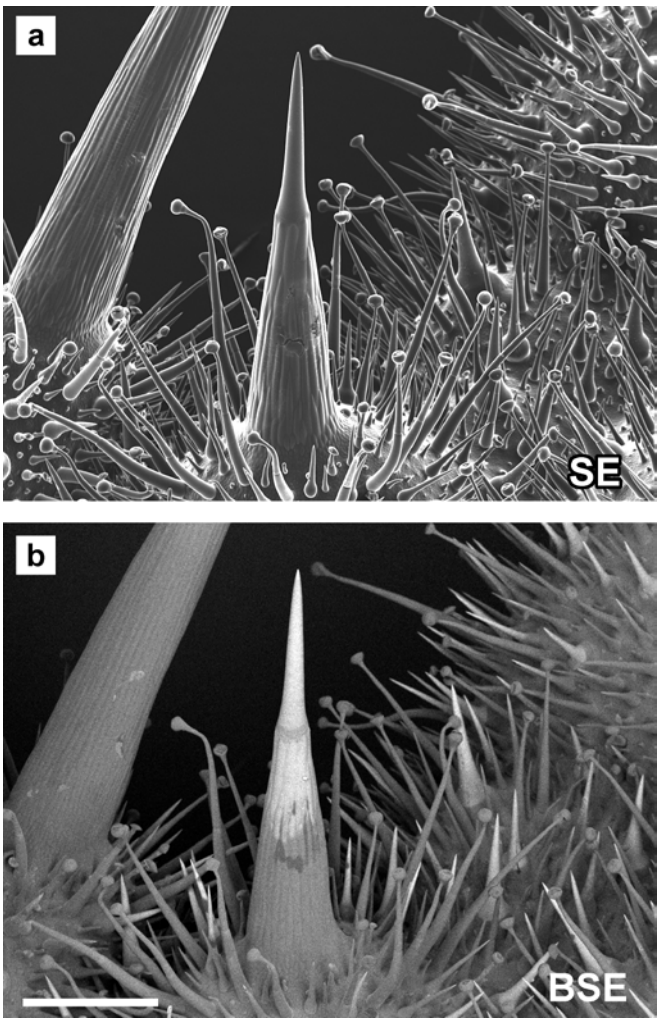


**Fig. S4.** Separate secondary electron (SE) and backscattered electron (BSE) images of Fig. 2a. The cryo-SEM images show (a) topographical and (b) compositional contrast of *Codon royenii* trichomes. Bright contrast in (b) indicates high concentrations of heavier elements (Ca, P). Scale bar = 400 µm.

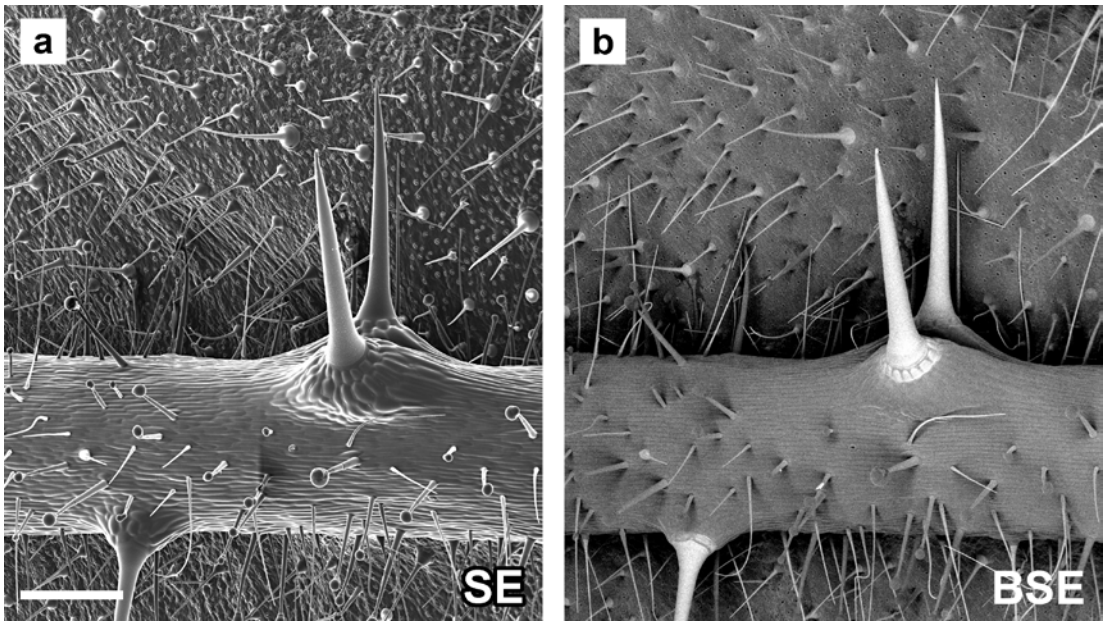


**Fig. S5.** Separate SE and BSE images of Fig. 2f. The cryo-SEM images show (a) topographical and (b) compositional contrast of *Phacelia malvifolia* trichomes. Bright contrast in (b) indicates high concentrations of heavier elements (Ca, P). Scale bar = 400 µm.

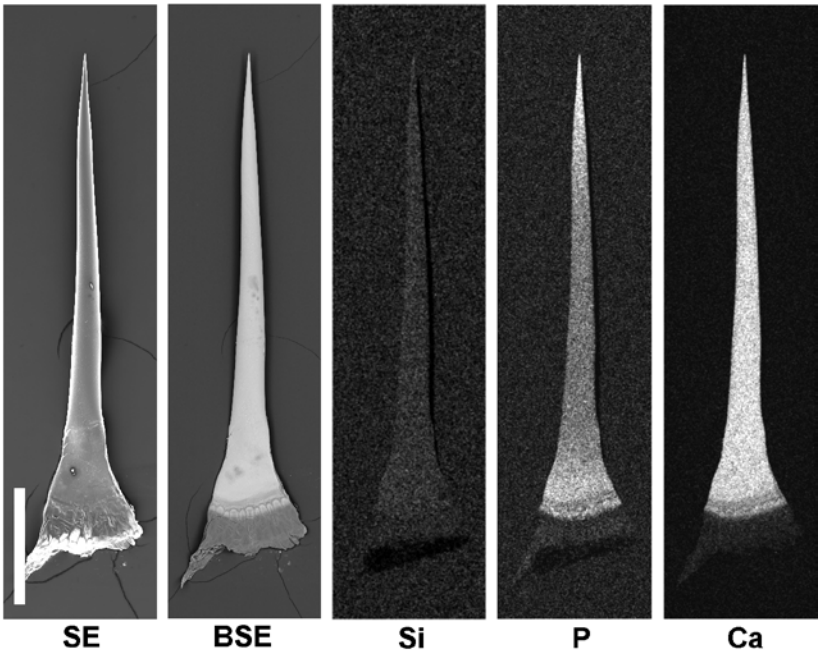


**Fig. S6.** SE-, BSE-, and element-mapping images of Fig. 2g. The *Phacelia malvifolia* trichome shows high Ca concentration in the entire shaft, whereas the P concentration is high in the trichome tip and base, but lower in the center. Si is not detected. Scale bar = 400 µm.

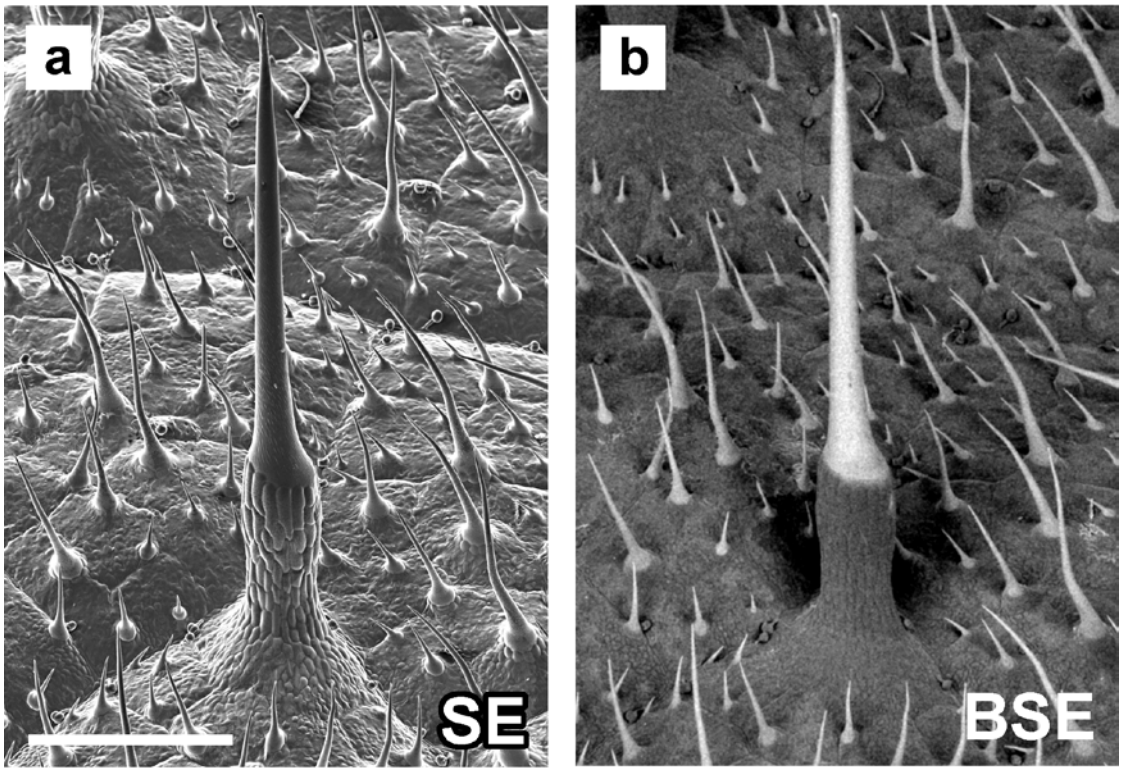


**Fig. S7.** Separate SE and BSE images of Fig. 3a. The cryo-SEM images of a stinging hair and small trichomes of *Urtica dioica* show (a) topographical and (b) compositional contrast. Bright contrast in (b) indicates high concentrations of heavier elements (Si, Ca, P). Scale bar = 500 µm.

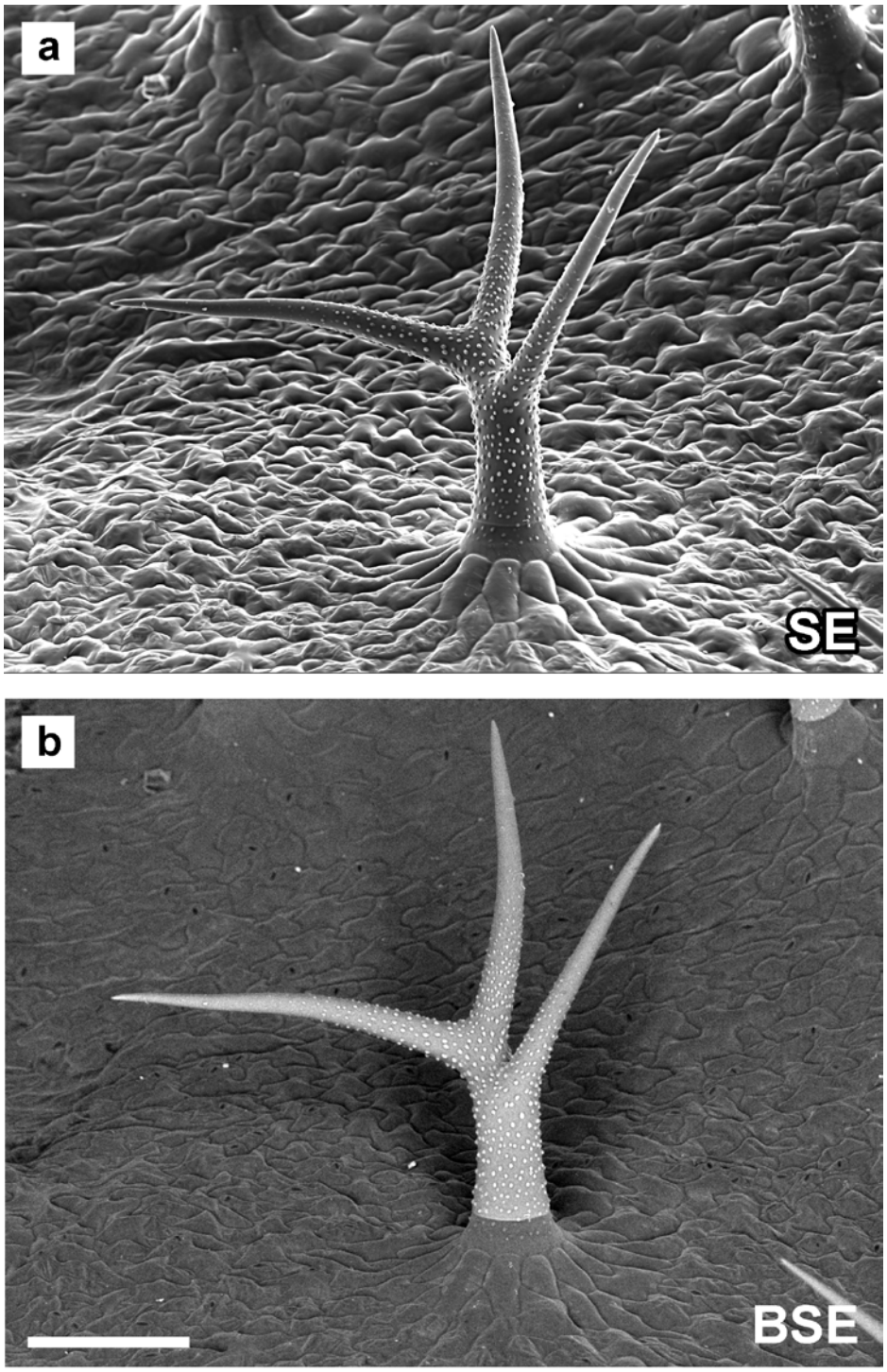


**Fig. S8.** Separate SE and BSE images of Fig. 4a. The cryo-SEM images show (a) topographical and (b) compositional contrast of an *Arabidopsis thaliana* trichome. Bright contrast in (b) indicates high concentrations of mineral elements (Ca, P, Si). Scale bar = 100 µm.

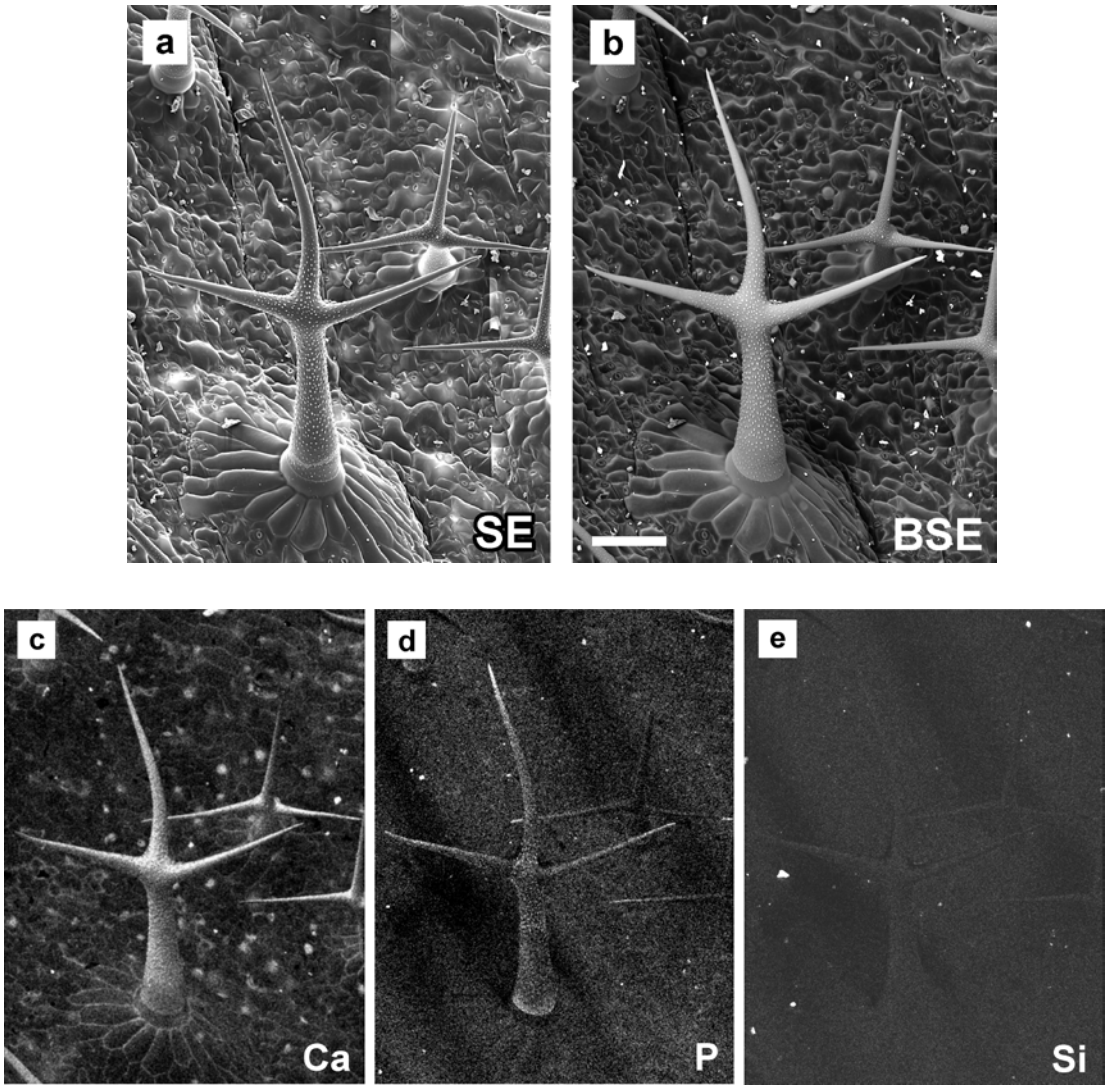


**Fig. S9.** SE-, BSE-, and element-mapping images of Fig. 4b. The SEM images of CP-dried *Arabidopsis thaliana* trichomes show high Ca concentrations in the entire trichomes, and high P concentrations mainly in tips and basal regions of the trichomes. Si is detected only in dust particles on the surface. The slight unevenness of detected Ca-distribution results from varying surface angles and does not reflect compositional differences. Remarkably high Ca contents in the epidermis cell walls may indicate a displacement of Ca compounds during preparation. Scale bar = 100 µm.

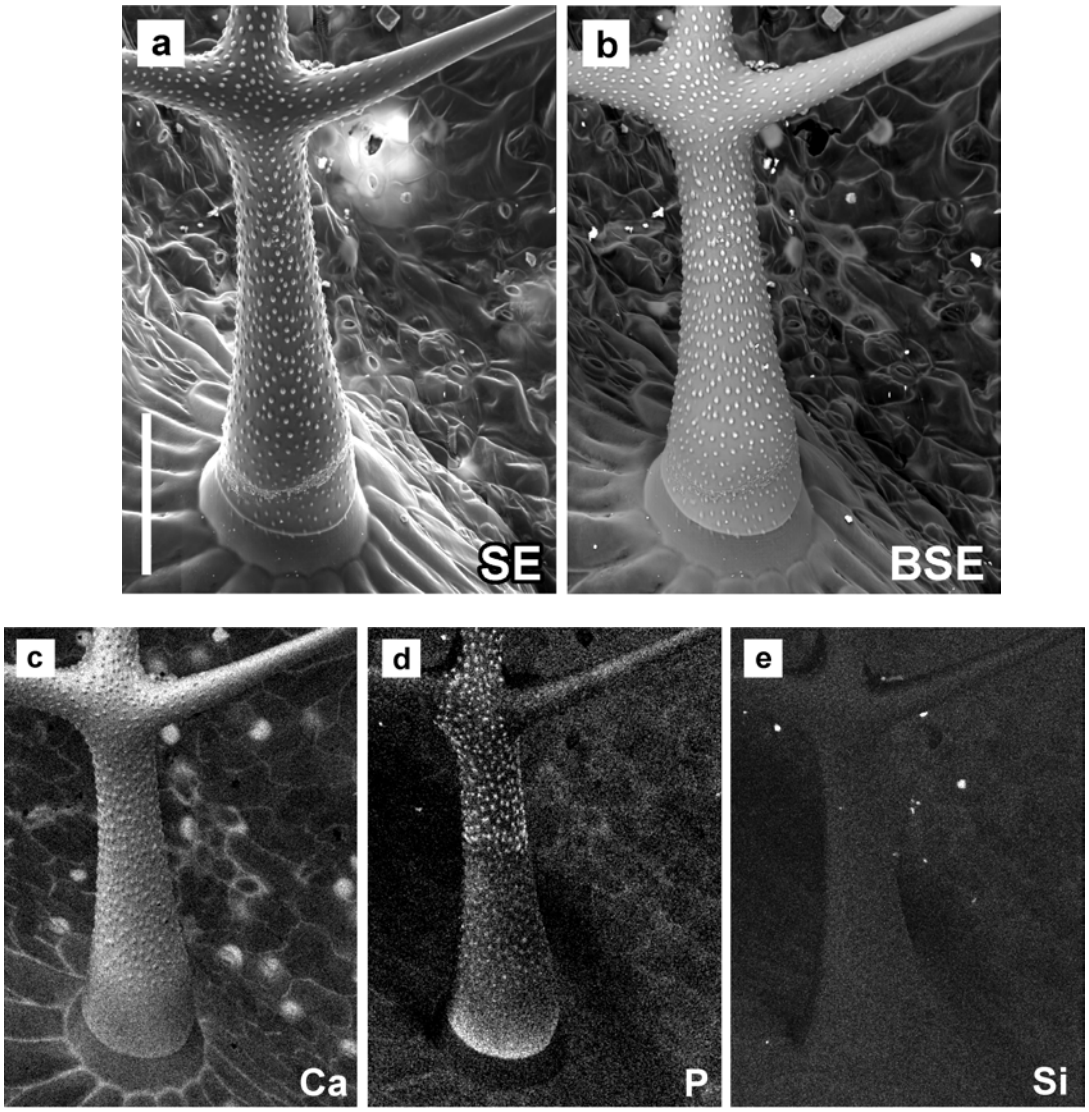


**Fig. S10.** SE-, BSE-, and element-mapping images of Fig. 4f,g. The SEM images of part of a CP-dried *Arabidopsis thaliana* trichome show high Ca concentrations in the entire trichomes, except for the non-mineralized lower end, and in some epidermis structures. High P concentrations occur in the grainy shaft structures and the basal region of the trichome. Si is found only in some dust particles. The uneven intensity in the Ca distribution of the trichomes results mainly from unfavorable orientations of the surface relative to the detector position. Elevated Ca contents in the epidermis cell walls may indicate a displacement of Ca compounds during preparation. Scale bar = 100 µm.

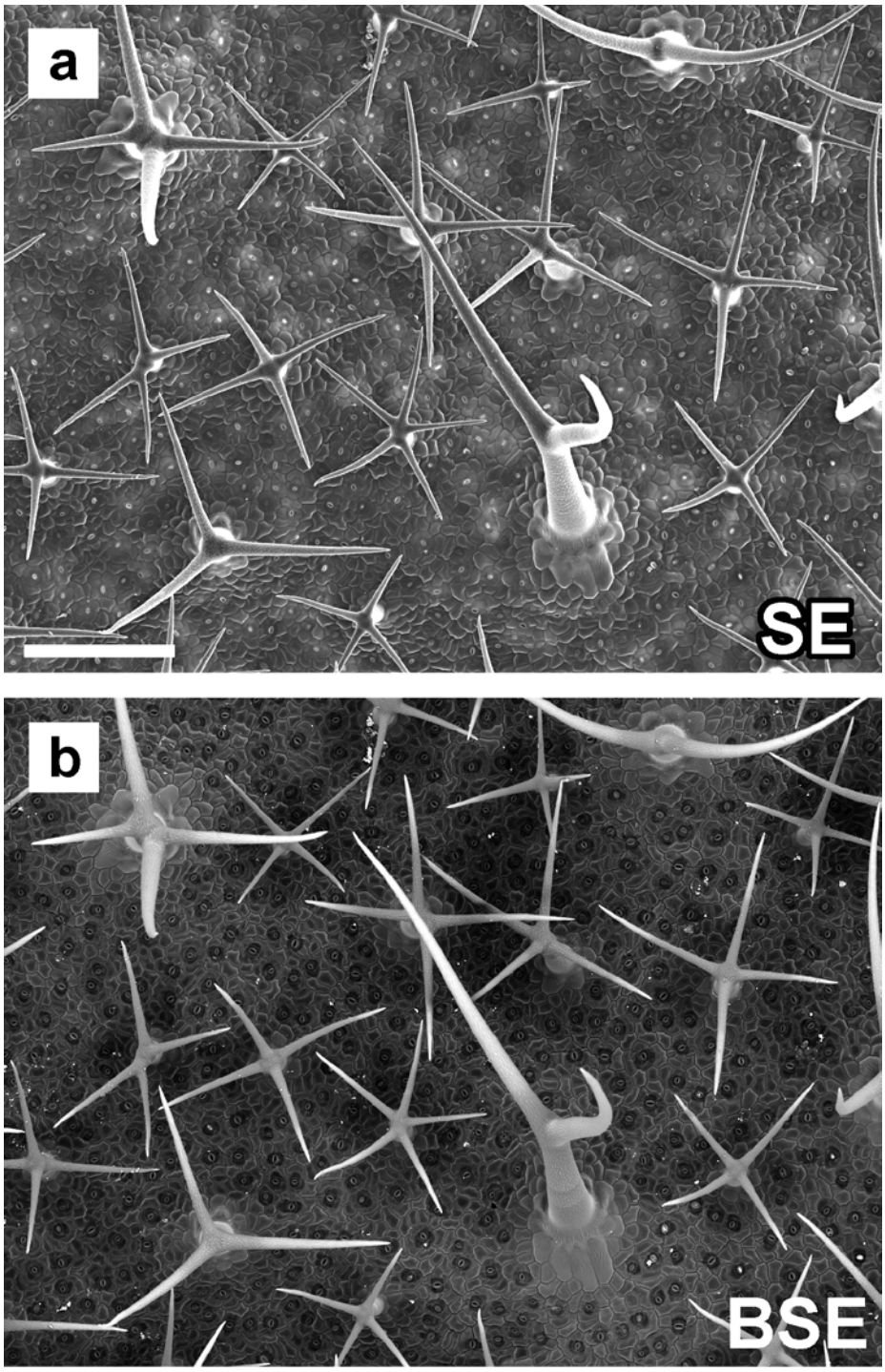


**Fig. S11.** Separate secondary electron (SE) and backscattered electron (BSE) images of Fig. 6a,b. SEM images of CP-dried *Aubrieta deltoidea* trichomes. Scale bar = 200 µm.

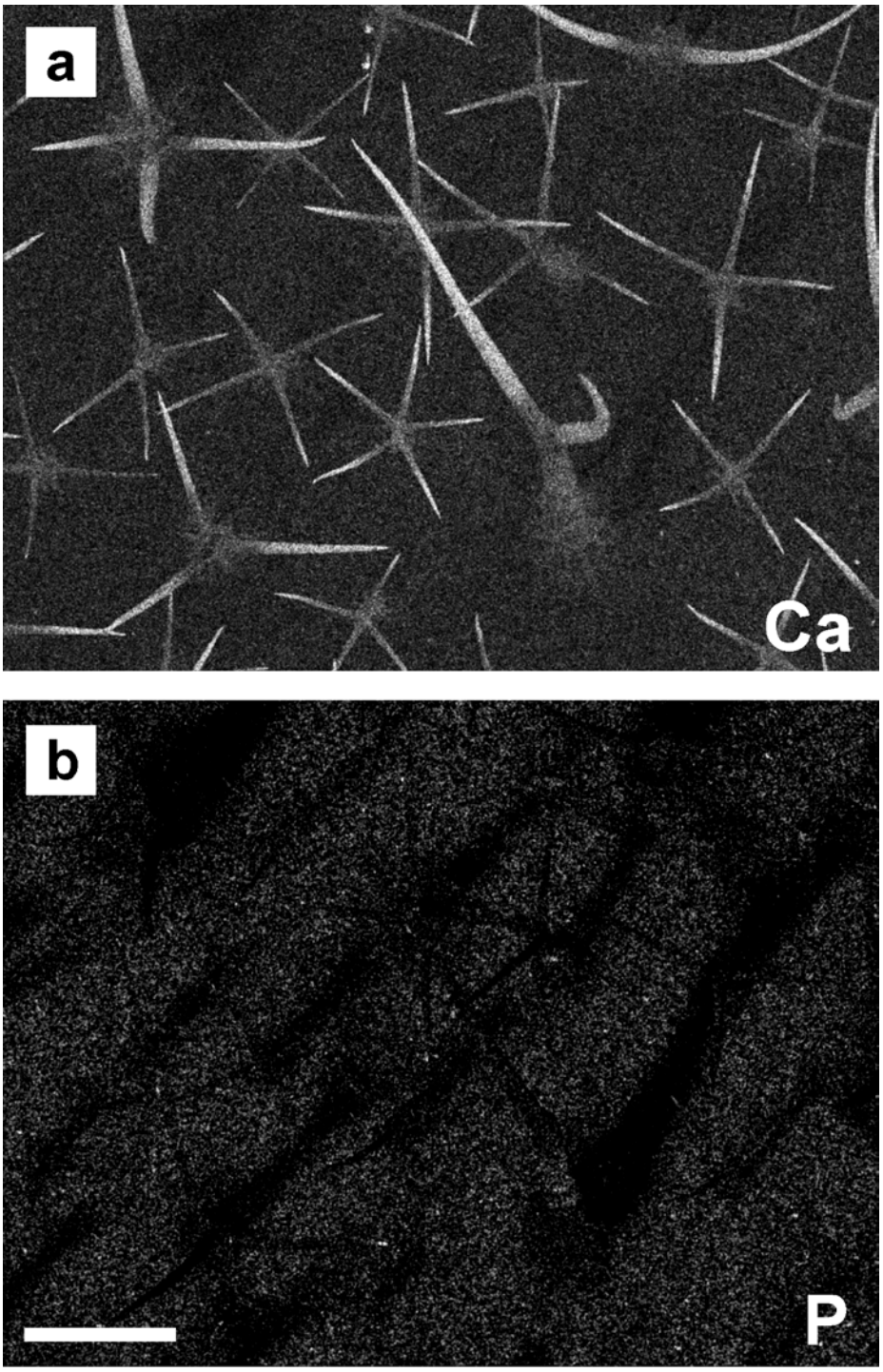


**Fig. S12.** Separate Ca and P element-mapping images of Fig. 6a, b from CP-dried *Aubrieta deltoidea* trichomes. High Ca concentrations occur in large distal parts of the trichomes whereas high P concentrations are restricted to minute areas at the very tips of the trichomes. Scale bar = 200 µm.

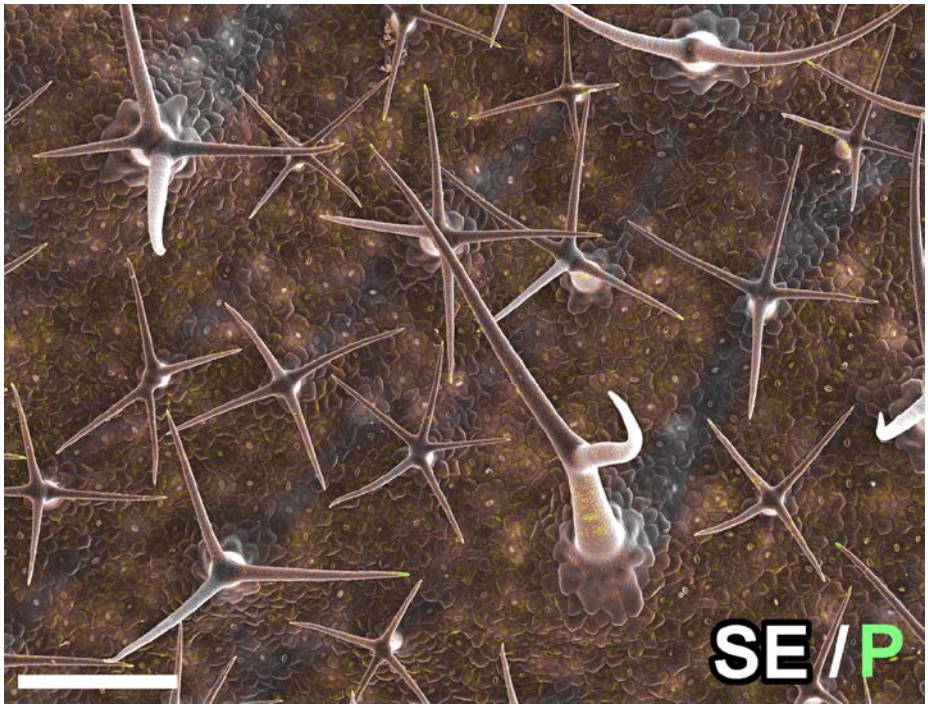


**Fig. S13.** Combined SE- and P-mapping image (= Fig. 6a) from CP-dried *Aubrieta deltoidea* trichomes. In the color image it is easier to recognize the P-rich trichome tips (green) than in the separate phosphorus mapping image (Suppl. Fig. S12 b). Scale bar = 200 µm.

# CURRICULUM VITAE

# PUBLICATION LIST

## Research papers

1) Ensikat, H. J., **Mustafa, A**., & Weigend, M. (2017). Complex patterns of multiple biomineralization in single-celled plant trichomes of the Loasaceae. *American Journal of Botany*, 104(2), 195–206.

2) **Mustafa, A**., Ensikat, H. J., & Weigend, M. (2017). Ontogeny and the process of biomineralization in the trichomes of Loasaceae. *American Journal of Botany*, 104(3), 367–378.

3) **Mustafa, A**., Ensikat, H. J., & Weigend, M. xxxx. Diversity of Biomineralization in Stinging trichomes of Different Plant Families: Silica, Calcium phosphate, or neither? **(**In preparation).

4) **Mustafa, A**., Ensikat, H. J., & Weigend, M. 2018. Mineralized Trichomes in Boraginales – Complex Microscale Heterogeneity and Simple Phylogenetic Patterns. *Annals of Botany* (In Press)

5) Weigend, M., **Mustafa, A**., Ensikat, H. J. 2018. Calcium phosphate in plant trichomes: the overlooked biomineral. *Planta*, 247(1), 277–285.

## Posters

1) **Mustafa, A**., Jeiter, J., Große-Veldmann, B., Ensikat, H. J., Chacon, J., Holstein, H., Weigend, M. (2016). Pflanzen die unter die Haut gehen.

2) **Mustafa, A**., Jürgen, H. J., & Weigend, M. (2016). Biomineral distribution in trichomes of Boraginales.

3) **Mustafa, A**., Jeiter, J., Ensikat, H. J., Holstein, H., Weigend, M. (2016). Biomineralisierung — bestechend schön und vielfältig.

4) Große-Veldmann, B., Jeiter, J., **Mustafa, A**., Poretschkin, C., Holstein, H., Weigend, M. (2016). Brennnesseln — gleich und doch verschieden.

5) Jeiter, J., **Mustafa, A**., Große-Veldmann, B., Chacon, J., Poretschkin, C., Holstein, H., Weigend, M. (2016). Brennhaarpflanzen — nur gucken, nicht anfassen.

## Conference contribution

1) Weigend , M., Jeiter, J., **Mustafa, A**., Ensikat, H. J., Luebert, F., Chacón (2017). Evolutionary trends in Boraginales. IBC 2017, XIX International Botanical Congress, Shenzhen China.

2) Ensikat, H. J., **Mustafa, A**., Weigend, M. (2017). Calcium phosphate biominerals in plants: more than exotic curios. MC 2017 Lausanne, Switzerland.

3) **Mustafa, A**., Ensikat, H. J., & Weigend, M. (2016). Biomineral distribution in trichomes of Boraginales. III. International Boraginales meeting, Nees-institute for biodiversity of plants, University of Bonn, Germany.